CONTROL OF VEHICLE LATERAL DYNAMICS BASED ON LONGITUDINAL WHEEL FORCES

Simon James O'Neill

A thesis submitted in fulfillment of the requirements
for the degree of Master of Science (MSc)

Department of Mechanical Engineering
School of Engineering
University of Glasgow
February 2012

Abstract

Trends show that on board vehicle technology is becoming increasingly complex and that this will continue to be the case. This complexity has enabled both driver assistance systems and fully automatic systems to be introduced. Driver assistance systems include anti-lock braking and yaw rate control, and these differ from fully automatic systems which include collision avoidance systems, where control of the car may be taken away from the driver.

With this distinct difference in mind, this work will focus on driver assist based systems, where emerging technology has created an opportunity to try and improve upon the systems which are currently available.

This work investigates the ability to simultaneously control a set of two lateral dynamics using primarily the longitudinal wheels forces. This approach will then be integrated with front wheel steering control to assess if any benefits can be obtained.

To aid this work, three different vehicle models are available. A linear model is derived for the controller design stage, and a highly nonlinear validated model from an industrial partner is available for simulation and evaluation purposes. A third model, which is also nonlinear, is used to integrate the control structures with a human interface test rig in a Hardware in the Loop (HiL) environment, which operates in real-time.

Frequency based analysis and design techniques are used for the feedback controller design, and a feedforward based approach is used to apply a steering angle to the vehicle model. Computer simulations are initially used to evaluate the controllers, followed by evaluation via a HiL setup using a test rig. Using a visualisation environment in Matlab, this interface device allows driver interaction with the controllers to be analysed. It also enables driver reaction without any controllers present to be compared directly with the controller performance whilst completing the test manoeuvres.

Results show that during certain manoeuvres, large variations in vehicle velocity are required to complete the control objective. However, it can be concluded from both the computer simulation and HiL results that simultaneous control of the lateral dynamics, based on the longitudinal wheel forces can be achieved using linear control methods.

Acknowledgements

I would like to express my gratitude to the many people that have helped to make this thesis possible. Firstly my two supervisors Dr Henrik Gollee and Prof. Ken Hunt, both of University of Glasgow. Ken, thankyou for the initial opportunity, and Henrik thankyou for your help, support and invaluable guidance. Also, to Geraint who I shared an office with for the duration of my studies. Our conversations and discussions were very helpful and motivational. Thanks also to Prof. John O'Reilly from University of Glasgow for your words of wisdom and suggestions. My thanks also goto the CRE group at Glasgow who helped to make a fun, cohesive and stimulating group.

Most importantly my family, and my parents in particular, who have both supported me and encouraged me tremendously throughout my life, especially during the past few years. For this I will always be grateful.

Finally, to my recently wed wife Emma. Thankyou for your understanding and putting up with the long nights and whole weekends of doing 'uni work'. We can now spend more quality time together and really enjoy married life!

Nomenclature

X	longitudinal distance	[m]
Y	lateral distance	[m]
v	vehicle velocity	[m/s]
a	vehicle acceleration	[m/s^2]
g	gravitational acceleration	[m/s^2]
F	forces in vehicle CG system	[N]
F_0	forces in earth fixed axis system	[N]
f	forces in tyre axis system	[N]
β	vehicle sideslip angle	[rad]
δ_f	front steer angle	[rad]
δ_r	rear steer angle	[rad]
γ	camber angle	[rad]
α	lateral tyre slip	[rad]
λ	longitudinal tyre slip	[-]
ψ	yaw angle	[rad]
$\dot{\psi}$	yaw velocity	[rad/s]
$\ddot{\psi}$	yaw acceleration	[rad/s^2]
μ	friction coefficient	[-]
ω_i	angular velocity of the wheel	[rad/s]
$\dot{\omega}_i$	angular acceleration of the wheel	[rad/s^2]
$C_{\alpha,i}$	cornering stiffness of the tyre	[N/rad]
J_w	moment of inertia of wheel	[kgm^2]
J_z	moment of inertia of vehicle	[kgm^2]
m	vehicle mass	[kg]
T_w	torque applied to the wheel	[Nm]
r_e	effective wheel radius	[m]
d_l	distance from centre of gravity to left wheel	[m]
d_r	distance from centre of gravity to right wheel	[m]
l_f	distance from vehicle centre of gravity to the front axle	[m]
l_r	distance from vehicle centre of gravity to the rear axle	[m]

ω_n	natural frequency	[rad/s]
ω_b	bandwidth frequency	[rad/s]
ω	frequency	[rad/s]
ζ	damping co-efficient	[-]
j	complex operator	[-]
s_m	vector margin	[-]
L	loop gain	[-]
K	controller	[-]
G	linear plant	[-]
$G_{\dot{\psi}}$	linear plant for yaw rate dynamics	[-]
G_{vx}	linear plant for longitudinal velocity dynamics	[-]
S	sensitivity function	[-]
T	complementary sensitivity function	[-]
K_1	longitudinal velocity controller	[-]
K_p	longitudinal velocity controller	[-]
K_{11}	longitudinal velocity controller	[-]
K_{33}	yaw rate controller	[-]
K_{p3}	yaw rate controller	[-]
β_{th}	sideslip controller threshold	[-]
M_s	peak value of sensitivity function	[-]
B	Pacejka's Magic Formula coefficient	[-]
C	Pacejka's Magic Formula coefficient	[-]
D	Pacejka's Magic Formula coefficient	[N]
E	Pacejka's Magic Formula coefficient	[-]
T_x	transformation matrix	$\in \mathbf{R^{4\times 2}}$
$\overrightarrow{F}$	force vector in CG axis system(x & y direction)	$\in \mathbf{R^{1\times 2}}$
$\overrightarrow{f}$	force vector in tyre axis system(x & y direction)	$\in \mathbf{R^{1\times 2}}$
$\overrightarrow{v}$	velocity vector in CG axis system(x & y direction)	$\in \mathbf{R^{1\times 2}}$
$\overrightarrow{F_0}$	force vector in earth fixed axis system(x & y direction)	$\in \mathbf{R^{1\times 2}}$
$\overrightarrow{v_0}$	velocity vector in earth fixed axis system(x & y direction)	$\in \mathbf{R^{1\times 2}}$

Indices

$i = 1$ front left wheel

$i = 2$ front right wheel

$i = 3$ rear left wheel

$i = 4$ rear right wheel

x longitudinal direction, positive forwards

y lateral direction, positive leftwards

z vertical direction, positive upwards

Abbreviations

BLDC Brushless Direct Current

CCD Charge Coupled Device

DAQ Data Acquisition

dof Degree of Freedom

EAKF Extended Adaptive Kalman Filter

EKF Extended Kalman Filter

GPS Global Positioning System

HIL Hardware in the Loop

ICD Individual Channel Design

IMC Internal Model Control

INS Inertial Navigational System

KF Kalman Filter

LCDM Linear Controller Design Model

LID Linear Inverse Dynamics

LQ Linear Quadratic

LTR Load Transfer Ratio

RCP Rapid Control Prototyping

RTSM Real-time Simulation Model

SMC Sliding Mode Control

VSM Verified Simulation Model

UDP User Datagram Protocol

Vehicle Terminology

2WD Two Wheel Drive
4WS Four Wheel Steering
ABC Active Brake Control
ABS Anti-Lock Braking System
ACC Adaptive Cruise Control
AFS Active Front Steering
ARC Active Roll Control
ASR Traction Control System
AWD All Wheel Drive
AWS All Wheel Steering
BbW Brake-by-Wire
BSS Brake Steer System
CAN Controller Area Network
CG Centre of Gravity
DSC Dynamic Stability Control
DYC Dynamic Yaw Control
EDiff electronic differential
ESC Electronic Stability Control
ESP Electronic Stability Program
EV Electric Vehicle
FWS Front Wheel Steering
LSD Limited Slip Differential
RMD Roll Moment Distribution
RWS Rear Wheel Steering
SbW Steer-by-Wire
SUV Sport Utility Vehicles
TCS Traction Control System
TVD Torque Vectoring Differential
VSC Vehicle Stability Control
VTD Variable Torque Distribution
XbW X-by-wire

Contents

List of Tables

List of Figures

Chapter 1

Introduction

> At least every second road accident will be prevented in the future if the vehicles are fitted with appropriate driver assistance systems.
>
> Prof. Klaus-Dieter Vöhringer
>
> Previous President of Research and Technology of DaimlerChrysler, 2002

Statistics show that on German roads 90% of registered accidents are caused by human error, with the remaining 10% by technical defects [2]. Another source quotes that 95% of accidents on Britain's roads involve human error [3].

In recent years, control systems have become readily available on motor vehicles. Ranging from anti-lock braking systems and traction control, to yaw rate and vehicle roll control systems, they are designed to improve the safety of the vehicle and the passengers within. As such, vehicles have become much more complex than their predecessors, aided with the availability of more complex electronics. These available electronics can be used to aid the driver in everyday driving situations, mainly in the area of lateral dynamics control.

Lateral dynamics are explicitly associated with lateral behaviour of the vehicle. Many control systems are designed to limit the lateral dynamics with the most common being yaw rate control. On the other hand, longitudinal dynamics are a result of longitudinal motion of the vehicle, and longitudinal wheel slip control is the most widely used. Predominately, lateral dynamics are controlled using actuators that are directly associated with lateral movement (for example, steering). However, this work approaches the problem from a different angle and will present a case for controlling a set of two lateral dynamics (vehicle yaw rate and

vehicle sideslip) using the longitudinal wheel forces.

1.1 Motivation

Production vehicles are becoming laden with complex technology, which leads to an increase in on-board control systems. Arguably the most prolific lateral dynamic system is ESP (Electronic Stability Program) and this is seen as being so fundamental to vehicle safety that the EU has proposed all vehicles produced after 2014 should have this system fitted. Furthermore, the National Highway Traffic Safety Administration[1] in USA has implemented legislation for all vehicles under 4536 Kg manufactured in 2012 onwards to be fitted with ESP.

The general consensus is that drivers would prefer to remain in control of their own vehicle at all times. The fundamental difference between driver assist and automatic control is that driver assist control will only aid the driver and does not take over control of the vehicle, as with the automatic control system.

Vehicle dynamics is an active and expanding area of research. A lot of work has been carried out using Four Wheel Steering (4WS), and as such this area has been very heavily researched. This, combined with the impracticalities of employing 4WS on production vehicles at present, has caused research to move to different actuator sets. However, very recently BMW have launched 4WS on its latest 7 series model as an optional extra, with the rear wheels being able to steer through $\pm 3^{\circ}$.

As the number of control systems in the vehicle grows, the need for these systems to interact becomes increasingly important. Therefore, the interactions between the subsystems must be considered in some capacity. ESP control systems can be used to limit the yaw rate but do not have the capability to control sideslip angle simultaneously. 4WS is seen as the ideal method for this simultaneous control, although as already mentioned it has been studied in great detail. Therefore, other means of achieving similar performance must be explored.

To this end, this work will focus primarily on using the longitudinal wheel forces to simultaneously control vehicle yaw rate and sideslip as a driver assist system. The system will then be integrated with front wheel steering control. The main advantage of this integrated

[1] http://www.nhtsa.gov

system is that the wheel force and front steering actuators are already available on many standard production vehicles today.

1.2 Current state of the art

This section presents the current state of the art of vehicle lateral dynamics control, and will also look briefly at other control systems which use the same actuators. This will highlight the broad range of applications in which vehicle lateral dynamics control has been used. This review is structured as follows. Firstly, the control of lateral dynamics using only individual longitudinal wheel forces is introduced, followed by how integrating steering with the longitudinal wheel forces can be used to control vehicle lateral dynamics. Finally, a review of four wheel steering (4WS) control is carried out to assess its influence in current research. The remaining sections review elements which are important for vehicle dynamics control, together with the methods and techniques associated with them, including parameter estimation and vehicle modelling. A discussion concludes this section which presents the argument for the main contributions of this thesis in section 1.4.

It has been mentioned that lateral control refers to the ability to control vehicle movements which are associated with lateral behaviour. The most common example of such a system is ESP, or yaw rate control. Within this chapter, many different systems are mentioned which are used to stabilise yaw rate. To this end, the following systems can be regarded as being used for the same purpose and are therefore comparable: Dynamic Stability Control (DSC), Dynamic Yaw Control (DYC), Electronic Stability Control (ESC), Electronic Stability Program (ESP) and Vehicle Stability Control (VSC). The different names of these systems arise from the different manufacturers, and each will retain their original name when discussed within this thesis.

Nowadays, Anti-Lock Braking System (ABS) and Electronic Stability Program (ESP) are included in most production vehicles as standard. ABS operates during vehicle braking and attempts to avoid wheel lock. This is made possible by reducing the braking force intermittently, allowing the longitudinal slip of the wheel to remain near its peak value, resulting in maximum traction at the road/wheel interface. Research work for ABS has progressed greatly since it was first started during the 1980's [4–8], with the market leader

being Bosch [9], and has evolved into ESP which was introduced to limit the vehicle yaw rate, and thus help to maintain stability of the vehicle [10]. ESP typically works by applying a torque to the outer front wheel of the cornering vehicle, resulting in a moment generated at the vehicle centre of gravity [11–13]. Engine intervention can be combined with the braking action to limit the yaw rate and maintain yaw stabilisation. More recently, Traction Control Systems (TCS) [14] have become common in larger production vehicles. These systems operate in a similar fashion to ABS, but attempt to maintain maximum traction during vehicle acceleration as opposed to vehicle braking. Traction Control is extremely advantageous when accelerating on low-friction surfaces where wheel spin is very likely to occur.

With the recent advances in technology, Brake by Wire (BbW) is now possible, resulting in individual wheel braking, and has created many exciting opportunities from a control design perspective. The ability to brake the four wheels independently of each other has enabled Brake Steer Systems (BSS) to be developed, where by altering the left/right and front/rear braking ratios a yaw moment can be generated [15]. It is the ability to vary the braking force to each wheel independently which makes it possible to control vehicle lateral dynamics using only the vehicle braking system, albeit the performance will be limited when using only braking forces.

Within this area of lateral dynamics control, most of the studies are simulation studies with very few of the control systems tested using a hardware in the loop (HIL) setup (for example [16–19]). Rarely are SbW test rigs used to evaluate controllers. The work carried out in [17] uses steering hardware, but is limited by computing power to a simple vehicle model.

1.2.1 Braking only control

When using the wheel braking system to control vehicle dynamics, one usually thinks of longitudinal dynamics control, for example vehicle velocity control or longitudinal slip control. However, as mentioned earlier, the emerging availability of BbW technology has resulted in the possibility to use the vehicle braking system more widely to control lateral dynamics. In the available literature, BbW can control yaw rate and vehicle speed. This can be used to either stabilise yaw rate in the presence of disturbances or uncertainties (as in ESP), or to make the car follow a desired trajectory (as in BSS). This is a fundamental yet very important

difference.

BSS have been investigated by a number of different researchers for improving vehicle handling in general driving situations. Pilutti et al. [20], were one of the first to propose the idea of differential braking as steering intervention, and the possibility that the limited steering function provided by BSS can be used to control lateral position in an unintended road departure system. Raksincharoensak also identifies the usefulness of differential braking for a lane departure warning system when used in conjunction with a camera [21]. However, for the latter to work in principle, the curvature of the road is required as an input to the controller, and as such the controller relies heavily on the accuracy of this signal. This can only be estimated, and Kalman filtering theory can be used for this, as described in [22].

The systems mentioned so far are classed as driver assistance systems. They are designed to assist the driver, but not take complete control of the vehicle. The other class of system is fully automatic, where the controller takes complete control of the vehicle from the driver, for example in an automatic collision avoidance system [23].

Many different control methods have been adopted in the literature. Pilutti et al. [20] favours LQ and pole placement techniques for their controller design, due to the quick reaction times which are possible, while Raksincharoensak [21] uses differential longitudinal forces to generate an assistive direct yaw moment in order to track a desired yaw rate with the control law obtained using Linear Inverse Dynamics (LID).

Vehicles and their computer based models are both associated with uncertainties (for example, the friction coefficient or modelling errors) [24–26]. This makes sliding mode control a popular method because of its inherent robustness properties [27, 28], and Ayat et al. [25] adopt a nonlinear based sliding mode controller using the torque vector at the wheels to control the yaw rate at a given velocity and steer angle.

The research reviewed so far, has concentrated on controlling only vehicle yaw rate. Studies exist which attempt to control an additional variable simultaneously to improve vehicle stability [26, 29], and Yi states that this is a necessity. As a result, sliding mode control with brake pressure inputs is used to regulate both sideslip angle and yaw rate [26]. An important method of determining the performance of the controller, is to compare them with Dynamic Yaw Control (DYC), where only yaw rate is controlled. Improvements in the control of sideslip angle can be seen with the simultaneous control. Zhao uses Fuzzy methods and chooses to

control lateral velocity and yaw rate using differential braking [29]. Using the vehicle brakes to regulate sideslip angle is also adopted by Toyota [30], to good effect over a large operating region.

1.2.2 Integrated steering and braking control

Using braking only control on its own utilises four actuators, which in turn limits what can be controlled. It is apparent that it can be combined with steering to extend the actuation. Obviously the extra actuator makes extra degrees of freedom available and as a result of this, more literature is available.

In general, the methods applied to integrated control are not as simplistic as those for braking only control, with nonlinear methods more common. The nonlinearities which occur from the steering input and coupling between the steering and braking systems are mainly responsible for this. Also, in the vehicle and tyre models, small angle assumptions for sine and cosine can easily start to become invalid.

Fuzzy logic was used in braking only control [29] due to its robustness properties. Other properties which make it a popular choice in automotive control, are that it is based on simple methods, where the control laws can be described in vague linguistic terms. Both of these advantages can make it particularly suitable to vehicle stability control [31–33].

Simultaneous control of vehicle sideslip angle and yaw rate is achieved by Boada et al. [31], through applying a braking torque on either front wheel and adding an additional steering wheel angle to the driver's wheel angle. A slightly different approach is adopted by Ahmadi et al. who, with Fuzzy control, designs two controllers, Dynamic Yaw Control (DYC) and Active Front Steering (AFS) individually and then integrates them [32]. The combined control performs better than the controllers employed on their own.

Stability of electric vehicles is studied using yaw rate control, and all wheel drive electric vehicles in particular [33,34]. Both fuzzy control and optimal control are used to good effect. When attempting to control the vehicle dynamics, reference signals need to be made available to the controllers. These can come from a variety of sources, but often it is desirable to make the vehicle behave like an 'ideal' vehicle. In this case, model matching techniques can be used. Nagai et al. employ this method to good effect, where feedforward steering decides the inputs to the steering wheel, and feedback braking eliminates any output errors [35].

Burgio [36] uses similar methods to derive a control law from a nonlinear tyre model, based on the assumption that the lateral front tyre force is a direct actuation and inverting it to compute the steering law.

All work considered so far involves integrated front wheel steering and individual wheel braking. However, another alternative is integrated four wheel steering (4WS) and individual wheel braking of all four wheels, which should offer scope to control lateral dynamics better, given the extra control input. Four wheel steering is discussed in more detail in section 1.2.3. Salman offers something similar to this, but uses only rear wheel steering control with four wheel braking for improving vehicle stability in combined braking and turning manoeuvres, while the driver uses the front wheel steering actuators [37]. The controller, designed using Davison's robust servomechanism control design methodology [38, 39], tracks vehicle deceleration and yaw rate. The advantage of this approach is that the driver is able to retain some control over the vehicle via the front wheel steering. Another study by the same author uses front wheel steering control with the rear wheels fixed, and four wheel braking [40]. Although the controllers improve stability in both cases, no clear advantages can be identified between either control setup.

It was seen earlier in [32] that DYC and active front steering (AFS) subsystems can be designed independently of each other and then integrated together. However, no consideration was given as to how the integration could be implemented. To expand on this, He et al. presents AFS and DSC subsystems and suggests a bottom-up approach to integrate them [41]. The AFS improves steerability at low to mid range lateral accelerations, while DSC bounds the sideslip during extreme manoeuvres. In this way, both systems complement each other. Another example of similar work is carried out by Guvenc et al. [42], who use a model regulator to improve yaw stability through steering and braking [43, 44]. Although only one variable is controlled in this work, it is found that again the steering compliments the braking well, and offers good disturbance rejection. The natural progression of this work would be to control two variables simultaneously to improve vehicle stability further, with possibly the extra variable being sideslip angle. Indeed, one of the main findings in [41] is that vehicle sideslip is directly related to the stability of the vehicle, and it is therefore accepted that it must be bounded in order to keep the vehicle stable. This seems to be the general consensus, and many other studies choose to control both sideslip angle and yaw rate simultaneously for

similar reasons.

Individual wheel braking integrated with steering is the most common approach, but Hac et al. include suspension as one of the actuators when controlling yaw rate [45], and therefore, use controllable brakes, steering and suspension.

One observation noted throughout the integrated braking and steering literature, is that most of the work considered involves steering applied as a feedforward signal, which avoids the delays associated with feedback control. Furthermore, the steering and braking subsystems are often designed independently of each other and integrated later. This seems to work well in most situations, although few studies have actively designed integrated subsystems.

Of course this feedforward steering signal needs to be generated. Also, the reference signals for the controllers need to be generated which is of great importance in contributing to the performance of the controller. If these reference signals are not meaningful (e.g for a lane change manoeuvre, they must be accurate enough to allow the manoeuvre to be completed), then the controllers performance could be compromised. Usually these are dependent upon the driver's steering input, based on the inversion of an ideal model, as in [15, 20, 21, 26] although some literature does not state how they are obtained.

Steering and braking control uses more nonlinear models for controller design than braking only control, and more commonly achieves simultaneous control.

1.2.3 Four wheel steering control

Currently, four wheel steering (4WS) control is an active area of research. However, a fundamental difference exists between 4WS control and control involving braking actuators. Braking removes energy from the system which holds advantages over 4WS control, especially in emergency manoeuvres where it may be desirable to reduce the vehicle velocity (e.g for vehicle stability). On the other hand, this reduction in velocity can be seen as a disadvantage, and several authors report that since 4WS does not greatly reduce the vehicle velocity, this is 'ideal' for controlling vehicle lateral dynamics in non stability based applications [31, 35].

Another difference is the most suitable application for each set of actuators. 4WS lends itself to reference tracking while braking only control is very useful for stability control because of the energy reduction in the system.

The two sets of actuators in 4WS (the front and rear road wheel steering angle) give

rise to the possibility of two control inputs, hence the ability to control two variables simultaneously. However, to achieve simultaneous control, it is necessary to ensure that the signals are not coupled. Simultaneous control with 4WS has been achieved by Villaplana et al. [46] and Ackermann [47]. Villaplana et al. track yaw rate and sideslip angle simultaneously, and decouple the system into two channels, allowing Individual Channel Design (ICD) [48] techniques to be applied. Similar methods are used by Ackermann to decouple yaw rate and lateral velocity. Both of these studies employ yaw rate feedback to achieve velocity independent yaw dynamics.

4WS and braking

It has been stated that 4WS can be seen as 'ideal' due to the relatively small reduction in vehicle speed [31,35]. However, if braking is integrated with 4WS then the vehicle velocity is more likely to vary. Jia and Yu both include braking to try improve vehicle stability [49,50], and like Villaplana and Ackermann, Jia also finds it necessary to decouple the 4WS model into three second order subsytems (velocity controlled by longitudinal forces, lateral motion controlled by front steering angle and yaw velocity controlled by rear steering). On the other hand, Yu considers only two subsystems: the first to interpret the driver's inputs of steering and braking, and the second to output the steering and braking commands, according to road conditions etc. A reduction in wheel slip on low friction surfaces is the contributing factor for the improved performance.

Matsumoto et al. argue that the closed loop dynamics should depend on vehicle velocity and cornering stiffness factor (both of which are assumed to be known). This is the basis of regulating vehicle lateral velocity and yaw rate, and solve an LQ problem in order to design control laws for front and rear wheel steering [51]. The gain scheduled control laws (with respect to velocity and cornering stiffness) give good results when compared with front wheel steering combined with (i) differential drive torque between the two front wheels and (ii) between the two rear wheels.

The longitudinal forces on the wheels can be responsible for generating lateral motion as well as longitudinal motion. This was seen for braking only control, where altering the left-to-right braking ratio results in a yaw moment being generated. For this reason, it is desirable to control the longitudinal forces at the wheel directly [52], which can provide the

added benefits of reduced wheel slip on low friction surfaces [33]. Lin et al. combine 4WS and braking with an earlier developed nonlinear tyre model to redistribute the longitudinal forces and improve vehicle stability and controllability via wheel slip, based on the maximum friction available [52]. However, instead of controlling longitudinal wheel forces, Horiuchi et al. [53] choose to control the torque at the wheel directly, and compare three strategies for combining 4WS with braking control, namely

- rear wheel steering control with front wheel steering and standard brake system,
- four wheel torque control plus front wheel steering, and
- front and rear wheel steering control plus four wheel torque control.

Any non-controlled actuation is generated via driver input, while the control is performed using nonlinear predictive control, with the reference signals generated from a reference vehicle model. Overall, the combination of front and rear steering with four wheel torque control performs best in most situations.

In terms of production vehicles, active rear wheel steering was employed on a 1997 model Toyota Aristo [54], where a combination of brushless D.C. motors and $H\infty - \mu$ control improved vehicle handling within the linear region of tyre characteristics. The main problem with any SbW system (including rear wheel steering systems) for production vehicles is the need for a working backup system to be put in place for the event of a system failure. Presently, the mechanical backup is a conventional steering system with steering column and rack. The result of this is that SbW has been deemed impractical, too expensive and unprofitable to implement [55].

In an attempt to overcome this impracticality, a method of ensuring a mechanical failure will remain safe is presented by Fujita et al. [54]. This involves ensuring that the rear wheels will remain in the failed position, which at ± 1.6 degrees, the effects can be overcome using the front steering wheels. A similar strategy has been adopted by BMW in their 2009 model 7 series vehicle, which allows ± 3 degrees of rear wheel steering[2].

However, some disadvantages are also associated with 4WS, the main one being 'swing-out' with negative phase[3] RWS. Swing-out is more evident in low speed manoeuvreing, where

[2] http://www.bmw.com

[3] Negative phase is steering the rear wheels in the opposite direction to the front wheels

the rear of the vehicle requires a larger area to turn than a traditional 2WS vehicle. To alleviate this, Akita et al. [56] propose swing-out reduction control which works by steering the rear wheels in positive phase initially, then in negative phase thus reducing the turning circle to match that of a 2WS vehicle. However, Velardocchia et al. [57] state that the turning circle of a vehicle can be reduced by around 15% when using 4WS, with the rear wheels again steered in negative phase. The control law manages to stabilise the vehicle through steering the rear wheels by as little as 2 degrees. However, like many other studies, the control law is dependent on the available road friction coefficient.

1.2.4 Modelling

Vehicle models and tyre models must capture the essential dynamics and reflect reality. The operating point of the vehicle and the tyres determine the effectiveness of any control system. Both linear and nonlinear models are commonly used. However, linear models are well suited for controller design, while nonlinear models are more often used to verify the controllers and evaluate them. The linear models have a limited operating range due to the assumptions that are made when they are designed, and allow linear control design and analysis tools to be used. On the other hand, nonlinear models tend to have a much larger operating region, which makes them very desirable for evaluating the controllers.

Vehicle modelling

Vehicle modelling describes modelling the dynamic behaviour of the vehicle. If the model is to be used for controller design purposes, it must be both accurate and adequately represent the necessary dynamics. One common observation which has been noted is that large braking or accelerating force inputs can greatly affect the vehicle speed. Generally this will not have an adverse effect on nonlinear models, but could possibly have disastrous effects on linear models. For example, the linear models with small angle approximations will tend to operate outside of their equilibrium point. In other words, linear models have a limited validity range due to the assumptions made, whereas non-linear models are valid over a wider range of conditions. It is further observed from the available literature, that controller performance will be limited by the assumptions made at the time of constructing the model. An example of this can be seen in [26] where various approaches are compared.

Linear modelling

For brake only control, linear two degree of freedom (dof) vehicle models are a popular choice [20, 21, 36], with yaw rate and either lateral velocity or sideslip angle as the other state.

Assumptions are normally made to keep the linear models as simple as possible, although the model must remain representative of the actual plant. The assumptions include both constant vehicle velocity and that all angles are small. These angles include steering angle and slip angle. The bicycle model, for example, is dependent on velocity, so assuming this remains constant simplifies the equations greatly. Hac et al. use a 3 dof linear vehicle model, but finds it adequate to ignore the effects of the vertical dynamics to generate two dimensional mapping [45]. Carlson [58] on the other hand, linearises a nonlinear vehicle model for the controller design, with yaw angle and longitudinal tyre forces as the model inputs, to enable yaw rate and roll angle to be controlled.

Nonlinear modelling

To the other extreme, Jang [15] uses an 8 dof highly nonlinear model for both design and simulation, while Drakunov [24] uses a nonlinear vehicle and tyre model for controller design. Under heavy braking and acceleration, the pitch angle of the vehicle can change significantly and as such Salman [37] includes the effect of vertical dynamics into a nonlinear 3 dof model for 4WS and braking control.

When considering severe driving conditions, a linear vehicle model is not entirely appropriate, and Nagai et al. [35] devise a nonlinear model which includes load transfer from braking and sidewinds, which is in sharp contrast to He et al. [41] who use a linear two dof model to design the required controllers to regulate yaw rate and sideslip angle, for severe driving situations. Burgio [36] too uses a nonlinear tyre model dependent upon vertical forces, friction co-efficient and longitudinal slip. A control law is derived from this tyre model, based on the assumption that the lateral front tyre force is a direct actuation and inverting it to compute the steering law.

Hauksdottir considers nonlinear control methods for a vehicle on dry roads under non-emergency conditions [59]. In this study, a nonlinear approach is followed because their

linearised model is only valid for a small range of operating points, whereas the nonlinear model is valid for a wide range of operating points, including extreme nonlinear behaviour. The nonlinearities in the model occur when the longitudinal dynamics are described in terms of vehicle velocity, dependent on the throttle position.

Vehicle models can be separated into single track (or bicycle model) and two track model, where the latter is an extension of the simplified single track. The single track model has the two front wheels lumped together and the two rear wheels also, leading to one front and one rear wheel in line with the vehicle centre of gravity (CG). Steering inputs are usually associated with this model, but due to the assumptions of the lumped wheels, differential style braking cannot be simulated. Therefore, the two track model can be used. This two track model is the simplest model that can accommodate both steering and braking together [42]. In [42] the bicycle model is used for the front wheel steering controller, while a linearised two track model with individual wheel braking is adopted for brake controller design.

Tyre modelling

The tyre dynamics must be considered in some capacity within the vehicle model, since the tyres are the only contact that the vehicle has with the road surface. Furthermore, it is the tyres that are responsible for generating the forces which act on the vehicle chassis. Their complexity must also reflect the operating conditions of the controller. Generally, the tyres are complex and behave very nonlinear over their whole operating region, but can be described linearly for some part of the operating conditions (i.e for small lateral slip angles). The following three tyre models are most commonly used in the reviewed literature:

Linear Tyre Models which are based on linearisation of the tyre forces, assuming all angles are small (i.e δ,α).

Pacejka Magic Formula Tyre Model [1] which is a nonlinear empirical tyre model, that can be easily parameterised.

Dugoff Tyre Model [60] which is a nonlinear tyre model.

A number of authors use the linear model (e.g. [15, 21]), with the rest split between the latter two models. Finally, some authors use an 'in-house' tyre model, designed to their

specific needs [24].

The linear tyre model, is used mainly for small input approximations (for example, small angle inputs or alternatively, small inputs which would result in small angles, like yaw angle, sideslip angle etc). The linear model is commonly used for controller design purposes, mainly because the whole design process can become greatly simplified. Also, using linear models allows linear design and analysis techniques to be used, which may otherwise be inappropriate. However, this tyre model is no longer valid once it is operating outside of its region of validity, and this must be considered.

The Dugoff tyre model is used by Zhao for controller design [29], to control vehicle lateral velocity and yaw rate using differential braking. Pilutti et al. [20] use a nonlinear tyre model for their controller design, and also carry out a further study to find the optimal operating region of their Brake Steer System using a Pacejka tyre model.

The Pacejka tyre model is commonly used because it can be easily parameterised. In this model, the lateral and longitudinal tyre forces can be defined as a function of their respective slip parameter. Combined slip can also be built into the model, making it very flexible. Sharp et al. present a method of obtaining the tyre curve from very limited data sets [61].

Salman [37] relies on a polynomial based tyre model in his work [40, 62], and the same tyre model is used in later work, when front wheel steering is used instead of 4WS. In both cases, 4 wheel braking is included. The importance of the tyre model is highlighted by Burgio et al. [36] who use a nonlinear tyre model in a relatively simple 2 dof vehicle model.

Many studies use nonlinear models, and some can be found in [31, 35–37, 40, 49]. In the area of integrated steering and braking control, fewer studies are carried out using linear models, but examples can be found in [41, 45].

1.2.5 Parameter and state estimation

Many of the signals used in automotive control systems are measurable on the vehicle, and the CAN network is often used to transmit these signals throughout the car. These include accelerations, steer angles, wheel speeds, yaw rate and brake pressures to name a few. However, not all desired signals can be measured but instead need to be estimated. External parameters often fall into this category. Sideslip angle and the road friction co-efficient are

estimated since they are not straightforward to measure, but some signals which are straightforward to measure are also estimated in an attempt to minimise the number of onboard sensors. This section introduces possible methods of estimating various parameters.

Sideslip angle estimation

Many studies described thus far choose to control vehicle sideslip angle. Generally, this is not a signal which can be measured directly but is instead usually estimated (conventionally through using a tyre model [63] or a suitable vehicle model [31]). However, Klier et al. [64] propose a method which does not use vehicle models nor tyre friction models. Instead, the lateral and longitudinal directional components of a commercial Domain Control Unit (DCU) with integrated inertial sensors for the vehicle body are used to estimate it. The estimation is however, based on multiple signals - three angular rates, three translational accelerations, four road wheel velocities and steering wheel angle and use a Kalman filter to provide the required robustness.

Other methods of estimating sideslip are also possible. One method is to use an observer, together with a gyro and knowledge of the vehicle model, while another is to integrate the two required directional accelerations to obtain velocities [45, 65]. However, with these methods, problems may occur from inaccurate vehicle models, or integrator drift to name a few. It would be desirable to avoid these issues and offer a more reliable source for estimation. Daily et al. present a method of achieving this using Global Positioning Systems (GPS) [66]. GPS systems eliminate the need to estimate sideslip since the necessary velocities can be measured directly and very accurately using the Doppler shift of the GPS carrier wave, or the phase difference between two consecutive samples. Using this method, the calculated velocity has a typical accuracy of 5 cm/s [67]. However, latency can have an effect, and must be taken into account. Racelogic [68] have further improved technology and offer more accurate GPS based velocity measurements, while a number of patents have been filed for calculating sideslip angle from GPS signals (e.g. [69]).

Another possibility to estimate sideslip angle is using a pseudo integral, which offers robustness against variations in road friction [70]. However, one potential draw back of this method is the possibility of increasing integral error. To try and avoid this, Nishio et al. use look up tables prepared offline for different friction surfaces depending on the lateral

acceleration of the vehicle [70]. However, these too have limitations, for example, they will be invalid if vehicle spin out were to occur.

These studies so far only consider a constant vertical plane. Therefore, any change in pitch or roll would affect the accuracy of the sideslip estimate. To overcome this problem, Fukada considers roll bank angle, road surface change, sensor errors and brake force effect when estimating sideslip angle [30]. Crucially, only four sensors are used in this estimation; yaw rate, lateral acceleration, steering wheel angle and vehicle speed.

Friction coefficient estimation

The friction coefficient of the surface that the vehicle travels on is very important to the performance of dynamic control systems. It cannot be measured directly, but if it can be accurately estimated then the majority of the available control systems could function better.

Fukada estimates sideslip angle [30], and the estimator is dependant upon the road friction coefficient, μ, which is acknowledged to be very difficult to measure in practice. In this case, the minimum friction co-efficient is set as the detected value of acceleration. Further work has been undertaken by Müller et al. to estimate the maximum tyre-road friction co-efficient during braking [71]. When braking only one wheel, the other wheels can be reliably used for vehicle velocity measurement. Wheel slip, normal force and tractive force estimates are all combined to estimate whether the coefficient is one of two levels (0.6 or 1.0). However, a misclassification of 20% results from significant noise in the slip measurements and μ-estimation, indicating that further refinements are needed.

On the other hand, Mando's ESP system uses look-up tables for the vehicle reference model, and wheel slip is monitored and limited using a solenoid valve to vary brake pressure [11]. There is a dependency on the friction coefficient. To overcome this, it is estimated immediately as the manoeuvre starts using a reference model and the measured yaw rate of the vehicle.

Vehicle velocity estimation

In 2 wheel drive (2WD) vehicles, the velocity is usually taken from one of the free rolling wheels, and accelerations may be incorporated in the velocity calculation. The driven wheels cannot be used for reliable measurements since wheel slip is likely to occur during acceleration

and braking. All Wheel Drive (AWD) vehicles present further problems when trying to measure vehicle velocity. Due to wheel slip, reliable measurements cannot be made using engine driven wheels, which is in theory every wheel. To overcome this, Kobayashi et al. [72] combine a fuzzy based Kalman Filter together with an accelerometer and four wheel speeds to estimate the vehicle velocity.

However, Jiang et al. [73] use only wheel speed sensors for the estimation. Adaptive filtering [74] is employed together with the assumption that a braking vehicle will not travel faster than its wheels, and field test data shows that the estimation is both smooth and representative of the actual data. However, the assumption made is only valid when no wheel lock is present, otherwise the vehicle will travel much faster.

However, some authors have noted that Kalman filters are not practical for use in test vehicles where real time applications are required. Imsland et al. in particular [75] suggest using nonlinear observers which combine longitudinal and lateral accelerations, yaw rate, steering angle and the four wheel speeds. Lateral and longitudinal velocities are estimated very accurately on high friction surfaces, but less so on low friction due to large wheel slip values. This work assumes that the friction coefficient is known. However, Grip et al. evolve the observer and parameterise it to allow different friction coefficients to be accommodated [76].

Kalman filters

Kalman filters are very popular for state estimation, with good, accurate results achievable. Best et al. [77] considers three accelerometers combined with Extended Adaptive Kalman Filter (EAKF) theory to estimate the adaptive vehicle states. Adapting the values of tyre stiffness based on the longitudinal acceleration produces good results. Results show that the EAKF design is an improvement on the standard linear Kalman Filter design, and suggest that improvements may arise from the use of a nonlinear tyre model.

Indeed, this work is continued using a low order bicycle model combined with nonlinear tyre characteristics [78]. Within this work, two shape factors of the Pacejka tyre model are adapted in real time to maintain reliable and accurate information about the tyre forces. While results look favourable for the state and parameter estimation, the authors note that caution is required when deciding what parameters are to be estimated online, else errors may occur.

Many other works use Kalman filters for parameter and state estimation [64,71,77,79–83], mainly to reduce the number of required sensors.

An intuitive concept is employed by Yu et al. in an active suspension system [79] to reduce the number of sensors using Kalman filters, through correlating the front and rear wheel road inputs (i.e. wheelbase preview information). This effectively provides the active suspension's rear actuator with feedforward information, although this concept does have limitations when the vehicle velocity is greater than 15 m/s when the time frame becomes too small for it to function accurately.

Venhovens et al. use Kalman filters in many of their advanced control systems [81], including some of their previous work dating to the mid 1990's [82, 83]. Examples include their Adaptive Cruise Control (ACC) and lane keeping support, together with estimating vehicle yaw rate and tyre slip angles using only four ABS wheel speed sensors.

Hac et al. [84] choose to avoid using Kalman filters, and are also able to estimate the yaw rate using fewer sensors than Imsland (who also avoids Kalman filters); with only steering wheel angle, wheels speeds and lateral acceleration. Two yaw rate estimates are generated from the latter two sensors, and a confidence level is associated with the quality of the estimates. In total, yaw rate, lateral velocity and sideslip angle are all estimated. The observer used in this work, relies upon the friction co-efficient, which is estimated primarily from the lateral acceleration. Like Fukada [30], Hac et al. realise that the lateral acceleration has to be corrected for roll and bank angle before it can be used to estimate the road friction coefficient.

Estimation to reduce the vehicle sensor set

Although the majority of signals can be measured directly in the vehicle, some are often estimated to reduce the number of onboard sensors. This is more applicable to production vehicles than 'one-off' research or prototype vehicles. Accurate and reliable estimation of signals helps to keep production costs down. Lateral velocity is one of these signals, which Cherouat et al. choose to estimate from vehicle velocities and accelerations. This is achieved using an observer which the controllers are dependent upon when regulating vehicle yaw rate, lateral velocity and longitudinal velocity [85].

Generally, it is noticeable that both parameter and state estimation play a very important

role in vehicle dynamics control. The use of estimators has great benefits, however, the method of estimation is also important, and the requirements of the application should be considered.

1.2.6 Integrating novel approaches with existing technology

Integrating subsystems which are already available on production vehicles with new control systems is another possible method to improve vehicle stability [15, 20, 24, 86]. This also helps to reduce both production costs and subsystem integration problems at a later stage (i.e designing subsystems to work together, rather than integrating stand alone systems). One example of this might be using Anti-Lock Braking Systems (ABS) or Traction Control Systems (TCS) to avoid excessive wheel slip when additional longitudinal forces from new stability controllers are exerted on the wheels, thus helping to reduce the uncertainty of the frictional forces at the road/tyre interface. Jang et al. [15] and Drakunov [24] both make use of these systems, with Jang using a PID controller to modify the ABS forces to control yaw rate, while Drakunov expands current ABS and Traction Control System (TCS) technology, also to control a yawing vehicle.

ABS/TCS systems are frequently used in conjunction with new control systems, and Kim et al. combine them with ESP to work under emergency conditions only [11]. Morgando adopts a different approach, and combines previous feedback control with some additional control to improve ESP performance [12]. Also different is the fact that both wheels on the same side of the vehicle are braked, and this braking command is based on the steering input. The work is tested on hardware setup to verify the control design [19].

Also using ABS signals, BMW developed both Cornering Brake Control (CBC), which is designed to correct a yawing vehicle whilst braking and cornering simultaneously, and Dynamic Stability Control (DSC), developed from a combination of existing control systems [86]. These two systems work in the same principle as ESP. Leffler accepts that this approach of subsystems is the way forward, and will probably lead to a new design approach, where one overall system will suffice. Presumably condensing multiple subsystems will also lead to a single actuator set.

Finally, in an attempt to test the usefulness of integrating new and previous subsystems, Mokhiamar investigates three different control combinations: DYC & Rear Wheel Steering

(RWS), DYC & Front Wheel Steering (FWS), DYC & 4WS [63]. Available results show that DYC & 4WS has the best performance due to a balanced use of front and rear tyre forces, which can maximise the yaw rate whilst minimising sideslip angle.

1.2.7 Other applications

There are other areas of research which use the same actuator set as will be considered in this thesis, or alternatively different actuator sets are used to control the same lateral dynamics. They will be briefly mentioned in this section and include rollover avoidance together with engine and driveline control.

Rollover avoidance

Rollover is classed in the area of vertical dynamics. It can be described by the tendency of the vehicle wheels to lift off the ground, and is common while cornering where the inner wheels are more lightly loaded. The vehicle mass and centre of gravity contribute greatly to the problem. However, both of these are difficult to determine in practice.

For this reason, Huh et al. [87] estimate the vehicle mass three times, once for each axis of the vehicle (e.g longitudinal, lateral and vertical axes) using the respective dynamics, which are then combined to obtain the vehicle mass during manoeuvreing. This method explicitly avoids Kalman filters and a reliance upon specific driving situations, as seen in other studies (e.g. Rajamani et al. [88]).

However, rollover can be controlled using either steering control, individual wheel braking control, or a combination of both. For example, Model Predictive Control (MPC) combined with Inertial Navigation Systems (INS) and Global Positioning Systems (GPS) to measure yaw rate and sideslip angle enables both the peak roll angle of the vehicle to be limited while tracking the vehicle yaw rate using a combination of steering and differential braking [58].

Other combined steering and braking control studies include work by Odenthal et al. [89], who aims to avoid rollover using three nonlinear feedback control loops of continuous operation: steering control, emergency steering control and emergency braking control. In this case nonlinear control is considered due to the nonlinearities in the vertical dynamics.
An alternative method of dealing with the nonlinearities of vertical dynamics, would be to use multiple models and switch between them using some predefined criteria. This method

is used by Solmaz et al. who stress that multiple models are deemed to be more optimal than fixed controller gains set for the worst case scenario [90]. The multiple models infer the vehicle CG height and suspension parameters online. The inferred values are then used to switch one of a number of pre-tuned controllers, designed for a range of certain conditions.

A higher centre of gravity contributes greatly to vehicle rollover problems, and Akita et al. [56] note this in the control of Sport Utility Vehicles (SUV), which are higher than normal passenger vehicles and have both increased mass and higher payload capacity. When towing a trailer, vehicle stability becomes more critical and Akita et al. have developed a 4WS controller to maintain stability and improve manoeuvrability at low speeds. This is achieved using feedforward control based on model matching techniques, combined with a trial and error based H_∞ feedback controller.

Engine and driveline Control

Engine/driveline control is often combined with braking control. This prevents the two actuator sets trying to work against each other. It is this combination of braking and engine control that is the basis of standard DSC based functions.

The first BMW Dynamic Stability Control system was fitted to a BMW 850ci in 1992 [91]. It is a system which uses a steering sensor to determine the intended course of the driver, together with brake and engine control to avoid understeer and oversteer. In a similar system, engine control is combined with brake control in Mando's ESP system to limit the vehicle yaw rate [11].

Today's technology has permitted very advanced engine management systems, enabling the engine output to be constantly regulated for a variety of applications. Examples of this are Adaptive Cruise Control (ACC) and ESP. Most systems use some form of steering control combined with brake force control, and furthermore, a difference in braking/driving forces from one side of the vehicle to the other. There are however, some approaches in which the torque is controlled directly [92, 93].

When using Limited Slip Differentials (LSD) [94], the torque is transferred to the slower wheel, and therefore, although the direction of the torque cannot be controlled, it is possible to control its magnitude. To overcome this problem and allow the direction to be controlled, 'overdriven' differentials have been introduced into vehicles [95, 96]. These enable directional

yaw moment control, and Hancock et al. [92] use the overdriven differential to regulate sideslip angle and yaw rate, and then compare its performance to brake intervention based control. Differential control is less likely to saturate the tyres since two wheels generate the yaw moment, whereas for ESP type systems only one wheel is used.

It was seen in section 1.2.6 that previously available subsystems can be used in conjunction with new control systems to good effect (e.g using ABS to regulate demanded wheel forces from new control systems), and driveline control is no exception [92,97]. Post et al. combine driveline control with Electronic Stability Control, where the All Wheel Drive (AWD) active driveline allows continuously variable torque control while the system's actuators are the vehicle brakes and the throttle [97]. This integration results in less control authority at the brakes, yielding more consistent longitudinal momentum and less severe jerking motions.

It has been observed that actuation of the brakes when the vehicle is at its physical limits, can have a negative impact on the drivability of the vehicle [84,92,93,98]. Therefore, to avoid using braking control, active driveline control is integrated with active suspension control to improve vehicle dynamics.

1.2.8 Discussion

The literature discussed in this chapter gives a broad overview of the work which has been carried out in the area of lateral dynamics control, and briefly mentions other related work in vehicle dynamics control that can be achieved using the same actuator set. It can be seen that coordinated steering and braking control is a more active area of research than braking only control, where the additional actuator offers the ability to improve the control performance of vehicle lateral dynamics.

So far different approaches and considerations to vehicle lateral dynamics control have been discussed, and this will now be put into context with regards to the work of this thesis. Two sets of actuators are generally used for lateral dynamics control: vehicle braking and also front steering. These will now be summarised in turn.

To ensure stability of the vehicle, it is important to regulate vehicle sideslip angle in addition to vehicle yaw rate [26, 63, 66]. Section 1.2.1 emphasises that the use of braking only control has thus far, only been used to control yaw rate, with the exception of Yi [26], who controls yaw rate and sideslip angle simultaneously, and Zhao [29] who controls lateral

velocity and yaw rate together. Various methods of obtaining an accurate sideslip signal for use in dynamic control systems has been discussed, ranging from Kalman filter theory to using GPS signals. However, estimation of this signal is not considered in this work. Instead it is assumed to be known and available.

Many different control methods are used to control vehicle lateral dynamics, for example linear control methods such as pole placement [20], PID control [15], and linear inverse dynamics [21]. Both Fuzzy and Sliding Mode control are popular for automotive applications [24–26, 29, 31–33, 50], mainly due to their robustness properties and ability to handle uncertainties, while optimal control is also a active area [34, 37, 40].

Section 1.2.1 also shows that Brake Steer Systems can successfully generate a yaw moment on the vehicle, and it is not strictly necessary to use neither nonlinear models nor nonlinear control methods to obtain adequate controllers. Linear models appear to be adequate for operating conditions when vehicle speed does not change substantially. This means that large wheel forces which will change the vehicle speed should be avoided when linear models are used, else the models may become invalid. Several authors note that using ABS/TCS in conjunction with BSS can avoid wheel lock-up during acceleration or deceleration, when the wheel forces are instantaneously applied.

In contrast to brake only control, section 1.2.2 shows that most of the studies discussed choose to control two variables simultaneously, usually both sideslip angle and yaw rate, or lateral velocity and yaw rate. The extra actuator makes it more natural to achieve the simultaneous control task. Feedforward based steering is used in conjunction with feedback braking in many studies with good success(for example [35, 66, 99]). Lateral dynamics are controlled simultaneously n all three of these studies, with both sideslip angle and yaw rate being the popular choice.

By reviewing the literature, it can be seen that nonlinear models are more widely used for simulation than linear models, when modelling both the vehicle and tyres. Yet even within the integrated control section, it is interesting to see that many vehicle models with differing levels of sophistication are used for designing similar performing controllers. With the integrated control, it is noted by He et al. that designing controllers individually is feasible, but thought must be given to ensure that they are integrated effectively to achieve good performance [41].

The generation of appropriate reference signals is important, and the majority of studies generate the yaw rate reference from the driver steering wheel input. Ahmadi [32] derives the yaw rate reference from the steering command of a single track model for steady state cornering [100]. Nagai et al. [35] sets the sideslip angle reference to zero — a value which is achievable using active rear steering. Boada follows the same approach [31].

Accurate parameter estimation is very important to be able to generate the signals required for the control laws. It was shown that GPS and INS systems can be a good source for measuring sideslip, which otherwise needs to be estimated. An increase in the accuracy of these navigation systems could help to improve vehicle stability. However, within this thesis, both the friction co-efficient and sideslip angle are assumed to be both known and available.

The concept of SbW has led to the introduction of approaches for 4WS vehicles and AFS, which is seen by many as the ideal way to control the lateral dynamics of a vehicle [29, 35]. 4WS enables simultaneous control of sideslip and yaw rate with the advantage of only slightly decreasing the vehicle speed, which cannot be achieved when using FWS only. The extra actuator in terms of the rear wheel steering allows a sum and difference concept to be applied to control the vehicle. However, four-wheel steering is not a practical solution at present. Therefore, there is a clear advantage to being able to control the lateral dynamics using only brakes or integrated brakes and front-wheel steering, and obtaining results which are similar to that of four wheel steering control. The prospect of SbW has given researchers the opportunity to study new applications of vehicle dynamics control.

Active front steering (AFS) can generate a variable steering ratio which provides low speed manoeuvrability and high speed stability. Unlike the other systems mentioned, AFS can generate yaw torques at low speeds, however, both front and rear steering can saturate the tyres, causing stability problems.

Four main actuator sets are used to control vehicle lateral dynamic performance in current literature. These are

- *Brakes*: where a yaw moment is generated by differential application of the brakes.
- *Active suspension*: where a yaw moment is generated by changing the handling balance of the vehicle.
- *Electronically controlled drivelines*: where drive torque is controlled across and between

axles.

- *Active front/rear steering*: where front and/or rear steering angles are generated to control vehicle dynamics.

It has been discussed that using the braking system to stabilise the vehicle will remove energy from the system. The effect of this is a reduction in the vehicle speed, which may be desirable in some instances. This reduction in speed is less evident as a result of using the other three control methods above. Using the brakes can increase safety but may be intrusive to the driver. The braking system is very able in generating understeer, and can generate oversteer with assistance from some form of engine management which manipulates the driveline on rear wheel drive vehicles.

Several points can be made when summarising the current state of the art. Braking control is popular both on its own and in conjunction with steering actuation, and the popularity is not restricted to lateral dynamics control, with longitudinal wheel forces commonly used to achieve close control. However, uncertainties are usually present in the control loop, ranging from vehicle uncertainties such as mass and centre of gravity to external parameters such as road surface friction coefficient. With these uncertainties, fuzzy control and sliding mode control are both popular choices with researchers. However, PID control also seems to be desirable, presumably due to the ease of fine tuning that is possible on-site.

In terms of vehicle modelling, linear models are popular for controller design tasks and they are normally simplified with approximations to allow the design to take place. Once the controllers are ready for evaluation and testing, they are generally implemented into detailed nonlinear models, which usually accurately represent the vehicle over a wider operating window.

Finally, human in the loop, or even hardware in the loop testing is rare in current literature. Instead, most works rely purely on vehicle model simulation or implementation in an actual test vehicle. Obviously the latter option is better, but it is a luxury that few can afford. Therefore, perhaps a test rig or hardware in the loop rig is a good approach.

From the review of current literature, there are some open issues which, in my opinion, could be addressed. The first issue is to asses why wheel forces have been used very sparingly to simultaneously control vehicle lateral dynamics. The second issue is to asses why frequency

based design and analysis techniques have not been used thus far in this area of vehicle dynamics control. The driver assist system is very different from a stability control system, in that the latter is designed to optimise the vehicle performance, so that steerability and stability are not lost. Therefore, the third issue is to develop a linear model to accomodate the operating conditions of the system, which in turn will justify the choice of control design techniques. Finally, the lack of HIL testing is intriguing. Indeed, this absence highlights an opportunity that exists within this work to use hardware in the loop in the form of a human interface test rig. However, for this to be achieved, a vehicle model must be available which is suitable for real time applications. This model will be integrated with a real-time steering rig, to allow human inputs to be applied to the control loop. To enable this to be effective, a real time visualisation to run within Matlab will be introduced.

1.3 Aims and objectives

The main aim of this work is to control lateral dynamics primarily using the longitudinal wheel forces. As such, the work contained within this thesis will look at simultaneously controlling vehicle sideslip and yaw rate using these wheel forces in a feedback control structure. Only in [26, 29] has sideslip angle and yaw rate been simultaneously controlled, with many others only controlling yaw rate. Therefore, it seems that there is an opportunity to use the vehicle longitudinal wheel forces to improve vehicle dynamic behaviour.

This work will then focus on integrating front steering input with the original feedback control structure, in an attempt to achieve enhanced performance. Finally, the control structures will be implemented with a steering test rig to evaluate what impact realistic human inputs have on the controllers and the desired trajectories using a visual feedback environment.

The three test manoeuvres to be used are constant yaw rate, a gentle lane change and a sidewind disturbance acting on the vehicle. All of these manoeuvres are not aggressive, and do not excite the physical limits of the vehicle. This indicates that the inputs to the vehicle model will remain small in magnitude, allowing assumptions to be made with regards to the choice of vehicle model for this task.

The following objectives can be drawn up to realise the above aims.

- The development of a vehicle model which is suitable for controller design will be carried out.
- The linear vehicle model will be used to design and analyse a two-channel feedback controller using frequency based techniques.
- The feedback controller will then be integrated with a front wheel steering input, and any improvement in the system performance will be evaluated.
- Specific manoeuvres designed to test the controller will be implemented, and the controller will be evaluated in a highly complex, nonlinear vehicle model which has been benchmarked against a production vehicle.
- Finally, the controller will be integrated with a human interface test rig with visual feedback of the vehicle trajectory in real-time, and evaluated. This will enable the effect of a human in the loop to be analysed. The human operator of the test rig will attempt to complete the same manoeuvres as the vehicle simulations, but in real-time.

1.4 Contributions of thesis

This thesis offers the following contributions to the field of vehicle lateral dynamics control:

1. Frequency design techniques are used to develop a novel feedback controller for longitudinal wheel forces, which is then combined with steering control to simultaneously regulate yaw rate and sideslip angle.
2. The controller structure has been integrated into a test rig setup where driver input is included in a real-time environment of both controller and simulation. The performance of the controllers in this setup is analysed and discussed.

The following two publications have resulted from this work.

1. Bevan, G. P., O'Neill, S. J., Gollee, H. & O'Reilly, J. (2007), 'Performance comparison of collision avoidance controller designs', in 2007 IEEE Intelligent Vehicles Symposium IEE (2007), pp. 468-473. [101]

2. O'Neill, Gollee, and O'Reilly. 'Control of Lateral Vehicle Dynamics Using Partial Pole Placement'. UKACC International Control Conference / EPSRC graduate workshop, Glasgow, August 2006.

1.5 Outline

The remaining chapters of this thesis are structured as follows. Chapter 2 introduces vehicle dynamics and the relevant axis systems. Modelling assumptions are made, which result in the design of a simplified linear vehicle model. In this section two nonlinear models of different complexities are presented for controller evaluation purposes. Chapter 3 introduces the principles behind frequency based design methods, which are then used to design and analyse the necessary feedback controller. Later in that chapter, a control structure is set in place to enable the feedback controller to be integrated with steering actuation, generated automatically from the reference yaw rate signal. A human interface test rig is presented in chapter 4.

The feedback controller is implemented within a highly nonlinear vehicle model in chapter 5 for evaluation purposes. Using repeatable test manoeuvres, the results are evaluated and discussed. The human interface test rig is used with visual feedback to the driver to complete the same test manoeuvres in chapter 6, with the addition of some extra tests. Finally, conclusions are drawn from the work and some suggestions on how the work could develop in the future are presented in chapter 7.

Chapter 2

Vehicle modelling

It is apparent that the design of control systems is highly dependent on the availability of an appropriate model. For the model to be suitable for controller design, it should accurately represent the important dynamics of the system. This chapter provides some background to the modelling of vehicle dynamics focusing on tyre modelling and chassis modelling. Three vehicle models will be introduced: firstly, a linear model which will be used solely for controller design purposes, followed by two nonlinear models for simulating and evaluating the designed controllers. Both of these nonlinear models have different levels of complexity, which for reasons described later, will enable one model to be used as a real-time simulation model (RTSM), and the other as a verified simulation model (VSM). Step inputs will be applied to all three models, evaluating them and ensuring that they all accurately represent the relevant dynamic behaviour.

Although vertical dynamics are present in both nonlinear models to allow them to resemble a real/production vehicle more accurately, only longitudinal and lateral motions will be considered in this work and the controller design vehicle model will represent this. Therefore, vertical dynamics/movement will be excluded.

In general, tyre modelling involves understanding the forces which act at the tyre-road interface, while chassis modelling involves understanding the effects that these tyre forces have on the chassis.

2.1 Vehicle coordinate systems

The axis system used within this work is adopted from Kiencke and Nielsen [102]. The positive direction of the three axis (x,y,z) is forward, leftward and upward respectively. This system conflicts with that of Milliken et al. [103] and Gillespie [100], who choose forward, rightward and downward as the positive directions.

Figure 2.1 shows the earth fixed coordinate system (X_o, Y_o) together with the centre of gravity coordinate (CG) system (X_{CG}, Y_{CG}). The earth fixed coordinate system is fixed to one arbitrary defined set of coordinates and does not travel with the vehicle. It is apparent, therefore, that a relationship should exist between the vehicle and the earth fixed coordinate system, else the vehicle's position could not be determined. The centre of gravity axis system travels with the vehicle and is also known as the vehicle body axis system. This is related to the earth fixed system via a rotation of the vehicle yaw angle, ψ, and translated by X and Y. It should be noted that this rotation of ψ is in the horizontal plane, and will suffice only for longitudinal and lateral motion.

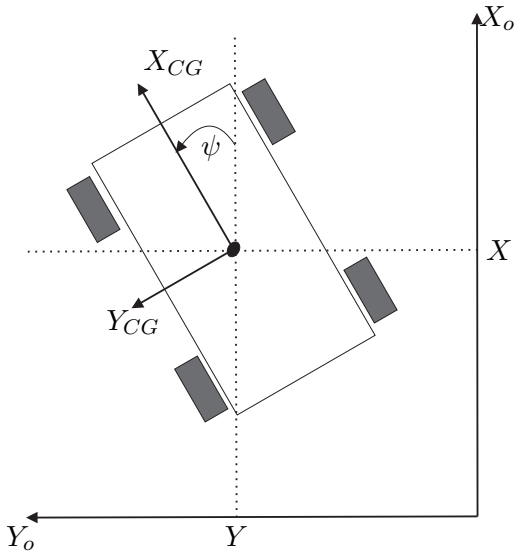

Figure 2.1: Earth fixed and CG coordinate systems

The wheel coordinate system is another coordinate system to exist on a vehicle. Each wheel can be assigned its own coordinate system, and each system moves with the wheel it represents. Importantly, it is orientated in the same manner as the two previously mentioned systems (using the right hand rule) and each wheel is given a subscript, i, as defined in table 2.1.

i	Wheel
1	Front left
2	Front right
3	Rear left
4	Rear right

Table 2.1: Wheel subscript system in use

The road wheels steer through an angle of δ_f for the front wheels ($i = 1, 2$) and δ_r for the rear wheels ($i = 3, 4$), which is measured as the angle between the x axis of the vehicle and the x axis of the tyre, as shown in figure 2.2.

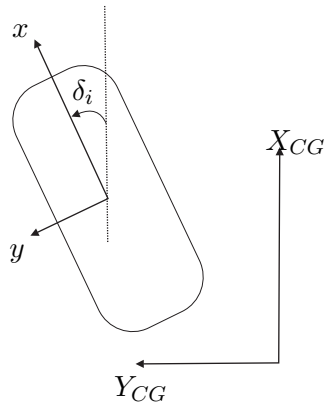

Figure 2.2: Definition of road wheel angle, δ_i

2.2 Tyre modelling

Under normal situations, the tyres are the only source of contact a car should have with the road. Each tyre has a contact patch with the ground, the size of which is generally no larger than the palm of a human hand. Therefore, it is critical to understand the way these forces behave; what influences them and what dynamics they in turn can influence. After all, it is these forces that can be used to alter the behaviour of the vehicle.

The tyre forces rely mainly on the friction coefficient of the road surface (μ) that the vehicle is travelling on. It was seen in section 1.2.5 that work has been carried out estimating this variable in an attempt to improve the performance of vehicle dynamics controllers. The friction coefficient greatly affects the amount of acceleration, a, available to the vehicle, which can be calculated as

$$a = \mu\, g, \tag{2.1}$$

where g is the acceleration due to gravity. The maximum available frictional force for each wheel, in any direction, is equivalent to

$$f_{max,i} = \mu\, f_z, \tag{2.2}$$

where f_z is the vertical load acting on the wheel (approximately one quarter of the vehicle mass). In theory the maximum force in any direction, $f_{max,i}$, represents a friction circle, but in practice the tread pattern and the profile of the tyre will vary the lateral and longitudinal components of friction coefficient, which in turn will effect the forces in equation (2.2). This results in generally larger forces in the longitudinal direction, hence the elliptical shape, outlined by the dashed line in figure 2.3.

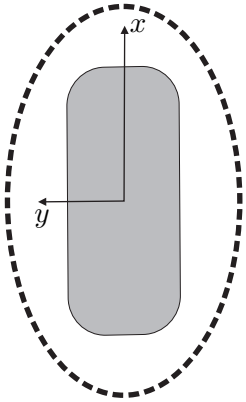

Figure 2.3: The friction ellipse for a single wheel

The friction coefficient is, in practice, very difficult to measure. Given what is mentioned above, the maximum available force at any wheel will vary greatly depending on the surface the vehicle is travelling on. Various different surfaces and their friction coefficients are listed in table 2.2. This table shows similarities between dry asphalt and dry cobblestones, however, when they become wet the friction characteristics of the two surfaces change dramatically. This phenomenon contributes greatly to vehicle dynamics control problems.

Road surface	Friction coefficient
Asphalt, dry	1.2
Asphalt, wet	0.85
Cobblestones, dry	1.2
Cobblestones, wet	0.4
Snow	0.2
Ice	0.05

Table 2.2: Road surface friction coefficient values

2.2.1 Wheel slip

When a vehicle is steered, the tyre does not turn instantaneously to the desired direction. Instead it 'scrubs' along the ground, generating an angle between the direction the tyre is heading and the direction in which it is travelling. This angle is known as *wheel slip angle* or *lateral wheel slip*. Lateral wheel slip, denoted by α, is depicted in figure 2.4 (a), and is calculated from

$$\tan(\alpha) = \frac{v_{y,i}}{v_{x,i}}, \tag{2.3}$$

where $v_{y,i}$ and $v_{x,i}$ are the lateral and longitudinal velocities of the tyre respectively.

As the wheel angle continues to increase, the deformation of the tyre also increases, resulting in lateral forces building up at the wheel. Initially, the slip angle and the lateral force increases rapidly in a linear fashion. The force then reaches its maximum value and starts to decrease as the frictional force acting against the tyre movement reaches its maximum. This behaviour can be described by the tyre curve, shown in figure 2.5 (a), for a μ value of 1.2 - representing a dry asphalt road.

One other slip quantity, *longitudinal slip*, denoted as λ, occurs when a torque (T_w) is applied to the wheel. In figure 2.4 (b), a driving torque is shown which is positive and accelerates the wheel, therefore a braking torque acting in the opposite direction will be negative. Essentially longitudinal slip is a measure of the difference in wheel speed to vehicle speed as the wheel deforms under load. λ can assume a value between $[-1; +1]$, where $\lambda = -1$ represents a spinning wheel with $v_x = 0$, $\omega > 0$, and $\lambda = +1$ represents a locked wheel with $v_x > 0$, $\omega = 0$. Longitudinal wheel slip is defined as

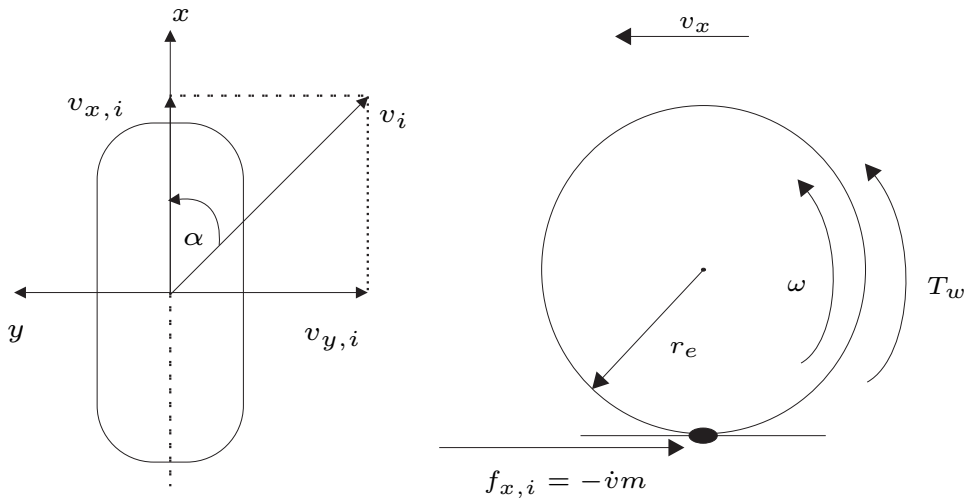

(a) lateral wheel dynamics (b) longitudinal wheel dynamics

Figure 2.4: Figures depicting the wheel dynamics for slip calculation

$$\lambda = \frac{v_x - \omega\, r_e}{\max(\omega\, r_e,\, v_x)}, \tag{2.4}$$

where v_x is the vehicle velocity and ω and r_e are the wheel rotational velocity and the effective wheel radius respectively. The effective radius is used, since the wheel changes shape and deforms under load. The force at the road/wheel interface is denoted by $f_{x,i}$. Typical longitudinal properties of the tyre are shown in figure 2.5 (b) for a range of the surfaces described in table 2.2. In this figure, a peak can again be seen for most values before the force drops off. This can be described in a similar manner to the lateral slip quantity, where the frictional force acting against the tyre reaches a maximum and is eventually overcome by the braking force of the wheel.

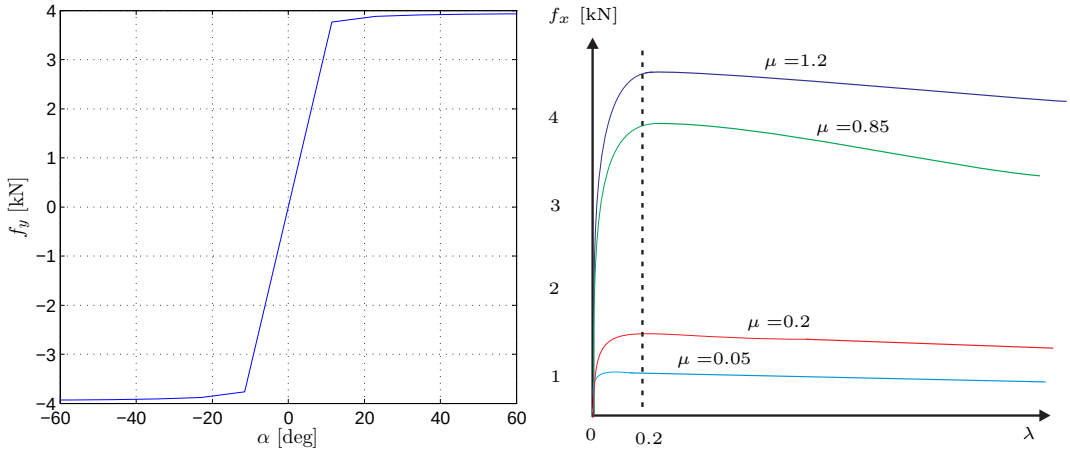

(a) Typical lateral properties of the tyre

(b) Typical longitudinal properties of the tyre

Figure 2.5: Figures showing typical tyre properties

2.2.2 Tyre models

Pacejka tyre model

From section 1.2, it was seen that Pacejka's 'Magic Formula' is a well known and often used tyre model [1]. This steady state empirical model describes the tyre forces as a function of the relevant slip parameter (i.e longitudinal force as a function of longitudinal slip, and lateral force as a function of lateral slip). Accepting the respective slip component as an input, the lateral or longitudinal tyre forces that would give rise to these slip values can be calculated. More accurately, the two forces (f_x and f_y) are a function of the camber angle, γ and the vertical load on the wheel, f_z.

The Magic Formula tyre model enables either combined slip or pure slip to be calculated. Pure slip is used most often and allows the forces to be calculated on the assumption that the other slip quantity is zero (e.g. longitudinal forces are calculated assuming lateral slip is zero, and vice versa). The force at the tyre which is a function of λ or α in the respective plane can be calculated by equations (2.5) and (2.6).

$$f_x(\lambda) = D_x \sin\left(C_x \arctan\left(B_x \lambda - E_x \left(B_x \lambda - \arctan\left(B_x \lambda\right)\right)\right)\right) \tag{2.5}$$

$$f_y(\alpha) = D_y \sin\left(C_y \arctan\left(B_y \alpha - E_y \left(B_y \alpha - \arctan\left(B_y \alpha\right)\right)\right)\right) \tag{2.6}$$

where the parameters B, C, D and E are tyre dependent and are described in table 2.3. They define the shape of the aforementioned tyre curves (see figure 2.5), allowing different tyre characteristics to be defined and modelled. These parameters are functions of friction coefficient of the road surface, camber angle of the wheel and the loading of the wheel. The parameters are generally not similar for both slip conditions. Some values are given in table 2.3 which define the shape of the lateral force vs slip tyre plot in figure 2.5(a).

Symbol	Description	Value for figure 2.5(a)
B	Stiffness Factor	15.0
C	Shape Factor	0.9
D	Peak Factor	1.0 [kN]
E	Curvature Factor	1.0

Table 2.3: Parameter definition for the Magic Formula [1]

Linearised tyre model

When introducing lateral slip, it was mentioned that the tyre forces behave initially linearly. This is typically until the slip angle, α, approaches approximately 15-20 degrees [100]. After this point, the tyre slip curve ($f_{y,i}$—α_i) reaches a peak, and the behaviour becomes nonlinear. Therefore, the possibility arises to simplify the tyre model, on the assumption that the slip angle will not exceed this peak value, but remain within the linear region.

During a turning manoeuvre, the lateral force (which is dependent on lateral slip) is the most critical quantity, since it is this force which enables the vehicle to turn. With this in mind, the lateral tyre force can be approximated to

$$f_{y,i} = C_{\alpha,i}\,\alpha_i\,, \tag{2.7}$$

where $C_{\alpha,i}$ is the cornering stiffness (or lateral tyre stiffness) of the respective wheel. The cornering stiffness can also be determined from the gradient of $f_{y,i}$—α_i curve (figure 2.5 (b)).

2.3 Chassis modelling

A brief overview of the different co-ordinate systems of a vehicle and the tyre properties has been given thus far. This information is now combined to present the equations that are used to determine how the tyre forces affect the vehicle behaviour.

All vehicle motion is given with reference to both the centre of gravity co-ordinates (X_{CG}, Y_{CG}), and the fixed inertial co-ordinates (X_o, Y_o). As mentioned previously, the origin of the CG co-ordinate system is at the centre of gravity of the vehicle body, whereas the fixed inertial system has an arbitrarily defined origin, and does not travel with the vehicle.

Firstly, the definition of vehicle sideslip angle will be presented. This will be followed by a brief introduction to the 'bicycle model', and then a description of the 'two-track model' which is used in the remaining sections of this work. In both models, vertical dynamics are ignored.

2.3.1 Vehicle sideslip angle

One of the control variables in this work is the vehicle sideslip angle, denoted by β. It is defined in the same manner as the tyre slip angle but in the vehicle body axis system, that is, the angle between the vehicle longitudinal axis and the velocity vector of the vehicle. The quantities v_x, v_y, v and β are shown in figure 2.6.

Therefore, the vehicle side slip angle can be calculated as

$$\beta = \arctan\left(\frac{v_y}{v_x}\right) \approx \left(\frac{v_y}{v_x}\right), \tag{2.8}$$

This equation shows that the sign of β will always have the same sign as the lateral velocity, v_y, as long as the vehicle is not reversing or stationary (i.e. $v_x > 0$). The approximation that has been made in equation (2.8) is only valid for small inputs that will result in v_y remaining small and for small changes in v_x.

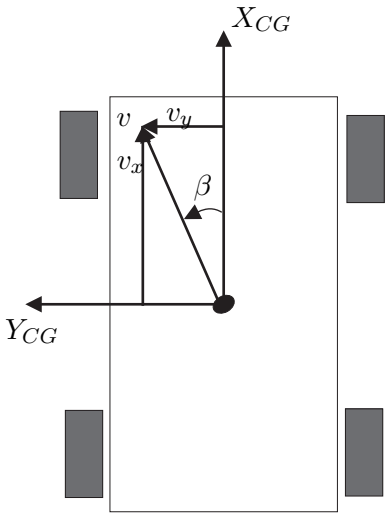

Figure 2.6: Definition of vehicle sideslip angle

2.3.2 Bicycle model

A bicycle model (or one track model) is the simplest adequate vehicle model. In this model description, the two front wheels are combined as are the two rear wheels, resulting in one wheel at the front axis and one wheel at the rear axis, both in line with the centre of the vehicle (see figure 2.7). The bicycle model incorporates two states; yaw rate ($\dot{\psi}$), and lateral velocity (v_y). The longitudinal velocity (v_x) is defined as constant for linearisation purposes, and the model input is the front steering angle (δ_f) - which is required to generate the lateral forces on the vehicle. Occasionally, rear wheel steering is also used as an input. The bicycle model is usually used only in conjunction with lateral dynamics. Brake inputs are not normally associated with this model, and with the small effect that the steering angle inputs will have on the velocity, it is justifiable to define v_x constant.

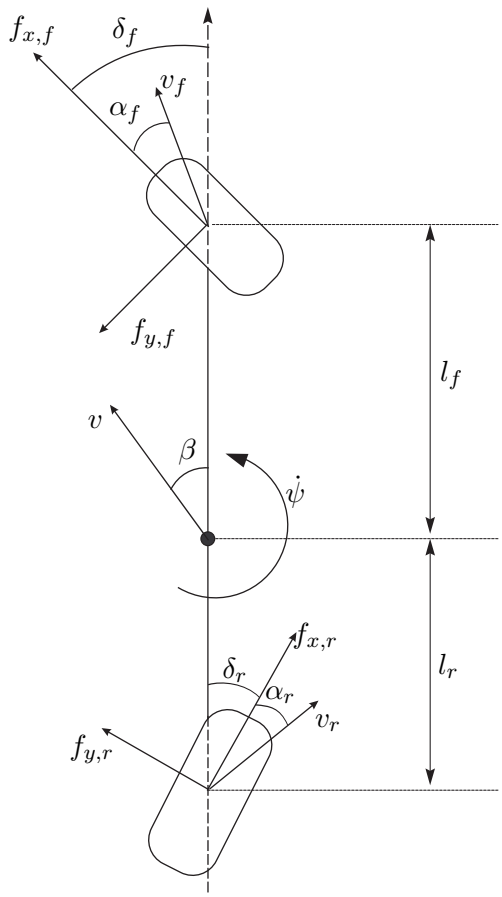

Figure 2.7: Diagram of a bicycle model

In figure 2.7, l_f and l_r define the distance from the centre of gravity to the front and rear wheels respectively. $f_{y,i}$ and $f_{x,i}$ are the lateral and longitudinal tyre forces at the respective wheels and β is the vehicle sideslip angle measured at the vehicle centre of gravity. α_i is the slip angle at the respective wheel and v_f, v_r is the velocity vector of the front and rear tyres. J_z is the vehicle moment of inertia.

Using these descriptions, the two state equations when derived from first principles are described as:

$$\dot{v_y} = \frac{1}{m}\left(-v_x\,\dot{\psi}\,m + f_{y,f} + f_{y,r}\right) \tag{2.9}$$

$$\ddot{\psi} = \frac{1}{J_z}\left(l_f\,f_{y,f} - l_r\,f_{y,r}\right). \tag{2.10}$$

2.3.3 Two track model

The two track model is an extension of the single track model. It has two axles and four wheels with a width w between the wheels of the same axle, (or alternatively $w/2$ distance from the centre of the wheel to the vehicle centre of gravity (CG)). From figure 2.8, the x and y directions can again be described as the longitudinal and lateral directions respectively. All other symbols are as defined for the bicycle model.

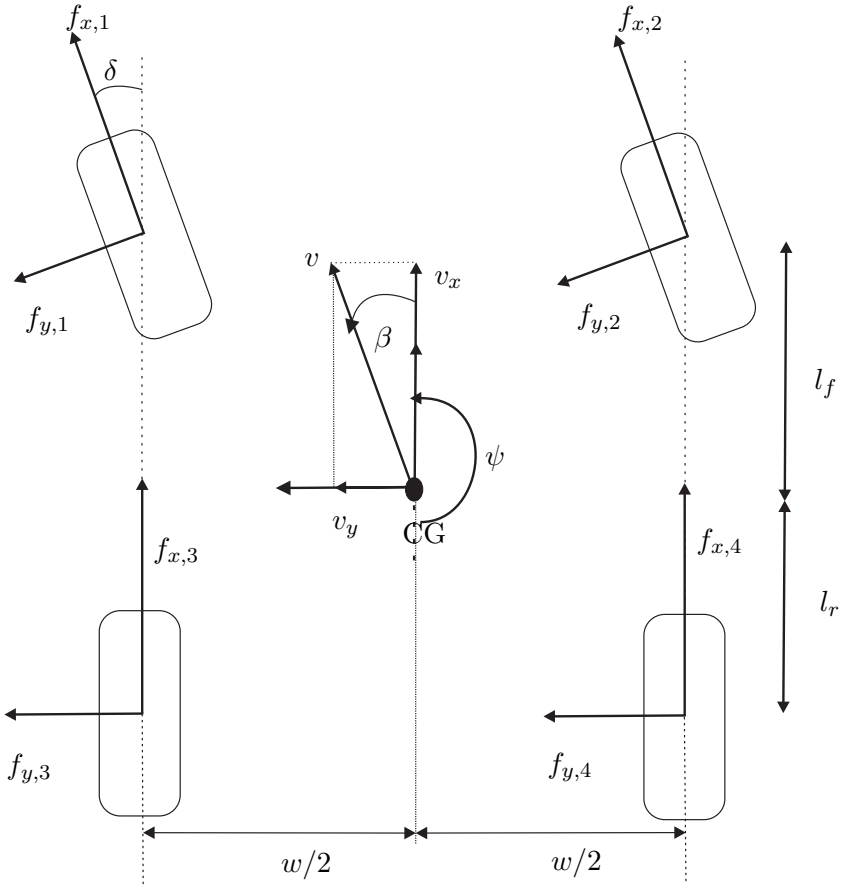

Figure 2.8: Two track vehicle model

For each of the four wheels in the two track model, the contribution of both longitudinal and lateral forces $f_{x,i}$ and $f_{y,i}$ (as shown in figure 2.8), can be translated into the vehicle axis system at the vehicle centre of gravity (CG), $F_{x,i}$ and $F_{y,i}$.

$$F_{x,i} = f_{x,i}\cos\delta_i - f_{y,i}\sin\delta_i \tag{2.11}$$

$$F_{y,i} = f_{x,i}\sin\delta_i + f_{y,i}\cos\delta_i. \tag{2.12}$$

To keep these expressions tidy, a *Rotation Matrix*, $\mathbf{D}(\delta_i)$ is introduced:

$$\mathbf{D}(\delta_i) = \begin{bmatrix} cos\delta_i & -\sin\delta_i \\ \sin\delta_i & \cos\delta_i \end{bmatrix} \tag{2.13}$$

and so,

$$\begin{bmatrix} F_{x,i} \\ F_{y,i} \end{bmatrix} = \mathbf{D}(\delta_i) \begin{bmatrix} f_{x,i} \\ f_{y,i} \end{bmatrix} \tag{2.14}$$

Applying Newton's second law of motion to the vehicle body, the following equations describe the forces at the vehicle centre of gravity in its own co-ordinate system.

$$m\left(\dot{v_x} - v_y\,\dot{\psi}\right) = \sum_{i=1}^{4} F_{x,i} \tag{2.15}$$

$$m\left(\dot{v_y} + v_x\,\dot{\psi}\right) = \sum_{i=1}^{4} F_{y,i} \tag{2.16}$$

Finally, the sum of the moments around the vehicle are equal to the moment around the centre of gravity,

$$J_z\,\ddot{\psi} = \sum_{i=1}^{4} M_{z,i}. \tag{2.17}$$

2.4 Vehicle models for use within thesis

In this section, three vehicle models which are used within this thesis are presented. Firstly, a linear model will be derived from basic principles and will be used in the controller design process. Next, a more complex nonlinear model will be introduced and will be integrated with the human interface test rig. This setup will allow us to evaluate human interaction with the controllers, and enable comparisons to be drawn between the automatic controllers and a human. Finally, a highly complex nonlinear model which has been validated against an actual passenger car will be presented. Comparisons will be made between all three models with regards to their limitations and complexity, and the differences between the two nonlinear

models in particular.

The vehicle to be modelled will be representative of a large passenger saloon car with rear wheel drive. As each of the three models are introduced, they will increase in complexity in both individual component level and subsystem integration/interaction.

2.4.1 Linear controller design model (LCDM)

Linear models are deemed desirable for controller design tasks, since tools have been made available to aid the controller design process which are unique to linear models. Therefore, this section will concentrate on deriving a linear vehicle model which accurately represents yaw rate and sideslip dynamics with respect to steering and wheel force inputs. The model derived in this section will be a linear, low complexity, three state model, containing both longitudinal and lateral dynamics, while ignoring vertical dynamics and any aerodynamics effects.

From section 1.2, it was seen that longitudinal velocity is often assumed to be constant when deriving vehicle models operating close to equilibrium (e.g. [26,99]). However, although in this model longitudinal velocity will be included as a state, the assumption that it remains constant around an equilibrium point will still be made.

The main assumptions made throughout are that the vehicle will operate close to equilibrium and the inputs/angles will be small, resulting in the tyres behaving in a linear manner. The main source of the nonlinearities are the angles which are related to trigonometric functions (i.e sine, cosine and tangent). Other assumptions which are made in this model, include that both the small steer angle and tyre slip angle have a negligible effect on the longitudinal tyre force. It is also assumed that the rear steering angle, δ_r, is zero throughout, and that both of the front wheels are steered to the same angle, δ_f.

The vehicle model is a three state, five input, three output model. The three states of this non-square model are the vehicle longitudinal velocity, v_x, vehicle lateral velocity, v_y and the vehicle yaw rate, $\dot{\psi}$. The five inputs are the front steer angle, δ_f and the four longitudinal tyre forces, $f_{x,1}$ to $f_{x,4}$, while the outputs are the three system states. This can be expressed in terms of state space modelling as

$$\dot{x} = f(x) + g(u) \tag{2.18}$$

$$y = x \tag{2.19}$$

$$x_0 = x(t = 0) \tag{2.20}$$

where x is a vector containing the system states, u is a vector containing the system inputs, y is the system outputs and x_0 are the initial conditions of the system. These can be expanded as

$$y = x = \begin{bmatrix} v_x \\ v_y \\ \dot{\psi} \end{bmatrix}$$

$$u = \begin{bmatrix} \delta_f \\ f_{x,1} \\ f_{x,2} \\ f_{x,3} \\ f_{x,4} \end{bmatrix}$$

$$x(t = 0) = \begin{bmatrix} v_{x0} \\ v_{y0} \\ \dot{\psi}_0 \end{bmatrix}$$

For linear systems, equations (2.18) to (2.20) can be expressed as

$$\dot{x} = A\,x + B\,u \tag{2.21}$$

$$y = x \tag{2.22}$$

$$x_0 = x(t = 0) \tag{2.23}$$

where A is the state matrix, and B is the input matrix and again, u are the system inputs,

y is the system outputs, x_0 are the initial conditions of the system.

The vehicle dynamic symbols in these expressions can be equated to the the diagram of the two track vehicle in figure 2.8.

Reminding ourselves of the control task — to simultaneously control vehicle yaw rate and vehicle sideslip angle using solely longitudinal wheel forces, and then integrated wheel force and steering control. This implies that expressions have to be formed that explicitly represent the yaw rate and sideslip angle dynamics with respect to steering angle and longitudinal wheel force inputs.

Therefore, looking firstly at the vehicle sideslip angle and in particular the expression for β in equation (2.8). It can be seen that changing either the lateral velocity or the longitudinal velocity, will result in a change in β. Furthermore, equation (2.8) can be obtained using two of the outputs of the state space model (v_y and v_x).

For this linear model derivation, it is assumed that the front steer angle δ_f is very small, so that the following approximations are valid

$$\cos(\delta_i) \approx 1 \tag{2.24a}$$

$$\sin(\delta_i) \approx 0. \tag{2.24b}$$

Applying these assumptions to the equations (2.11) and (2.12) results in the following expressions

$$F_{x,i} = f_{x,i} \tag{2.25}$$

$$F_{y,i} = f_{y,i}. \tag{2.26}$$

Now substituting equations (2.25) and (2.26) into equations (2.15) and (2.16) will result in the following simplified expressions

$$\dot{v}_x = \frac{1}{m} \sum_{i=1}^{4} f_{x,i} + v_y \dot{\psi} \tag{2.27}$$

and

$$\dot{v}_y = \frac{1}{m} \sum_{i=1}^{4} f_{y,i} - v_x \dot{\psi}. \tag{2.28}$$

Equation (2.27) can be simplified further. Assuming that the steering angle is small, v_y will be small, and $\dot{\psi}$ will be similarly small. As a result, the product of the two will be small, and hence negligible.

As with many literature associated with normal driving situations (i.e not in situations where the car and the tyres are at their physical limits) [29, 46], the lateral tyre force at each tyre can be assumed to be linear with respect to the tyre sideslip angle, α. As such it can be described as a function of α, [100, 102] (as expressed in equation (2.7), and repeated in equation (2.29))

$$f_{y,i} = C_{\alpha,i}\, \alpha_i, \tag{2.29}$$

where $C_{\alpha,i}$ is the cornering stiffness of the respective tyre. When operating in the linear region, α_i can be calculated from

$$\alpha_f = \delta_f - \beta - \frac{l_f \cdot \dot{\psi}}{v_x} = \delta_f - \frac{v_y}{v_x} - \frac{l_f \cdot \dot{\psi}}{v_x} \tag{2.30a}$$

$$\alpha_r = \delta_r - \beta + \frac{l_r \cdot \dot{\psi}}{v_x} = \delta_r - \frac{v_y}{v_x} + \frac{l_r \cdot \dot{\psi}}{v_x} \tag{2.30b}$$

where $\alpha_f = \alpha_1 = \alpha_2$, and $\alpha_r = \alpha_3 = \alpha_4$, and all of the symbols are represented in figure 2.8.

Once the expressions for α_i in equation (2.29) have been replaced with their linear equivalent in equations (2.30a) and (2.30b), the full expression can be written as

$$f_{y,f} = C_{\alpha,f} \left(\delta_f - \frac{v_y}{v_x} - \frac{l_f \cdot \dot{\psi}}{v_x} \right) \tag{2.31}$$

and

$$f_{y,r} = C_{\alpha,r}\left(\delta_r - \frac{v_y}{v_x} + \frac{l_r \cdot \dot{\psi}}{v_x}\right). \tag{2.32}$$

To obtain an expression for the lateral acceleration in terms of yaw rate, lateral velocity, steer angle and longitudinal tyre forces, equations (2.31) and (2.32) should be substituted into equation (2.28). The resulting equation is therefore

$$\begin{aligned}\dot{v}_y = \frac{C_{\alpha,i}}{m}&\left[\left(\delta_i - \frac{v_y}{v_x} - \frac{l_f \cdot \dot{\psi}}{v_x}\right) + \left(\delta_i - \frac{v_y}{v_x} - \frac{l_f \cdot \dot{\psi}}{v_x}\right)\right] \\ +\frac{C_{\alpha,i}}{m}&\left[\left(-\frac{v_y}{v_x} + \frac{l_r \cdot \dot{\psi}}{v_x}\right) + \left(-\frac{v_y}{v_x} + \frac{l_r \cdot \dot{\psi}}{v_x}\right)\right] \\ &-v_x\,\dot{\psi}\end{aligned}$$

Similar to v_x and v_y, an expression for $\ddot{\psi}$ can be found by summing the forces around the vehicle

$$\ddot{\psi}\, J_z = l_f(f_{y,1} + f_{y,2}) - l_r(f_{y,3} + f_{y,4}) - d_l(f_{x,1} + f_{x,3}) + d_r(f_{x,2} + f_{x,4}) \tag{2.33}$$

which can be expanded by including the terms in equations (2.31) and (2.32) to give

$$\begin{aligned}\ddot{\psi}\, J_z = C_{\alpha,f}\, l_f&\left[\left(\delta_f - \frac{v_y}{v_x} - \frac{l_f \cdot \dot{\psi}}{v_x}\right) + \left(\delta_f - \frac{v_y}{v_x} - \frac{l_f \cdot \dot{\psi}}{v_x}\right)\right] \\ -C_{\alpha,r}\, l_r&\left[\left(-\frac{v_y}{v_x} + \frac{l_r \cdot \dot{\psi}}{v_x}\right) + \left(-\frac{v_y}{v_x} + \frac{l_r \cdot \dot{\psi}}{v_x}\right)\right] \\ &-d_l\,(f_{x,1} + f_{x,3}) + d_r\,(f_{x,2} + f_{x,4})\end{aligned}$$

Finally, these equations can be combined to obtain a state space model described in equation (2.34), where the system can be represented as follows,

$$\begin{bmatrix} \dot{v_x} \\ \dot{v_y} \\ \ddot{\psi} \end{bmatrix} = \begin{bmatrix} 0 & 0 & 0 \\ 0 & \frac{-(C_{\alpha,1}+C_{\alpha,2}+C_{\alpha,3}+C_{\alpha,4})}{m\,v_x} & \frac{-l_f(C_{\alpha,1}+C_{\alpha,2})+lr(C_{\alpha,3}+C_{\alpha,4})}{m\,v_x} - v_x \\ 0 & \frac{-l_f(C_{\alpha,1}+C_{\alpha,2})+l_r(C_{\alpha,3}+C_{\alpha,4})}{v_x\,Jz} & \frac{-lf^2(C_{\alpha,1}+C_{\alpha,2})-lr^2(C_{\alpha,3}+C_{\alpha,4})}{v_x\,Jz} \end{bmatrix} \begin{bmatrix} v_x \\ v_y \\ \dot{\psi} \end{bmatrix} \tag{2.34}$$

$$+ \begin{bmatrix} 0 & 1/m & 1/m & 1/m & 1/m \\ \frac{(C_{\alpha,1}+C_{\alpha,2})}{m\,v_x} & 0 & 0 & 0 & 0 \\ \frac{l_f\,(C_{\alpha,1}+C_{\alpha,2})}{J_z} & \frac{-d_l}{J_z} & \frac{d_r}{J_z} & \frac{-d_l}{J_z} & \frac{d_r}{J_z} \end{bmatrix} \begin{bmatrix} \delta_f \\ f_{x,1} \\ f_{x,2} \\ f_{x,3} \\ f_{x,4} \end{bmatrix}$$

$$y = \begin{bmatrix} 1 & 0 & 0 \\ 0 & 1 & 0 \\ 0 & 0 & 1 \end{bmatrix} \begin{bmatrix} v_x \\ v_y \\ \dot{\psi} \end{bmatrix} + \begin{bmatrix} 0 & 0 & 0 & 0 & 0 \\ 0 & 0 & 0 & 0 & 0 \\ 0 & 0 & 0 & 0 & 0 \end{bmatrix} \begin{bmatrix} \delta_f \\ f_{x,1} \\ f_{x,2} \\ f_{x,3} \\ f_{x,4} \end{bmatrix}$$

$$x(t=0) = \begin{bmatrix} v_{x0} \\ v_{y0} \\ \dot{\psi}_0 \end{bmatrix}$$

This vehicle model is very similar to a single track (bicycle) model, with the exception that this model has been expanded to accommodate the four wheel forces as inputs. This is the simplest model that can accommodate combined steering and braking [42]. In this linear model the steering input can be made equal to zero, resulting in a vehicle model which has only four wheel force inputs.

Since frequency based design techniques will be used to design the controllers, the equations for the plant must be converted from the time domain to the frequency domain. Laplace transforms are used to for this conversion, and the Laplace operator is denoted by the symbol s. Firstly, taking laplace transforms of the equation describing the vehicle longitudinal velocity results in

$$v_x(s) = \frac{1}{s\,m} \sum_{i=1}^{4} f_{x,i}(s), \tag{2.35}$$

where m is the vehicle mass, and the expression is a simple integrator.

Similarly, the expression representing yaw rate dynamics can be converted to the frequency domain using. Firstly simplifying the expression to

$$\ddot{\psi} = M_1(v_x)\, v_y + P(v_x)\, \dot{\psi} + M_2\, f_{x,odd} + M_3\, f_{x,even} \tag{2.36}$$

where

$$\begin{aligned}
M_1 &= \frac{-l_f(C_{\alpha,1} + C_{\alpha,2}) + l_r(C_{\alpha,3} + C_{\alpha,4})}{v_x\, J_z} \\
P(v_x) &= \frac{-lf^2(C_{\alpha,1} + C_{\alpha,2}) - lr^2(C_{\alpha,3} + C_{\alpha,4})}{v_x\, J_z} \\
M_2 &= \frac{-d_l}{J_z} \\
M_3 &= \frac{d_r}{J_z} \\
f_{x,odd} &= (f_{x,1} + f_{x,3}) \\
f_{x,even} &= (f_{x,2} + f_{x,4})
\end{aligned}$$

and taking Laplace transforms of equation (2.36) results in

$$\dot{\psi}(s) = \frac{M_1(v_x)}{s + P(v_x)}\, v_y(s) + \frac{M_2}{s + P(v_x)}\, f_{x,odd}(s) + \frac{M_3}{s + P(v_x)}\, f_{x,even}(s) \tag{2.37}$$

These two equations (2.35) and (2.37) will be used in chapter 3, to design the feedback controller.

2.4.2 Real-time simulation model (RTSM)

A real-time simulation vehicle model has been developed outside the scope of this work. It is a nonlinear, 21 state model developed and written in C code and interfaced using an S-function in Simulink. Because the original code is available and the workings of the model can be understood, this model will be used in conjunction with the human interface test rig. The

rig will be introduced in chapter 4. This RTSM model, with nonlinearities present, is more representative of an actual vehicle for a wider operating envelope than the LCDM. It can be run in real time and connected to the test rig using Simulink interface tools, which enables human input via the rig to be implemented together with the controllers. Comparisons can be made between automatic control, driver only steering input, and a combination of both. This vehicle model has the following characteristics:

- Translational and Rotational Dynamics
- Vertical dynamics including load transfer
- Nonlinear tyre model
- Pitch, roll and yaw dynamics
- Integrated driveline
- Included friction coefficient of the road surface, μ, for each wheel
- Position of necessary sensors (e.g. lateral acceleration) and centre of gravity
- Brake actuator dynamics
- The ability to apply lateral and longitudinal road wheel forces to each wheel individually

Additionally, rear wheel steering is also a possible with this model, but will be disabled for this work. The tyre model used is a customised model.

2.4.3 Verified simulation model (VSM)

A highly nonlinear model was available for simulation and evaluation purposes as part of the CEMACS project [1]. This model is highly complex, has been validated against a real vehicle, and is presented as a 'black box' model in the sense that its workings are not known to the user. It is for this reason that both the linear controller design model and the real-time simulation model are available. Because of the level of detail, this proprietary model is very useful for simulation but is not suitable for controller design purposes or real time applications.

[1] Complex Embedded Automotive Control Systems: A research program funded via the European Union's Sixth Framework Program contract 004175

The model contains very detailed information including, but not limited to:

- Nonlinear tyre model using look up tables based on test data
- Translational and Rotational Dynamics
- Anti lock Braking System
- Electronic Stability Program
- Vertical dynamics
- Gearbox modelling
- Locations of onboard sensors
- Active Body Control
- Actuator modelling
- Engine modelling
- Internal model control loops (mentioned in more detail below)
- Ability to apply external disturbances

It is important to note at this stage that wheel slip controllers are not used directly in this study. Instead it is assumed that the ABS/TCS controller, which is integrated into the proprietary model, will control the wheel slip when the wheel forces are demanded by the lateral dynamics controllers. Also, because this model has been verified against an actual production/research vehicle, it can be used as a benchmark for simulation.

Importantly, this vehicle model contains a driver model. This model will accelerate the vehicle to a nominal velocity of 20.5 m/s, or decelerate to the same value when necessary. The acceleration is very moderate and equates to approximately 0.17 m/s^2. Obviously the main implication of this is that the vehicle will not remain at a steady state velocity until it reaches the value of 20.5 m/s.

2.4.4 Model evaluation and verification

Verification of the three vehicle models is carried out to establish if all three models behave in a similar manner. To achieve this, identical step inputs are applied to each model. The verified simulation model emulates a passenger vehicle, so all three vehicle models will be loaded with the same parameter values (this includes vehicle dimensions, moment of inertia, vehicle mass etc.) as listed in table 2.4.

symbol	value	units
v_{x0}	11.11	[m/s]
v_{y0}	0	[m/s]
$\dot{\psi}_0$	0	[rad/s]
μ	1.0	[-]
C_f	70000	[N/rad]
C_r	130000	[N/rad]
J_z	4700	[kgm^2]
m	2360	[kg]
d_l	0.787	[m]
d_r	0.787	[m]
l_f	1.67	[m]
l_r	1.41	[m]

Table 2.4: Vehicle parameters used in the three models

The following chapter will present the control design section of this work. The controllers will be designed to operate at moderate vehicle speeds, and for this reason, the initial velocity was set to 11.11 m/s (which equates to 40 km/h).

The behaviour of the three models should be similar for a set of given inputs which are designed to excite the lateral dynamics. In all of the simulations, the following initial conditions for the models were set

$$v_{x0} = 11.11 \text{ [m/s]} \tag{2.38}$$

$$v_{y0} = 0 \tag{2.39}$$

$$\dot{\psi}_0 = 0 \tag{2.40}$$

Also, the inputs during the manoeuvres are designed to keep the vehicle within the linear operating region. In figures 2.9 and 2.10, the following abbreviations are used for the legends:

LCDM Linear controller design model

RTSM Real-time simulation model

VSM Verified simulation model

Steering input

Firstly, a 'double step' (to the right, then to the left) steering input is applied to the vehicle. A step input for a road wheel angle will excite both yaw rate and sideslip angle, and figure 2.9 shows the results for the three different models for each of the following: vehicle velocity, vehicle yaw rate and vehicle sideslip angle. The road wheel angle in figure 2.9(d) is approximately ± 0.5 degrees, which equates to a steering wheel angle of approximately 10 degrees.

Figure 2.9(a) shows the results for yaw rate response to the steering input. Firstly, it can be seen that all three responses have the same sign, and that the steady state magnitudes are almost identical. The VSM response is more oscillatory, but these oscillations merely reflect the complex properties of the model. Importantly, the rise times of all three model responses are identical.

Figure 2.9(b) shows the results for the vehicle sideslip response to the steering input. Again the magnitudes of all three responses are very similar, while the verified simulation model is much more oscillatory than the other two models. Also, the responses from all three models have the same sign, and a similar rise time. The latter of these properties is important since it shows that the dynamics are similarly represented in all three models.

In the last of the steering input plots, figure 2.9(c) shows how the vehicle velocity responds to the steering input. Generally, the steering input has very little effect on the velocity. The LCDM and RTSM both remain undisturbed and are plotted directly on top of each other. Initially, the proprietary model looks to behave rather oddly. Within the first second, the model goes through a settling down period, after which the vehicle starts to accelerate slowly. This can be explained by the driver model described earlier in section 2.4.3.

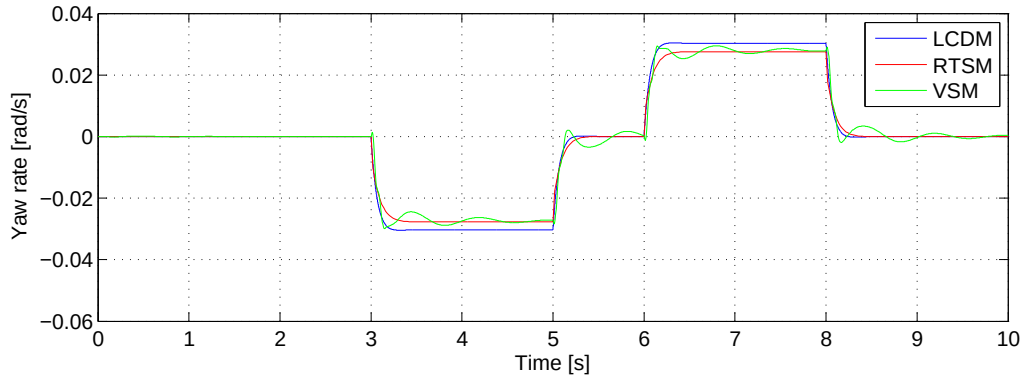

(a) Vehicle yaw rate, $\dot{\psi}$

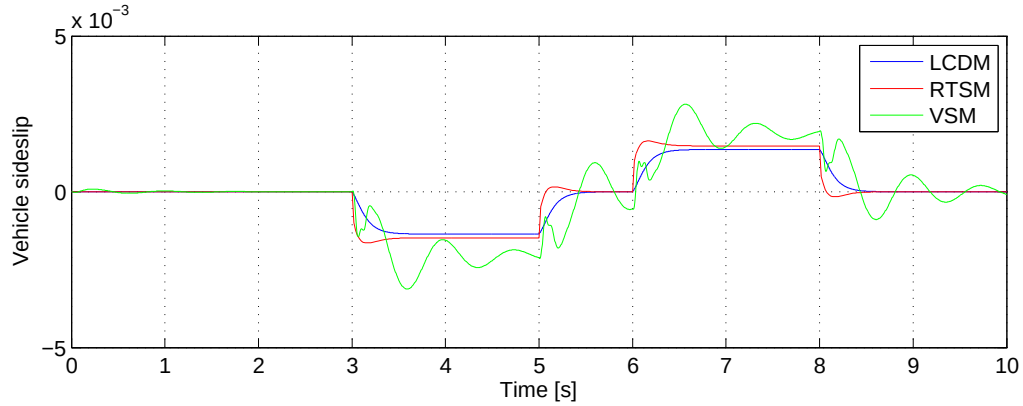

(b) Vehicle sideslip, β

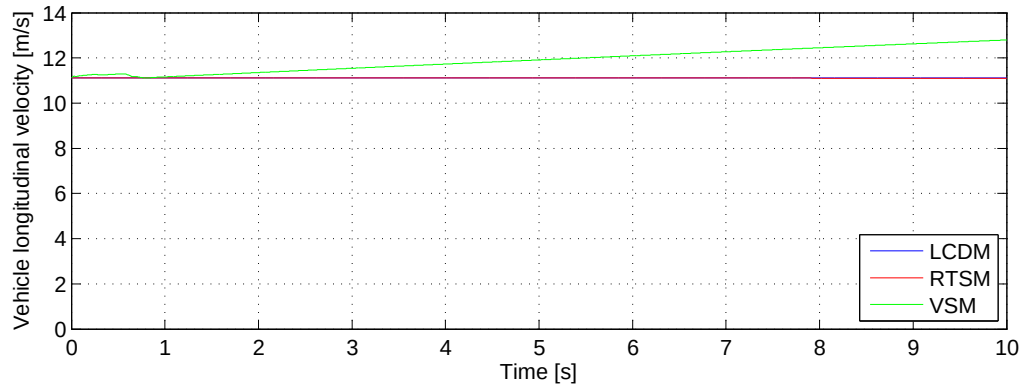

(c) Vehicle longitudinal velocity, v_x

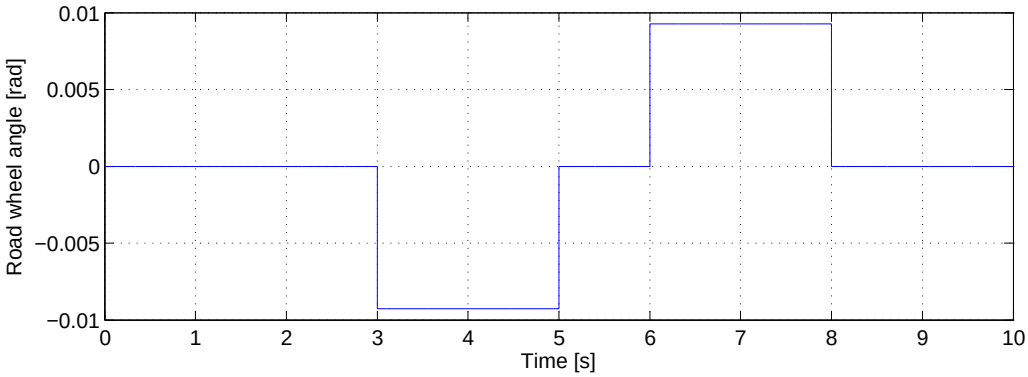

(d) Road wheel angle, δ_f

Figure 2.9: Vehicle response to step-steering input

Wheel force input

A step input to simulate wheel braking is applied to both wheels on the right hand side of the vehicle, and zero input applied to both wheels on the left hand side. This step input induces differential style braking, and will generate a yaw moment together with some vehicle sideslip. Comparisons between the three vehicle models will again be made, with the results presented in the same way as for the steering input. With a vehicle mass of 2360 Kg, a friction coefficient of 1.0 and gravitational constant set to 9.81 m/s, the applied wheel force is approximately half of the maximum force available (which is approximately 5000 N per wheel as described in equation (2.2)).

Figure 2.10(a) shows how the vehicle yaw rate compares for the three different vehicle models, when the same wheel force is applied to all models. The verified simulation model again behaves more oscillatory than the other two models, which can be accounted for by the nonlinearities present in the model. There are differences in the peak magnitudes of the yaw rate (approximately four times in magnitude), but the rise times are similar, indicating that the dynamics are similar.

Figure 2.10(b) shows differing vehicle sideslip responses for all models. The verified simulation model is very oscillatory and never reaches steady state during the step phase. It is also different in peak magnitude to the other two models. On the other hand, both the linear controller design model and the real time simulation models are very similar in magnitude and rise time, reflecting that overall the sideslip dynamics are captured well within these two models.

One other comment to make regarding figure 2.10(b) is that when comparing it to figure 2.9(b), the sign of β is seen to change for all three models. This can be explained from equations (2.30a) and (2.30b) which can be rearranged as below, to show the contribution of the front and rear wheels to the sideslip angle.

$$\beta = \frac{l_f \cdot \dot{\psi}}{v_x} - (\alpha_f - \delta_f) \tag{2.41a}$$

$$\beta = -\frac{l_r \cdot \dot{\psi}}{v_x} - \alpha_r \tag{2.41b}$$

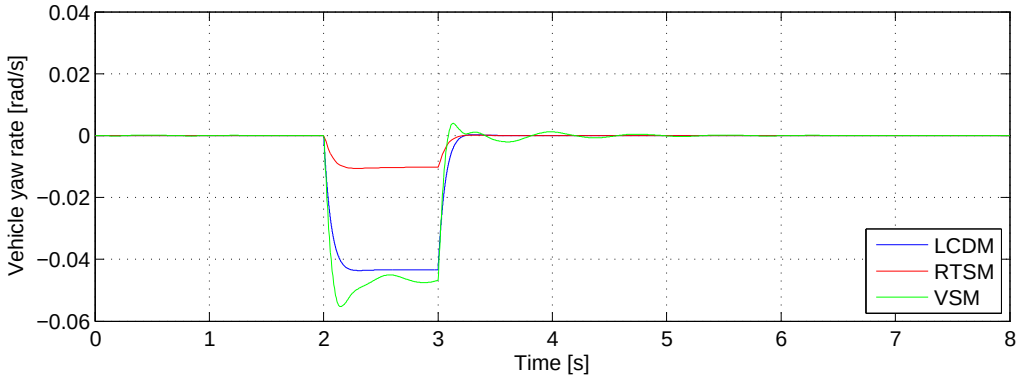

(a) Vehicle yaw rate, $\dot{\psi}$

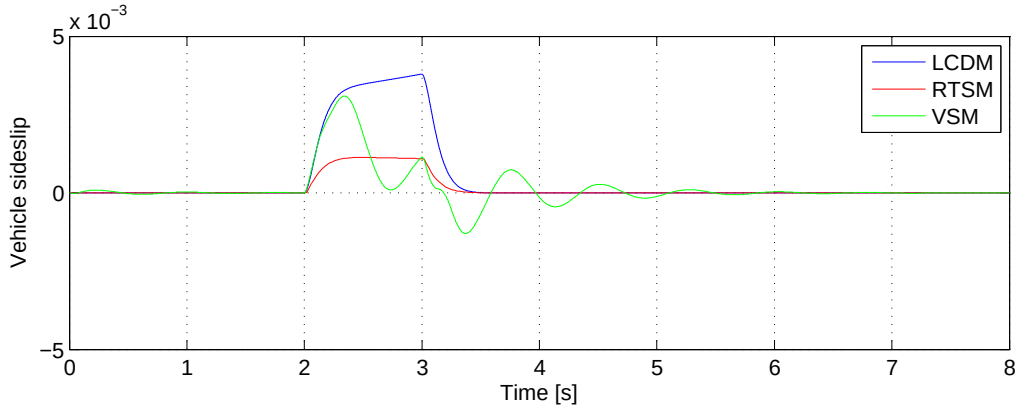

(b) Vehicle sideslip, β

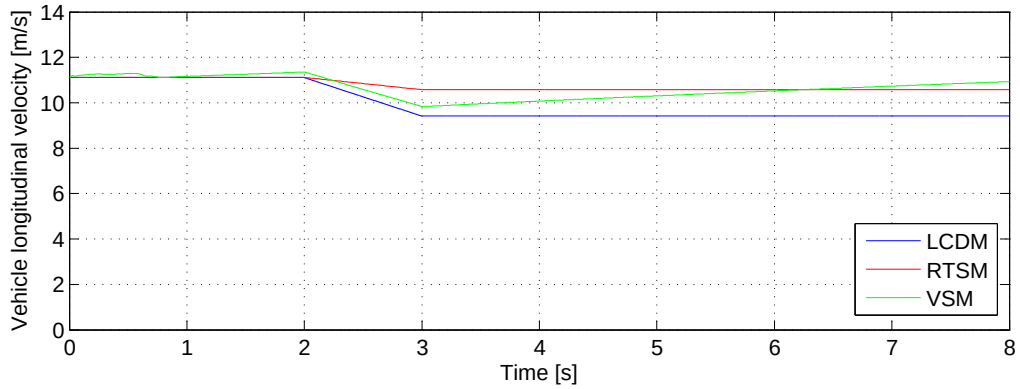

(c) Vehicle longitudinal velocity, v_x

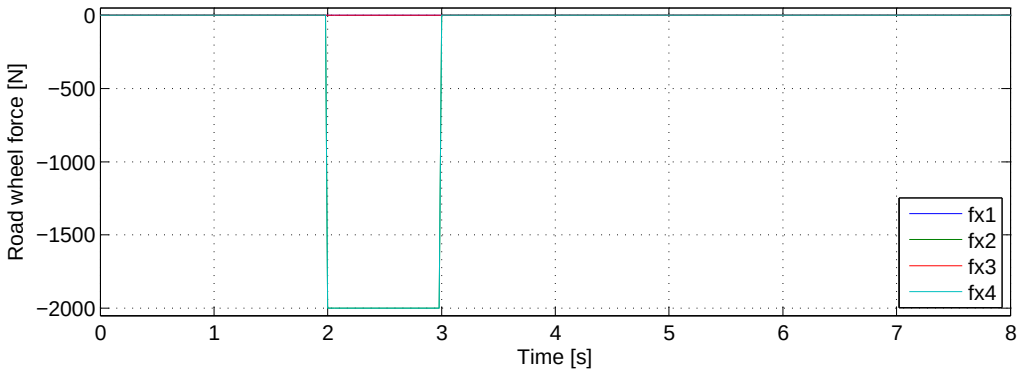

(d) Road wheel longitudinal force, $f_{x,i}$

Figure 2.10: Vehicle response to step-brake input

These two equations show that a different magnitude for vehicle sideslip will result when δ_f changes from being zero to non-zero. Under certain conditions, the sign of the sideslip angle will also change.

Finally, the plots for vehicle velocity can be seen in figure 2.10(c). All three models show the same characteristics; a small decrease in velocity while the brakes are applied. After this decrease, both the LCDM and RTSM remain at a constant value, while the VSM starts to accelerate slowly. This behaviour of the VSM can be explained as before. Importantly, in this figure the velocities of all three models remain very similar, indicating that the braking dynamics are accurately represented in all models.

2.5 Conclusions

Overall, it can be concluded that the simulation results of all three models are dynamically similar. Therefore, it can be said that the linear model seems to contain the fundamental dynamics that are also present in the nonlinear models. This implies that any analysis from using the linear model should reflect the general properties of the nonlinear models. However, the nonlinearities of the VSM become visible through the oscillatory behaviour when each set of inputs is applied.

In this chapter three vehicle models have been introduced. A linearised model is designed specifically for linear control design and analysis techniques to design a robust feedback controller. On the other hand, two nonlinear models (RTSM and VSM) will be used for controller evaluation through simulation and real time experiments using a human in the loop. The simulation manoeuvres for this will be introduced at the beginning of chapter 5.

The following chapter will introduce the control structure and the feedback controller will be designed.

Chapter 3

Controller design

This chapter introduces the controller design process and the implementation of the control laws, which leads to evaluation and testing in chapters 5 and 6. Section 1.2 highlighted that vehicle modelling can be rather complex, however, with the assumptions applied in chapter 2, the resultant model to be used for controller design is simplified to a linear Multi-Input-Multi-Output (MIMO) system.

A brief summary of the important aspects of the design process will be given, leading to the development of control laws which can be implemented in both of the nonlinear models (the real-time simulation model (RTSM) and the verified simulation model (VSM)). The proposed control structure will then be discussed and finally conclusions will be drawn on the derived control laws.

3.1 Control design methods

This section will look at the theory behind designing feedback controllers using frequency based design methods, leading to the proposed controller design criteria.

3.1.1 Principle of frequency based design

The principle behind frequency based design is to perform 'loop-shaping' on the open-loop frequency response in order to design adequate controllers for the closed loop system. This can be achieved through designing controllers to obtain desired characteristics at certain frequencies for the complete system. These desired characteristics will be introduced as this

chapter proceeds. Frequency based design has one major limitation, in that it can only be applied to linear systems. It can be described as an iterative process, where the design process is revisited until the design criteria are satisfied.

3.1.2 Methods of measuring robustness and stability

Control laws are often designed using a linear model and are then tested and simulated using a nonlinear system. The control laws are expected to work in both of these environments, since the linear model should capture all of the important dynamics from the real system. However, higher frequency dynamics and general nonlinear behaviour are often neglected or inaccurately described in linear models, but the control laws should still work with these uncertainties present. The capability of the controllers to work in the presence of these uncertainties, is a measure of their robustness.

From the control loop shown in figure 3.1, some general expressions can be derived which help analyse the stability of the overall system and the robustness of the designed controllers.

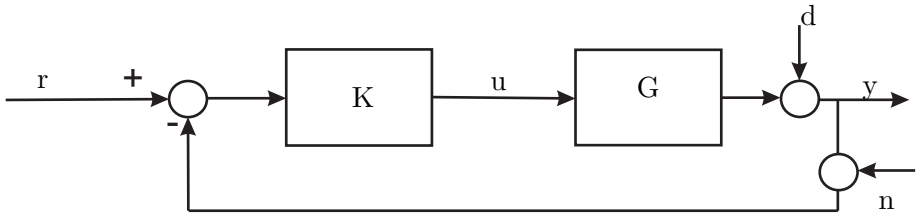

Figure 3.1: General closed loop control system

In this figure,

- r is the reference signal
- K is the feedback controller
- u is the control signal
- G is the plant
- d is the output disturbance
- y is the system output, and

- n is the measurement noise signal

The plant, G, is also sometimes known as the *nominal plant*. This is generally a linear model which approximates the actual plant and provides the basis for control design and analysis. Therefore, in this work the linearised plant is equivalent to the nominal plant, and the nonlinear vehicle models are equivalent to the actual plant.

Starting with an expression for the output of the closed loop, and assuming that the Laplace domain is considered, y can be expressed as

$$y(s) = \frac{K(s)\,G(s)}{1 + K(s)\,G(s)}\,r(s) + \frac{1}{1 + K(s)\,G(s)}\,d(s) - \frac{K(s)\,G(s)}{1 + K(s)\,G(s)}\,n(s). \tag{3.1}$$

For simplicity, the s term will be dropped in any expressions from here onwards.

From equation (3.1), it can be seen that the expression for the transfer function from d to y determines the influence that any disturbances have on the output. This is known as the *'sensitivity function'*, denoted by S. Furthermore, the transfer function from n to y determines the influence of any measurement sensor noise on the output. This transfer function is known as the *'complementary sensitivity function'*, denoted by T. Therefore, in summary, these two functions can be expressed as

$$S = \frac{1}{1 + K\,G} = \frac{1}{1 + L} \tag{3.2}$$

$$T = \frac{K\,G}{1 + K\,G} = \frac{L}{1 + L} \tag{3.3}$$

where $L = K\,G$ is the loop gain, allowing equation (3.1) to be expressed in compressed form as

$$y = T\,r + S\,d - T\,n. \tag{3.4}$$

It is clear from equation (3.3), that the complementary sensitivity function also describes the closed loop transfer function, and is confirmed by the fact that it describes the response from the reference signal, r, to the output, y, as seen in equation (3.1). Symmetry can be proven between S and T. It can be shown that the sensitivity of T w.r.t plant variations

can be determined by S, and the sensitivity of S is determined by T. Furthermore, adding equations (3.2) and (3.3) together equals unity, i.e.

$$S + T = 1. \tag{3.5}$$

It can also be shown that over the frequency range where S is small, T will be largely unaffected by plant variations, and similarly, for the frequency range where T is small, S becomes largely unaffected by plant variations. This description of S and T gives an insight into the tradeoff which exists, since from equation (3.5), both S and T cannot be made small at the same frequency.

If a peak occurs in the sensitivity plot $|(S(j\,\omega))|$, then the maximum value of this peak, M_s, can be used as a measure ofthe performance and robust stability of the closed loop system. For greater magnitudes of this peak, the system is seen to be less robust and may be closer to instability, where the stability of a system is measured in the presence of uncertainties.

Closed loop stability must be achieved at all times for a control system to function properly. The sensitivity and complementary sensitivity functions can be used as a measure of how robust and stable a system is, and the loop gain is responsible for defining the S and T functions for a range of frequencies. When we say how stable the system is, we mean: is the system stable in the presence of uncertainties? — also known as robust stability. Furthermore, the gain margin, phase margin and vector margin are indicators of system stability, and these indicators can be translated between open loop Bode plots of the loop gain L, the sensitivity and complementary sensitivity plots (S and T) and step responses, all of which are mentioned briefly here.

The open loop Bode plots of L can indicate the performance of a given system from plotting the forward loop, and expressing some important information in terms of gain and phase margins. The Gain margin represents the increase in the system gain when the phase crosses -180° that will result in the system becoming unstable. That is

$$g_m = \frac{1}{|L(j\,\omega_o)|},$$

where $L(j\,\omega_o)$ is the point of crossing, and ω_o is the frequency at which it crosses. The Phase margin represents the amount of phase shift that the system can accommodate before it

reaches instability at unity magnitude.

Therefore, the margins are a good measure of the robustness of the system, and large margins indicate that the system is more robust. From control theory textbooks [104, 105] suitable margins are generally 30° for phase and 2dB for gain. These are the minimum recommendations, but are of course application dependent.

An example open loop Bode plot is shown in figure 3.2 with the two margins indicated. The gain margin is equal to 12dB and the phase margin is equal to 74.5°. This figure is calculated for a non-specific system with transfer function

$$L = \frac{2}{s^3 + 2\,s^2 + 4\,s}. \tag{3.6}$$

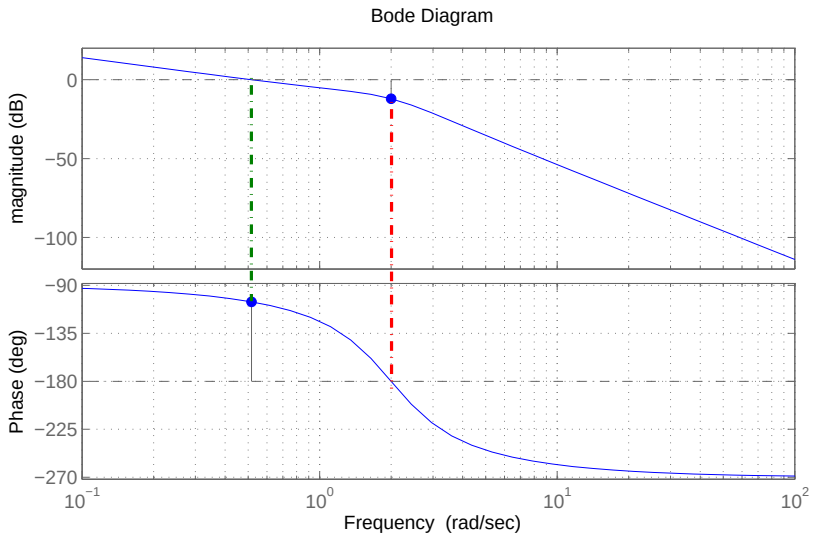

Figure 3.2: Open loop Bode plot indicating stability margins

When shaping the open loop Bode plots of the loop gain, L, the magnitude plot should be characteristically shaped to have a steeper roll off at high frequencies (no less than 20dB/decade, but preferably 40dB/decade). This is designed to limit the influence of any high frequency and unmodelled dynamics which may impair the performance of the controller. In conjunction with this, the low frequency gain should be high, to avoid any steady state errors.

In summary, a lot of information can be obtained from open loop Bode plots of the system

loop gain, the sensitivity plots and the complementary sensitivity plots. This information can be used in the controller design process, to iteratively design robust controllers which are capable of keeping the plant stable. Loop shaping will be used to create a loop transfer function, L, so that $|T|$ is small at high frequencies and $|S|$ is similarly small at low frequencies. Example sensitivity and complementary sensitivity plots are shown in figure 3.3, for a system loop gain of

$$L = K\,G = \frac{100}{s+1}. \tag{3.7}$$

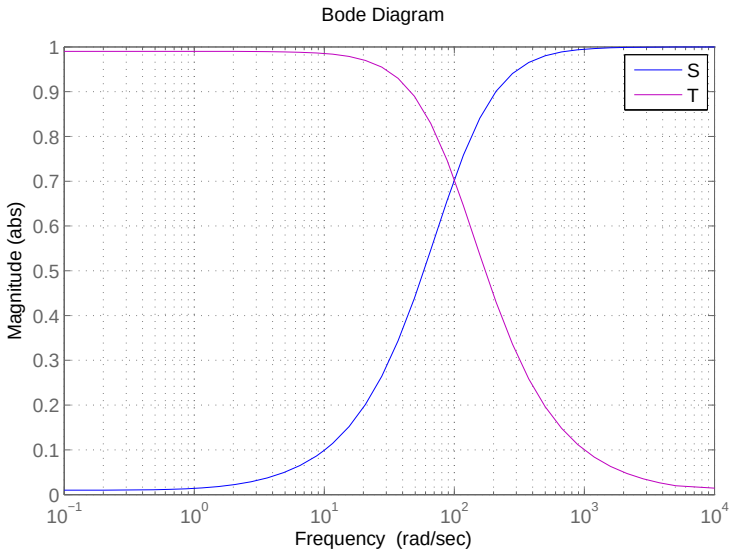

Figure 3.3: Example Bode plot indicating desired $|S|$ and $|T|$ plots

Finally, the closed loop step response can be used to calculate the steady state error for the system using equations (3.8) and (3.9) below,

$$e_{ss} = \frac{1}{1+mag} \times 100\% \tag{3.8}$$

and

$$mag = 10^{(\frac{M(dB)}{20})}, \tag{3.9}$$

where M(dB) is the low frequency gain, measurable from the open loop bode plot. As mag is much greater than 1, the steady state error will tend to zero.

3.1.3 Design specification for controllers

Two different variables will be controlled within this work — vehicle sideslip and vehicle yaw rate. It has been shown in chapter 2 that vehicle sideslip can be altered by changing either v_y or v_x. Therefore, it is proposed to design a relationship between the actual vehicle lateral velocity, actual vehicle sideslip and desired vehicle sideslip. This setup will allow a reference signal for v_x to be calculated, based on a comparison between actual vehicle sideslip and desired sideslip. Thus, v_x can be controlled as a means of regulating vehicle sideslip, β. The second variable to be controlled is the vehicle yaw rate, $\dot{\psi}$, which is achievable via braking each side of the car by different amounts.

When the design process for both controllers is being carried out, some criteria must be met to ensure that they are realistic, implementable and can function properly. From various literature [29, 36, 42], setting the bandwidth for channel 2 — for vehicle yaw rate, to approx 7 rad/s should give an adequate rise time, and therefore desirable system performance.

A similar bandwidth setting can be made for channel 1 — for vehicle sideslip. From works by Boada and Morgando [12, 31], vehicle sideslip has a bandwidth of approximately 5 rad/s. From this, it can be assumed that the velocity should be in this same range since it is used to calculate the sideslip. Therefore, the bandwidth of channel 1 should be approximately 5 rad/s.

It has been mentioned that minimum acceptable gain and phase margins are 2dB and 30°. However, when the controllers are included in the loop, the system should be able to handle small time delays. These are already incorporated into the verified simulation model. Time delays are known to reduce the phase margin of the open loop system. A small time delay of 20ms (equal to 1 simulation step in the vehicle models) will reduce the phase margin by approximately 6° on channel 1 and 8° on channel 2. With this in mind, the minimum phase margin for both channels should be 40°. In terms of gain margin, this is not constrained, but should be large enough to give good $|S|$ and $|T|$ functions as described earlier in this chapter.

3.2 Proposed control structure

The control structure chosen is the classical feedback control structure shown in figure 3.4. This control structure has the reference signal, y_{ref}, subtracting the output of the system, y,

to obtain the error, e. This error is used as the input to the controller, K, which outputs a control effort, u, which is in turn applied to the plant G. In this case, the plant, G, is the linear vehicle model which was derived in chapter 2.

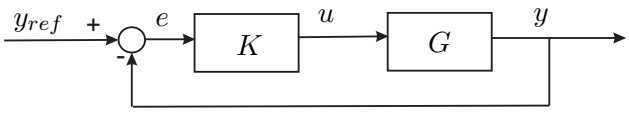

Figure 3.4: Classical feedback control problem

However, it was seen from chapter 2 that the plant can be separated into two SISO channels (to allow each channel to be individually analysed and then for the controllers to be designed, as described by ICAD theory [46,48]). This then enables the structure in figure 3.4 to be expanded as illustrated in figure 3.5.

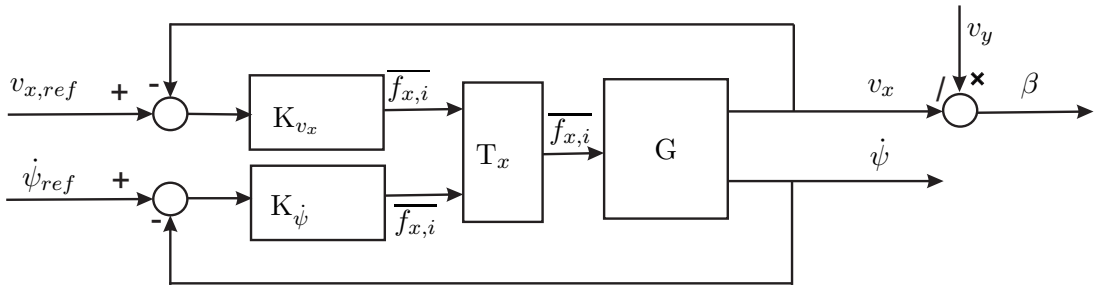

Figure 3.5: Outline of control problem

This new structure differs from the previous structure by having two controllers, and hence, two reference signals and two output signals. Also included in this figure is the calculation of the vehicle sideslip, β, from two of the model outputs, v_x and v_y. The two controllers will be regarded as one controller with two channels. Pairing two controller outputs with four plant inputs, creates a control allocation problem and this is now investigated in further detail.

3.2.1 Control allocation problem

The linear controller design model (LCDM, presented in chapter 2) can be separated into two channels (as per figure 3.6), where $T_{x,vx}$ and $T_{x,\dot{\psi}}$ are described by equations (3.10) and (3.11). Also introduced in this figure are the terms f_{x,v_x} and $f_{x,\dot{\psi}}$. These symbols are associated with

the demanded force output from the respective dynamics controller. Also, the terms G_{v_x} and $G_{\dot{\psi}}$ indicate that only the equations which describe the appropriate channel used (e.g for the yaw rate channel, only the plant dynamics which describe the yaw rate response are used).

Therefore, in summary, each channel can be used to create a Single Input, Single Output (SISO) system which will simplify the control design task. As a result, the two individual channels formed are,

- Channel 1 - v_x: which relates wheel forces to vehicle velocity
- Channel 2 - $\dot{\psi}$: which relates wheel forces to vehicle yaw rate.

From now on these are the two controlled variables. In the case of channel 1, a reference signal will be calculated for v_x online, and it is this reference value which will give desired vehicle sideslip behaviour.

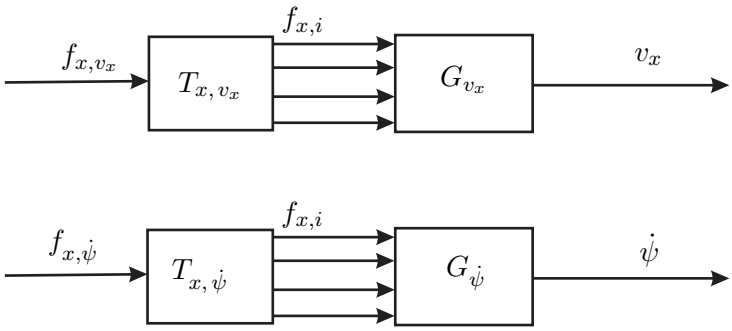

Figure 3.6: Model loops for both channels

Combining the two model loops in figure 3.6 results in figure 3.7. It now becomes evident that T_x must be a $[4 \times 2]$ matrix, with the first column corresponding to channel 1 and the second column corresponding to the channel 2. Therefore, this transformation matrix relates the outputs of both channels to the four longitudinal wheel forces, which are used as inputs to the vehicle model.

A sum and difference concept can be applied, where the sum of the longitudinal wheel forces on either side of the vehicle can control the velocity, while the difference of either side will generate a yaw moment. Using this concept allows a unity gain matrix to be used for the transformation, where the sign of each individual matrix element is dependent upon the wheel configuration of the vehicle.

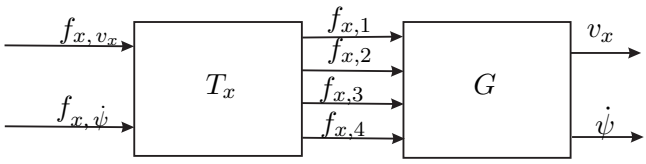

Figure 3.7: Concept of the transformation matrix

Studying channel 1 in figure 3.6, which relates f_{x,v_x} to $f_{x,i}$ (where i is the wheel number 1 to 4), it can be noted that the sign of all the elements in the first column of the transformation matrix should be positive. This will ensure that the output from the controller will be applied to all four wheels, with the same sign. Denoting T_{x,v_x} as the first column of the transformation matrix, and therefore for channel 1, it can be expressed as

$$T_{x,v_x} = \begin{bmatrix} +1 \\ +1 \\ +1 \\ +1 \end{bmatrix}. \tag{3.10}$$

A similar thinking can be applied to the second column of T_x for channel 2, relating $f_{x,\dot{\psi}}$ to $f_{x,i}$. One control input must be translated into four wheel forces, and in order to generate a yaw moment at the vehicle centre of gravity, differential style braking must occur. This implies that a different force is applied to one side of the car than the other. In keeping with the configuration of the vehicle, the following matrix can be defined for $T_{x,\dot{\psi}}$

$$T_{x,\dot{\psi}} = \begin{bmatrix} -1 \\ +1 \\ -1 \\ +1 \end{bmatrix}. \tag{3.11}$$

Equations (3.10) and (3.11) can be combined to give a 2 input, 4 output matrix as per equation (3.12)

$$T_x = \begin{bmatrix} +1 & -1 \\ +1 & +1 \\ +1 & -1 \\ +1 & +1 \end{bmatrix}. \tag{3.12}$$

It is important to note that the matrix in equation (3.12), which is represented by the unity gains, only distributes the wheel forces calculated by the controllers. Occasions may exist when non-unity is preferred, for example, it may be desirable to distribute the brake forces between the front and rear of the vehicle.

3.3 Design of feedback controller

Starting with the model expressions in equation (2.28), it can be seen that the longitudinal wheel force inputs have no direct actuation on the lateral velocity (or its derivative), and as a result only two states are directly controllable from the inputs: v_x and $\dot{\psi}$. These two linear SISO channels can now be analysed using frequency design methods, and each channel will be used separately to design their respective controllers.

3.3.1 Channel 1 controller design

To be able to analyse channel 1 using frequency analysis and design techniques, the system must be represented in the frequency domain. From chapter 2, the expression for the channel 1 in the frequency domain was found to be

$$v_x(s) = \frac{1}{s\,m} \sum_{i=1}^{4} f_{x,i}(s). \tag{3.13}$$

The open loop step response for channel 1, with the transformation matrix included (as per channel 1 in figure 3.6 and equation (3.14)) is shown in figure 3.8, where the response continues to rise linearly.

$$\dot{v}_x = \frac{1}{m} \begin{bmatrix} +1 \\ +1 \\ +1 \\ +1 \end{bmatrix} (f_{x,1} + f_{x,2} + f_{x,3} + f_{x,4}) \tag{3.14}$$

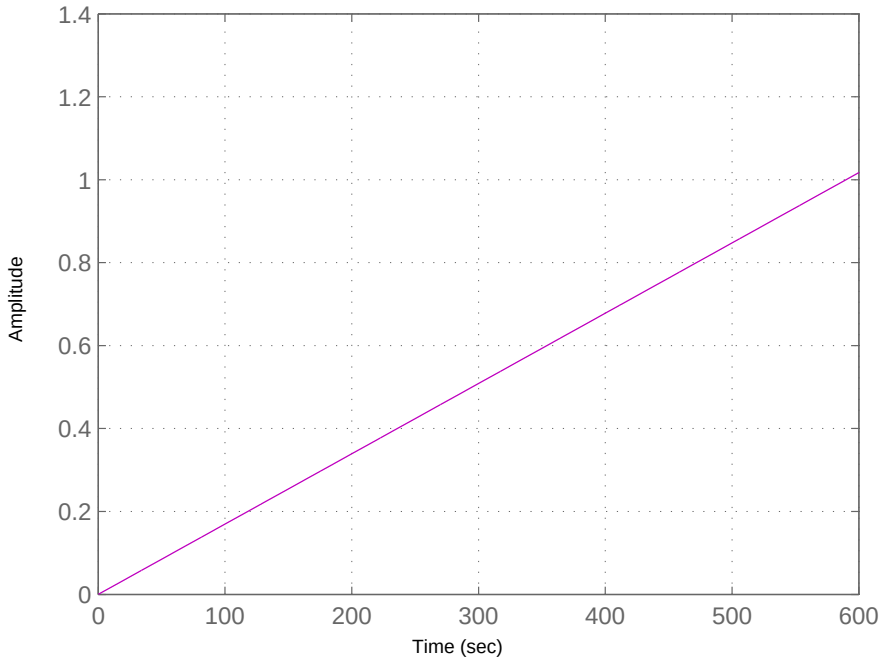

Figure 3.8: Open loop step response of $G_{v_x} T_{x,v_x}$

Equation (3.13) has no velocity dependency, therefore the plots will be identical for all velocities, given that all other parameters remain fixed.

Figure 3.9 shows the phase and magnitude plots for two systems for channel 1. Focusing on 'without K_p' for now, the crossover frequency, ω_c, for the system is very low and the gain is also very low (approximately zero dB at 0.001rad/s). To achieve satisfactory performance, the low frequency gain of the system needs to be increased. This will naturally increase the bandwidth of the system, which is presently very low ($\approx$ 0.00168 rad/s). Introducing some pure proportional gain into the control loop will achieve this. Looking for a bandwidth of approximately 5 rad/s, equation (3.15) shows that a gain, K_p of approximately 3000 will increase the current crossover frequency to the desired level. Due to the approximate values

for desired bandwidth and actual bandwidth, the proportional gain for the controller is set to 3000.

$$K_p = \frac{5}{0.00168} \approx 3000 \tag{3.15}$$

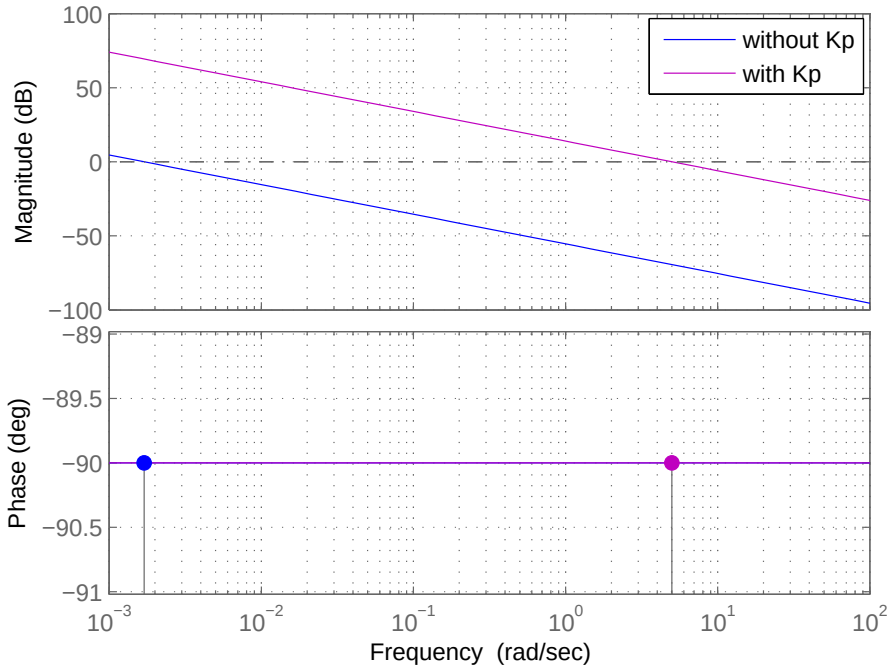

Figure 3.9: Open loop Bode plot of $G_{v_x} T_{x,v_x}$

The effect of the inclusion of the proportional gain in the loop, can be observed in the open loop Bode plot in figure 3.9, for the 'with K_p' plot. An increase in the crossover frequency can be clearly seen, which has now been increased to 5 rad/s as desired. The characteristics of the integrator plant are still visible, through the constant $-90°$ phase and the 20dB/decade slope on the magnitude plot. The markers on the phase plot indicate the crossover frequency for the two systems. The gain has increased over the whole system, which importantly includes the low frequency gain which is essential for rejecting disturbances. The effectiveness of the plant to reject the disturbances can be seen from figure 3.10, from the S and T plots. In these plots the desired characteristics can be found for the sensitivity and complementary sensitivity plots. The S plot indicates that the system will reject disturbances

at low frequencies, and the T plot shows that at low frequencies the system output will be 100% of the closed loop transfer function.

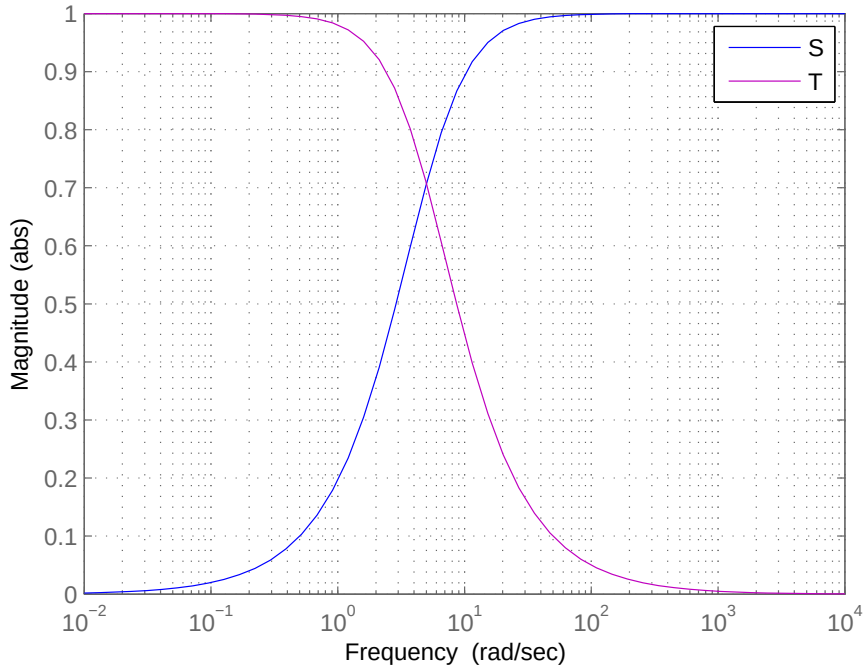

Figure 3.10: Sensitivity and complementary sensitivity plots of $G_{v_x}\, T_{x,v_x}\, K_p$

However, although the bandwidth of the system is in the correct region, there remains an issue with this control law. The shape of the open loop Bode plot of L is not desirable. It was mentioned previously that the open loop Bode plot should be shaped to have high frequency roll off of 40dB/decade, which is not the case. However, the low frequency gain should be high, which does not give cause for concern.

Currently, the integrator supplies the high gain at low frequency (since $|L(j\,\omega)|_{\omega=0} = \infty$), but does not supply the desired shape elsewhere. Introducing an extra pole into the controller, and hence the loop, L, will shape both the magnitude and phase parts of the bode plot.

Placing a pole at (s=-10) will alter the phase margin and shape the open loop Bode plot of L, expanding the controller to

$$K_1 = \frac{K_p}{s+10} = \frac{3000}{s+10}. \tag{3.16}$$

The effect of introducing this pole is reflected in the open loop Bode plot of L in figure 3.11. The first noticeable difference is the shaping of the phase plot, together with the 40dB/decade roll off at the higher frequencies on the magnitude plot, both of which are desirable properties. However, as a result of introducing these two properties, the crossover frequency has now shifted to the left and reduced to approximately 0.4 rad/s. Secondly, the inclusion of the extra pole in the loop gain (at s=-10), leads to a drop in phase to $-180°$ (since the integrator in the plant is responsible for the original $-90°$ phase). The S and T plots in figure 3.12 again highlight the properties of the system, and its ability to effectively reject disturbances. In the S plot, a small peak can be seen to start at approximately 1 rad/s. This indicates that the system is more sensitive at this frequency. Because this peak is very small in magnitude, it can be regarded as having little effect on the system robustness.

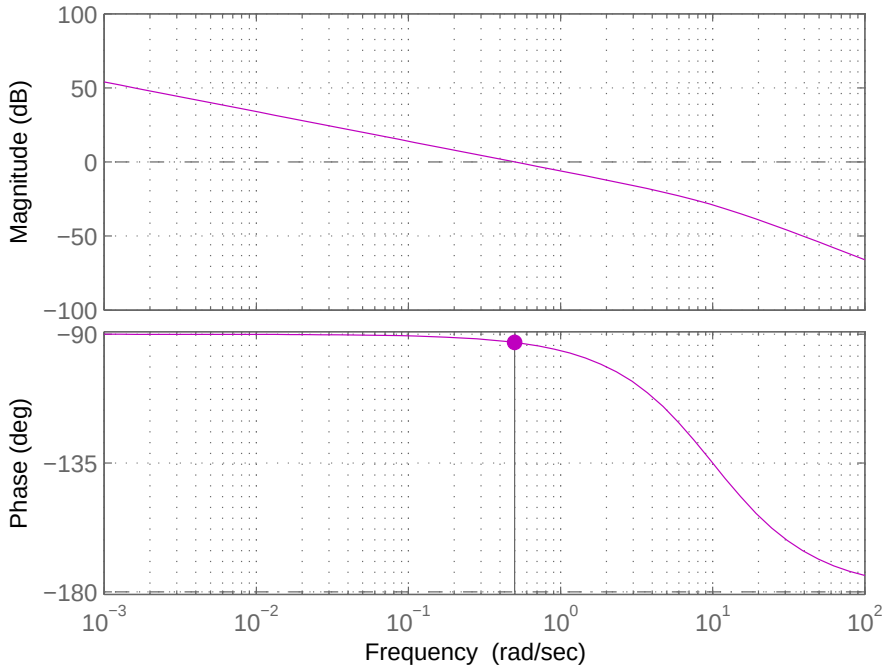

Figure 3.11: Bode plots of $G_{v_x}\, T_{x,v_x}\, K_1$

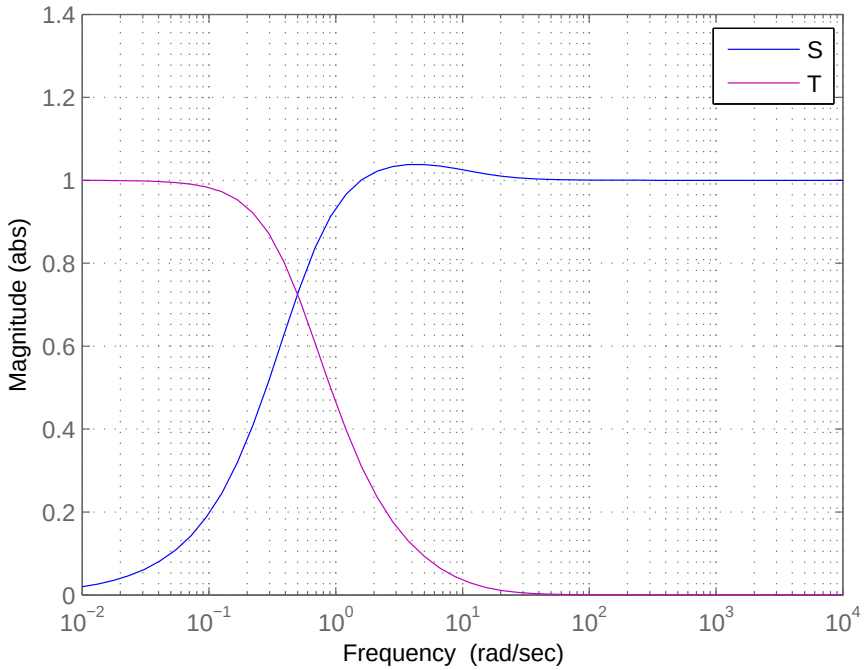

Figure 3.12: Sensitivity and complementary sensitivity plots of $G_{v_x}\, T_{x,v_x}\, K_1$

In order to keep the shape of the open loop Bode plot but increase the bandwidth, the loop gain can be increased by a factor of 8. This will increase ω_c from 0.5 rad/s to 4 rad/s. It will decrease the phase margin slightly though as the magnitude plot is shifted upwards, in turn shifting the crossover point to the right, where the phase angle heads towards $-180°$.

Therefore, the controller gain is adjusted to

$$K_{11} = \frac{8\,K_p}{s+10} = \frac{24000}{s+10}, \tag{3.17}$$

for which the open loop Bode plot is shown in figure 3.13. The phase margin is decreased to 69.5° and the gain margin is infinite, since the phase plot does not cross through the $-180°$ line. The crossover frequency is now 4 rad/s, and the bandwidth is approximately 5.5 rad/s, which meets the design criteria set out in section 3.1.3.

Closed loop step responses can be calculated and compared to see the difference between the original (pure gain) controller, K_p and the controller with the pole (at s=-10) included, K_{11}. Closing the loop using negative feedback, the step responses are obtained and combined

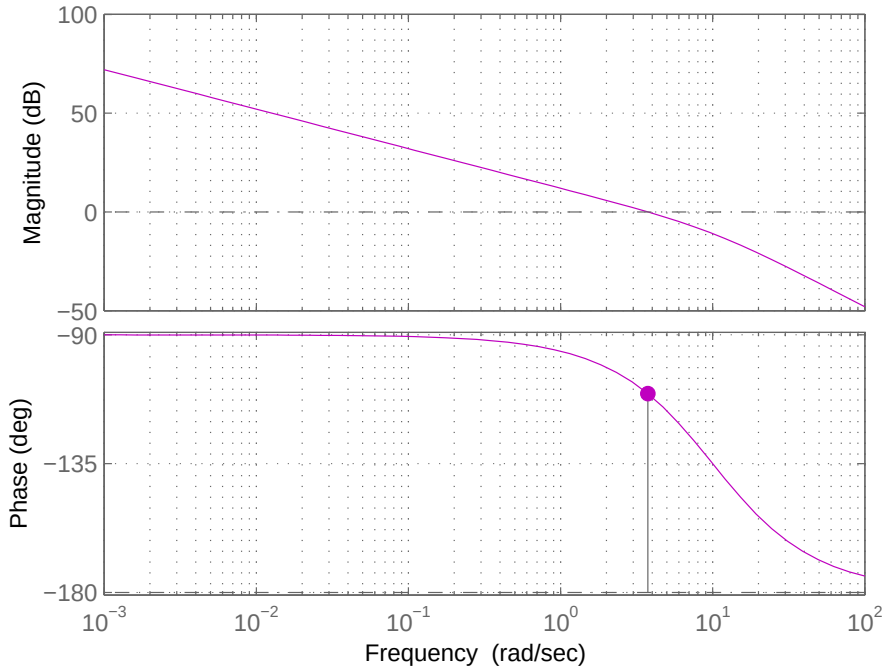

Figure 3.13: Bode plots of $G_{v_x}\, T_{x,v_x}\, K_{11}$

into figure 3.14. These plots are compared because they both met the design criteria for the crossover frequency, however the shape of the open loop Bode plot for the pure proportional gain controller was not desirable. Adding the pole to the latter controller has made the system second order, which explains the introduction of the small overshoot (approximately 3%).

The rise times can be found as the time taken to reach 90% of the final value from 10% of the final value, and are both equal to just under 0.5 seconds. When comparing both controllers, the settling time for the revised controller is quicker by around 0.2 seconds, and the rise time for the revised controller is quicker by approximately 10%. Table 3.1 compares some important values for controller K_p and K_{11}, and shows that for most criteria K_{11} performs best.

The information obtained from the open loop Bode plots of L and step response look favourable for the refined controller design, K_{11}. Finally the ability for the controller to reject disturbances must be considered. The sensitivity function of channel 1 with controller

Measure	K_p	K_{11}
ω_c [rad/s]	4.5	4
Overshoot [%]	0	1.7
Rise time [s]	0.44	0.385
Settling time [s]	0.782	0.583

Table 3.1: Comparison values of the two controller designs for channel 1

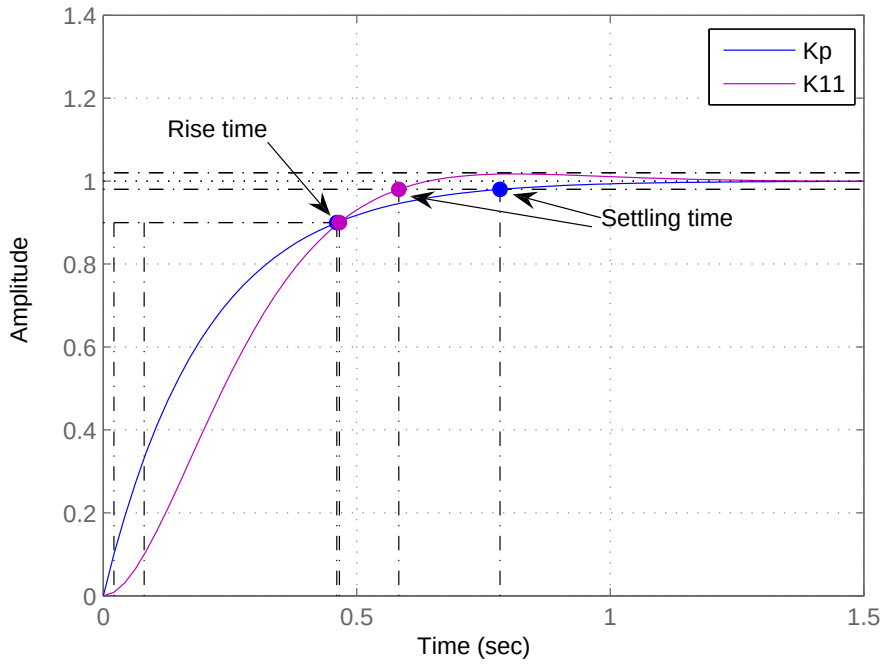

Figure 3.14: Comparison of closed loop step response of $G_{v_x} T_{x,v_x}$ for different controller designs, (equations (3.15) and (3.17))

K_{11} from equation (3.17) is combined shown with the complementary sensitivity function and shown in figure 3.15.

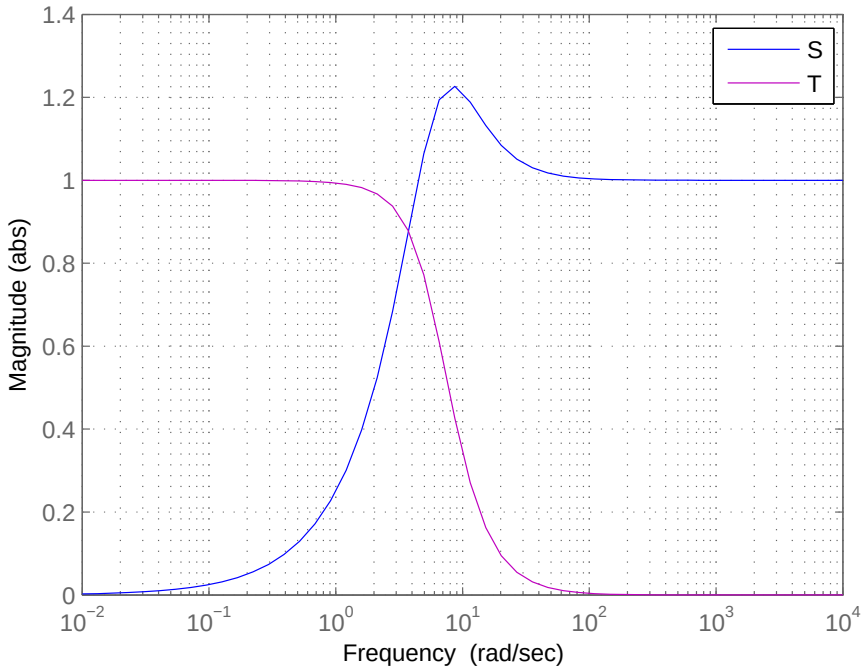

Figure 3.15: Sensitivity and complementary sensitivity plots of $G_{v_x}\, T_{x,v_x}\, K_{11}$

From the sensitivity plot in figure 3.15, a small peak can be seen to appear after a frequency of 4 rad/s. The complementary sensitivity function behaves well. The frequency at which these two plots cross is the crossover frequency (ω_c) on the Bode plot - and is approximately 4 rad/s. Comparing figure 3.15 with figure 3.12, the revised controller design can be seen to improve the sensitivity of the system at low frequencies.

This control law now meets the desired criteria, and is ready to implement into the verified simulation model for evaluation. A similar process will now be applied to channel 2 to design the yaw rate controller.

3.3.2 Channel 2 controller design

Similar to channel 1, the equations describing channel 2 must also be represented in the frequency domain. From equation (2.37), the expression for the yaw rate dynamics in the frequency domain was found to be

$$\dot{\psi}(s) = \frac{M_1(v_x)}{s + P(v_x)}\, v_y(s) + \frac{M_2}{s + P(v_x)}\, f_{x,odd}(s) + \frac{M_3}{s + P(v_x)}\, f_{x,even}(s) \tag{3.18}$$

where

$$\begin{aligned}
M_1(v_x) &= \frac{-l_f(C_{\alpha,1} + C_{\alpha,2}) + l_r(C_{\alpha,3} + C_{\alpha,4})}{v_x\, J_z} \\
P(v_x) &= \frac{-lf^2(C_{\alpha,1} + C_{\alpha,2}) - lr^2(C_{\alpha,3} + C_{\alpha,4})}{v_x\, J_z} \\
M_2 &= \frac{-d_l}{J_z} \\
M_3 &= \frac{d_r}{J_z} \\
f_{x,odd} &= (f_{x,1} + f_{x,3}) \\
f_{x,even} &= (f_{x,2} + f_{x,4})
\end{aligned}$$

Again, it is useful to start the controller design process for channel 2 by assessing the open loop step response of the plant. For this the transformation matrix, $T_{x,\dot{\psi}}$ is included in the forward loop, to transform one control input, $f_{x,\dot{\psi}}$ into four longitudinal wheel forces, $f_{x,i}$. The open loop step response for a range of vehicle velocities is shown in figure 3.16. It can be seen that the steady state values are small, indicating that the plant gain is low. However, the speed of response is much quicker than that of channel 1, and is a first order response depending on v_x, with a pole at location $-P(v_x)$. The corresponding open loop Bode plot of L can be seen in figure 3.17, which is again plotted for a range of vehicle velocities. However, in all open loop Bode plots hereafter which show a range of velocities, the phase margin will not be marked so that the plots remain presentable and clear.

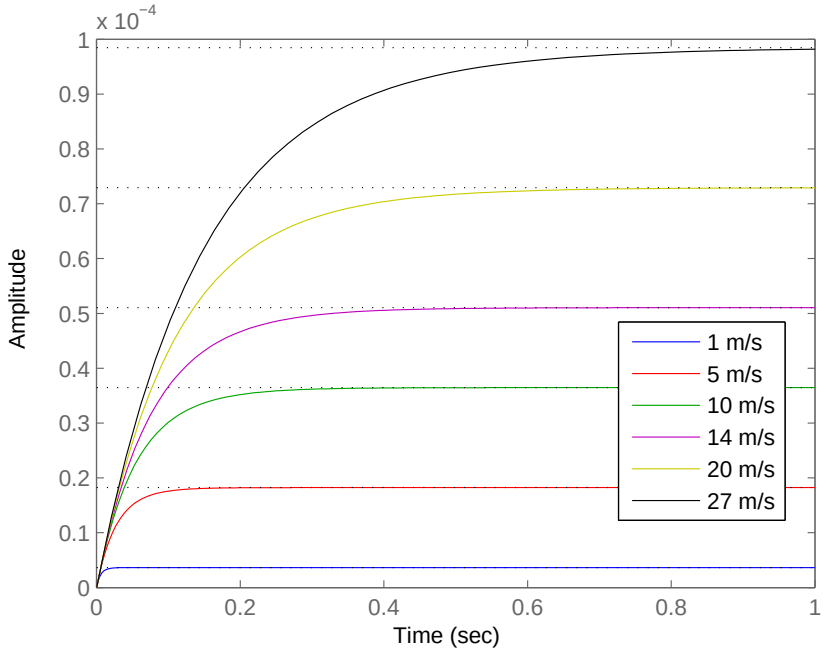

Figure 3.16: Open loop step response of $G_{\dot{\psi}}\,T_{x,\dot{\psi}}$ for varying v_x

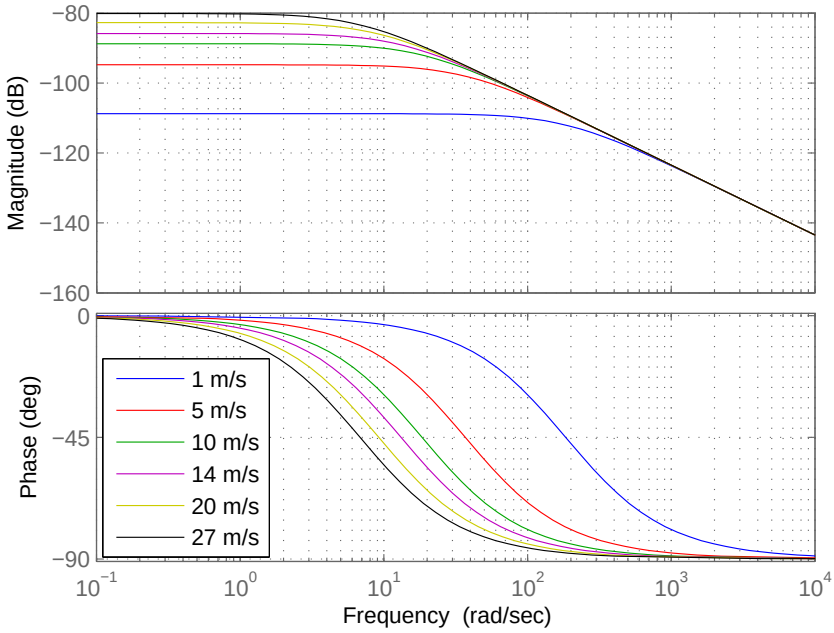

Figure 3.17: Open loop Bode plots of $G_{\dot{\psi}}\,T_{x,\dot{\psi}}$ for varying v_x

Importantly, the shape of the open loop Bode plots of L in figure 3.17 is not undesirable, but the magnitude of the low frequency gain is extremely low, and as such will not possess good disturbance rejection properties. Furthermore, a steeper roll off at high frequencies will help with disturbance rejection. As before, one solution to increase the low frequency gain, is to use some pure proportional gain for the controller. Therefore, looking to increase the crossover frequency to approximately 7 rad/s it can be calculated that moving the magnitude plot upwards 95 dB to 0 dB is almost equivalent to $10e^4$. This is a good starting point, and so the proportional gain for channel 2 is set as

$$K_{p3} = 10e^4,$$

where the subscript 3 is used to identify this as the yaw rate controller — the 3rd state of the vehicle model. Plotting the open loop Bode plots for $(G_{\dot{\psi}}\, T_{x,\dot{\psi}}\, K_{p3})$ for the range of velocities, produces the plots in figure 3.18.

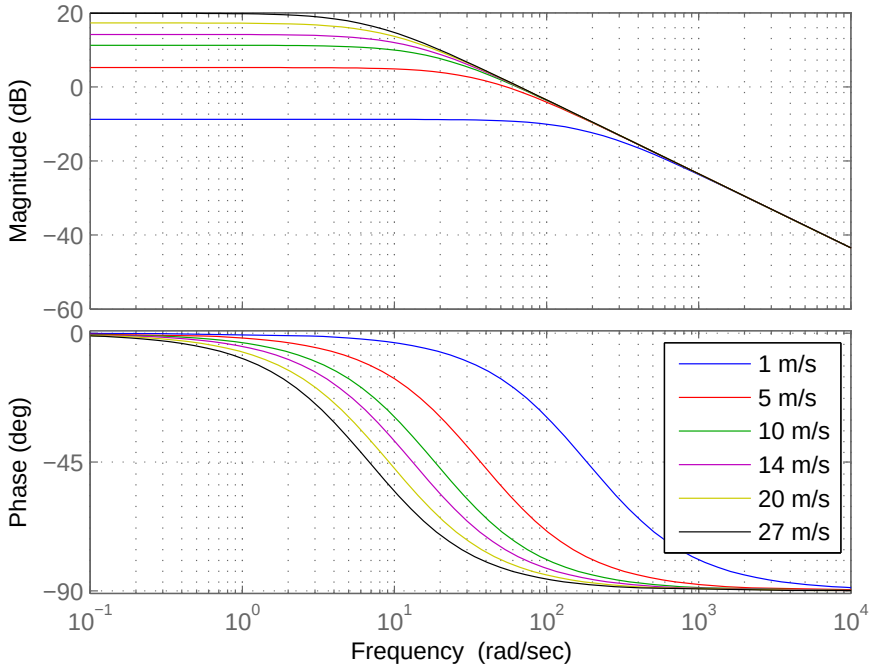

Figure 3.18: Open loop Bode plots of $G_{\dot{\psi}}\, T_{x,\dot{\psi}}\, K_{p3}$ for varying v_x

The proportional gain has shifted the magnitude plot upwards, and allowed a phase margin

to be defined for every vehicle speed with the exception of 1 m/s, since the magnitude plot is still below the 0dB line. However, there is an argument to say that the controller would not be necessary for low speeds and surely not at 1 m/s, — although it is plotted here to complete the velocity spectrum. The gains for the range of other velocities are not very large, and as a result may still lead to disturbance rejection problems. This will be evaluated in the same manner as for the design of the controller for channel 1, using S and T plots. It can also be seen that the crossover frequency is approximately 60 rad/s, which would indicate a bandwidth of similar magnitude. From available literature [29, 36, 42], and the design specification, this would appear too large. Instead a bandwidth in the region of approximately 7 rad/s is required. In summary, the large gain is required to move the magnitude plot upwards above the zero dB line. Now the loop gain has the be further shaped, while maintaining the large gain.

Before progressing and altering the controller, the S and T plots for the system with the current controller gain can be examined to confirm if the fears of poor disturbance rejection are correct. If so, information from the plots can be used to improve the controllers and hence, the system performance. Using the previously defined expressions for S and T (equations (3.2) and (3.3)), the respective plots are computed and shown in figures 3.19 and 3.20.

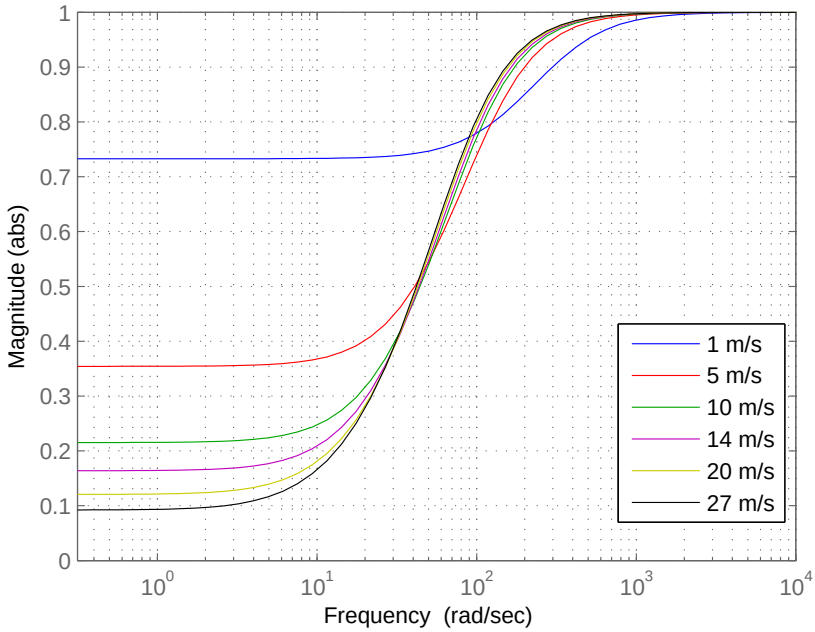

Figure 3.19: Sensitivity plots of $G_{\dot{\psi}}\, T_{x,\dot{\psi}}\, K_{p3}$ for varying v_x

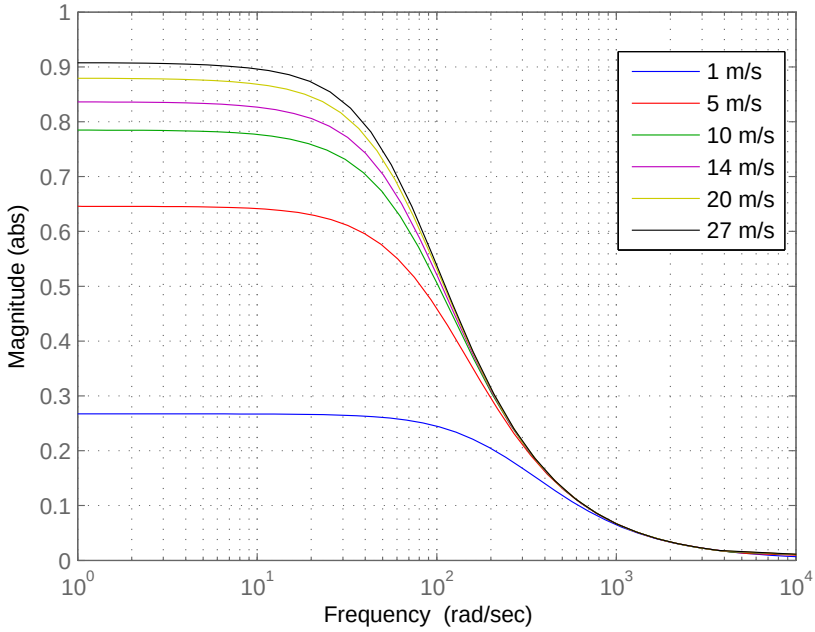

Figure 3.20: Complementary sensitivity plots of $G_{\dot{\psi}}\, T_{x,\dot{\psi}}\, K_{p3}$ for varying v_x

It is clear from figures 3.19 and 3.20, that the system does not possess good disturbance rejection properties, and the controller will not perform as desired. A sensitivity plot with a magnitude very close to zero at low frequencies shows that the system will reject disturbances effectively, and they will have no effect on the output of the system. It can be seen that this is not the case, but as the vehicle velocity increases, the behaviour of the system improves. In conjunction with this, the complementary sensitivity plot should be one at low frequency indicating that the output of the system is 100% of the closed loop transfer function. It can be concluded from this, that disturbance rejection must be improved — especially at low frequencies, since at higher frequencies the ideal characteristics are observed.

Figure 3.21 shows the closed loop step response of $G_{\dot{\psi}}\, T_{x,\dot{\psi}}\, K_{p3}$. From this figure it can be seen that the yaw rate response is a first order response with a rise time dependent upon v_x. Furthermore, the slower the speed of the vehicle, the larger the steady state error becomes.

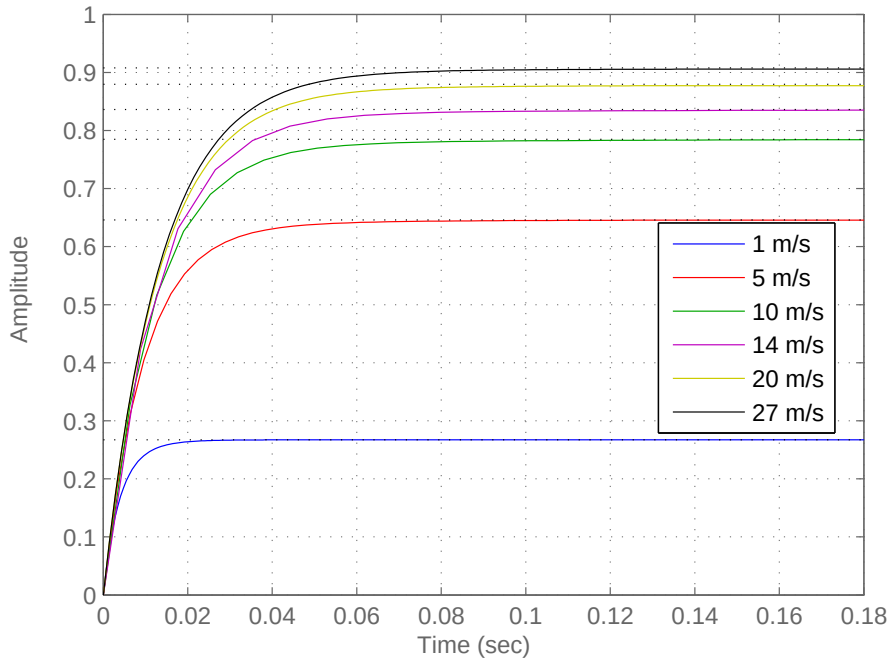

Figure 3.21: Closed loop step response of $G_{\dot{\psi}}\, T_{x,\dot{\psi}}\, K_{p3}$ for varying v_x

The widely ranging steady state errors would indicate that some scheduling with respect to vehicle velocity is required. However, neglecting the two lower velocities and the largest

velocity also, (since they are far away from the equilibrium position) there remains three plots which are relatively similar, as can be confirmed by the open loop Bode plot of L in figure 3.18.

The plots of sensitivity and complimentary sensitivity functions, together with the closed loop step response, highlight the need for the low frequency gain to be increased. However, increasing the proportional gain of the controller will increase the gain of the system over all frequencies, and increasing the high frequency gain may result in amplification of unwanted high frequency dynamics. Furthermore, it will increase the crossover frequency through lifting the magnitude plot upwards, which results in a decrease in the phase margin and as described earlier, will make the system less robust. Ideally, the low frequency gain should be increased, the crossover frequency decreased and the gain at higher frequencies should continue to roll of quickly, to avoid any effects of the high frequency dynamics.

Placing a pole at the origin allows a steeper roll off at higher frequencies and provides infinite low frequency gain, removing any steady state error. Therefore, expanding the proportional gain (K_{p3}) to include a pole at the origin (s=0) will result in the expression

$$K_{33} = \frac{K_{p3}}{s}, \tag{3.19}$$

and the system now becomes second order.

Implementing this controller into the current structure, results in the open loop Bode plots of L in figure 3.22. Upon comparison with figure 3.18, it can be seen that at low frequencies the constant value has now changed to a slope of 20 dB/decade, giving infinite gain at zero frequency. A decrease in the crossover frequency has also been achieved, where it now occurs between 4 rad/s and 7 rad/s depending on the velocity of the vehicle. At higher frequencies, the roll off is now 40 dB/decade due to the addition of the second pole. This fast roll off will help to keep the effect of high frequency unmodelled dynamics to a minimum.

The gain margin from the open loop Bode plot in figure 3.22, can be calculated to always be infinite since the phase plot does not cross the $-180°$ line. The phase margin however, changes considerably as the vehicle speed changes. Varying from almost 90° at v_x =1 m/s to approximately 60° at v_x = 27 m/s. This spread of gain margin remains greater than the accepted minimum of 30° at all times, and include ample 'cover for the effect of time delays'.

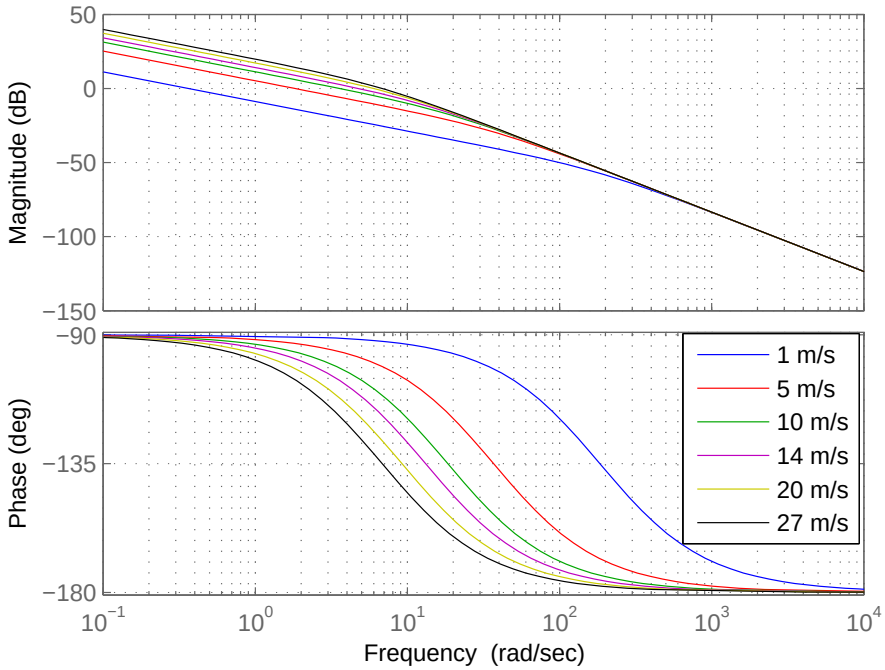

Figure 3.22: Open loop Bode plots of $G_{\dot{\psi}}\, T_{x,\dot{\psi}}\, K_{33}$ for varying v_x

It can therefore be concluded that the controller will remain robust enough when the vehicle is travelling within this range of velocities. It is observed that ω_c at 1 m/s and 5 m/s is too small, and arguably 27 m/s is too quick for our system. However, the other four velocities meet the design criteria well and it is these four velocities which will be most commonly used whilst controlling the vehicle dynamics (although on one or two manoeuvres the vehicle velocity decreases to roughly 5 m/s).

The closed loop step response for the revised controller is shown in figure 3.23, again for varying vehicle velocity. Two important points can be identified from this figure. Firstly, as the velocity increases, the rise time decreases and secondly (and most importantly), there is no steady state error. Removing the quickest and the two slowest velocities, similarities can be found between the remaining responses. The rise times are of the same order, and it can be concluded that the controller will perform similarly when the vehicle speed is within this range.

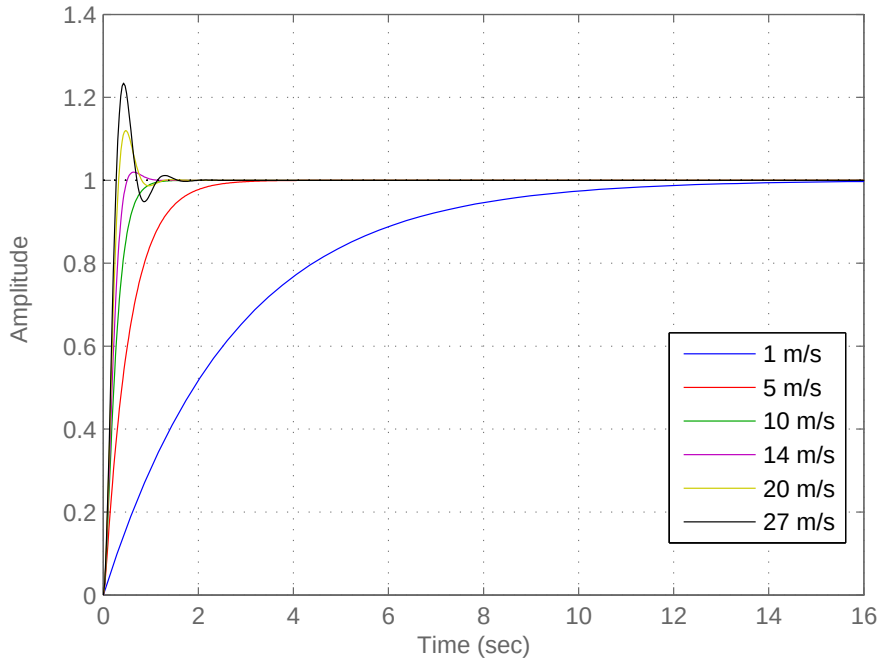

Figure 3.23: Closed loop step response of $G_{\dot{\psi}}\, T_{x,\dot{\psi}}\, K_{33}$ for varying v_x

The other plots which are used to aid and validate the controller design process are the sensitivity and complementary sensitivity plots, shown in figures 3.24 and 3.25. Both of these plots show that the system now possesses the correct disturbance rejection properties The sensitivity plot (see figure 3.24) shows that as the vehicle velocity increases, the system becomes more sensitive, and furthermore, a peak occurs, which also increases in magnitude as the velocity increases. However, these peaks are relatively small and give no cause for concern in terms of system stability.

3.3.3 Summary

The two designed channels of the feedback controller appear to be satisfactory in terms of possessing the correct robustness and stability properties. As such, they are now ready to be implemented into the nonlinear models for evaluation through simulation in chapter 5, and hardware in the loop in chapter 6.

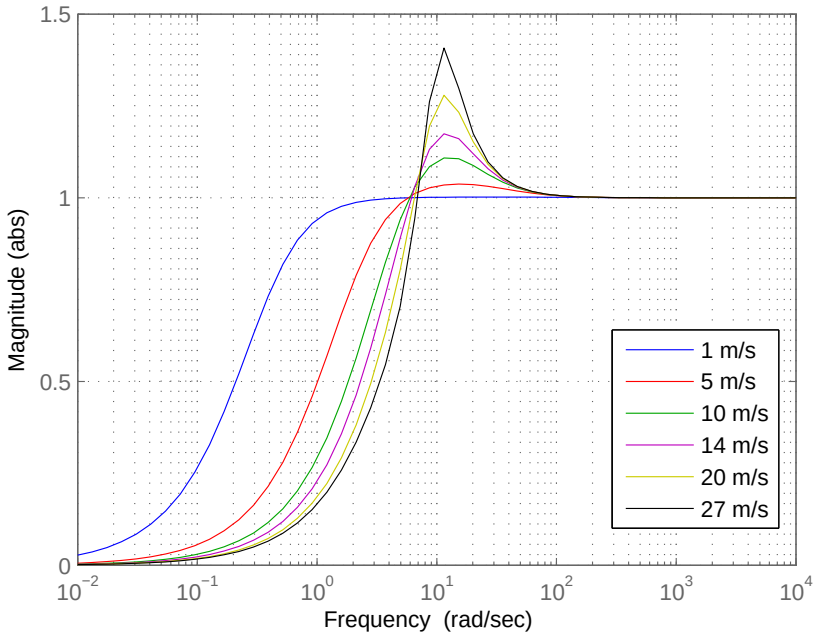

Figure 3.24: Sensitivity plots of $G_{\dot{\psi}}\, T_{x,\dot{\psi}}\, K_{33}$ for varying v_x

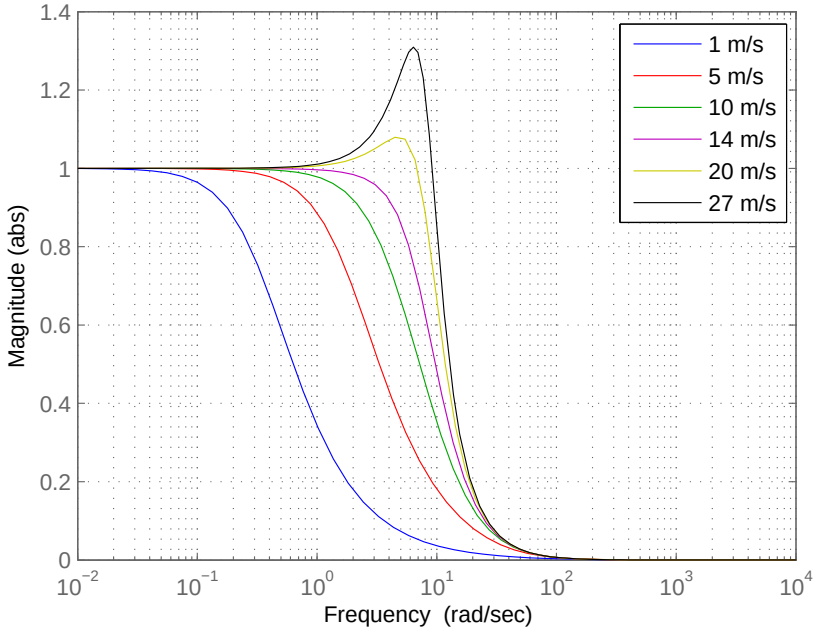

Figure 3.25: Complementary sensitivity plots of $G_{\dot{\psi}}\, T_{x,\dot{\psi}}\, K_{33}$ for varying v_x

3.4 Integrated feedback and steering control

One further aim of this work is to integrate front wheel steering with the already designed feedback controller, to evaluate if any advantage can be gained from using integrated steering and wheel force control.

Steering control has to be included without having a negative impact on the performance of the two channels of the feedback controller. One possible method is to use feedforward based control to act directly on the plant. By doing this, the delays associated with feedback control are avoided. The steering angle is calculated directly from an 'ideal' vehicle model based on the yaw rate reference, and methods have similarly been adopted in [32, 35]. Importantly, in line with the modelling assumptions in chapter 2, this steering angle will be small, since the yaw rate from which it is generated is small, hence the assumptions will not be violated by this extra control loop.

Figure 3.26 shows the proposed feedforward based structure combined with the feedback control of wheel forces. $(G_{\dot{\psi}})^{-1}$ denotes an inverse model, mentioned in more detail later. Importantly, this G is not the same G used earlier in this chapter. It is referred to as *feedforward based* because it is applied to the model in a feedforward manner, but is constantly updated with v_x.

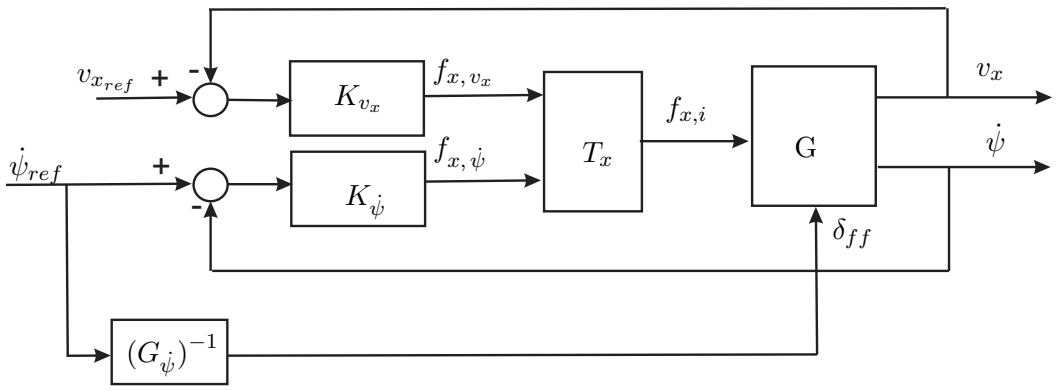

Figure 3.26: Feedforward based control structure

Firstly, a relationship between steering angle and yaw rate is identified in [85] as

$$\dot{\psi}_{ref} = \frac{a\, v_x}{1 + b\, {v_x}^2}\, \delta \tag{3.20}$$

where a and b are constants,

$$a = \frac{1}{l_f + l_r} \qquad\qquad b = \frac{m}{(l_f + l_r)^2}\left(\frac{l_r}{c_f} - \frac{l_f}{c_r}\right).$$

Equation (3.20) can be rearranged to obtain the required steering command, δ_{ff}, from the desired yaw rate, $\dot{\psi}_{ref}$,

$$\delta_{ff} = \dot{\psi}_{ref}\,\frac{1 + b\,{v_x}^2}{a\,v_x}, \tag{3.21}$$

and it is this expression (equation (3.21)) that appears inside the box labelled '$(G_{\dot{\psi}})^{-1}$' in figure 3.26. The expression must be accurate, otherwise the steering angle which is applied will not have the desired effect on the vehicle, and the wheel force control system may become more active to overcome negative effects from inaccurate feedforward steering signals. This signal is a steering angle which is calculated in real-time using, amongst others v_x and $\dot{\psi}_{ref}$. v_x is likely to change during the test manoeuvres, so although the yaw rate reference does not change, the steering angle will change as v_x does in an attempt to always achieve the value of $\dot{\psi}_{ref}$. This expression is based on work by J. Ackermann where the behaviour of δ and $\dot{\psi}$ has been accurately mapped. It has also been tested within the three available models to ensure that the output is correctly calculated.

3.5 Regulating vehicle sideslip

Controlling the vehicle longitudinal velocity allows the vehicle sideslip to be regulated. However, some meaningful reference signals must be generated. It was described earlier in this chapter that the velocity reference can be generated using the sideslip reference and the current lateral velocity.

While it would be desirable to control sideslip to zero, in this work it is not practical. Either v_x would have to be infinitely large, or v_y would need to be zero. Therefore, the sideslip reference is defined simply as a range of β around a reference value of zero (i.e $\beta_{ref} = 0 \pm \beta_{th}$, where β_{th} is the threshold or deadband region). When this is the case, the controller should remain inactive. However, when this region is exceeded, the controller should become active to reduce the sideslip. As such, the reference signal for the vehicle

velocity is always calculated in real-time, regardless of whether the controller is active or not. This is depicted in figures 3.27 and 3.28, where β_{th} is the threshold value for β.

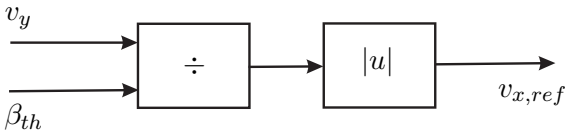

Figure 3.27: Generation of v_x reference signal

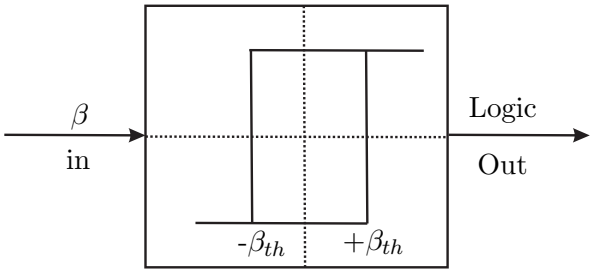

Figure 3.28: Control logic using vehicle sideslip deadband

Figure 3.27 is derived from the basic equation for calculating the vehicle sideslip, i.e

$$\beta = \frac{v_y}{v_x} \tag{3.22}$$

The block labelled $|u|$ is used to ensure that the sign of the output signal, $v_{x,ref}$, is always positive. If this was not used, a scenario will exist where the reference value for velocity is negative, which indicates that the vehicle must reverse.

The logic signals used to activate and deactivate the velocity controller are shown in figure 3.28. In this case, the current value of β is compared with the upper limit and lower limit of the threshold. Within this work, these limits will both have the same magnitude and only the sign will differ. However, it is feasible to have different magnitudes to represent the upper and lower limits of the threshold. If β is larger than the threshold, then the output will be logic 1, else logic 0 will be output. This logic signal is finally multiplied by the controller output, so logic 1 indicates that β needs to be reduced, and logic 0 indicates that no action is required at that time step.

The diagram of the complete control structure is shown in figure 3.29. This figure includes

the calculation of β and the generation of the reference signal for v_x. The box labelled 'fig.3.28' contains the contents of figure 3.28.

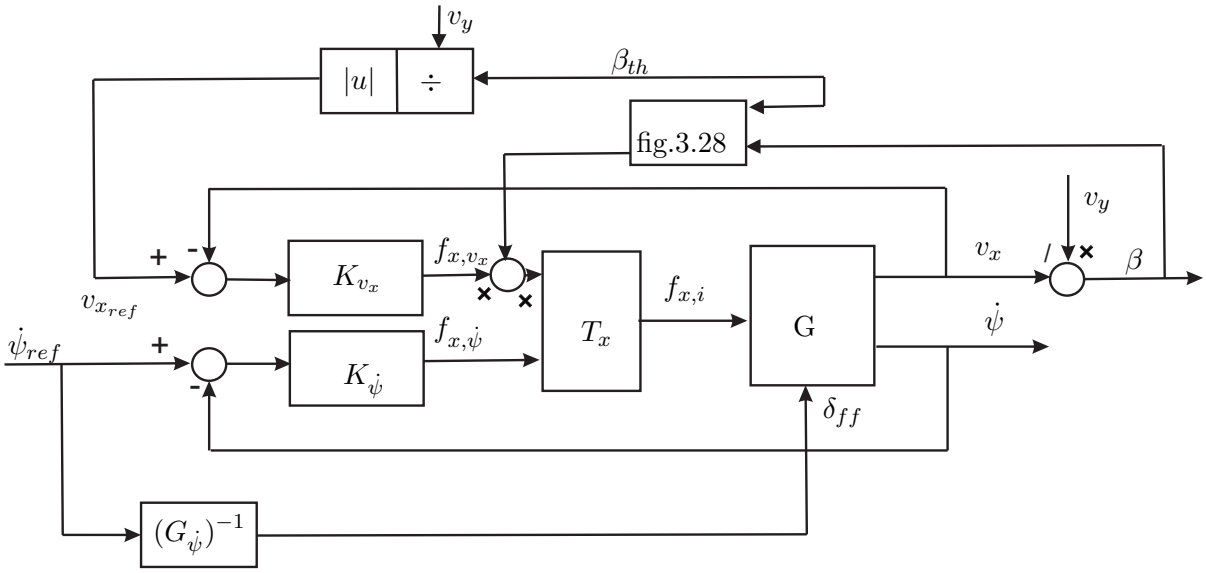

Figure 3.29: Complete control structure

3.6 Conclusions

In this section frequency based methods have been used to design a 2 channel feedback controller. Moreover, available methods have been used to assess the likely performance of the system in the presence of disturbances. The structured approach has shown that the design process is fairly straightforward, when some design principles are understood and implemented. The two channel feedback controller has been designed with system stability and robustness in mind.

The feedforward based steering signal is used to complement the feedback control structure, in that it is designed to reduce the work load on the feedback controller when regulating yaw rate. The steering angle is calculated from a simple expression relating steering angle to yaw rate. Ideally, the feedback will no longer be required to control the yaw rate, but only be used to control the velocity, while the steering control is present.

Chapter 4

Human interface test rig

This chapter introduces and describes a human interface test rig which is used within this thesis. The test rig is integrated with a vehicle model, and the outputs of the vehicle model are used to plot the trajectory of the vehicle in real-time, resulting in an effective driver simulation environment.

4.1 Aim of the driver interface test rig

The aim of the driver interface test rig is to allow a human to interact with a vehicle model running on an office PC. By applying a steering wheel angle from the test rig direct to the model, the driver will be able to dictate the intended direction of the vehicle. The human interface test rig will be integrated with a visual feedback setup to allow the driver to complete manoeuvres and see the vehicle trajectory in real time. In addition to the vehicle position being fedback to the driver, force feedback from the test rig will also be experienced. The RTSM vehicle model from chapter 2 is used to interact with the test rig.

4.2 Test rig - component level

This section describes the working components of the driver interface test rig in some detail. The rig is useful for designing and testing a wide range of possible steer by wire systems, ranging from velocity dependent steering ratios, to the other extreme of a car turning left when the steering wheel is turned to the right. However, more importantly it allows driver interaction with hardware and software testing.

Figure 4.1 shows a steer-by-wire (SbW) system. In such a system, the steering wheel is connected to a sensor which measures the angle of the steering wheel, and a motor which provides feedback to the driver. Motor 2 applies the required angle to the road wheels, with the pinion angle sensor measuring position of the pinion. The components of the test rig used in this work are highlighted by the dashed black circle. This test rig could fit into a more technical setup in possible real cars.

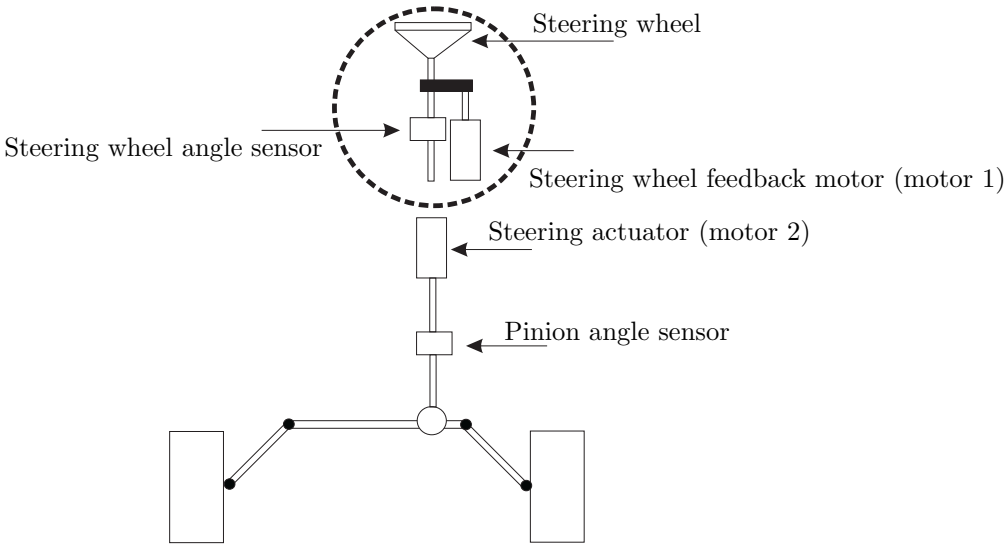

Figure 4.1: Diagram of a steer by wire system, including components of the interface test rig

Motor 1 in figure 4.1 is used to provide torque. The motor (RBE03014, Kollmorgen [1], Germany) is a Brushless Direct Current (BLDC) servomotor and is used to provide feedback to the driver (in a similar fashion to a traditional steering system). If the steering system is power assisted, there is seldom any need for an output torque in excess of 5 Nm [106]. However, in order to generate a feedback torque to the driver which resembles a traditional steering system, the motor must be capable of handling higher torques. This results in motor 1 being able to generate a continuous torque of 40.9 Nm and peak torque of twice as much. The torque which is supplied to the motor is controlled using current and a motor interface with a reference signal given as a voltage between $\pm$ 10 V, where 10 V relates to the maximum torque while the sign dictates the direction. At 0 V the torque is zero. This means that for a given voltage, a certain torque is applied. The motor interface (TWR34,

[1] http://www.kollmorgen.com

Maccon, Munich, Germany) is supplied with 28 V.

The position of the steering wheel motor is measured using a 2-pole resolver [2], which is converted to a quadrature encoder signal using a 12 bit resolver-to-digital converter. The resolver, which is integrated within the steering wheel motor, measures the driver's input as the angular position of the steering wheel, and the motor provides the driver with a torque feedback generated from the steering system.

The quadrature incremental encoder signal is connected to a four channel quadrature encoder input board (PCI QUAD04, Measurement Computing) [3] with 24 bit resolution. Two inputs to this board are used — Phase A and Phase B, which are generated with 90° offset to each other, and give information about position, velocity and direction.

A data acquisition (DAQ) card (NI6025E, National Instruments, Austin, Texas, USA) is used to interface the test rig with the PC. This allows data to be read in and out of the PC and Test rig.

Incorporated into the test rig is an emergency stop button which cuts off the power supply to the rig.

4.3 Complete system

The complete system overview is shown in the diagram in figure 4.2. The driver uses the interface test rig to input a steer angle, while attempting to complete a pre-defined test manoeuvre. The steer angle is accepted as an input to the vehicle model running on the xPC target machine in real time. The manoeuvre which the driver attempts to complete through steering is shown as a trajectory on the monitor of the animation PC (anim PC), which provides visual feedback for the driver. Finally, the host PC is used to collect the data from and interface with the target PC.

[2] http://www.maccon.de
[3] http://www.measurementcomputing.com

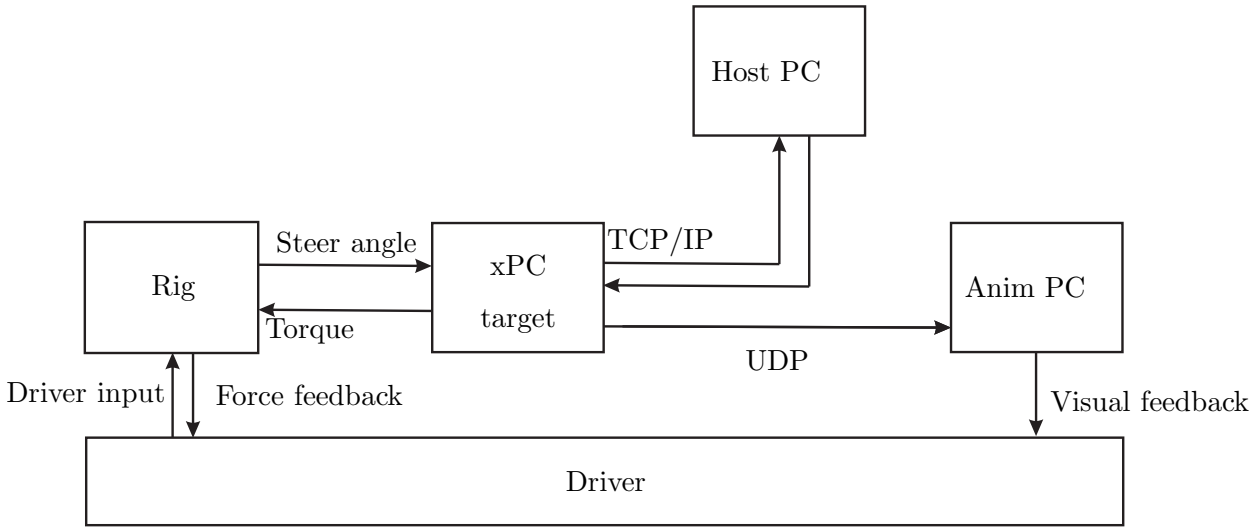

Figure 4.2: Overview of the system communication

In the laboratory, the full system is setup as shown in figure 4.3. In this figure, starting from the right hand side, the test rig is shown next to the target and host PC's. The latter two of these will be explained in the next section. From figure 4.3 the driver interface test rig can be seen highlighted in yellow. The animation PC is the laptop enclosed inside the red box, and this is the monitor that the driver uses when attempting to complete the test manoeuvres. The target PC can be seen just out of the picture at the bottom right hand corner, enclosed within the pale blue box. Finally, the host PC is shown on the left of the photograph, highlighted in green.

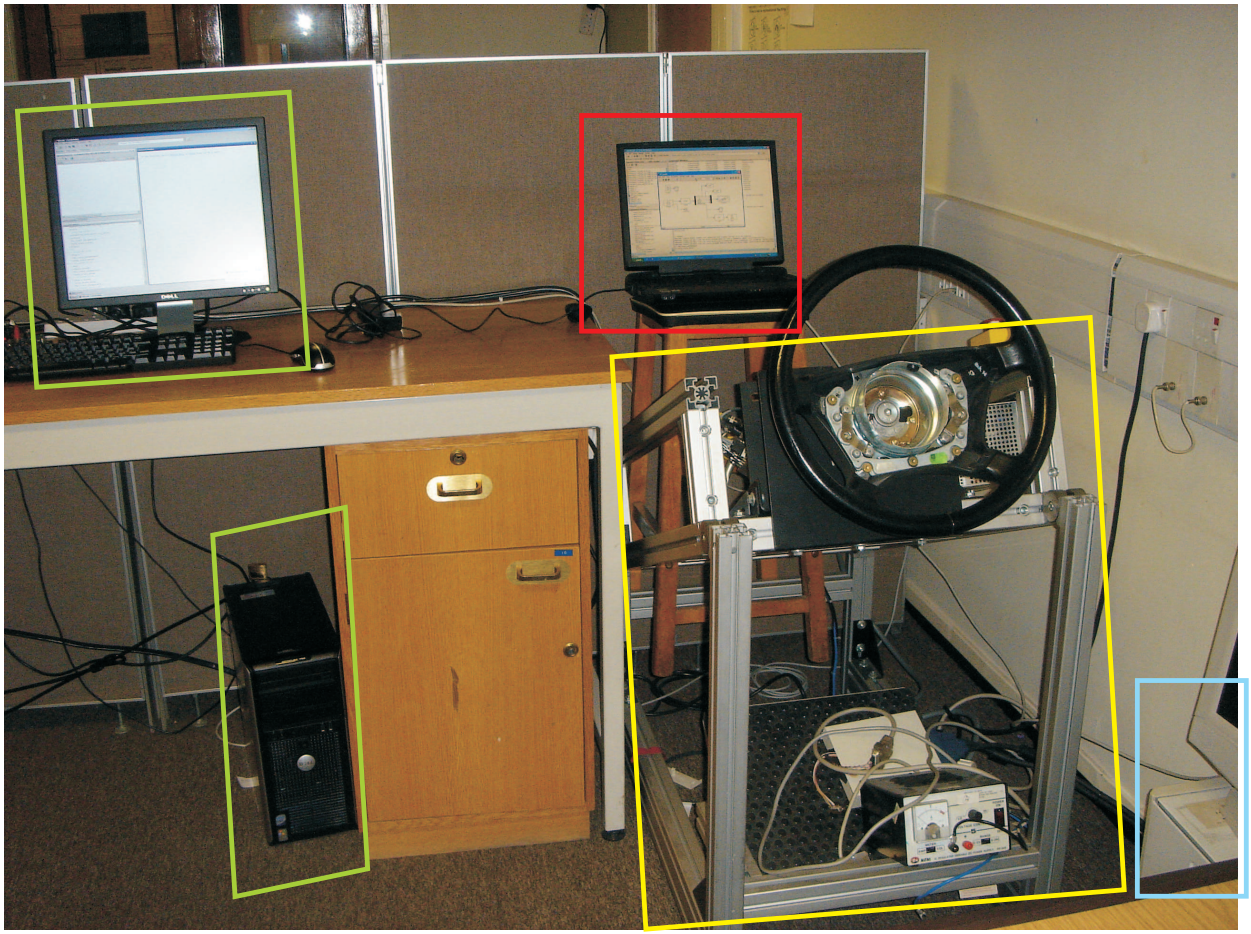

Figure 4.3: Photograph of the test rig, target, host and anim PC

4.3.1 Simulation model: xPC target/host PC

xPC-Target is an extension of the MATLAB software from Mathworks and is an application for Rapid Control Prototyping (RCP). The xPC-Target kernel can run on any PC-compatible computer system in hard-real-time. For the purpose of this work the xPC target machine was a standard PC for office use with a Pentium II processor working at 400MHz and with 256MB of RAM memory. The target PC interfaces directly to the test rig. The real-time simulation model (RTSM) described in chapter 2 is configured to accept the steering wheel angle from the interface test rig as an input, and also generate torque feedback. Then it is loaded onto the target PC from the host PC. The RTSM was simulated with a sample time of 0.02 seconds.

In addition to communicating with the test rig, the target PC is also linked to the host PC, which is a Pentium dual-core processor running at 2GHz, and with 2GB of RAM memory.

The two machines are configured to communicate using a TCP/IP connection, and a variety of information can be exchanged between them, including:

- The target application
- Control signals used to start/stop the simulation, change sample times and get information about the performance of the application/CPU
- Signal data (either post-simulation or soft-real-time transfer)
- Parameter values (again, either post-simulation or soft-real-time transfer)

4.3.2 Animation PC

The purpose of the animation PC is to provide visual feedback to the driver/human operator of the test rig. A soft-real-time animation runs on this PC, while the target PC simulates the vehicle model. The animation PC is a Pentium 4 laptop PC running at 2GHz with 512MB of RAM memory.

For the animation to be meaningful, some vehicle quantities must be made available to the animation PC. The target PC and the animation PC are linked using a User Datagram Protocol (UDP) connection, which allows the necessary data to be transferred. In order to plot the trajectory of the vehicle, the animation running on the animation PC requires the following signals: the longitudinal and lateral positions, the yaw angle, the road wheel angle and the vehicle velocity. This information must be packed into a single output vector prior to sending, and unpacked when received by the other PC before it can be used.

Real time animation

An animation has been created using an S-function in the Simulink environment, which is designed to display the current position of the vehicle and the trajectory travelled, both in real-time. To assist the driver, the dimensions of a gentle lane change manoeuvre described in chapter 5 have been plotted in the animation, which allows the boundaries of the manoeuvre to be displayed. The generated animation is a graphics object, created within a figure window. Updating this figure regularly enough enables it to be treated as a real-time visualisation. When the figure window is refreshed, the pre-programmed road layout and the position of

the vehicle relative to this road are updated. The animation model contains a real-time synchronisation function which samples at 0.06 seconds and ensures soft real-time using the windows clock.

Relative longitudinal movement between the road and the vehicle is shown by the road moving forwards or backwards. Thus the vehicle only moves laterally (steering and yaw etc.) Markers are used to visualise how fast the vehicle is travelling when the outlined trajectory is straight ahead. The markers are placed along the side of the road at 10 metre intervals to give an indication of the vehicle velocity. These markers, together with the trajectory/road and vehicle, can be seen in figure 4.4. The longitudinal and lateral position of the vehicle are also indicated. The front steer angle and vehicle yaw rate cause the vehicle to move laterally. At the top of this figure the road layout narrows at the point where the lane change area ends. The vehicle is shown during turning to complete the manoeuvre, and this figure was captured while carrying out a manoeuvre in real time.

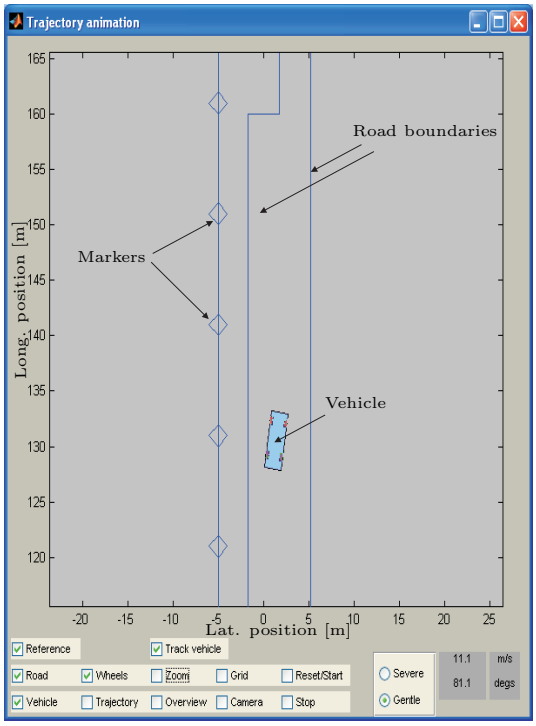

Figure 4.4: Screen shot of the trajectory animation, for driver aid

The dimensions of a desired test manoeuvre can be pre-programmed, to show the boundaries which the vehicle must remain within. For example, the outline of a lane change manoeuvre, or a straight ahead road to counteract disturbances acting on the vehicle can

be plotted on the animation, and the vehicle trajectory will be plotted in real time. This provides feedback using the real time information to a human to assist him/her to complete the test manoeuvres.

The vehicle starts from co-ordinates (0,0), and the coordinate system of the animation output is the same as the vehicle coordinate system.

Several check box options at the bottom of the animation figure enable the user to change the layout of the screen, all of which are self-explanatory.

4.4 Conclusions

This chapter has introduced the human interface test rig, which is used within this thesis to aid the driver in carrying out the test manoeuvres. This has been made possible by implementing a real-time animation within the Matlab environment, to accurately show the position and velocity of the vehicle. This will allow driver interaction with the vehicle lateral dynamics controller which was designed in chapter 3. Furthermore, driver interaction with the controller can be assessed, and the response of the controller can be compared with the response of the driver when completing the same test manoeuvres. The manoeuvres used to test the controller are described in more detail in chapter 5, and results from the experiments are shown in chapters 5 and 6.

Chapter 5

Evaluation using vehicle simulation

This chapter presents the results for the controller which was designed in chapter 3 using frequency based design techniques. The controller will be simulated using both the linear controller design model (LCDM) and verified simulation model (VSM) while carrying out the test manoeuvres described below. Following on from the description of the manoeuvres, results will be presented for a constant yaw rate test. First only the feedforward based steering response will be considered, followed by the feedback controller performance. Finally, the two control structures will be combined. Then results for a lane change manoeuvre will be presented, again with the three control structures: feedforward based steering only, feedback control and feedback control with feedforward based steering. Finally the main discussion will follow the presentation of the results.

It is important to mention here that the VSM contains TCS/ABS functions that ensures the applied longitudinal wheel forces are realistic and avoid excessive wheel slip.

5.1 Introduction of test manoeuvres

5.1.1 Constant yaw rate manoeuvre

The first manoeuvre to be defined is a vehicle travelling with a constant yaw rate. This manoeuvre is frequently used for testing vehicle dynamics controllers, especially in the case of lateral dynamics control and rollover avoidance [107]. In this work it will assess the capability of the controller to track two reference signals (v_x and $\dot{\psi}$) simultaneously. For this manoeuvre to be accomplished, both vehicle yaw rate and vehicle longitudinal velocity

must become constant at steady state. It follows that with a constant yaw rate and vehicle longitudinal velocity, the vehicle lateral velocity will also be constant, and since the vehicle sideslip is calculated from lateral and longitudinal velocity, it too will be constant.

The reference signal for vehicle velocity will be calculated to keep β within the threshold region. As introduced in chapter 3, $\beta_{ref} = 0 \pm \beta_{th}$, allowing the longitudinal velocity reference, $v_{x,ref}$, to vary depending on the magnitude of the lateral velocity at that given point in time. On the other hand, the yaw rate reference signal, $\dot{\psi}_{ref}$, will be defined as constant.

The vehicle will start with an initial velocity of 11.11 m/s (40 km/h), an initial lateral velocity of 0 m/s and an initial yaw rate of 0 rad/s. These are the same initial conditions as those used to compare the three different models in chapter 2.

5.1.2 Gentle lane change manoeuvre

The second manoeuvre is a gentle lane change manoeuvre which will provide a more realistic test for the controller.

This gentle lane change is a scaled version of the ISO lane change (ISO-3888:1991,2002) [108]. The ISO standard assumes a lateral shift of 5.6 metres within a longitudinal distance of 30 metres, and an initial vehicle velocity of 22 m/s. However, the scaled version used in this work dictates that the lane change will take place within a lateral shift of 3.25 metres and a longitudinal distance of 45 metres with an initial vehicle velocity of 11.11 m/s. These changes will relax the constraints on the vehicle during the manoeuvre and will also result in small magnitude inputs.

The scaled manoeuvre will return lateral accelerations at the vehicle centre of gravity (CG) of approximately 0.4 m/s^2, or 0.04 g. Therefore, the inputs to the vehicle will be small and will allow the approximations which were made to linearise the vehicle model to remain valid. Because the vehicle yaw rate changes sign and magnitude, the lateral velocity of the vehicle will also change, and as a result, so too will the vehicle sideslip. It is these changes of sign and magnitude that make this manoeuvre a good test for the controller.

Figure 5.1 shows the outline of the lane change as a dashed line labelled *cones*. The solid blue line marks a typical trajectory which could be taken.

This manoeuvre is used only to provide a yaw rate reference signal that is reflective of a genuine test manoeuvre. It is not intended to try and complete the lane change manoeuvre -

feedback of the vehicle position would be required for that. The aim of this test manoeuvre is to see if it is possible to simultaneously control a set of two realistic lateral dynamic signals, using primarily the longitudinal wheel forces.

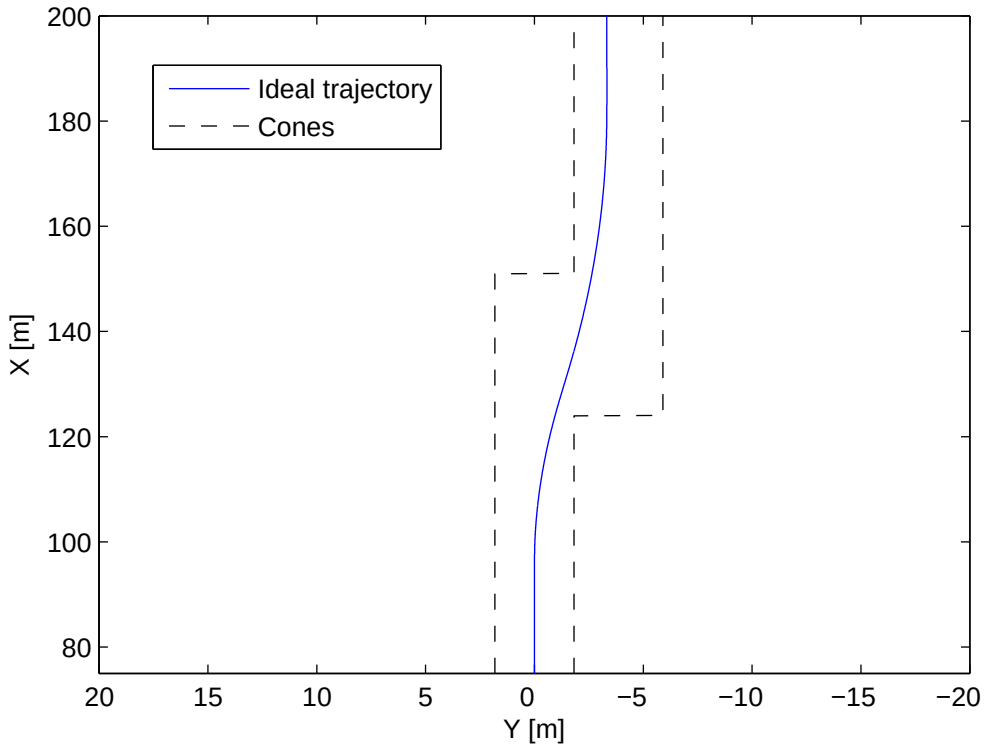

Figure 5.1: Gentle lane change manoeuvre definition

5.1.3 Controller architectures

In all sets of results, the *feedforward based steering* case is obtained first. The manoeuvre is acquired with no feedback control active, but only the feedforward steering signal with v_x dependency is connected (which is obtained from the inverse model $((G_{\dot{\psi}})^{-1})$ in figure 3.26 of chapter 3). Therefore, the applied steering angle will vary with v_x to achieve the desired yaw rate, which will be the same yaw rate reference signal as that used in the other controller architectures. Therefore, it provides a response against which the feedback controller can be compared.

Two other controller arrangements are used in addition to this setup. The first is the *feedback only* controlled setup. In this case, only the feedback controller is connected and

active while no steering input is applied. The other setup is *feedback control and feedforward based steering*. This arrangement combines feedback control and steering input.

In all cases when the feedforward based steering is active, it will generate the yaw rate as desired by the same reference signal that is used for the feedback controller. In some instances when only feedback control is used, only one of the two channels of the feedback controller may be activated (e.g vehicle sideslip channel activated whilst the yaw rate channel is deactivated, or vice versa). This will be performed to highlight how the channels perform individually, especially if their performance deteriorates somewhat when the two channels are combined.

Finally, the caption on each set of results will indicate which vehicle model was used. This will be abbreviated as

LCDM Linear controller design model

VSM Verified simulation model

5.2 Constant yaw rate manoeuvre

5.2.1 Feedforward based steering

The results shown in this section have been obtained with only the feedforward based steering active using the verified simulation vehicle model (VSM). A steering wheel angle is applied as a feedforward signal, designed to give a vehicle yaw rate of 0.05 rad/s. This value for yaw rate has been chosen for all controller architectures for this test manoeuvre, allowing comparisons between the different setups to be easily made.

Therefore, the results in figure 5.2 show how vehicle with only front wheel steering can generate a yaw rate of $\dot{\psi}$=0.05 rad/s. Using the feedforward based steering signal, a road wheel angle, as shown in figure 5.2(d) is applied to the vehicle resulting in the yaw rate in figure 5.2(b). This yaw rate is very close to 0.05 rad/s, with a steady state error of approximately 3%. The value for the yaw rate reference in the controlled plots later in this section. This yaw rate gives rise to the sideslip angle in figure 5.2(c) at the vehicle velocity in figure 5.2(f). Figure 5.2(a), shows the trajectory which the vehicle follows as a result of the steering input.

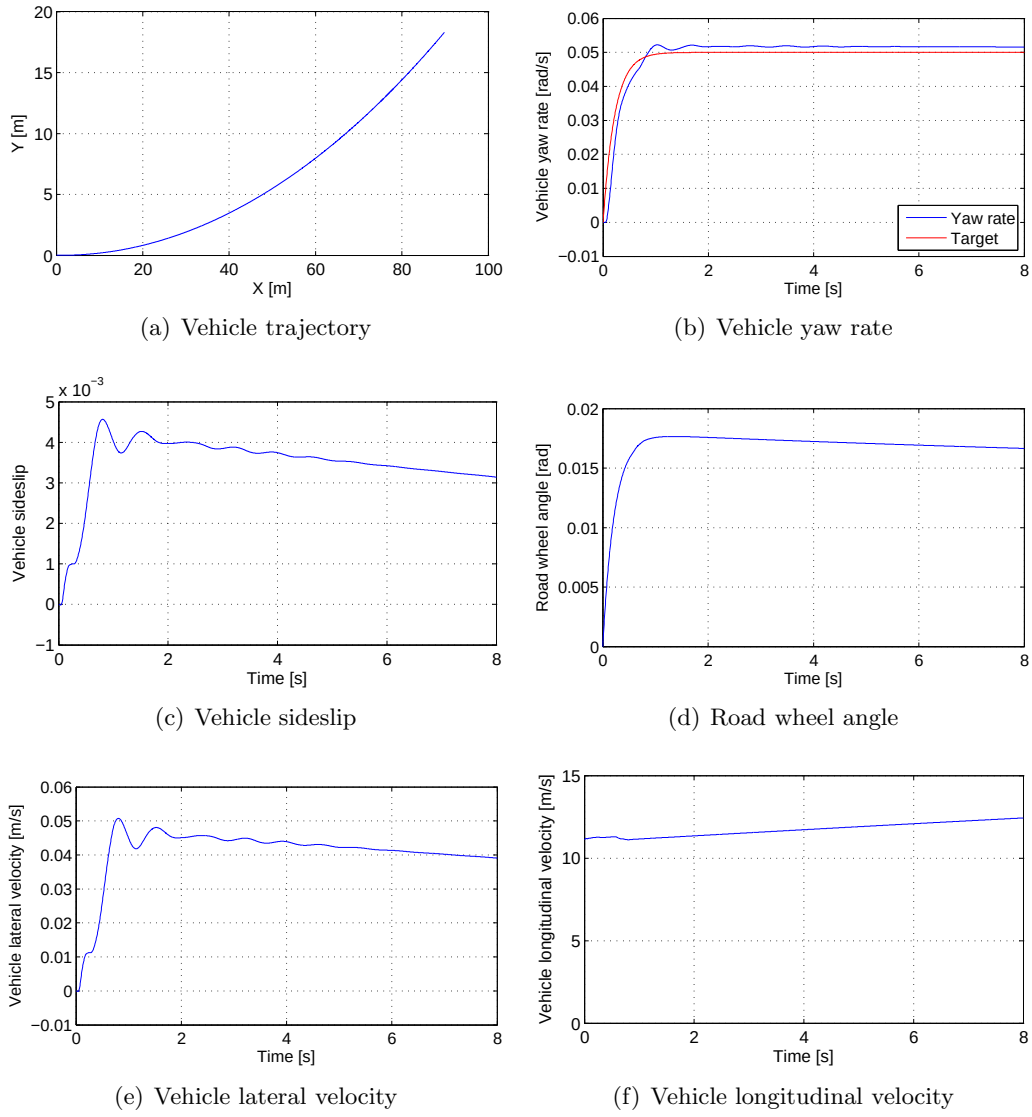

(a) Vehicle trajectory

(b) Vehicle yaw rate

(c) Vehicle sideslip

(d) Road wheel angle

(e) Vehicle lateral velocity

(f) Vehicle longitudinal velocity

Figure 5.2: Feedforward based steering for the constant yaw rate manoeuvre, using VSM

The yaw rate is seen to settle down and remain constant after approximately 2 seconds. From 2 seconds onwards, the road wheel angle starts to decrease as the vehicle longitudinal velocity increases, enabling a constant yaw rate to be achieved. This increasing longitudinal velocity and decreasing lateral velocity (figure 5.2(e)) gives rise to a decreasing vehicle sideslip, as shown in figure 5.2(c). Furthermore, this decrease in δ is due to the steering signal being dependent on v_x.

5.2.2 Feedback control

In this section, only feedback control is considered. Therefore, no steering is applied and both channels of the feedback controller are active at the same time. The linear controller design model is used first to evaluate the feedback controller, followed by the verified simulation model. It is expected that the controller will perform very well when used in the linear controller design model, since the controller was designed using that model. A yaw rate reference signal with the same magnitude as that in figure 5.2 is generated, and individual wheel force control is used to regulate the yaw rate while simultaneously controlling the vehicle sideslip to stay within the predefined range of $[-0.001 \ +0.001]$.

The value of ± 0.001 was chosen based on the results in figure 5.2(c). In this figure, the vehicle sideslip is seen to rise to 0.004 and remain larger than 0.003 at all times. Therefore, in order to determine if the controller is effective, the threshold must be smaller than the actual sideslip value, forcing the controller to demand a reduction in sideslip.

Using the linear controller design model

Figure 5.3(a) shows the trajectory of the controlled vehicle. The first thing to notice is the much larger distance that the vehicle travels compared to figure 5.2(a). The vehicle yaw rate and the reference signal are both plotted in figure 5.3(b), where no error can be seen, as the controlled signal follows the desired signal very closely. Vehicle sideslip is plotted in figure 5.3(c) together with the threshold signal — the value which the sideslip should not exceed. However, it can be seen that the threshold is initially exceeded, and after approximately 1.5 seconds the sideslip is reduced to the negative limit of the threshold, where, according to figure 5.3(h), the sideslip controller is deactivated. The delay in control is due to the vehicle reaching the desired speed. Obviously if the initial velocity was nearer the velocity required for the sideslip to be within the threshold, then the overshoot would be reduced — both in magnitude and duration. The vehicle sideslip is controlled by altering the vehicle longitudinal velocity, and once the sideslip angle is within the threshold region, the controller is deactivated. It would be re-activated if the threshold is exceeded.

As shown in figure 5.3(d), the small difference between left and right wheel forces after 1.5 seconds can be associated with generating and maintaining the desired yaw rate, since the

vehicle sideslip does not require to be controlled. Moreover, the demanded wheel forces peak at a magnitude that is excessive in terms of what is achievable from the wheel. Importantly, there are no actuator limits within this linear vehicle model. However the the RTSM and VSM both represent the nonlinearities of the real system more accurately, with the latter of the two doing so more significantly. The road wheel angle in figure 5.3(e) is zero, and the lateral velocity, v_y, generated by the differential style wheel force distribution is shown in figure 5.3(f), which has the correct behaviour at steady state for a constant yaw rate and vehicle longitudinal velocity. Finally, the longitudinal velocity and the corresponding reference signal are shown in figure 5.3(g). The performance of this controller is very good, but an initial delay can be seen between the two signals, due to the sideslip controller not being immediately activated at time $t = 0$, while the vehicle sideslip is within the threshold. Also, at time $t = 0$, the vehicle has not started to turn, therefore $v_y = 0$ and hence $v_{x,ref} = 0$.

Figure 5.3(g) shows a very quick increase in vehicle velocity to regulate the vehicle sideslip. This increase equates to an acceleration of approximately 30 m/s^2, which is very fast and impractical to implement. The demanded increase in the vehicle velocity is calculated using the model, so while the model may be adequate for control design it may not accurately represent a real vehicle when simulating manoeuvres, due to the lack of actuator limits etc. The same effect is also seen with the LCDM in the feedback control and feedforward based steering manoeuvre in figure 5.5(g).

Attention is drawn to the plots showing the longitudinal velocity of the vehicle and the reference signal, both in this figure and all of the remaining figures. Firstly, the reference signal is only shown when the value of sideslip exceeds the threshold, otherwise no reference is required (when the sideslip controller is deactivated). Secondly, because the reference signal for the longitudinal velocity, $v_{x,ref}$ is calculated instantaneously at each time step and does not take into account the acceleration/deceleration dynamics of the vehicle, an error is likely to exist between the reference signal and what is physically possible for the vehicle to deliver.

Overall, the controller behaves well when evaluated with the LCDM. This is expected since this model was used to design them. However, the verified simulation model (VSM) will provide a more challenging test for the linear controller — in an environment where nonlinearities and modelling errors exist.

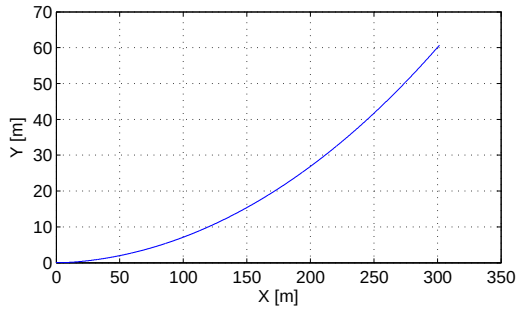

(a) Vehicle trajectory

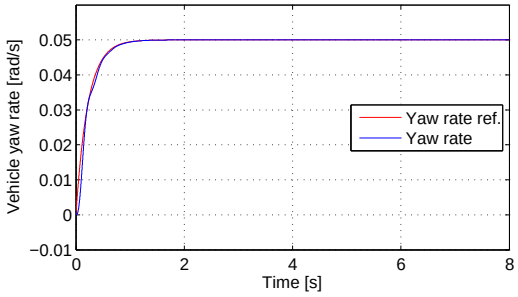

(b) Vehicle yaw rate

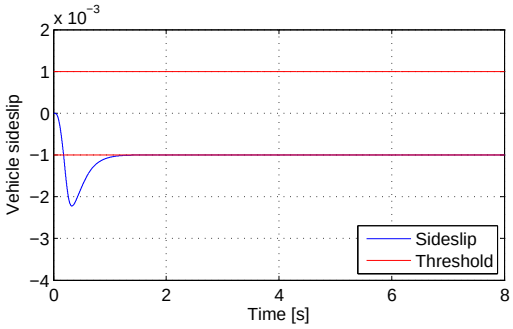

(c) Vehicle sideslip

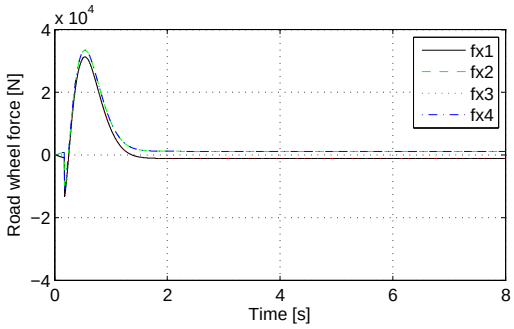

(d) Demanded longitudinal road wheel forces

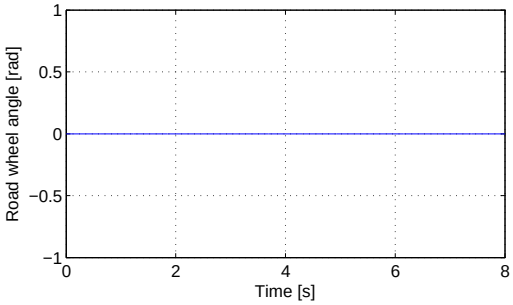

(e) Road wheel angle

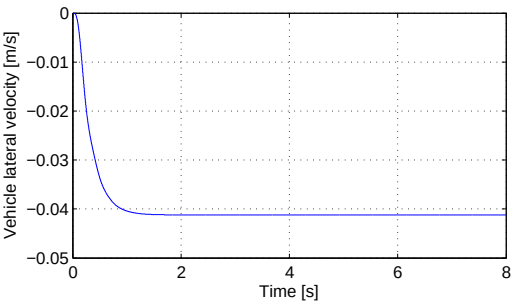

(f) Vehicle lateral velocity

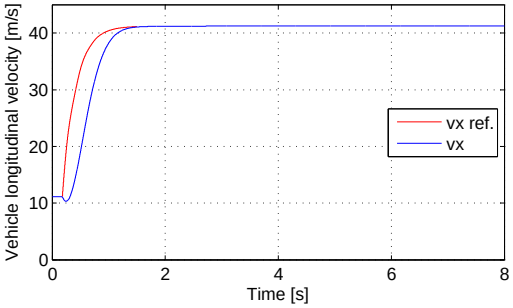

(g) Vehicle longitudinal velocity

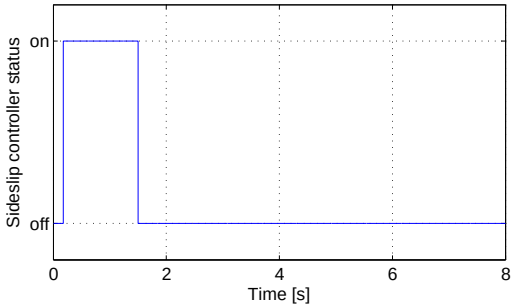

(h) Sideslip controller status

Figure 5.3: Feedback control for the constant yaw rate manoeuvre, using LCDM

Using the verified simulation model

The verified simulation model (VSM) is setup in the same manner as the LCDM and the results in figure 5.4 were obtained. This simulation was run for 15 seconds instead of 8 because the increasing velocity caused the sideslip to be very close to the threshold after 8 seconds. To show how the controller would cope with this, the simulation was run for a further 7 seconds.

The results show that there are indeed some nonlinearities and oscillations present when compared with figure 5.3. However, the yaw rate in figure 5.4(b) is well controlled with neither an offset nor a steady state error. There are oscillations at approximately 0.5 seconds and 10 seconds, which can be attributed to the change of longitudinal velocity. This change in velocity requires a change in differential wheel forces to generate the desired yaw rate, which initially overcompensates - and causes the peak. The required extra wheel forces can be seen in figure 5.4(d), which are realistic and feasible in behaviour and magnitude.

In figure 5.4(c), the sideslip and the threshold are plotted together. The control concept is again to try and keep the vehicle sideslip within the threshold. However, the threshold is exceeded for the first 0.75 seconds, while the velocity is decreased as necessary. After this initial 0.75 seconds, the sideslip controller is turned off which can be verified from both figures 5.4(d) and 5.4(h). Similar to the LCDM results, the difference between the forces on the left and right hand sides of the car can be identified as generating and maintaining the required yaw rate. Only the demanded longitudinal wheel forces are used for the control objective, and this can be seen from figure 5.4(e), where the road wheel angle is zero for the whole duration of the manoeuvre, and the applied longitudinal road wheel forces are steady state non-zero and within the actuator limits.

Finally, the vehicle velocity and its reference signal in figure 5.4(g) also show that after the initial 0.75 seconds, the controller turns off and the velocity starts to increase steadily but slowly due to the internal driver model. As the longitudinal velocity starts to increase, so too does the lateral velocity. This non steady state lateral velocity is responsible for the non steady state vehicle sideslip, which heads towards the lower limit of the threshold. However, the controller deals with this well and decreases the vehicle speed momentarily.

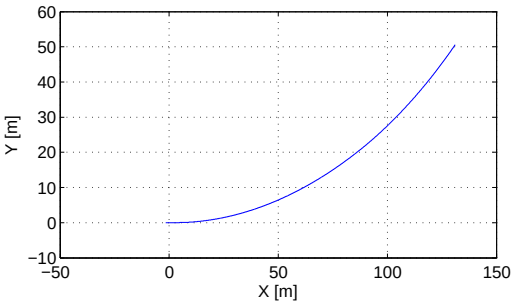

(a) Vehicle trajectory

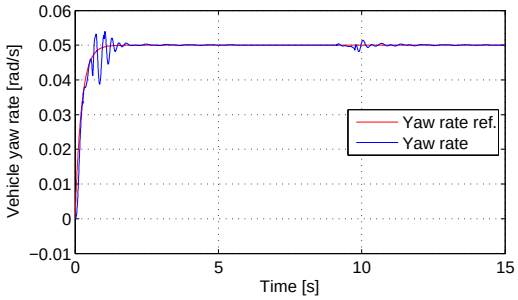

(b) Vehicle yaw rate

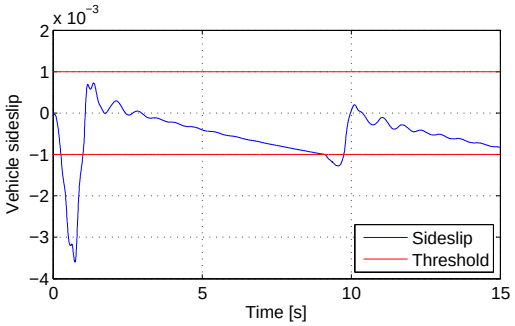

(c) Vehicle sideslip

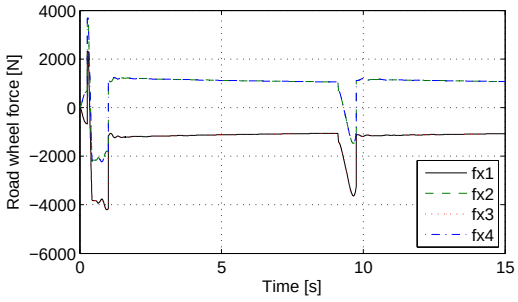

(d) Demanded longitudinal road wheel forces

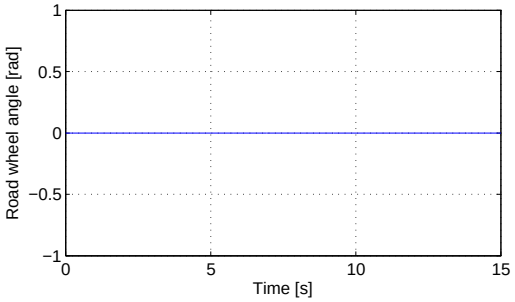

(e) Road wheel angle

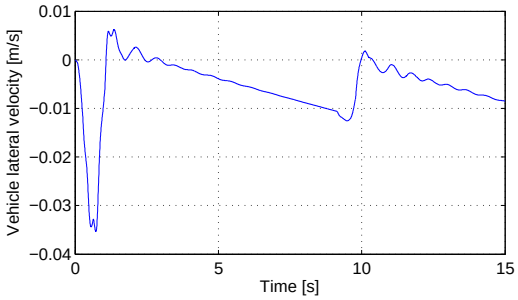

(f) Vehicle lateral velocity

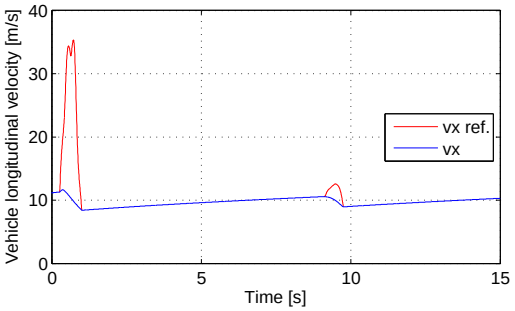

(g) Vehicle longitudinal velocity

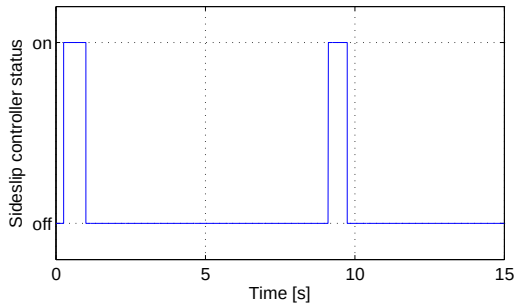

(h) Sideslip controller status

Figure 5.4: Feedback control for the constant yaw rate manoeuvre, using VSM

Therefore in the presence of nonlinearities, close control of yaw rate is evident, and the vehicle sideslip is greatly reduced from the feedforward based steering input in figure 5.2. There are some over/undershoot present which can be explained by the controller overcompensating when v_x changes throughout the manoeuvre. It can therefore be concluded that the feedback control seems capable of controlling vehicle sideslip and yaw rate simultaneously in cornering manoeuvres. It can also be concluded that both the target velocity and the initial velocity of the vehicle when the sideslip controller is activated are critical for the performance of the system.

5.2.3 Feedback control and feedforward based steering

This section presents the results for the combined steering and feedback control of longitudinal wheel forces for the constant yaw rate test. Feedforward based steering is applied to the vehicle as described in section 5.2.1 and also in chapter 3, and is accompanied by the feedback controller. Simultaneous control of vehicle sideslip and yaw rate was seen to be possible for the feedback control setup, now simulation results will be presented and discussed to evaluate if steering input helps or hinders the performance of the feedback controller.

The controller is again tested in the linear controller design model (LCDM) first, followed by the verified simulation model (VSM).

Using the linear controller design model

Evaluation with the LCDM gives the results shown in figure 5.5. Accurate control of yaw rate can be seen in figure 5.5(b) and control of vehicle velocity in figure 5.5(g) allows vehicle sideslip to be reduced to within the threshold in figure 5.5(c). Importantly, the difference between the left and right wheel forces in figure 5.5(d) has disappeared, or has become very small now that the steering actuation has been introduced. This allows the longitudinal wheel forces to concentrate primarily on controlling the longitudinal velocity, to keep sideslip within the threshold region. Unfortunately the wheel forces exceed the physical limits of the wheel.

The sideslip controller status is plotted in figure 5.5(h) and directly relates to figure 5.5(c). The road wheel angle in figure 5.5(e) reduces in magnitude slightly after approximately 0.5 seconds, as the velocity changes quickly.

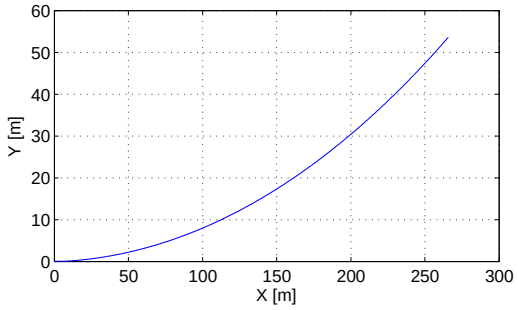

(a) Vehicle trajectory

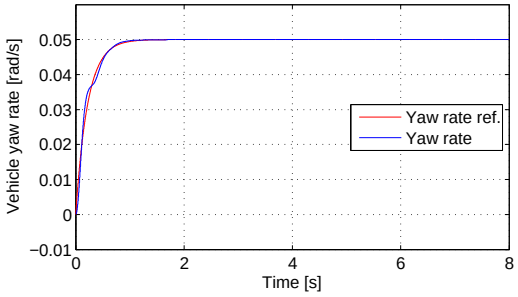

(b) Vehicle yaw rate

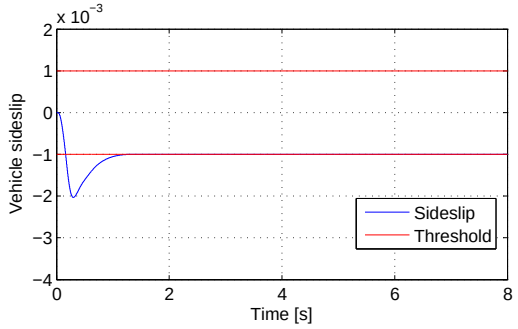

(c) Vehicle sideslip

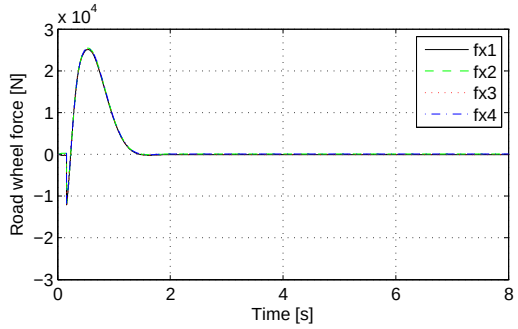

(d) Demanded longitudinal road wheel forces

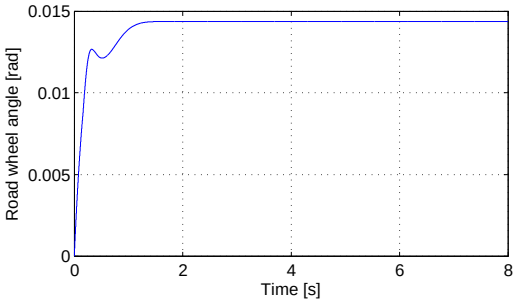

(e) Road wheel angle

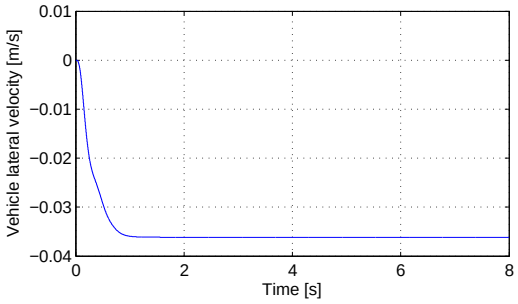

(f) Vehicle lateral velocity

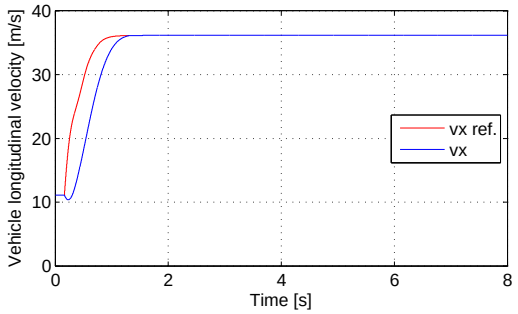

(g) Vehicle longitudinal velocity

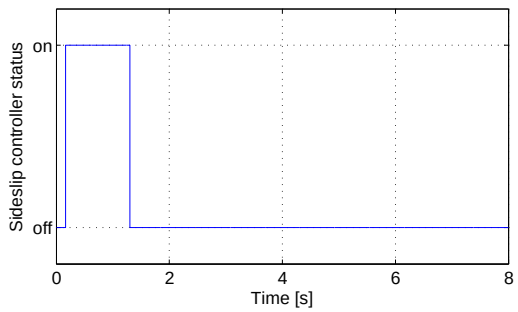

(h) Sideslip controller status

Figure 5.5: Feedback control and feedforward based steering for the constant yaw rate manoeuvre, using LCDM

This reduction in steering angle compensates for the change in velocity, to attempt to keep generating the desired yaw rate through the feedforward signal. This velocity together with its reference signal can be seen in figure 5.5(g). Good control can be seen allbeit with a small amount of lag in the control loop.

Overall, the feedback controller performance is very good. The feedforward steering does not seem to impart any negative behaviour, but instead assists with the generation of the desired vehicle yaw rate. This conclusion has been drawn mainly from figure 5.5(d) where there is no significant difference between the longitudinal wheel forces at either side of the vehicle. This enables the wheel forces to be used primarily to regulate the vehicle velocity.

Using the verified simulation model

Implementing and testing the controller in the nonlinear model will allow the controller performance in the presence of uncertainties and unmodelled dynamics to be assessed.

The results shown in figure 5.6 suggests that the nonlinear vehicle model can also be controlled using the feedback controller in conjunction with feedforward based steering. The combined wheel forces and steering actuation has several improvements together with several degradations in the vehicle behaviour when compared with the feedback only control in the nonlinear model of figure 5.4.

The purpose of the steering being included as an input is solely to generate the desired yaw rate, and the feedback control will correct for any of the small errors that occur in the yaw rate, together with controlling v_x to regulate vehicle sideslip. The plot of yaw rate in figure 5.6(b), can be seen to follow the reference signal, but at the expense of some small oscillations - no more than 2% in magnitude. These oscillations (at approximately 1 Hz) are caused by the controllers trying to correct for some small errors in the yaw rate which are generated by the applied steering angle (in figure 5.6(e)), and further enlarged by an increase in v_x. The oscillations are also reflected in the longitudinal wheel forces in figure 5.6(d), and both the vehicle sideslip and lateral velocity behave in a similar oscillatory manner. However, the oscillations become more evident after the sideslip controller is switched off at approximately 1.5 seconds when the sideslip returns to within the threshold region (as seen from figures 5.6(c) and 5.6(h)). The oscillations found on the vehicle sideslip and lateral velocity signals are due to the small yawing effect of the vehicle from one side to the other and

back again. Importantly, the inclusion of the steering input has reduced the large undesireable under/over shoots that were observed in figure 5.4.

After 1.5 seconds, any demanded wheel force will assist only the yaw rate controller, because the sideslip controller is inactive. This demanded force is very small (see figure 5.6(d)) - a value in the region of ±100N, decreasing to a value very close to zero. Between 1.5 seconds and 4 seconds, the oscillations suggests that a small error exists in the automatic steering generation and the wheel forces try to compensate for this. In figure 5.6(g), the vehicle longitudinal velocity increases while the sideslip controller is active, in order to reduce vehicle sideslip to within the threshold.

The figures for the combined braking and steering control have shown that both yaw rate and sideslip can be controlled simultaneously. Furthermore, the velocity of the vehicle can be controlled well, to a value dictated by the current value of the lateral velocity and the desired vehicle sideslip. The road wheel angle is very small for this manoeuvre, and could be implemented using AFS or a SbW system. When comparing figure 5.6 to figure 5.4 a much smaller difference in $f_{x,l}$ and $f_{x,r}$ can be observed. This is due to the inclusion of the automatic steering, resulting in the feedback controller maintaining rather than generating yaw rate.

One other difference between the two figures is the larger distance that the combined feedback and feedforward based steering controlled vehicle covers within the same time frame. The larger steady state velocity is responsible for this.

It is important to note that if no feedback control was applied in this instance, then the results would be identical to those presented in figure 5.2. This earlier set of results was obtained using only the feedforward based steering to achieve a vehicle yaw rate of 0.05 rad/s. Conclusions can therefore be drawn on the effect that the feedback wheel force control has on the vehicle and the control problem.

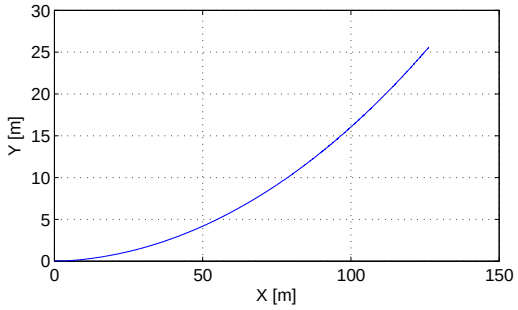

(a) Vehicle trajectory

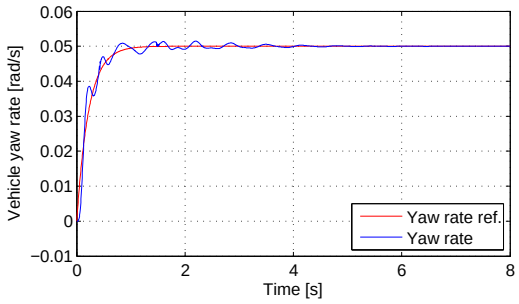

(b) Vehicle yaw rate

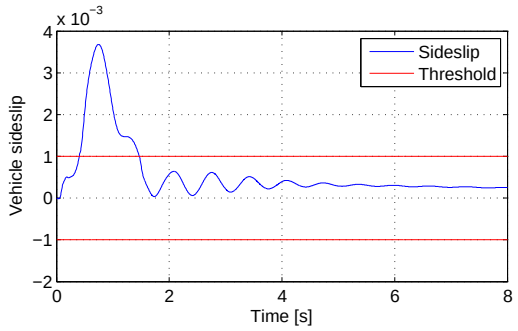

(c) Vehicle sideslip

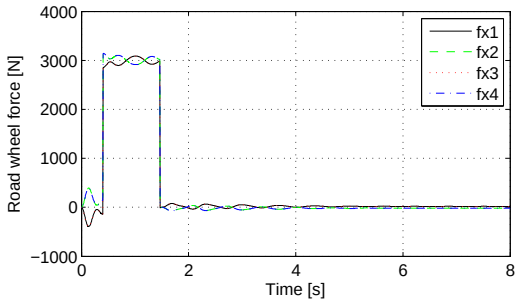

(d) Demanded longitudinal road wheel forces

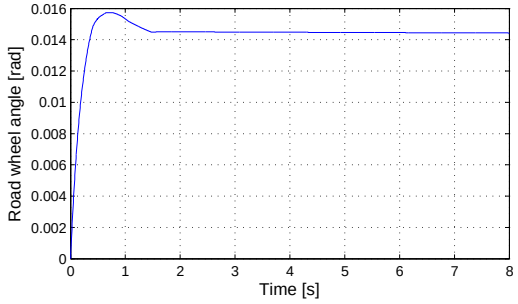

(e) Road wheel angle

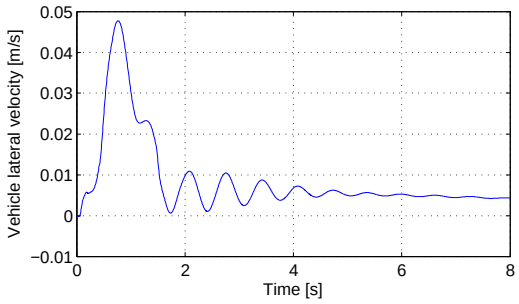

(f) Vehicle lateral velocity

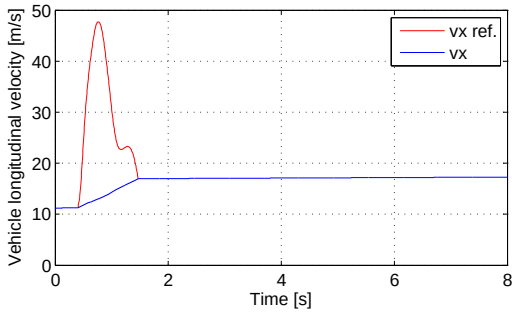

(g) Vehicle longitudinal velocity

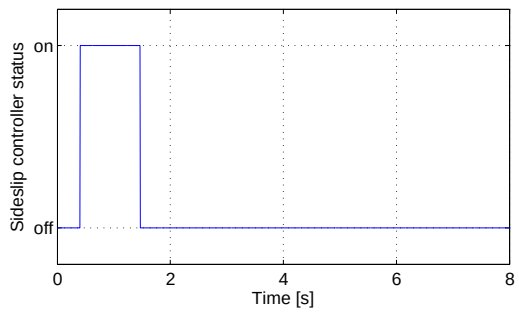

(h) Sideslip controller status

Figure 5.6: Feedback control and feedforward based steering for the constant yaw rate manoeuvre, using VSM

5.2.4 Discussion

It can be concluded that by using the integrated control (both feedback and feedforward based control) vehicle sideslip is greatly reduced (by an average of approximately 80%) but at the expense of a change in the vehicle velocity (by an average of approximately 40%). Although these values will depend on the vehicle sideslip threshold value.

One further advantage exists if this integrated control structure is implemented into a real system. It is known that the feedforward based steering is used primarily for generating the desired yaw rate, and this can leave the feedback controller to regulate predominately the vehicle sideslip.

Therefore, the scenario can exist when the front wheel steering controller is being used to generate the yaw rate, and the feedback controller is not used since sideslip is within the threshold - which is an advantage over using feedback control. Furthermore, if only the feedforward based steering is active at any point in time, then the vehicle speed will be less likely to change than if the feedback controller was active. This of course assumes that the feedforward based steering is generated from an accurate relationship of yaw rate to steering angle.

This constant yaw rate test manoeuvre is very good for testing the controller performance and to determine if both vehicle sideslip and yaw rate can be controlled simultaneously. The fact that steady state conditions are reached enables a more straightforward assessment to be made in comparison to other manoeuvres. However, one problem exists with this manoeuvre — it is very benign and would not be used often in real life scenarios. To this end, the next test manoeuvre (a gentle lane change) will be more realistic of every day driving.

The actuator limits were calculated earlier to be approximately 5000N per wheel. However no actuator limits are incorporated into the linear model. Physical actuator dynamics are modelled in the verified simulation model (VSM), which will help to make the results more realistic. Therefore, only the VSM model will be used to simulate the gentle lane change manoeuvre.

5.3 Gentle lane change manoeuvre

As described in section 5.1, this test manoeuvre is a more relaxed version of the ISO-3888 part 1 standard [108]. The main difference to the constant yaw rate manoeuvre is the non constant reference value for yaw rate during the lane change. The reference values for yaw rate will be generated offline using a series of step functions, while the reference values for the vehicle velocity will continue to be calculated in real time using the lateral velocity and the value of the sideslip threshold.

Similar to the previous section, figures for the feedforward based steering plots will be shown first. These results will again be obtained by applying a steering input as a feedforward signal, with no feedback control connected. The feedforward signal is again derived from the reference yaw rate signal, assuming an ideal vehicle model, and will vary with v_x. The second set of results to be presented will be for feedback control, which uses only the feedback controller. Finally, the steering input will be incorporated with the feedback control. For both of the setups involving feedback control, simultaneous control of yaw rate and sideslip angle will be attempted.

The vehicle model used for all of these simulations is the verified simulation model (VSM). The simulation will be run for a period of time of typically 20 seconds but will ultimately depend on the velocity of the vehicle.

For the lane change manoeuvres, the same reference signals are used for the three different control structures. This introduces consistency and offers comparisons by explicitly highlighting the differences between the various control methods. For example, it was seen from the constant yaw rate test manoeuvres, that different control actuators resulted in differing vehicle velocities. These different velocities will have an effect on both the yaw rate and the vehicle trajectory.

It is important at this point to stress that completing a lane change manoeuvre is not an objective in this task. As discussed at the end of section 5.2.4 the lane change manoeuvre is chosen because it better resembles everyday driving events, more so than the constant yaw rate test manoeuvre. Strictly speaking, position would have to be controlled if the trajectory of the vehicle throughout the manoeuvre was important. Instead, the primary objective remains to track the desired vehicle yaw rate and regulate the vehicle sideslip simultaneously.

It is for these reasons that the vehicle trajectory throughout the manoeuvre will not be shown in the relevant figures.

5.3.1 Feedforward based steering

In the same manner as the constant yaw rate test, the feedforward based steering lane change plots are generated from the road wheel input (which can be related to a steering wheel angle), without any active vehicle-assisting controllers, and are shown in figure 5.7.

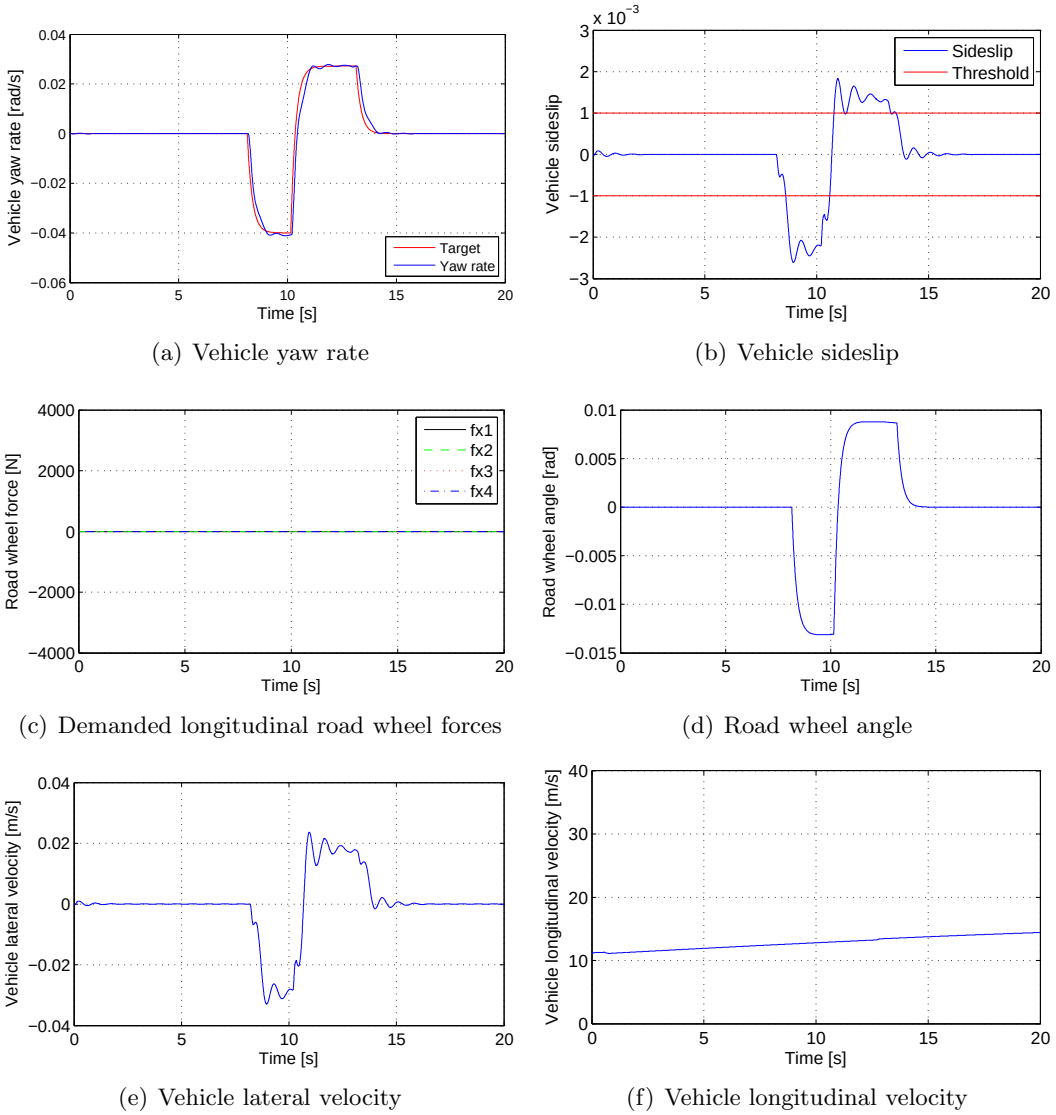

(a) Vehicle yaw rate

(b) Vehicle sideslip

(c) Demanded longitudinal road wheel forces

(d) Road wheel angle

(e) Vehicle lateral velocity

(f) Vehicle longitudinal velocity

Figure 5.7: Feedforward based steering input for the gentle lane change manoeuvre, using VSM

The applied road wheel angle in figure 5.7(d) induces the yaw rate and sideslip shown in figures 5.7(a) and 5.7(b) respectively. The threshold is included in the sideslip plot as a visual

aid to enable easy reference with the controlled plots at a later stage. It can be seen that the magnitude of the sideslip angle decreases as the vehicle velocity in figure 5.7(f) increases.

Both figures 5.7(c) and 5.7(f) show that the longitudinal wheel forces are not demanded by the controller and the velocity is not controlled throughout this manoeuvre. Furthermore, figure 5.7(a) shows the vehicle yaw rate and also the target yaw rate. All plots hereafter will refer to this as *Yaw rate ref.* Of course in figure 5.7(a) it is not a reference signal since there is no control applied to the system, but it is only plotted here to show how accurate the feedforward based steering is at generating the required yaw rate.

5.3.2 Feedback control

In this section the setup is changed to accommodate only the feedback controller. Steering input is not considered here. Therefore, only feedback control is enabled and the same reference signals are used for $\dot{\psi}$ and for the β threshold value as in section 5.3.1. The plots in figure 5.8 are obtained using the verified simulation model (VSM).

The longitudinal velocity, v_x, changes as expected when the vehicle sideslip is being regulated. After this, the vehicle velocity is in the correct range for β to be within the threshold and the sideslip is reduced. This shows that altering v_x (and in this case by only 3 m/s) can effectively reduce sideslip. The yaw rate is controlled very well in figure 5.8(a). Both signals are controlled using only one set of actuators, and the demanded wheel forces are neither excessive nor unrealistic. these wheel forces are shown in figure 5.8(c), while the road wheel angle is shown to be zero indicating no steering input.

The vehicle sideslip in figure 5.8(b) peaks at a value of more than twice the threshold. This is due to the inability of the vehicle velocity to change quickly enough, as was observed for the constant yaw rate test (figure 5.4). This peak value is very similar to that seen with the feedforward based steering setup. However, it now decreases much quicker due to the change in vehicle velocity. The magnitude of sideslip is drastically reduced after the initial peak at around 8 seconds. There is another peak at 11 seconds, but again this is much reduced than with the feedforward based steering plot in figure 5.7.

Importantly, the sideslip controller (via controlling v_x) is only active for two short durations (see figure 5.8(g)). During the periods of controller inactivity, the wheel forces generate the desired yaw rate which is confirmed by the differential style wheel forces in figure 5.8(a).

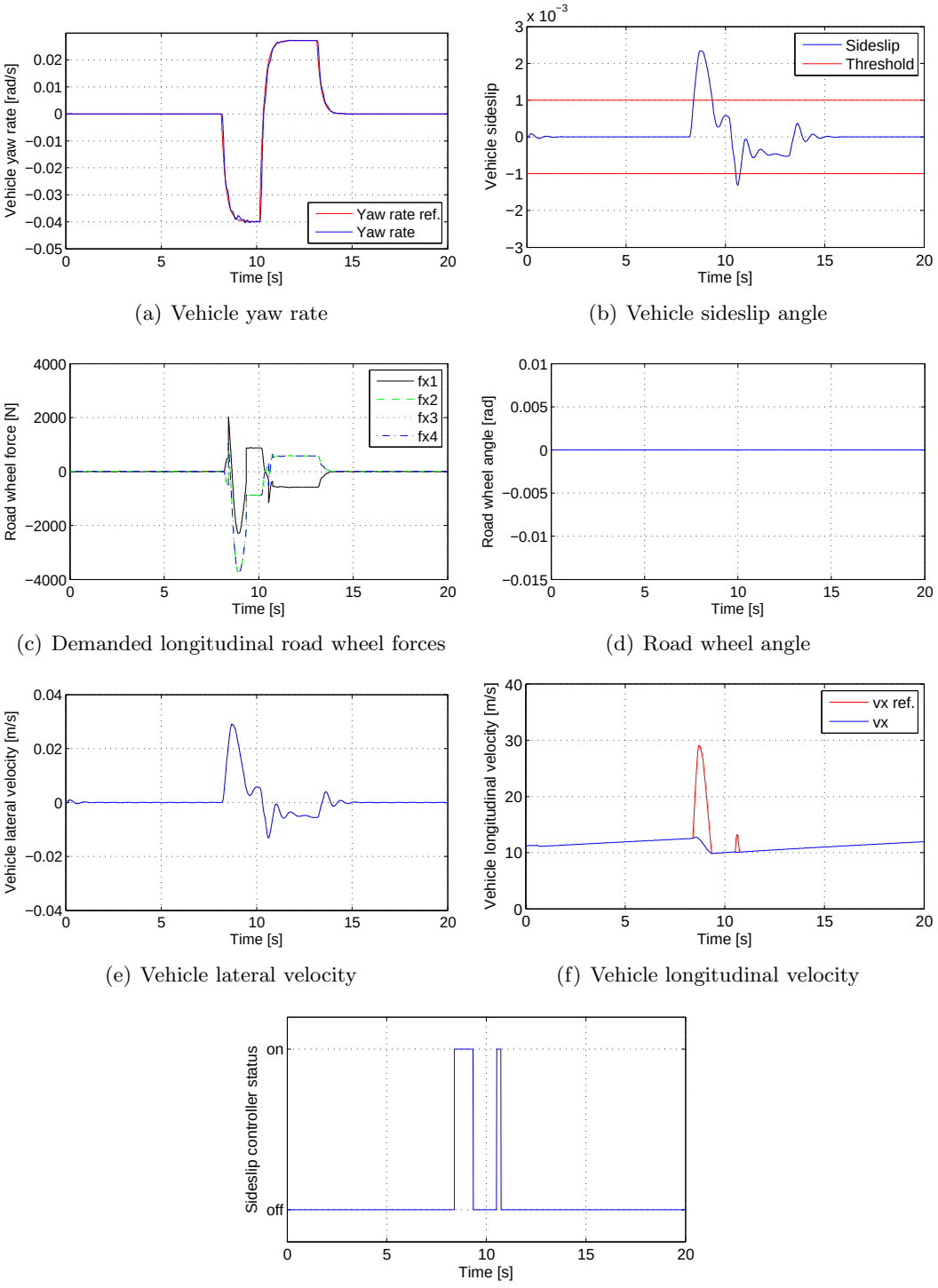

(a) Vehicle yaw rate

(b) Vehicle sideslip angle

(c) Demanded longitudinal road wheel forces

(d) Road wheel angle

(e) Vehicle lateral velocity

(f) Vehicle longitudinal velocity

(g) Sideslip controller status

Figure 5.8: Feedback control for the gentle lane change manoeuvre, using VSM

The increasing velocity in figure 5.8(f) which is not due to any demanded wheel forces is the same phenomena as seen earlier, and described in chapter 2.

5.3.3 Feedback control and feedforward based steering

Figure 5.9, shows the results for the combined feedback control and feedforward based steering lane change manoeuvre and first impressions are that the system appears to contain a lot of oscillations. Again these oscillations mainly occur when the channel of the feedback controller, which demands road wheel forces to alter the vehicle velocity has been deactivated (i.e when the vehicle sideslip is within the threshold).

While the controller is active, the sideslip response is fast and the yaw rate response quicker still, with negligible overshoot. There are some very small, low frequency oscillations which, similar to those observed in the constant yaw rate manoeuvre when both steering and wheel force actuators are used, are no more than 2% and approximately 1 Hz. The oscillations on the sideslip angle occur between approx 11 seconds and 13 seconds when the sideslip controller is deactivated. As mentioned earlier, this behaviour is not a direct result of the controller. Instead, it seems to be the vehicle model reacting to the velocity controller being deactivated. Also, the peak at 11s is much enlarged compared to the feedback control plots.

Figure 5.9(a) shows that close control of yaw rate is possible, which is mainly due to the applied feedforward based steering angle in figure 5.9(d). The demanded longitudinal wheel forces in figure 5.9(c) are within the physical limits of the actuator and contribute mainly to controlling v_x in order to regulate sideslip. This can be confirmed by the lack of wheel force difference from one side of the vehicle to the other.

The longitudinal velocity in figure 5.9(f) increases throughout the manoeuvre. However, this increase causes a larger lateral velocity when the vehicle changes direction. This explains the two large peaks in figure 5.9(e), which are translated into figure 5.9(b) for sideslip. Interestingly, when comparing figures 5.8(c) and 5.9(c), the only significant difference is caused by the wheel forces trying to regulate yaw rate. Otherwise, the demanded forces are similar in magnitude.

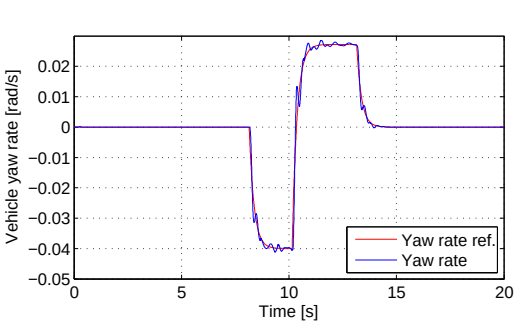

(a) Vehicle yaw rate

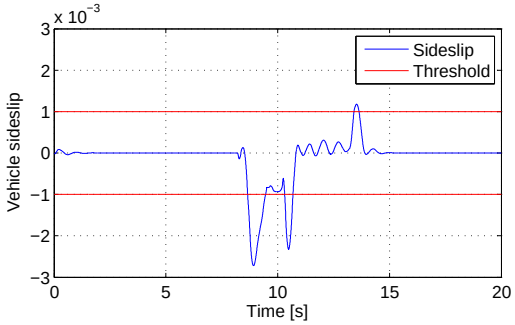

(b) Vehicle sideslip angle

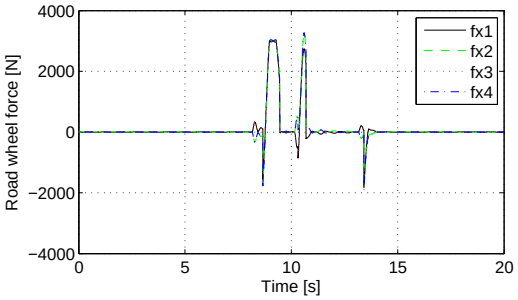

(c) Demanded longitudinal road wheel forces

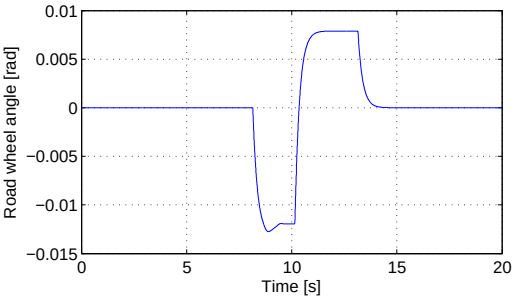

(d) Road wheel angle

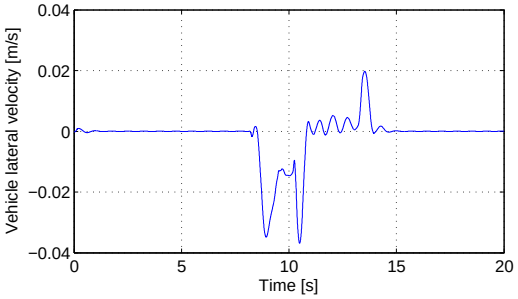

(e) Vehicle lateral velocity

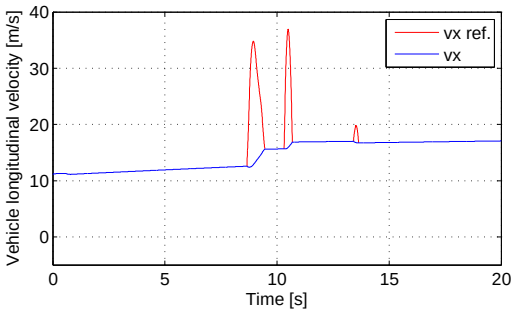

(f) Vehicle longitudinal velocity

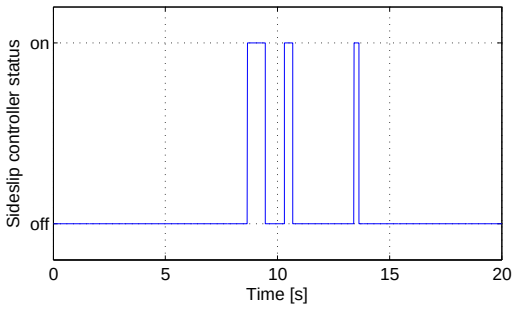

(g) Sideslip controller status

Figure 5.9: Feedback control and feedforward based steering for the gentle lane change manoeuvre, using VSM

5.3.4 Discussion

Three different controller architectures have been simulated using the gentle lane change manoeuvre, and their results presented. The feedforward based steering plots were shown for benchmarking the performance of the remaining two architectures.

Results for both feedback control and integrated feedback control with feedforward based steering show that it is possible to control vehicle yaw rate and vehicle sideslip simultaneously. Furthermore, the results for the feedback controller show that sideslip can be reduced in comparison to the feedforward based steering response (driver steering in a passive vehicle) through reducing the vehicle velocity by as little as 3 m/s. Also, the demanded longitudinal wheel forces are realistic and within the limits of the actuators. Very close control of yaw rate can be seen, which gives better performance than the integrated steering and feedback controller. This is disappointing and indicates that the feedforward based steering and the longitudinal road wheel forces are working against each other. This is also highlighted by the more oscillatory nature of the integrated controller while simulated in the VSM, although it must be accepted that the increased velocity will result in the system becoming more sensitive.

The sideslip controller is active for a longer duration overall for the integrated controlled system. This fact combined with the information above and the figures showing the results of both systems, it is fair to say that the feedback controller performs better when working on its own.

5.4 Discussion for computer simulation manoeuvres

Using two different test manoeuvres, it has been shown that both sideslip and yaw rate can be simultaneously controlled, allbeit to different extents. In both manoeuvres, the combined steering and feedback control produced small oscillations around the reference yaw rate, and oscillations were observed on the lateral channels (v_y and β) when the sideslip controller was deactivated. However, the steering input reduces the workload of the feedback controller to controlling mainly only v_x, and correcting for small errors in yaw rate. Excluding the peak forces, the demanded wheel forces are always close to zero — a large contrast to when only feedback control was used. When operating on its own, the feedback control did generate

undershoots and overshoots on the yaw rate channel for the constant yaw rate manoeuvre. However, this was much improved for the gentle lane change.

There are some important points to consider while analysing the presented results. Firstly, the sign of the vehicle sideslip angle changes depending on whether the front steering is applied or not. It is known that understeer, neutral steer or oversteer will occur whilst steering a vehicle on a constant radius turn. This can be corrected using the vehicle velocity as shown in figure 5.10, assuming the steer angle does not change.

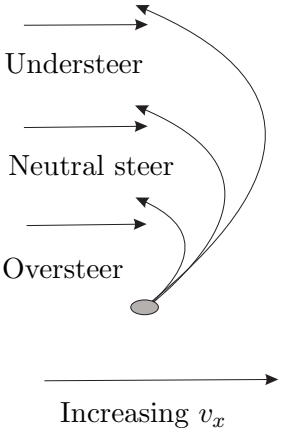

Figure 5.10: Effect of increasing velocity on constant steer angle

Furthermore, an oversteering vehicle has positive sideslip angle for a negative turn (i.e to the right), while for an understeering vehicle it will be negative. Reducing the longitudinal velocity of an understeering vehicle will reduce the understeer, eventually experiencing neutral steer and then oversteer. On the other hand, an increase in the vehicle longitudinal velocity will reduce the oversteer of a vehicle, again bringing it towards neutral steer, and eventually into understeer.

In chapter 2 it was shown that the front tyre sideslip angle, α_f is related to yaw rate, vehicle velocity and front steer angle. Therefore, from equation (5.1) below (which was introduced in chapter 2), β_f, the sideslip angle at the front axle (translated from the vehicle CG) will change sign depending on the magnitude of δ_f.

$$\beta_f = \delta_f - \alpha_f \tag{5.1}$$

This is evident in the two sets of controlled plots for the constant yaw rate manoeuvre:

figures 5.4 and 5.6 where the natural response of the vehicle sideslip changes sign depending on whether front steering is applied or not (before the sideslip controller is activated). Also, when steering is enabled, the velocity required to maintain the sideslip angle within the threshold will be different from that when the steering is disabled. This too is derivable from the above equation, when β_f is replaced with its expanded form.

There is a possibility that continued use of the feedback controller could lead to uncomfortable driving conditions and in the extreme case, tyre saturation. However, this is thought to be minimised because the controller should demand small inputs, as designed with the linear model. In the linear region of the tyre, the following relationship exists for the lateral tyre force

$$f_{y,f} = C_f \, \alpha_f \tag{5.2}$$

where, α_f can be replaced with equation (5.1) above to give the expression in equation (5.3).

$$f_{y,f} = C_f \, (\delta_f - \beta_f) \tag{5.3}$$

Equation (5.3) shows that the front steer angle plays a big part on possible saturation and overall tyre performance. Also, the equation shows that under certain conditions the lateral tyre force may be greater with no front steering. In other words, if (δ_f =0, β_f $\neq$0) may result in a larger force than if δ_f $\neq$0. In essence the tyre will saturate when the largest forces are exerted on it, and this can be calculated from the following equation.

The effect of the zero/nonzero steering angle can be seen in figure 5.11, which shows 2 plots for the gentle lane change manoeuvre, obtained from the VSM. The lateral tyre force at the wheel during the manoeuvre for feedforward based steering only and also for feedback control of channel 2 only ($\dot{\psi}$) can be seen. Therefore, no sideslip control is active in this case. It is merely a comparison between a passive steering response and differential type wheel force inputs.

Figure 5.11(a) represents a vehicle with front wheel steering. As the front wheels turn the lateral forces on all 4 wheels change in the same magnitude and direction simultaneously. However, figure 5.11(b) is very different. As the vehicle 'steers' through the manoeuvre using only the feedback controller, the force on the front wheels act in the opposite direction to the

rear wheels. Furthermore, the lateral force at the front wheels is reduced in comparison to figure 5.11(a), and the lateral forces at the rear wheels are much larger.

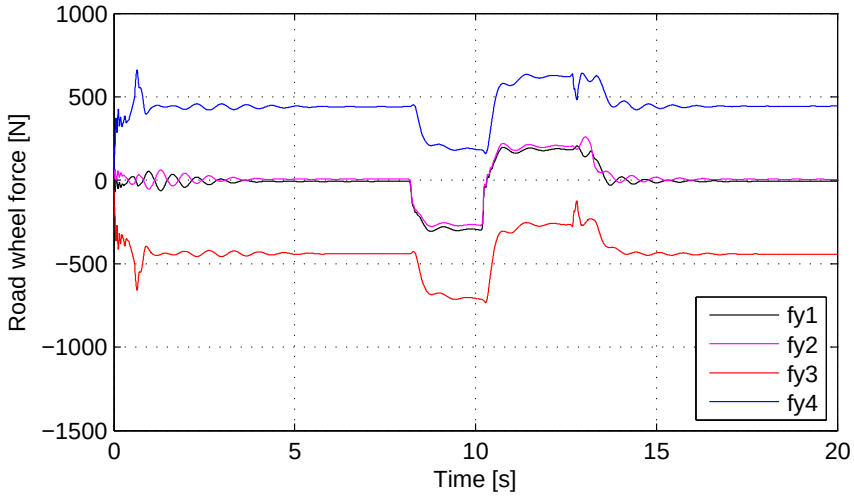

(a) Lateral tyre forces for the steer only vehicle

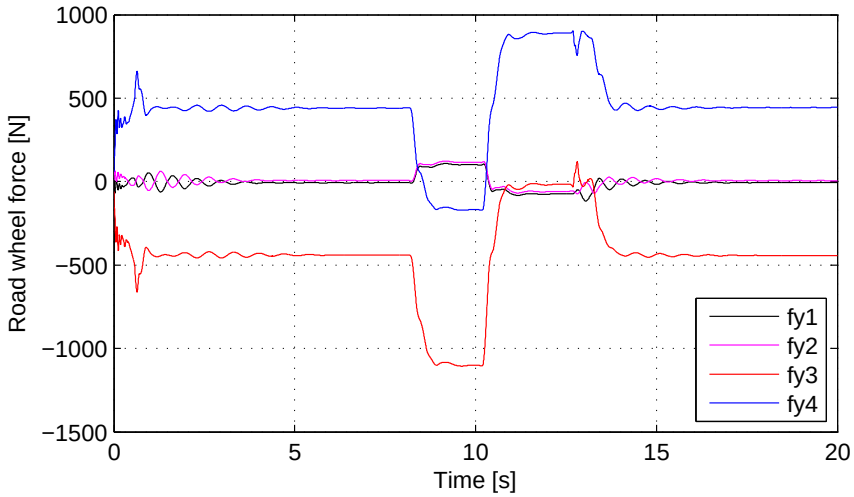

(b) Lateral tyre forces for the differential style longitudinal wheel force controlled vehicle

Figure 5.11: Lateral road wheel forces for the lane change manoeuvre, obtained using VSM

AFS is becoming readily available in the market place[1], and with road wheel angles in all of the simulations in the region of ±1 degrees, it is feasible that AFS could be used in the application of these vehicle dynamics control systems — for this sort of manoeuvre.

The initial velocity of the vehicle at the beginning of the manoeuvre is critical to the performance of this control system. Obviously, the closer the initial velocity is to the desired velocity, $v_{x,ref}$ (which is calculated from the lateral velocity), the quicker the vehicle sideslip

[1]BMW, ZF and Bosch amongst other manufacturers have developed AFS systems, currently in use.

can be contained within the threshold. It is important to remember that this controller is not an 'at the vehicle limits' controller, but instead is merely a 'driver assist' controller. For both test manoeuvres presented here, lateral accelerations are of the order of 1 m/s^2 or 0.1g, which is very tame for accelerations; in [101], an aggressive collision avoidance controller achieved accelerations in the magnitude of 10 m/s^2 or 1g.

For the lane change manoeuvres, the yaw rate reference generation is not ideal because of the varying velocity whilst controlling vehicle sideslip. Vehicle yaw rate is dependent on the vehicle velocity, so as the velocity changes the yaw rate will also change, and the reference signal should accommodate this. Therefore, for the aim of completing a lane change manoeuvre one generic yaw rate reference signal is not practical. Instead it should be at least be dependent on v_x, similar to the dependency of the feedforward based steering angle.

The generation of the reference yaw rate signal is neither optimal nor automatic. However, this has been studied in other works [23] where novel optimisation techniques are employed to calculate the optimal trajectory for different lane change specifications.

5.4.1 Conclusions

This chapter has presented simulation based results for the linear feedback controller. The results are promising and show that simultaneous control of yaw rate and vehicle sideslip is possible with both control architectures, under certain circumstances. The next chapter will present results using the driver interface test rig and the real-time nonlinear vehicle model (RTSM).

Chapter 6

Evaluation using human interface

6.1 Overview

This section presents results from the experiments using the human interface test rig and the real time simulation model (RTSM). The test rig is setup as described in chapter 4, and is used to allow human interaction with the vehicle model which runs on a PC. For the experiments where it is deemed necessary, visual feedback will be available to the driver. Within this human interface study, unless described otherwise, the driver's steering angle is added to any angle generated from the feedforward based steering before being added to the vehicle model as an input.

This chapter will present three different test situations. First a driver disturbance acting during a constant yaw rate manoeuvre, secondly some lane change manoeuvres similar to the previous chapter and finally, a disturbance acting on the vehicle in the form of a sidewind. Within this set of manoeuvres, different architectures will be used including the feedforward based steering on its own, driver steering using the test rig to generate the input, feedback control and various permutations of all of these. This range of setups will allow comparisons to be made and conclusions to be drawn. The same driver will be used to obtain each set of results for all manoeuvres, with the exception of the sidewind disturbance manoeuvre where an additional driver is also used.

Finally, the caption on each set of results will indicate that the RTSM (real-time simulation model) was used to obtain the results. Also, the plots which show the road wheel angle will generally have two signals plotted with an appropriate legend. The legend refers to

controller input and *rig input*. It is important to emphasise at this point that the rig input is generated from the driver at the human interface test rig, while the controller input is the automatic feedforward based steering input introduced in chapter 3.

6.2 Constant yaw rate manoeuvre with disturbance input

The first manoeuvre to be evaluated is the constant yaw rate manoeuvre, as before but now a disturbance input is applied via the test rig. Feedforward based steering is applied to generate the desired yaw rate, with no feedback control considered. A disturbance is applied via some step steering input from a human operator using the test rig. This causes the road wheels to turn more, resulting in larger than desired vehicle yaw rate and sideslip angle.

The steering disturbance input is very difficult to repeat precisely on the rig. Therefore, it is generated using a human operator and the test rig which is recorded. This recorded signal is then fed back into the vehicle model offline. The main advantage of this method, is that the signal is consistent for all control architectures, providing repeatability and accuracy. The disturbance input from the rig should be rejected by the feedback controller and continue to track the steady state reference values. In essence, this test is the same as the constant yaw rate test with an added disturbance from the human operator of the test rig.

The initial conditions for this test are an initial vehicle longitudinal velocity of 11.11 m/s, an initial yaw rate of 0 rad/s and an initial lateral velocity of 0 m/s.

6.2.1 Feedforward based steering

A steering angle is calculated from the ideal vehicle model to give a desired yaw rate of 0.05 rad/s. An additional steering angle is then applied to the vehicle model using the driver interface test rig. Since no feedback control is used in this case, the results will be referred to as 'feedforward based steering' results. These are shown in figure 6.1.

The feedforward based steering vehicle follows the elliptical trajectory in figure 6.1(a) since the applied steer angle is non constant while the vehicle velocity remains constant. The road wheel inputs of figure 6.1(e) are summed together before being applied to the vehicle model as one steering angle for the front wheels. The only other possible input, the longitudinal wheel forces, are zero throughout the manoeuvre (see figure 6.1(d)).

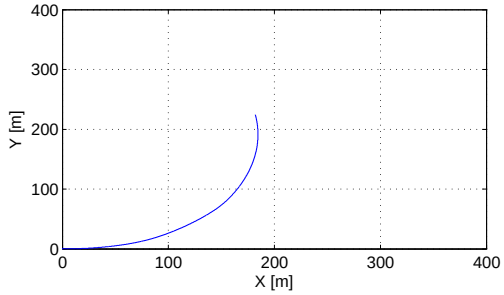

(a) Vehicle trajectory

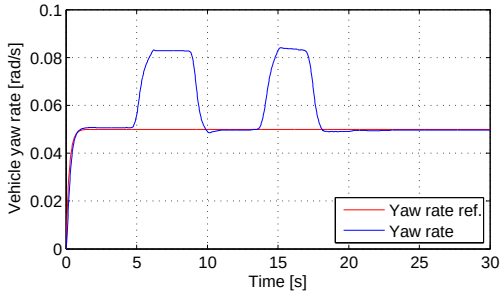

(b) Vehicle yaw rate

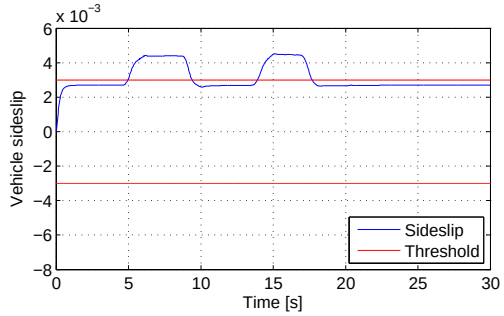

(c) Vehicle sideslip

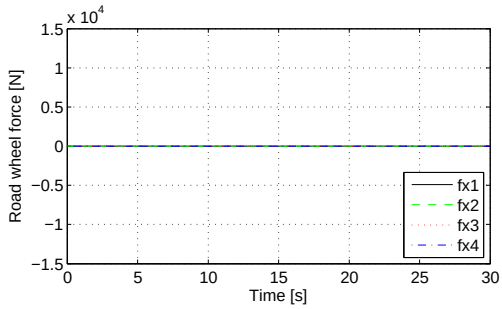

(d) Demanded longitudinal road wheel forces

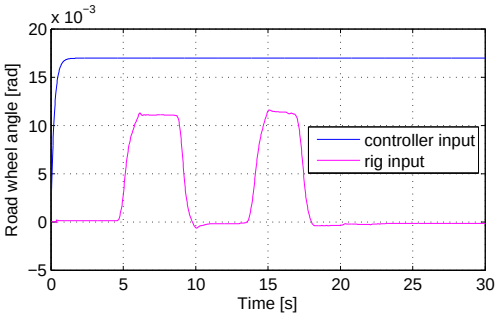

(e) Road wheel angle

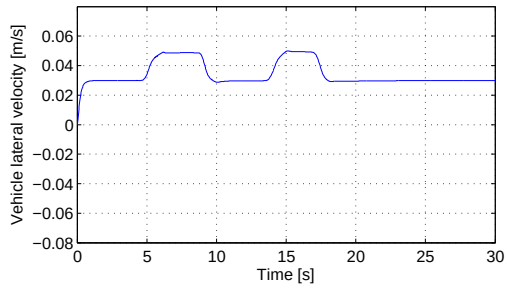

(f) Vehicle lateral velocity

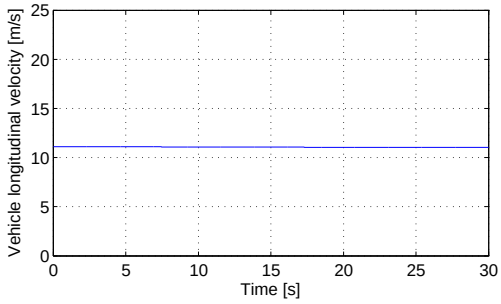

(g) Vehicle longitudinal velocity

Figure 6.1: Feedforward based steering for the constant yaw rate manoeuvre with disturbance input from test rig, using RTSM

The feedforward based steering angle which is labelled as *controller input* in figure 6.1(e) is responsible for generating the steady state values for vehicle sideslip and yaw rate. The second data set in the plot is the disturbance input that the driver applies via the test rig. The effects of this steering disturbance input can be seen on both yaw rate and sideslip plots. It is important to note that the vehicle sideslip in figure 6.1(c) is plotted together with the sideslip threshold. This threshold has a value of 0.003, chosen because with the RTSM, the natural sideslip response to a front steering vehicle at steady state is equal to approximately 0.0028. Choosing this value for the threshold allows the sideslip response to remain unaltered until the steering disturbance is applied. Only once the disturbance input is applied will the vehicle sideslip require to be reduced using the controller.

From figure 6.1, the steering angle applied from the controller input in figure 6.1(e) can be seen to give the desired yaw rate of 0.05 rad/sec very effectively. The yaw rate plot in figure 6.1(b) does indeed show that the before the disturbance signal acts on the model, the yaw rate and its reference signal are very close that the difference is almost negligible.

6.2.2 Feedback control

Feedforward based steering is now disabled and the feedback controller is activated. Yaw rate will always be controlled to 0.05 rad/s and vehicle sideslip will be controlled whenever it exceeds the threshold value of 0.003. During the simulation, the generic disturbance input seen in figure 6.1 will be applied.

The results for the feedback controlled plots in figure 6.2 show that the trajectory covers a much smaller distance than the feedforward based steering manoeuvre. This can be explained by the decrease in velocity for the controlled manoeuvre (see figure 6.2(g)). The velocity is controlled in order to keep the vehicle sideslip within the threshold, which is achieved through altering the vehicle speed by demanding the longitudinal road wheel forces. This velocity is halved within a time frame of 5 seconds, and is greatly reduced by the end of the manoeuvre. Direct comparisons can be made between the plots of yaw rate and sideslip in figures 6.1 and 6.2, and it can be observed that the yaw rate control is actively working to reduce both the magnitude and duration of the acting disturbance. Similar effects can be observed for the sideslip, where it is almost always maintained within the threshold although it now acts in the other direction because the steering angle is not used as an input.

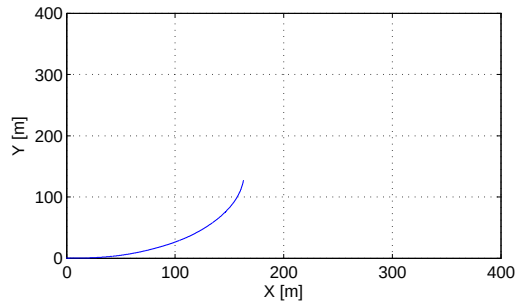

(a) Vehicle trajectory

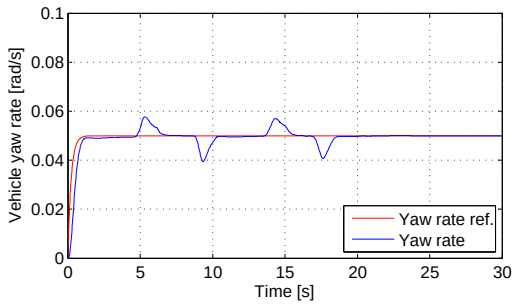

(b) Vehicle yaw rate

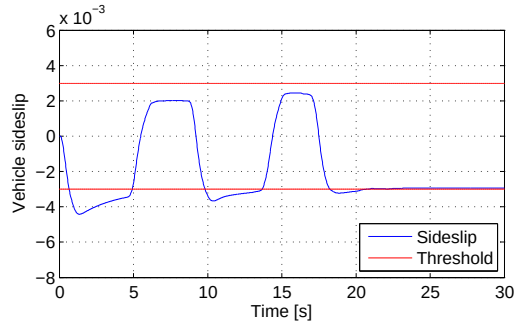

(c) Vehicle sideslip

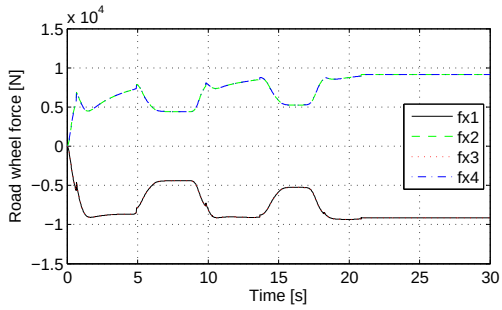

(d) Demanded longitudinal road wheel forces

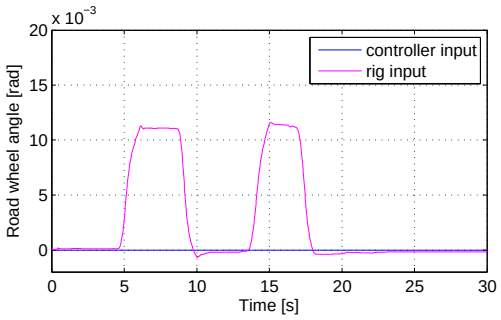

(e) Road wheel angle

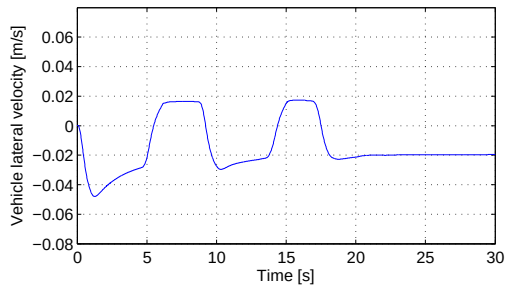

(f) Vehicle lateral velocity

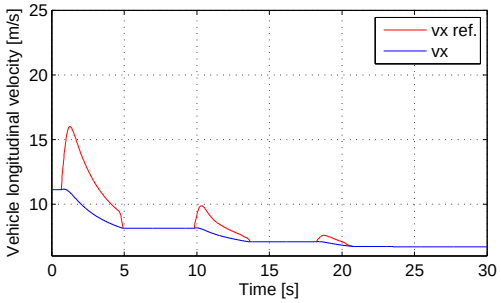

(g) Vehicle longitudinal velocity

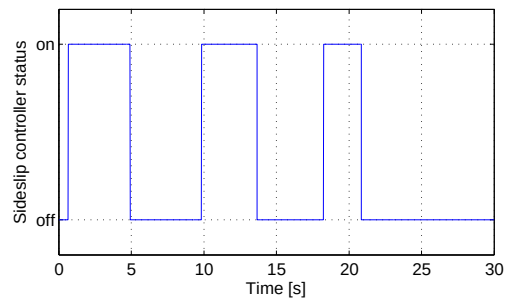

(h) Sideslip controller status

Figure 6.2: Feedback control for the constant yaw rate manoeuvre with disturbance input from test rig, using RTSM

The sum and difference concept of the wheel forces in figure 6.2(d) can be separated to show that the magnitude of the individual wheel forces controls sideslip, while the difference (left to right) is responsible for generating the desired yaw rate. Importantly, sideslip angle is only controlled when it exceeds the threshold value, else it could become more of a hindrance than assisting the driver, although in this circumstance a case could be made that the large reduction in vehicle velocity is not very beneficial to the driver. The status of the sideslip angle controller is shown in figure 6.2(h), and in figure 6.2(e), no feedforward based steering is applied to the vehicle but only the disturbance via the rig is applied.

The feedforward based steering response in figure 6.1 shows that the vehicle sideslip naturally exceeds the threshold when the steering input is applied. However, in figure 6.2, the disturbance steering input via the test rig actually brings the sideslip back within the threshold. Even with this occurring, the change in v_x can still be seen to have an effect on β since the duration of time that the sideslip controller is active, reduces with each disturbance step input. This can be seen in figure 6.2(h).

6.2.3 Feedback control and feedforward based steering

Applying the same disturbance input to the vehicle model with integrated feedforward based steering and feedback control, results in simultaneous control of both variables as shown in figure 6.3. Both vehicle sideslip and yaw rate reject the disturbance effectively. The wheel forces are more dynamically active, allbeit they are greatly reduced in magnitude in comparison to the feedback only control (98% steady state reduction from 10000N for the feedback control case to 200N for the integrated control case at the end of the manoeuvre). The use of these forces to minimise the effect of the disturbance on yaw rate can be seen in the figure 6.3(d)). A difference in demanded wheel forces from one side of the vehicle to the other can be observed while the disturbances are acting, and afterwards. It can be seen that before the disturbance acts, the feedforward based steering was more than capable of generating the desired yaw rate.

The increase in velocity is effective in reducing the vehicle sideslip, but it can be argued that the increase is too excessive with approximately a 100% increase from the initial velocity. Figure 6.3(h) shows how active the sideslip controller is during the simulation.

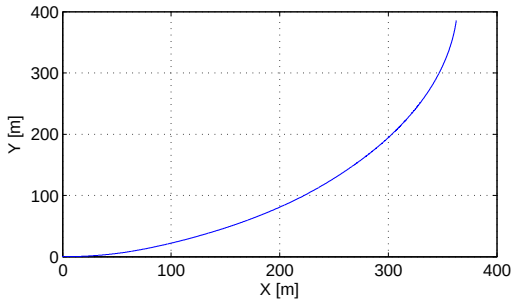

(a) Vehicle trajectory

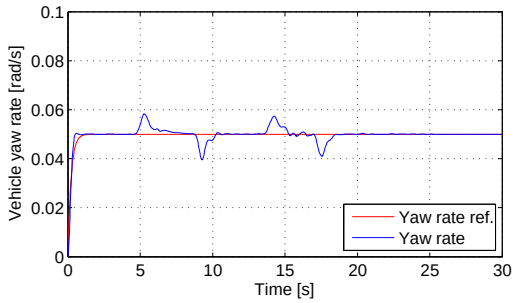

(b) Vehicle yaw rate

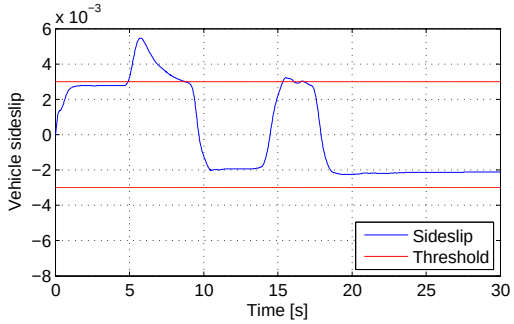

(c) Vehicle sideslip

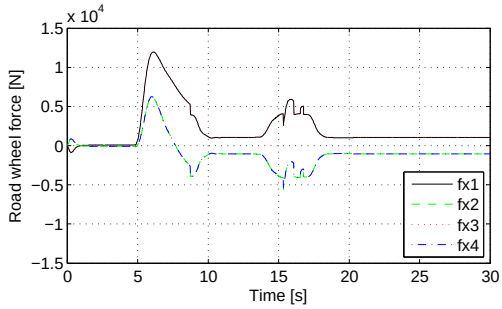

(d) Demanded Longitudinal road wheel forces

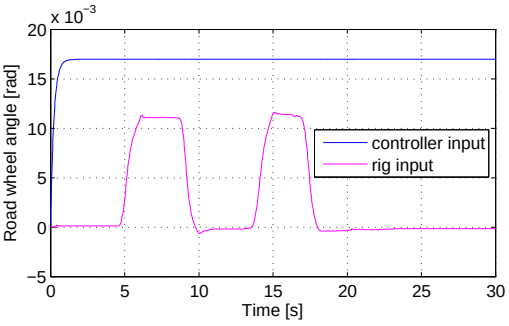

(e) Road wheel angle

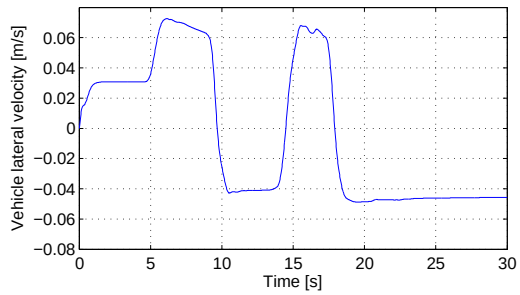

(f) Vehicle lateral velocity

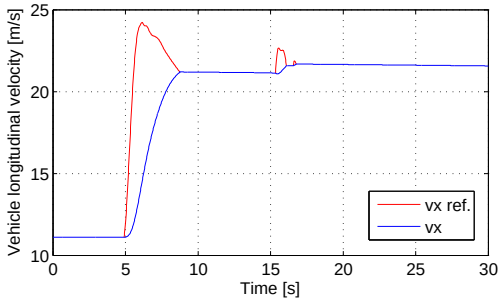

(g) Vehicle longitudinal velocity

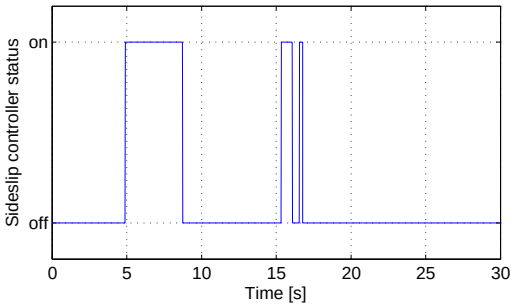

(h) Sideslip controller status

Figure 6.3: Feedback control and feedforward based steering for the constant yaw rate manoeuvre with disturbance input from test rig, using RTSM

In terms of time duration that the controller was active, it is reduced in comparison to the feedback controller, while in both cases the controller was activated on three occasions. Importantly, towards the end of the simulation the sideslip controller is active for a much shorter duration than at the beginning. This can be explained by the increase in the vehicle velocity which by the end of the manoeuvre, has increased to a value which will generate a sideslip value within the threshold for the current lateral velocity. This is of course the principle behind the control.

6.2.4 Discussion

It can be concluded that both control structures (feedback and integrated control) are able to complete the task of simultaneously controlling yaw rate and sideslip while effectively rejecting disturbances. Each structure has positive and negative effects in doing so. Looking at both structures, the vehicle velocity varies greatly while the controllers are working. The greatest effect of this is witnessed in the trajectory plots (plot (a) of each figure). For the same steering inputs, a larger velocity will allow the vehicle to travel further as seen in the integrated control case. On the other hand, a reduced velocity will prohibit the vehicle from travelling as far, as seen in the braking only control case. The impact of this on the vehicle could be deemed undesirable for the driver and certainly a large increase or decrease in velocity can be both impractical and dangerous.

For both control architectures, yaw rate disturbances were rejected very effectively — even in the presence of the changing vehicle velocity. What is of concern though, is the large longitudinal wheel forces that are required for this control, particularly for the feedback controller where the required steady state values are impractical towards the end of the simulation. Although the longitudinal wheel forces that are demanded by the integrated control architecture are much more realistic. The vehicle sideslip is controlled in both architectures. However, better results can be seen when using the combined feedback and feedforward based steering control.

Overall it has been shown, in principle, that simultaneous control can be achieved.

6.3 Gentle lane change manoeuvre

In this section, a gentle lane change manoeuvre is attempted using the various control setups. Firstly, just driver input using the interface test rig is assessed. Then combinations of feedback and feedforward based control are used without any test rig input. Finally, various combinations of active controllers and test rig inputs are considered. It is important to state that the manoeuvres have not been rehearsed by the test rig operator in any way. Visual feedback of the vehicle trajectory is provided via the animation PC as described in chapter 4. The RTSM is again used for the vehicle model. The setup for this lane change manoeuvre is an initial longitudinal velocity of 11.11 m/s — the same initial velocity for all manoeuvres so far. The initial lateral velocity is 0 m/s and an initial yaw rate also of 0 rad/s.

6.3.1 Driver steering input via test rig

In this section, five attempts of a gentle lane change, with a few minutes rest in between each run are carried out and the results plotted. Five different runs were used in order to obtain a representative average of the driver's behaviour. Only inputs from the driver interface test rig are used in this section.

The driver was given a clear set of instructions to carry out the manoeuvre. He was to sit on a stool at a comfortable height for the steering wheel, ensuring that the visual display on the laptop in front of him could be clearly seen. When ready to start, the start button was pressed in the Simulink model on the host PC by an assistant. The animation then starts running together with the simulation of the vehicle model. The aim is for the driver to try and keep the vehicle within the road boundary at all times. A rest period of between 3 and 5 minutes was allocated between runs.

The trajectories of the five manoeuvres using the test rig as input with human in the loop have been combined in figure 6.4. These trajectories are all very similar, with the vehicle following almost the same path on each run. In all 5 runs the vehicle remains within the coned boundary.

The road wheel angle which was generated by the human using the test rig is shown in figure 6.5. Again, only run 1 differs greatly and a good average seems to have been obtained by runs 2, 4 and 5, which being equal to ± 0.04 rad (approx 3degrees) is considered very

small. The steering wheel angle sensor is very sensitive and picks up very small movements (the very small variations from zero to nine seconds on the plot are a good example of this). Varying driver input has been recorded and the yaw rate and sideslip response to this input has been obtained. These responses will be useful in evaluating the controlled manoeuvre results. No feedback control of the wheel forces is considered here, hence the longitudinal road wheel forces are not presented since they are a constant zero. Similarly, the vehicle longitudinal velocity does not change and is therefore not shown either.

The average for runs 2, 4 and 5 for the yaw rate is -0.08 rad/s and changes direction to 0.12 rad/s, while for vehicle sideslip it is approximately -3.5×10^{-3}, changing direction to 4×10^{-3}. Both of these sets of values will become apparent when they are compared to the controlled values later. It does appear that run 1 of each plot is significantly different from the remaining 4 runs. This could be due to the driver learning how to improve the route through repeating the lane change. We will call this the *'training effect'*. Although no time provision for training was allowed, it can be assumed that the driver is not familiar with the equipment on the first run. It is good to see that there are no significant differences between the last 4 runs, indicating that no further learning of the manoeuvre took place. This highlights that the responses are both realistic and representative.

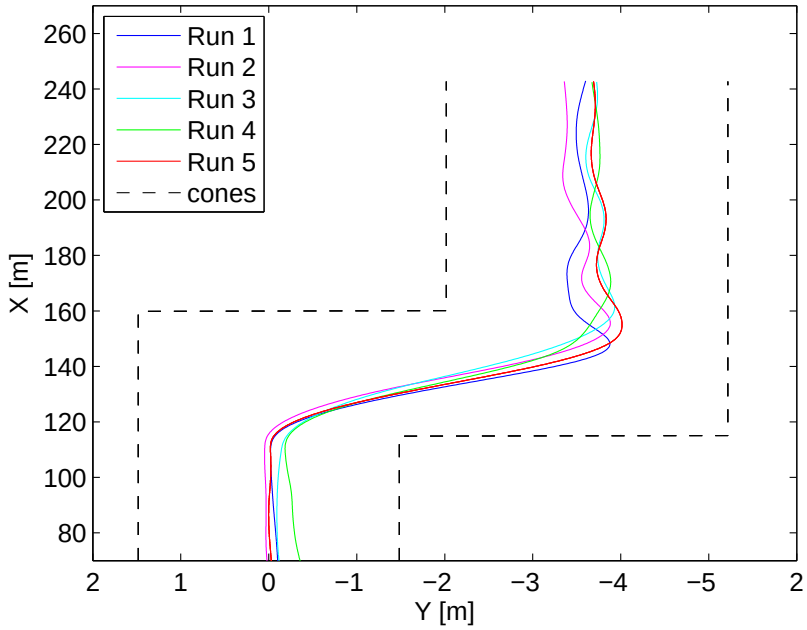

Figure 6.4: Combined trajectories for 5 gentle lane change manoeuvres, using RTSM

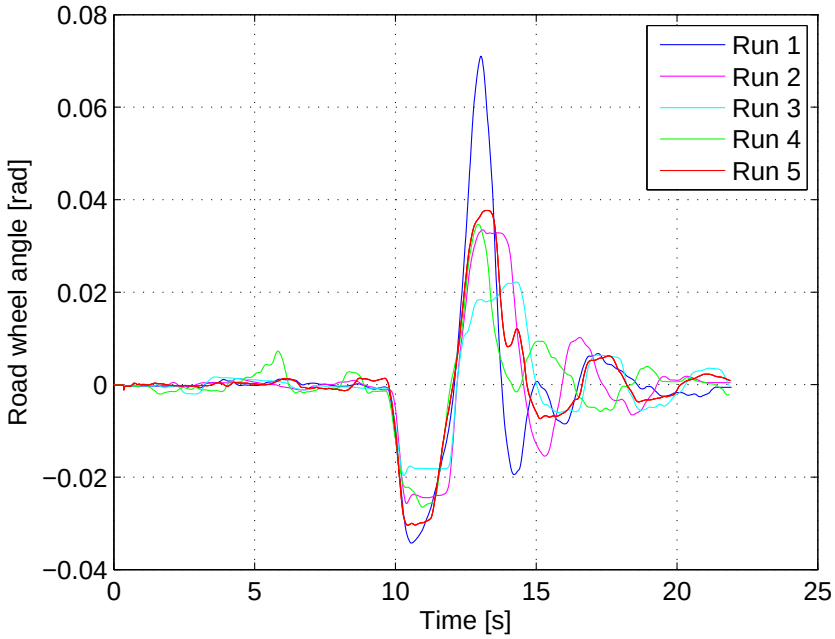

Figure 6.5: Combined road wheel angles for 5 gentle lane change manoeuvres,using RTSM

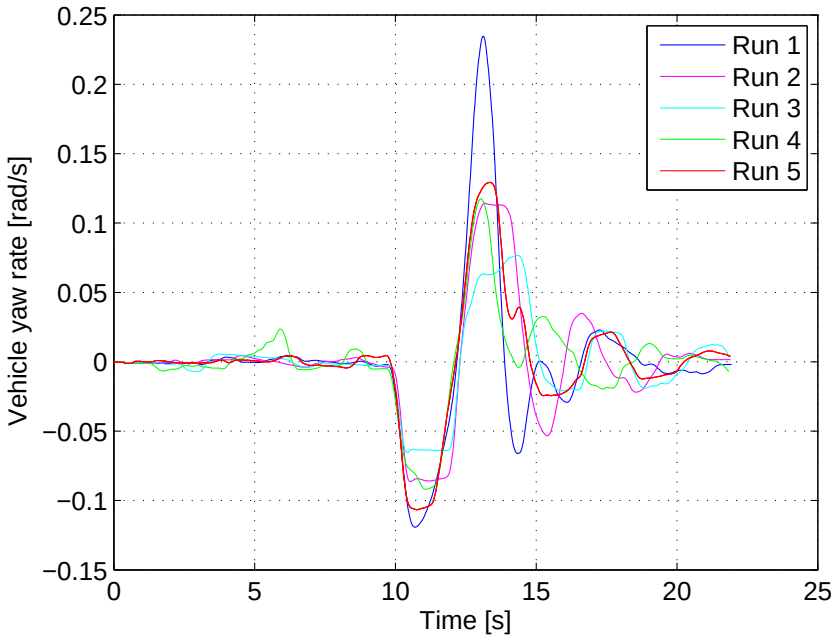

Figure 6.6: Combined yaw rate for 5 gentle lane change manoeuvres, using RTSM

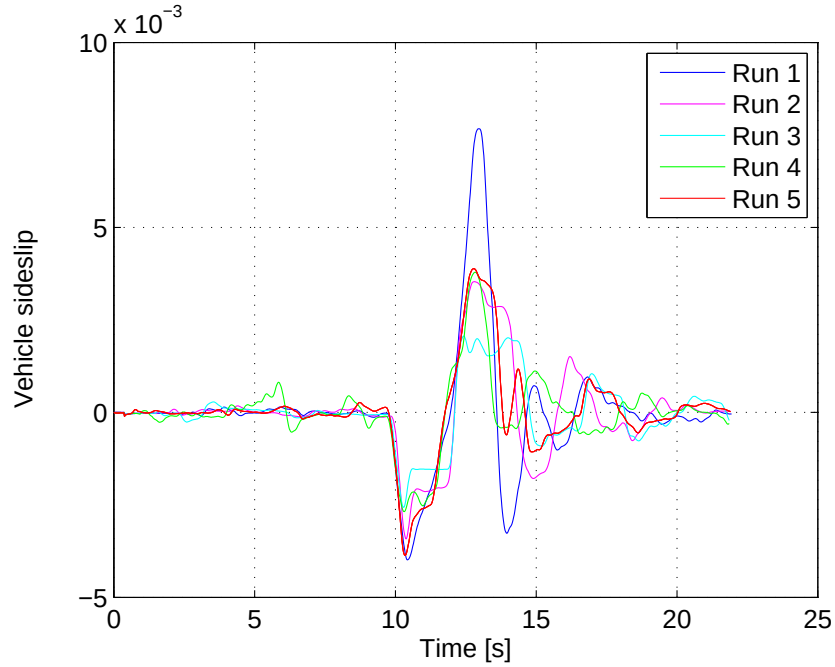

Figure 6.7: Combined sideslip for 5 gentle lane change manoeuvres, using RTSM

6.3.2 Automatic control - no driver input

In this section feedback control is considered first, followed by feedback control integrated with feedforward based steering. Driver input via the test rig is not used in this section, however, the RTSM is still used to simulate the vehicle behaviour.

Similar plots for lane change manoeuvres were seen in chapter 5. However, those results were obtained using VSM whereas the RTSM will be used in this chapter. These two models were comparatively similar when given the same step inputs in chapter 2. The average values for yaw rate and sideslip angle in the human response section were briefly mentioned from the relevant plots (figures 6.6 and 6.7), and it is apparent that for the controllers to have any usefulness, the reference values must be less than these average values. To this end, the threshold above which sideslip control will be activated is 3×10^{-3} — the same value used in section 6.2. This value is greater than the threshold used in chapter 5, but the manoeuvre in this chapter generates a larger yaw rate and sideslip with driver steering via the test rig. The threshold is set higher to try and avoid excessive changes in the vehicle velocity during the manoeuvre. The yaw rate reference will be generated from a series of step functions, and may have a timeshift for each manoeuvre to accommodate the required change in vehicle velocity.

Feedback control

The results for the feedback control setup are shown in figure 6.8. They show a well controlled vehicle yaw rate, while sideslip varies with v_x, but is not controlled as effectively. The sideslip plot travels towards the threshold but does not reach it in the required timescale, despite a recognised change in vehicle velocity. However, overall the vehicle sideslip has been reduced when compared to the driver only input plot in figure 6.7. The change in vehicle velocity is responsible for this, and β is greatly reduced between 12 and 16 seconds because the vehicle velocity has been regulated to be 'in the correct region' for the smaller lateral velocity. A reduction in vehicle velocity by around 17% is enough to regulate the sideslip. The demanded road wheel forces by the controller do not exceed the limitations of the actuators, but peak close to the calculated maximum. Finally, the sideslip controller is only required once throughout the manoeuvre to reduce sideslip for a duration of approximately 3 seconds, as seen in figures 6.8(c) and 6.8(h).

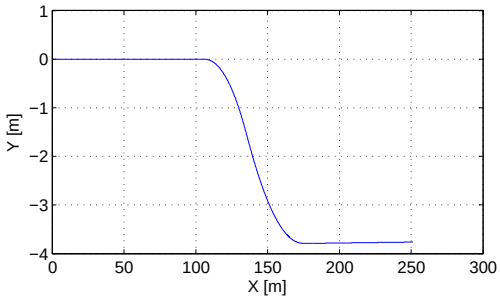

(a) Vehicle trajectory

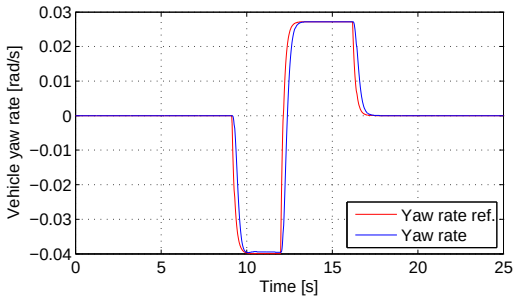

(b) Vehicle yaw rate

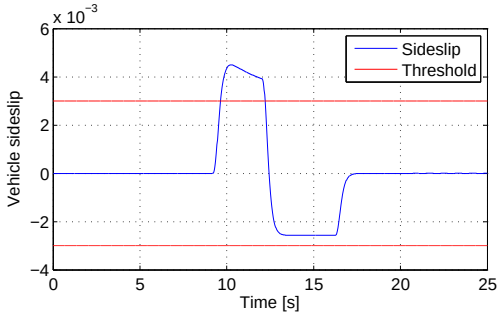

(c) Vehicle sideslip

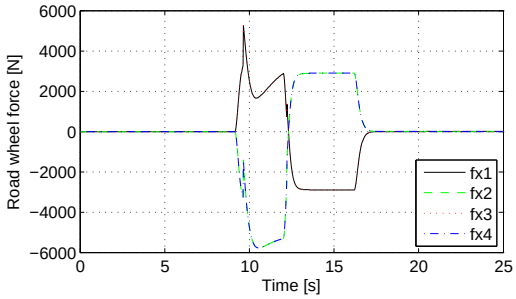

(d) Demanded longitudinal road wheel forces

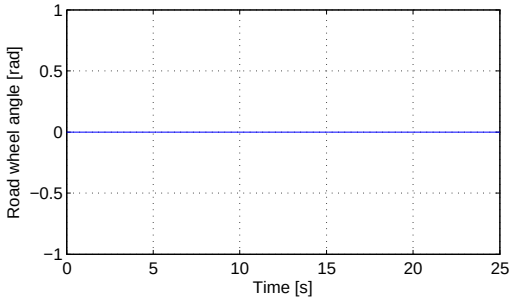

(e) Road wheel angle

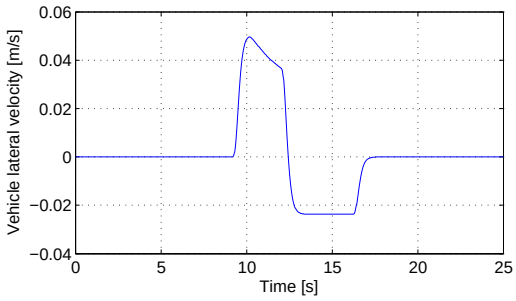

(f) Vehicle lateral velocity

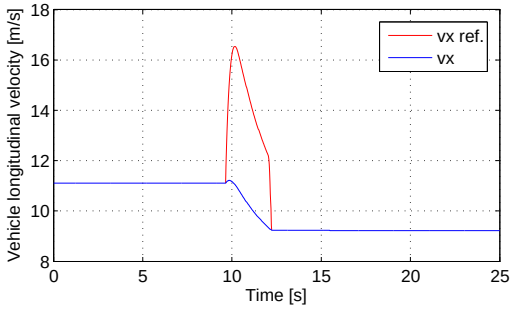

(g) Vehicle longitudinal velocity

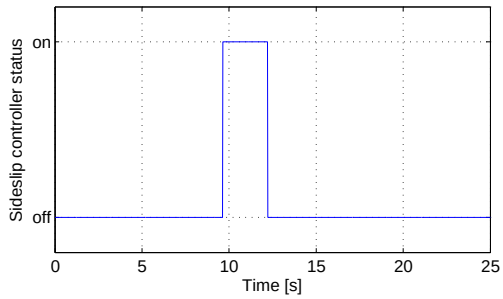

(h) Sideslip controller status

Figure 6.8: Feedback control for the gentle lane change manoeuvre, using RTSM

The trajectory of the vehicle in figure 6.8(a) shows that a lateral shift of almost 4 metres takes place during the manoeuvre.

The results in figure 6.8 can be directly compared with figure 5.8 since both sets of results are obtained using feedback control. The two figures showing yaw rate are very similar indeed. The vehicle longitudinal velocity decreases by a similar amount in both models, although the demanded wheel forces in the RTSM are approximately 50% larger at the peak value. The main difference occurs with the figures showing vehicle sideslip. The initial peak value from the RTSM model is almost double that from the VSM, and the RTSM takes much longer to reduce sideslip to within the threshold. In fact in the RTSM, the sideslip does not return to within the threshold, but only reduces somewhat towards the threshold. Overall, the results obtained from the VSM are more oscillatory then those obtained from the RTSM, the reasons for which have been discussed in earlier chapters.

Feedback control with feedforward based steering

In this section, feedforward based steering is combined with the feedback controller to simultaneously control vehicle sideslip and yaw rate during the gentle lane change manoeuvre. Again, no driver input via the rig is considered. The results are shown in figure 6.9, which highlight some interesting results.

The yaw rate is controlled very well with a small overshoot and no oscillations (see figure 6.9(b)). Also the small lag which was present when only the feedback controller was used, has disappeared now that feedforward based steering is used. However, the vehicle sideslip naturally occurs within the threshold at the initial velocity of the vehicle. Hence no control is required. As such, the vehicle velocity does not change in figure 6.9(g). Peaks do occur in the demanded road wheel forces, however these occur purely to counteract the overshoot on the yaw rate signal. It is important to note that the sideslip controller is not activated with the current threshold value. Obviously if this threshold was reduced in magnitude then controller intervention would be necessary.

However, reducing the threshold value for all controller setups would result in much larger variations in the vehicle velocity. Also, if different threshold values were were used for each manoeuvre, then comparisons between the results would become more difficult.

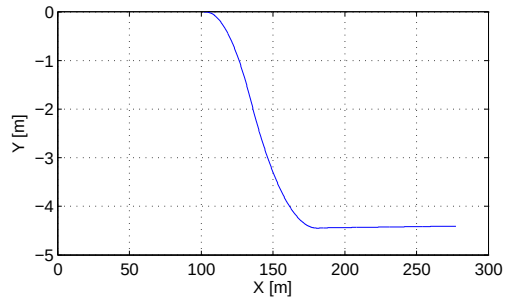

(a) Vehicle trajectory

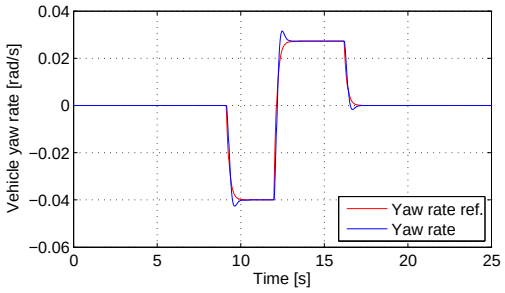

(b) Vehicle yaw rate

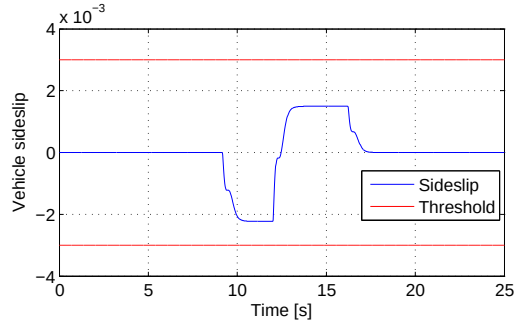

(c) Vehicle sideslip

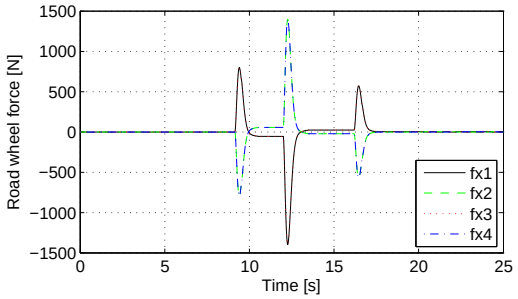

(d) Demanded longitudinal road wheel forces

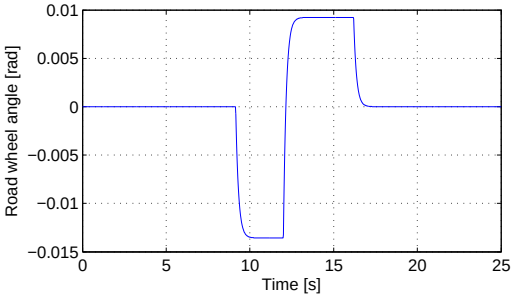

(e) Road wheel angle

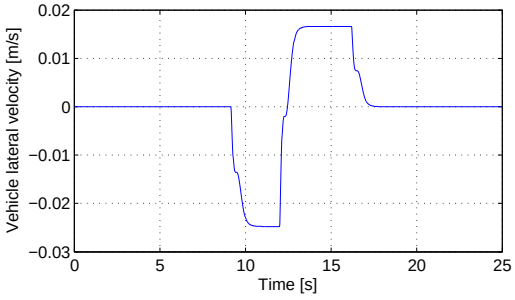

(f) Vehicle lateral velocity

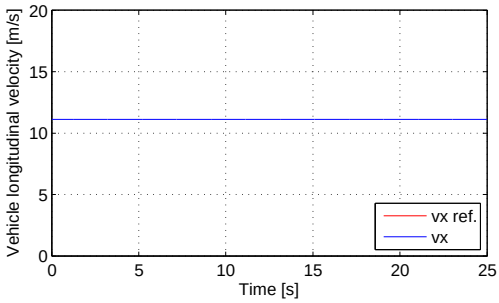

(g) Vehicle longitudinal velocity

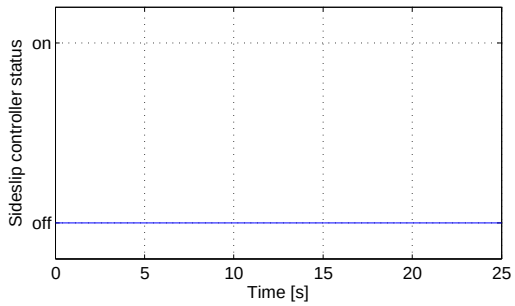

(h) Sideslip controller status

Figure 6.9: Feedback control and feedforward based steering for the gentle lane change manoeuvre, using RTSM

More precise control of yaw rate is possible when the feedforward based steering is included in the control structure, and approximately three to four times less wheel forces required to achieve the precise control when compared to figure 6.8.

The trajectory in figure 6.9(a) shows that although the reference signals were the same for the feedback control, the higher velocity for integrated control has meant that the vehicle has travelled further to the right.

Overall, this control structure has been able to control yaw rate while vehicle sideslip did not require controlling. Furthermore, it would appear that the integrated control is better at completing the control task than using only feedback control. The lag which occurred for the feedback control of yaw rate has now been removed by the feedforward based steering. There is an added bonus with the fact that in the integrated steering and feedback control setup, vehicle sideslip does not require controlling. Again, this is only because the predetermined threshold value.

6.3.3 Driver steering input and yaw rate control

This section still continues to simulate a gentle lane change manoeuvre, but the inputs to the vehicle model now change together with the control variables. The inputs to the vehicle model are now human (or driver) input via the interface test rig, and feedback control of yaw rate. Therefore, feedforward based steering is inactive. This experiment is a single test with one driver, and the instructions to the driver remain the same as those detailed in section 6.3.1, with the exception of the rest period between runs since there is only 1 run for this test. The driver will continue to use the visual feedback monitor of the animation PC whilst attempting to navigate the manoeuvre. Figure 6.10 shows results for this setup.

The yaw rate is the only controlled variable and follows the reference signal well until approximately 16 seconds, where an overshoot occurs due to the driver's input at the rig (see figure 6.10(e)). This overshoot is quickly eliminated back to the reference of zero. Vehicle sideslip is not controlled but is plotted together with the threshold signal that will be used when the controller is active, in figure 6.10(c). The magnitude of the sideslip angle is relatively large, and since it is not controlled, the vehicle velocity in figure 6.10(g) does not change.

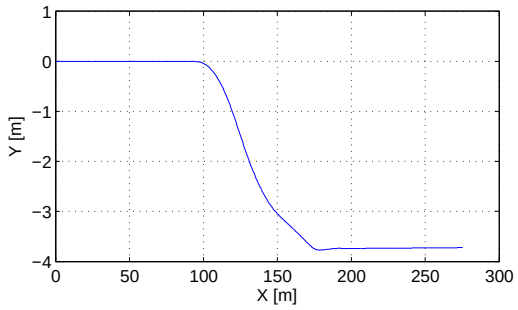

(a) Vehicle trajectory

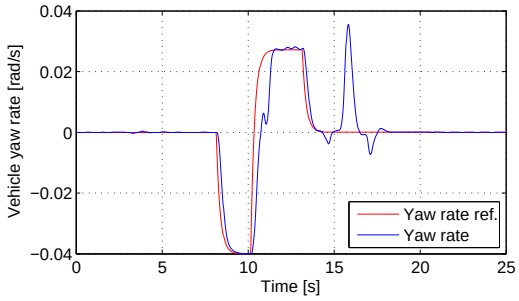

(b) Vehicle yaw rate

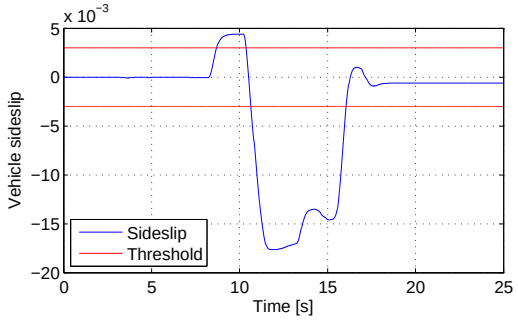

(c) Vehicle sideslip

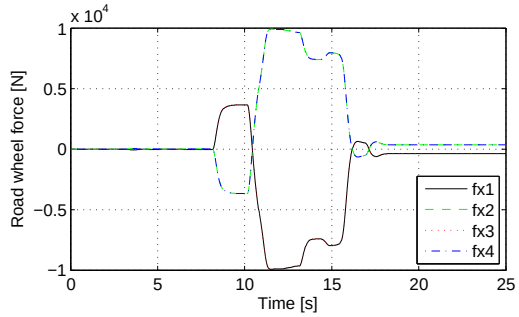

(d) Demanded longitudinal road wheel forces

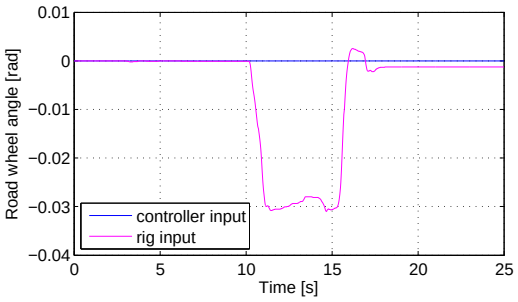

(e) Road wheel angle

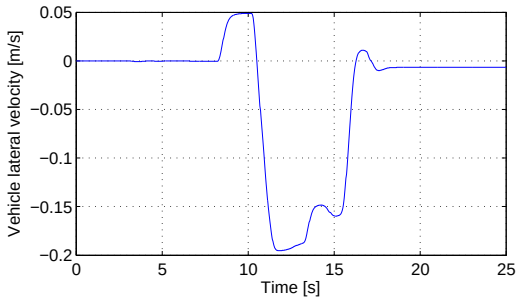

(f) Vehicle lateral velocity

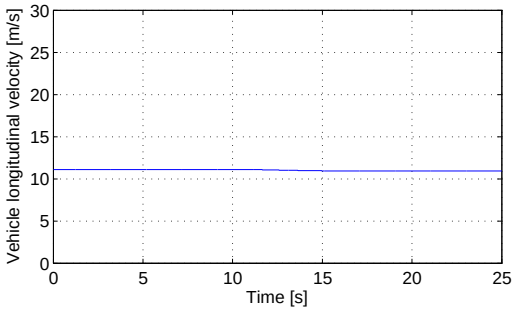

(g) Vehicle longitudinal velocity

Figure 6.10: Driver input and yaw rate control for the gentle lane change manoeuvre, using RTSM

The road wheel angle which is derivable from the driver's steering input via the steering ratio can be compared to the reference yaw rate, and the two should have some similarities (in earlier results in chapter 6, the feedforward based steering angle was used to generate the desired yaw rate and there were similarities in shape). However they do not — even the sign is not common. This explains the large forces demanded by the feedback controller, which almost fight against the driver at the rig. Despite this, a good lateral shift is achieved as shown in figure 6.10(a)). It is important to stress here that the test rig input is the driver's natural reaction when attempting the lane change manoeuvre, and may act against the automatic reference signal for yaw rate if the driver feels that the reference signal is not natural.

One final point to note is that the driver does not start to turn the vehicle until 10 seconds, whereas the yaw rate controller is activated 2 seconds earlier.

6.3.4 Driver steering input and sideslip control

The setup for this section is the same as the previous section with the exception of controlling vehicle sideslip instead of yaw rate. Therefore, driver input is applied via the rig, and channel 1 of the feedback controller is activated to control sideslip. Again, the driver has visual feedback and attempts to steer the vehicle through the same gentle lane change manoeuvre, while the sideslip controller works alongside. This is again a single experiment with one driver.

The trajectory of the vehicle shown in figure 6.11(a) is more oscillatory than the previous control architectures. This can be explained largely by the widely varying road wheel angle in figure 6.11(e) which the driver uses to steer the vehicle through the manoeuvre. In figure 6.10(e), the road wheel angle remains in a steady state like condition for longer, and importantly is constant for the last 8 seconds of the manoeuvre. In figure 6.11(e) it continues to vary until the end of the manoeuvre.

The steer angle for this manoeuvre is not as smooth when compared to the other manoeuvres when yaw rate control was active. This verifies that the yaw rate control helps to 'steer' the vehicle through the manoeuvre, while the sideslip controller does not.

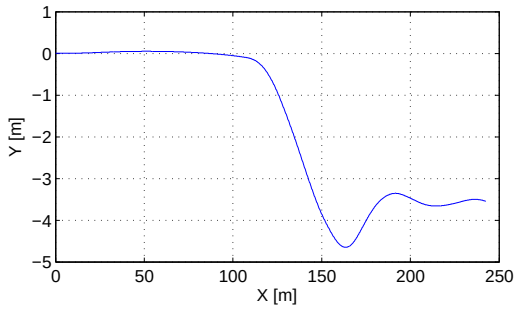

(a) Vehicle trajectory

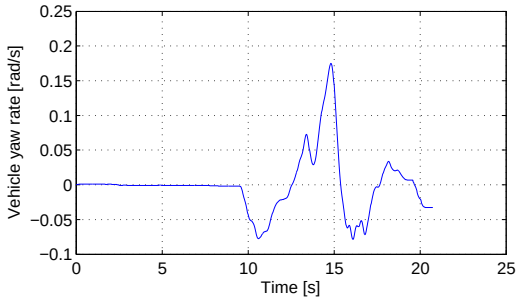

(b) Vehicle yaw rate

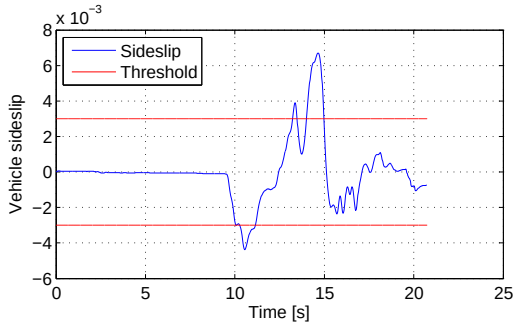

(c) Vehicle sideslip

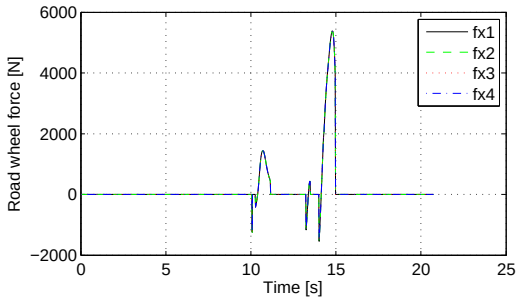

(d) Longitudinal road wheel forces

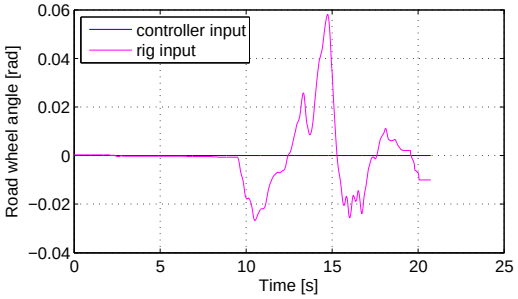

(e) Demanded longitudinal road wheel angle

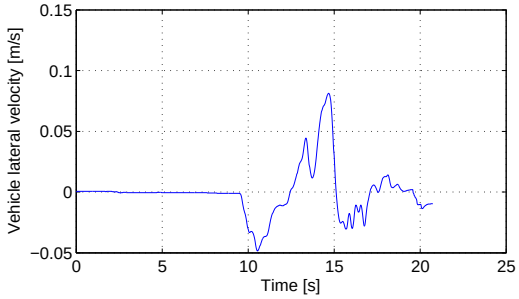

(f) Vehicle lateral velocity

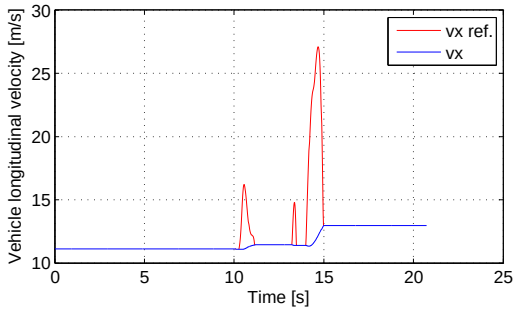

(g) Vehicle longitudinal velocity

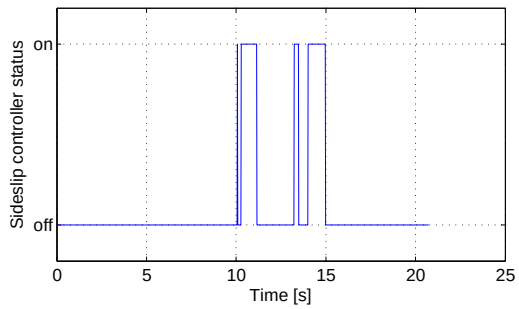

(h) Sideslip controller status

Figure 6.11: Driver input and sideslip control for the gentle lane change manoeuvre, using RTSM

The general shape of the steering input is reflected in the plots for vehicle sideslip and lateral velocity. Overall the sideslip is being controlled in figure 6.11(c), however with the varying test rig input, it becomes difficult to determine exactly what is contributing to the peaks in the plot. The sideslip controller is also not as responsive in this vehicle model, resulting in a required longer time frame to reduce/increase the vehicle speed.

For example, the large peak occurring at approximately 15 seconds is generated from the steering input at the rig. To counteract this large peak, the feedback controller demands a large force on all four wheels to increase the vehicle velocity and reduce vehicle sideslip. However, by the time the longitudinal velocity has increased, the steer angle has changed and hence the sideslip has too. Overall the demanded wheel forces are not excessive as can be seen in figure 6.11(d).

The uncontrolled yaw rate has remained similar to the driver only responses in figure 6.6, indicating that controlling only sideslip does not have a negative effect on the yaw rate response of the vehicle. The sideslip controller status in figure 6.11(h) highlights that the controller is never active for long periods of time, but instead only for short bursts. This can be explained by the controller working and the rig input changing quickly, hence the vehicle sideslip changes quickly also. Consequently, v_x never gets the same opportunity to increase or decrease enough to regulate β, as it does in the constant yaw rate manoeuvre, where steady state values were reached.

6.3.5 Driver steering input and feedback control

This section progresses naturally from the previous section, and the setup is now changed to accommodate simultaneous feedback control of yaw rate and sideslip with human input via the rig. However, no feedforward based steering is included. Therefore, the only difference in setup between the results for this section and figure 6.8 is that no driver input from the test rig is considered in the latter figure. Comparing these two sets of figures can help determine how the controllers interact with the driver's steering input.

Figure 6.12 shows the collection of plots for this simulation. First observations are that there are a lot of oscillations present, although the trajectory of the vehicle is smooth. The yaw rate and the corresponding reference signal are shown in figure 6.12(b). The yaw rate is very oscillatory and is due in part to the driver input in figure 6.12(e).

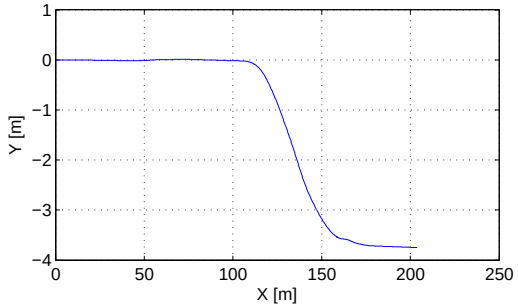

(a) Vehicle trajectory

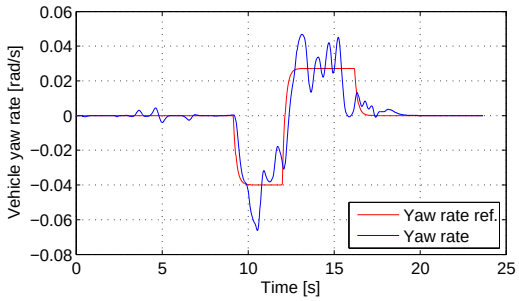

(b) Vehicle yaw rate

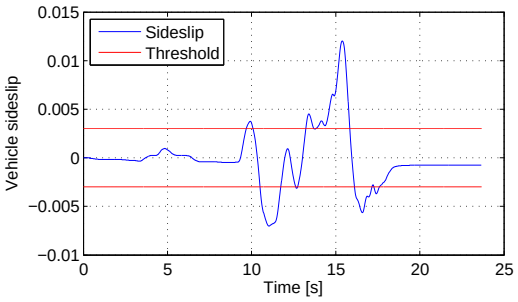

(c) Vehicle sideslip

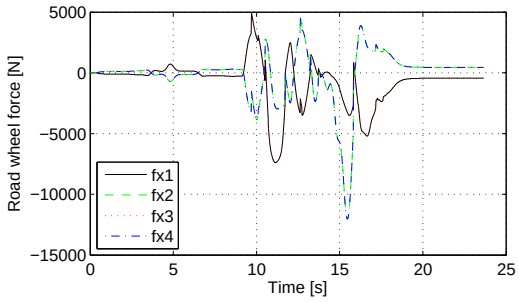

(d) Demanded longitudinal road wheel forces

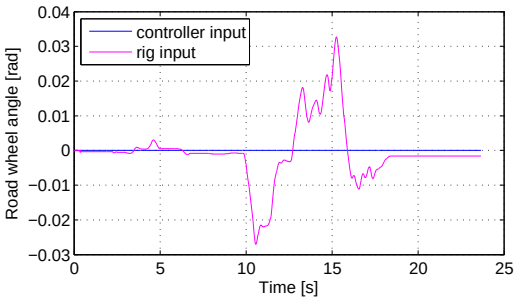

(e) Road wheel angle

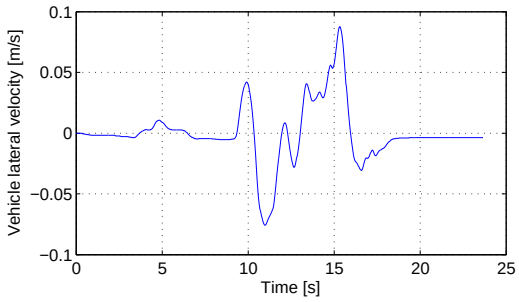

(f) Vehicle lateral velocity

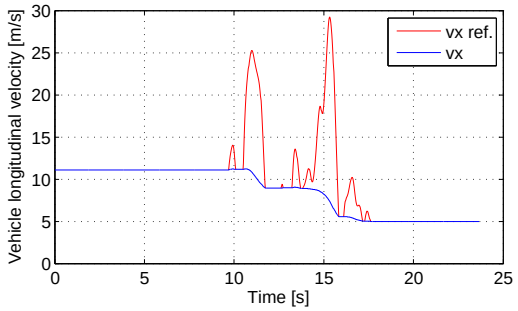

(g) Vehicle longitudinal velocity

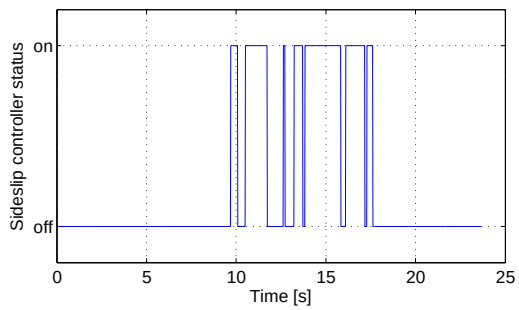

(h) Sideslip controller status

Figure 6.12: Driver input and feedback control for the gentle lane change manoeuvre, using RTSM

These oscillations occur around the reference signal and the yaw rate reference is still followed somewhat. The changing steering angle input prohibits the yaw rate from reaching steady state, instead the controller is always working to remove the error. The changing vehicle velocity also contributes to these oscillations.

Throughout figure 6.12(d) the longitudinal wheel forces are actively working to reduce the yaw rate error, which is confirmed by the different forces on each side of the vehicle. Meanwhile, figure 6.12(h) shows the sideslip controller activity during the manoeuvre. The sideslip controller is much more active, although still only for short durations at a time.

After 15 seconds there is a large difference between the demanded longitudinal wheel forces from one side of the car to the other (see figure 6.12(d)). It can be shown that when the demanded longitudinal wheel forces have the same magnitude and sign, that the sideslip controller is actively working. Likewise, when there is a large difference from side to side, the yaw rate controller is working. This large input is triggered by the steering input from the rig, which generates an excessively large yaw rate. It is this yaw rate that the large longitudinal wheel forces are trying to compensate for.

However, the sideslip controller is slow in bringing the sideslip back to the threshold value. Again, the steering input is large at times when the sideslip is being controlled, which generates extra sideslip, taking it further from the threshold value, giving the impression that it is not being controlled. However, the decreasing velocity occurs when the sideslip threshold is exceeded, indicating that the controller is demanding a change in velocity. Indeed, by the end of the manoeuvre, the vehicle velocity has decreased by 60% of its initial velocity.

Finally, it is interesting to compare figure 6.12 and figure 6.8. The demanded wheel forces increase in magnitude and are more widely varying when the test rig input is considered. This extra input also generates more vehicle sideslip and as a result, the longitudinal velocity of the vehicle is required to decrease in an attempt to control sideslip.

6.3.6 Driver steering input and feedback control with feedforward based steering

This is the final combination of control structures for lane change manoeuvres with the test rig input. This combination includes feedback control, feedforward based steering and the rig input connected.

Figure 6.13 shows the results for this simulation. The addition of the feedforward based steering seems to have made the system respond in a less oscillatory manner, and behave in a more controlled-like manner (when compared to figure 6.12 with no feedforward based steering). The trajectory of the vehicle throughout the manoeuvre, shown in figure 6.13(a) is barely adequate to perform the lateral lane change as it turns towards the left hand side (positive direction) of the lane at the end of the simulation. The yaw rate follows the shape of the reference signal, but is somewhat oscillatory around the reference value. Two things can be responsible for this: firstly, the steering input from the rig causes extra yaw rate and the feedback controller attempts to correct this, causing the vehicle to sway slightly from side to side. Secondly, the changing velocity has an effect on the yaw rate (remember from the model equations that the yaw rate response is first order and dependent on v_x). Most commonly, it is a combination of both, with the velocity increasing by around 80% in 7 seconds from 11 m/s to 19 m/s. Also, large differences in the demanded longitudinal wheel forces can be seen from one side of the vehicle to the other, which corresponds to a correction of yaw rate to try and minimise the error. This error is most likely generated via the steering input from the test rig.

The demanded longitudinal wheel forces are very large (see figure 6.13(d)), especially at approximately 11 seconds when a large differential style force is required for yaw rate correction. At this stage of the manoeuvre, the feedback controller is counteracting the two steering inputs that have been summed together. This is due mainly to the steering angle which has more than doubled in magnitude from the 'required' wheel angle, calculated from an inverse model.

Finally, the vehicle sideslip in figure 6.13(c) has very similar peak magnitudes to the simulation without feedforward based steering. However, when the feedforward based steering is applied, is sideslip controller is required for a shorter duration of time.

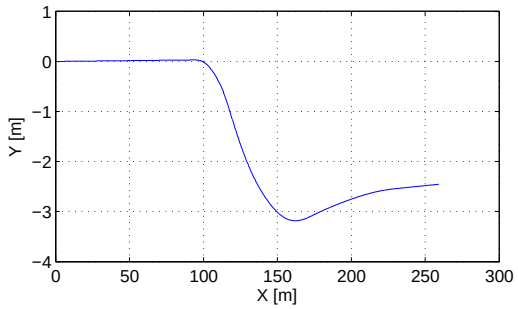

(a) Vehicle trajectory

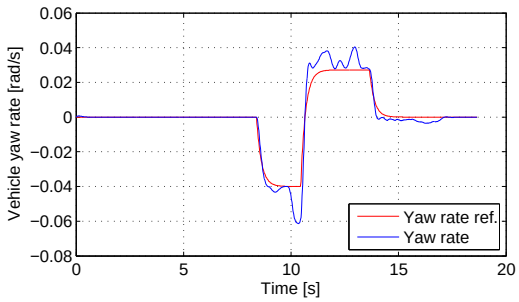

(b) Vehicle yaw rate

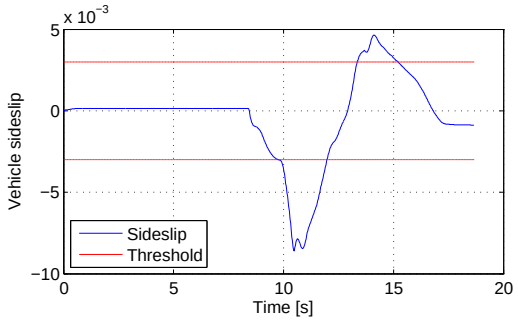

(c) Vehicle sideslip

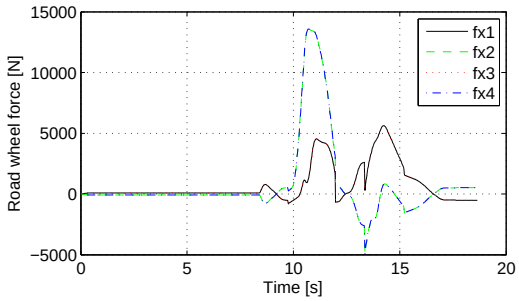

(d) Demanded longitudinal road wheel forces

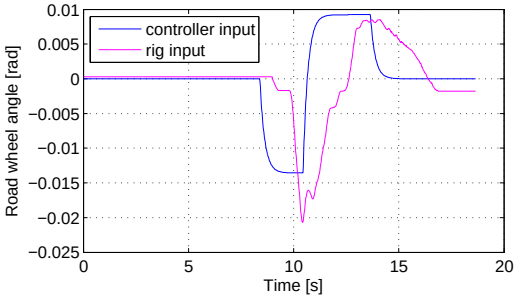

(e) Road wheel angle

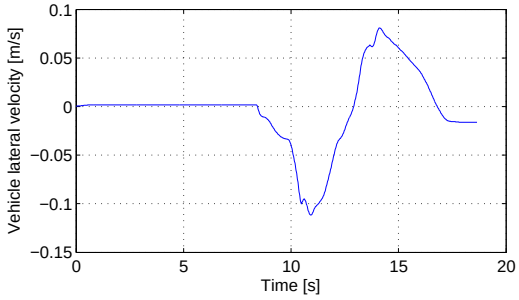

(f) Vehicle lateral velocity

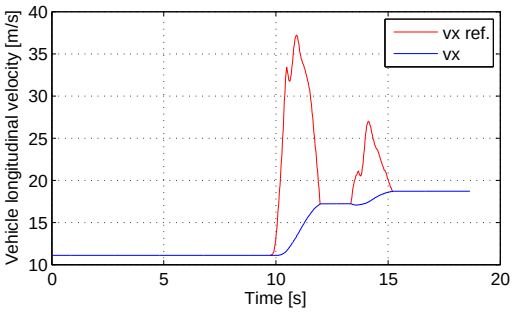

(g) Vehicle longitudinal velocity

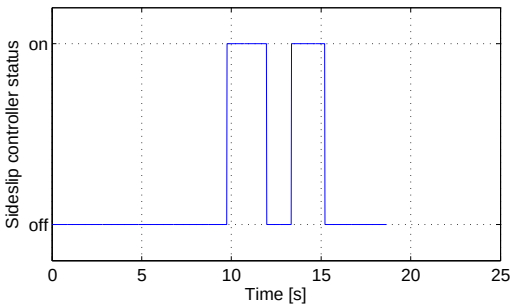

(h) Sideslip controller status

Figure 6.13: Driver input and feedback control with feedforward based steering for the gentle lane change manoeuvre, using RTSM

But again, when the sideslip is being controlled, a steering input from the rig is applied making it difficult to assess how successful the controller is, since a small change in β requires a fairly large change in v_x to correct it.

6.3.7 Discussion

Experimental results have been presented for a gentle lane change manoeuvre using various control architectures. This involved a combination of the 2 channel feedback controller, feedforward based steering input and steering input from the human interface test rig. Visual feedback for driver aid was also used when required.

Firstly, five attempts of a gentle lane change manoeuvre were made with driver steering from the test rig being the only input to the vehicle model. At this stage all other controllers were inactive. The results were similar for each run, and some indication of how the vehicle behaves to the driver's steering input during the manoeuvre was obtained. Feedback control without any human input was then assessed to evaluate how the controller compared with the driver's steering input. Both the sideslip and yaw rate of the vehicle were reduced when the feedback controller directed the vehicle through the lane change. Next, the feedback controller was combined with feedforward based steering which contributed more positively to the simultaneous control task.

Next, driver steering input was combined with feedback control of yaw rate and then feedback control of sideslip with driver steering input. For each case, it is useful to compare the uncontrolled variable to the driver input plots to ascertain if controlling one variable has a negative impact on the uncontrolled variable. When controlling sideslip the yaw rate did not vary much from the values seen in the driver input only plots. However, when controlling yaw rate, the sideslip increased by a factor of 2. This is due mainly to the increased lateral velocity as a result of controlling the yaw rate.

Driver input and sideslip control saw a reduction of approximately 20% for a 15% increase in vehicle velocity, when compared to driver input and yaw rate control. However, compared to the driver only steering input runs, the sideslip response was larger.

The driver input and feedback control of both channels resulted in a much larger sideslip and a more oscillatory yaw rate response. However, adding feedforward based steering resulted in figure 6.13, which is more acceptable in terms of the β and $\dot{\psi}$ response.

The best results in terms of controllability came from the combined rig input, feedforward based steering and feedback control. Although the feedback controller is working hard to counteract the excessive yaw rate which is generated when the two steering angles are added together, the yaw rate and sideslip are both controlled although slightly oscillatory. The vehicle sideslip in this case is actually larger than the feedback controller only setup, and slightly larger than the human/rig input only.

From these observations, it seems that the rig input changes too quickly for the controllers to cope, especially when the sideslip channel of the controller is trying to vary v_x quickly.

6.4 Sidewind disturbance manoeuvre

In everyday driving a situation exists where a sidewind disturbance acts on the vehicle, generating a large lateral velocity while longitudinal velocity remains relatively unchanged (e.g. overtaking a high sided vehicle). In this section, the different control architectures are implemented to study how effectively a sidewind disturbance can be rejected. A step disturbance input is added to the RTSM vehicle model via the tyres to represent a lateral force. The step function is rate limited to avoid an unrealistic rise in lateral components (e.g. f_y and v_y). The disturbance applied is shown in figure 6.14 below.

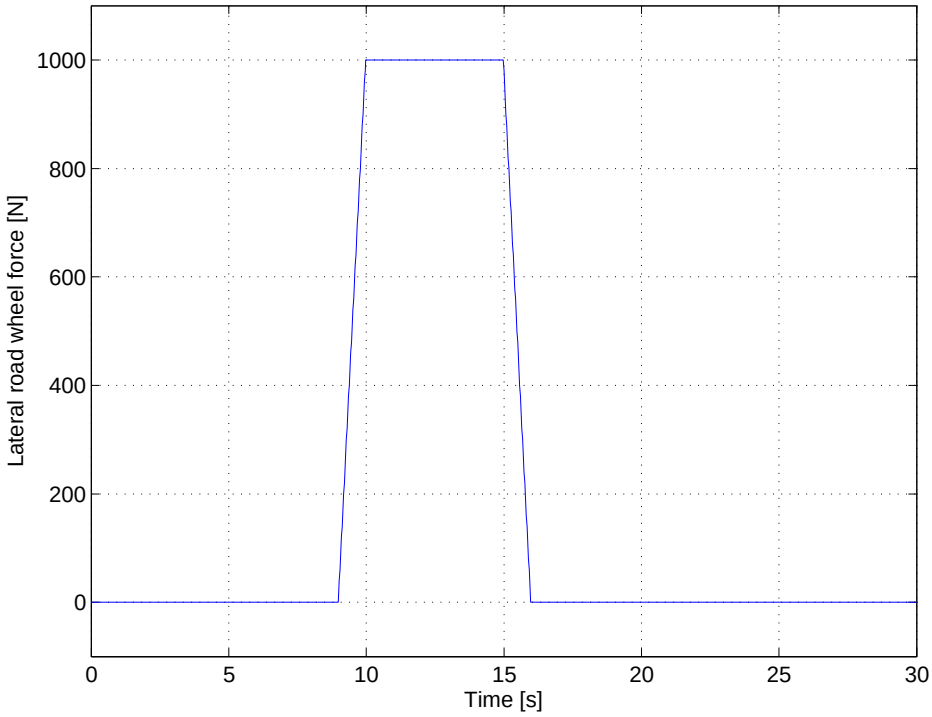

Figure 6.14: Step input to represent a sidewind disturbance

The sidewind will be acting directly at all four wheels of the vehicle simultaneously, creating an additional lateral velocity together with a small amount of yaw rate because of the different moment arms from the centre of gravity to the front and rear axle. The driving scenario for the simulations in this section is as follows. A vehicle is travelling straight ahead (with a heading angle of zero), and an initial velocity of 11.11 m/s. After a duration of 9 seconds, the side wind disturbance acts on the vehicle tyres. It was seen from chapter 2 that vehicle movement is created by forces acting on the tyres, and in this instance the lateral forces should create a lateral motion, resulting in a sudden change in vehicle sideslip. The

step has a magnitude of 1000 N, acting for a duration of 6 seconds, after which time the step is deactivated. The effects of this disturbance should be minimised when any of the controllers are activated. The reference for yaw rate will be constantly zero, but the reference for sideslip will again be limited to a threshold value, as before. This threshold value will be determined relative to the value of sideslip that is seen from a passive vehicle, to ensure that the threshold is realistic.

A time delay between the front and rear wheels was initially considered. But the time delay, t_d calculated in equation (6.1) was deemed small enough to be considered negligible. The time delay, t_d can be calculated as

$$t_d = \frac{(d_l + d_r)}{v_x} = 0.277 \text{ secs}, \tag{6.1}$$

where the term $(d_l + d_r)$ is the distance between the two axles (3.08m), and assuming that the velocity will not change from the initial value, v_x is equal to 11.11 m/s.

Firstly, the step disturbance is applied to the vehicle model without any controllers or driver input connected. This enables the natural, uncontrolled response of the vehicle to be obtained, so that it can be compared to the controlled responses later in this chapter.

Next, the same disturbance is applied to the vehicle with only driver input connected via the human interface rig, and the driver alone tries to counteract the sidewind disturbance. This enables the driver's reaction to the disturbance to be analysed and to see how the vehicle behaves under these circumstances. The behaviour in this case will be compared directly to the automatic controller response (both with and without driver input). From all of the results, conclusions will be drawn on the usefulness and effectiveness of the designed feedback controller. In this manoeuvre, feedforward based steering cannot be used because the wheel angle is generated from the desired yaw rate, which in this case is zero.

Finally, in all plot where it is deemed applicable, the period of time that the disturbance acts is marked with a solid black line along the bottom of the x-axis. This will be mainly for the plots showing the vehicle trajectory throughout the manoeuvre, but will also appear on the figures showing the driver's input from the test rig. All other plots are generally self explanatory where the disturbance acts.

6.4.1 Sidewind only

In this section, the natural response of the vehicle to the sidewind disturbance is obtained. No steering input via a driver at the test rig is considered, and neither are any control systems. Therefore, this is only the sidewind acting on a passive vehicle.

Figure 6.15 shows the plots of interest for this manoeuvre. Figure 6.15(a) shows the effect that the sidewind disturbance has on the vehicle trajectory. Instead of travelling straight ahead, the vehicle deviates a total of 16 m to the left within a longitudinal distance of slightly greater than 100 m by the end of the simulation. The resultant yaw rate and sideslip angle of the vehicle are shown in figures 6.15(b) and 6.15(c) respectively. In both of these figures a step function can be identified which returns to the initial value when the disturbance is no longer acting on the vehicle. The lateral velocity follows the same step function shape for the same duration as the other two plots. Both the longitudinal wheel forces (figure 6.15(d)) road wheel angle (figure 6.15(e)) are zero for the duration of the manoeuvre.

Finally, the velocity remains unchanged throughout the simulation, which was also seen in chapter 2 for a step steer input. Therefore it can be said that the vehicle sideslip is created purely by the change in lateral velocity.

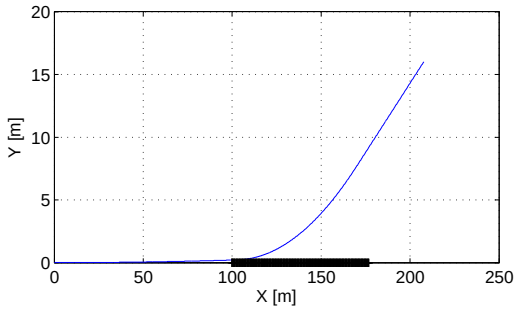

(a) Vehicle trajectory

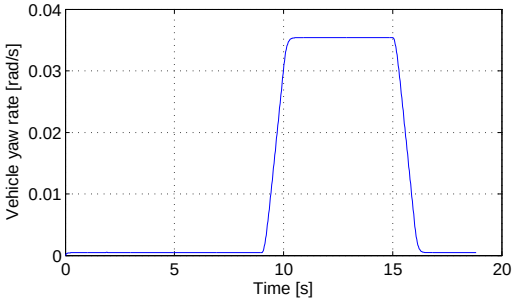

(b) Vehicle yaw rate

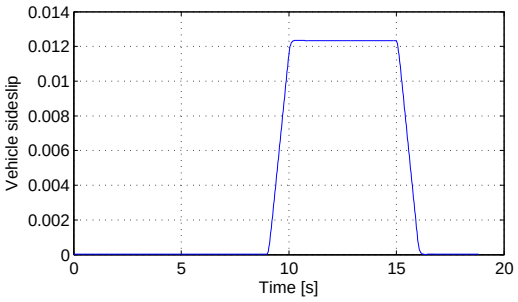

(c) Vehicle sideslip

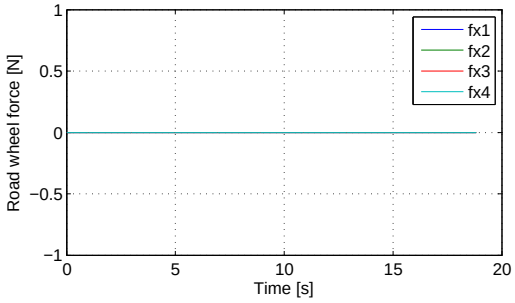

(d) Demanded longitudinal road wheel forces

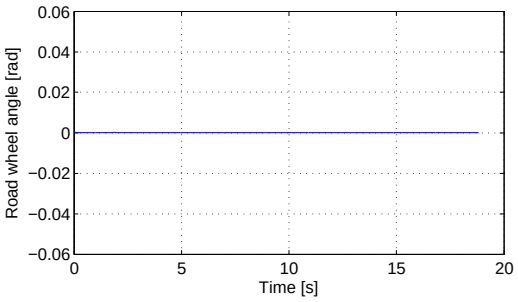

(e) Road wheel angle

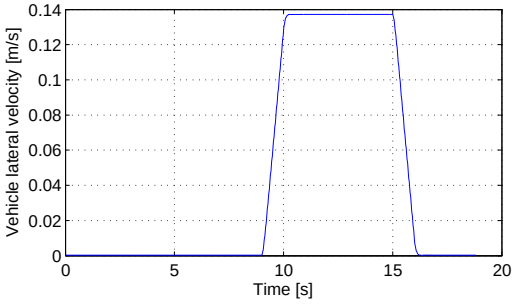

(f) Vehicle lateral velocity

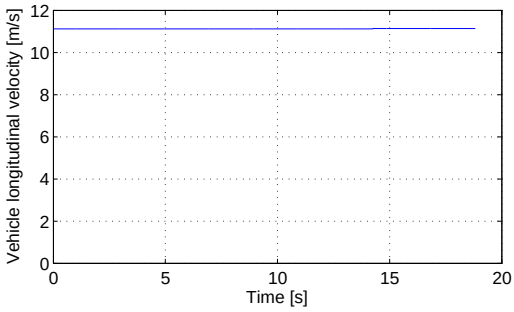

(g) Vehicle longitudinal velocity

Figure 6.15: Passive vehicle response to the sidewind disturbance manoeuvre, using RTSM

6.4.2 Driver steering input via test rig

The same sidewind disturbance is again applied to the vehicle model, but the setup is altered to allow a steering input from a driver/human to be applied via the human interface test rig. Still travelling straight ahead, the sidewind will force the vehicle off course. The driver will attempt to steer the vehicle and bring it back on course using the real-time vehicle/trajectory visualisation.

For this manoeuvre, one driver that has not completed any of the tasks so far was used to complete the manoeuvres. Thus the driver has no experience of the human interface hardware. Furthermore, five different runs were completed, with a rest period of between 3 and 5 minutes applied between the runs. This was designed to avoid the driver learning the manoeuvre. Also, the task was not rehearsed beforehand.

Figures 6.16 to figure 6.20 show the total of 5 runs mentioned above. For all of these figures, there is a solid black line plotted along the x-axis, indicating when the disturbance was acting on the vehicle.

The trajectory plot in figure 6.16 shows a variety of different paths as the driver steers the vehicle to try and counteract the sidewind. As the disturbance acts, the driver can be seen to try and steer the vehicle back onto the original course. Overall this is quite successful, but when the disturbance stops acting the car steers heavily to right. The change in vehicle velocity is negligible during the period when the disturbance acts on the vehicle, and it is therefore not shown. The driver uses the rig to generate the road wheel angles shown in figure 6.17, and all angles are similar and follow the same trend. Importantly, the large inputs after approximately 16 seconds occur because the disturbance has stopped acting, but the vehicle is still trying to counteract the disturbance and travels too far right. So the driver must correct for this and steer the vehicle back towards the ($x = 0$) position. The lateral velocity plots are shown in figure 6.18, and the yaw rate and sideslip responses to the driver input complete the set of outputs (shown in figures 6.19 and 6.20 respectively). Positively, there does not appear to be any 'learning effect' as defined in chapter 5. Instead all of the 5 runs are similar to one another. Finally, it can be seen that the yaw rate responses and the steer angle responses follow a similar trend, while the lateral velocity and sideslip responses follow another similar trend.

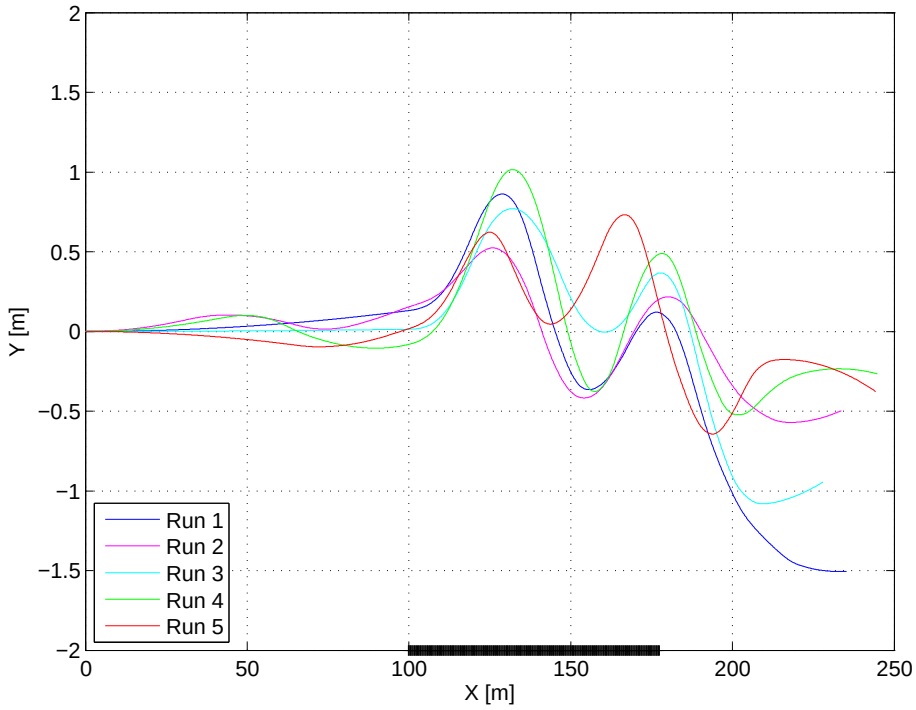

Figure 6.16: Combined trajectories for 5 sidewind disturbance manoeuvres, using RTSM

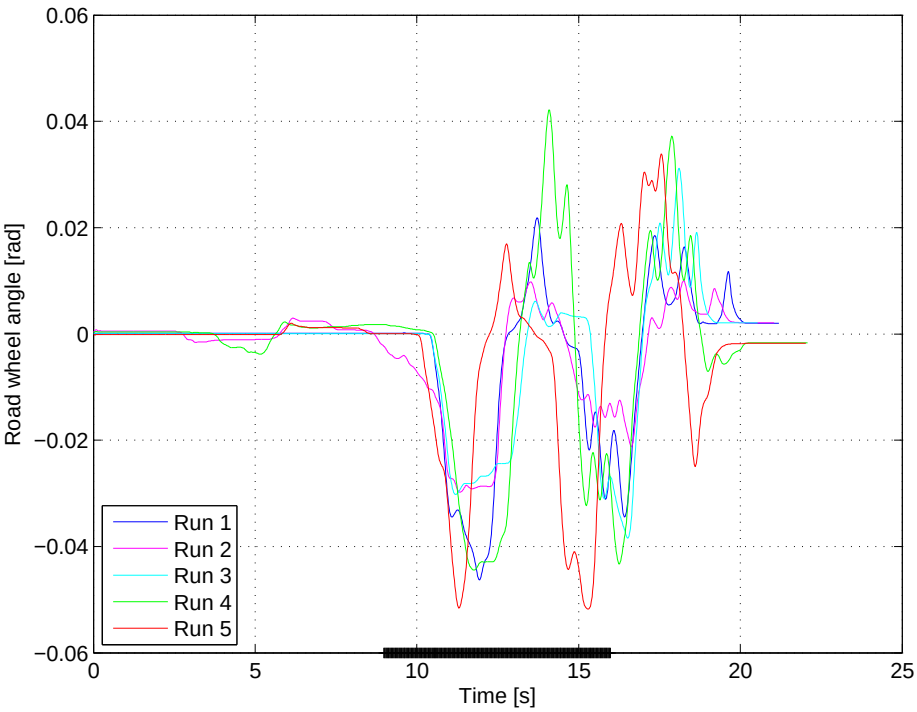

Figure 6.17: Combined road wheel angles for 5 sidewind disturbance manoeuvres, using RTSM

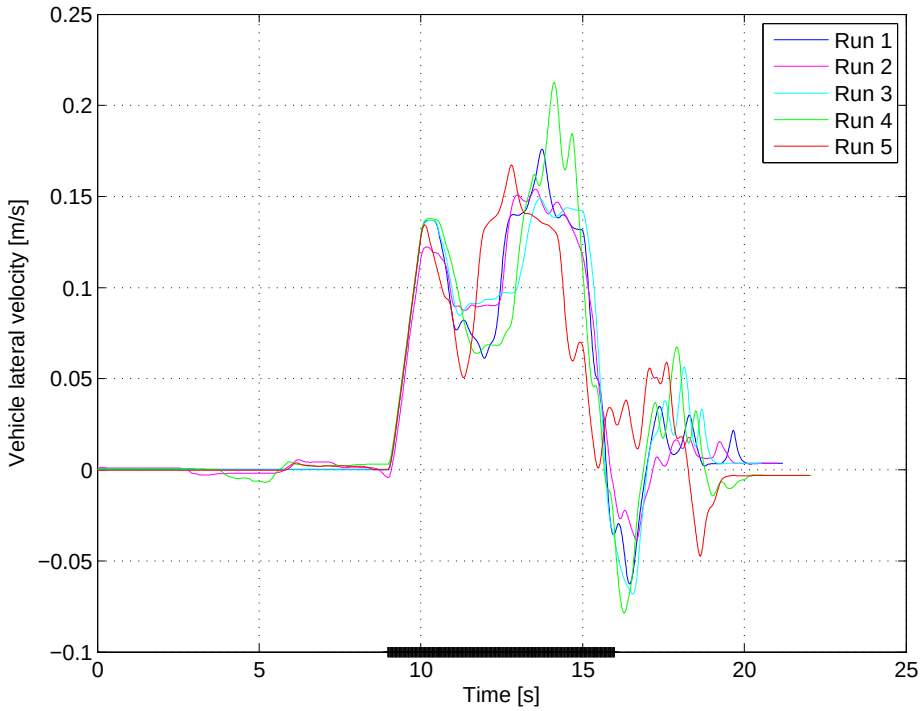

Figure 6.18: Combined lateral velocities for 5 sidewind disturbance manoeuvres, using RTSM

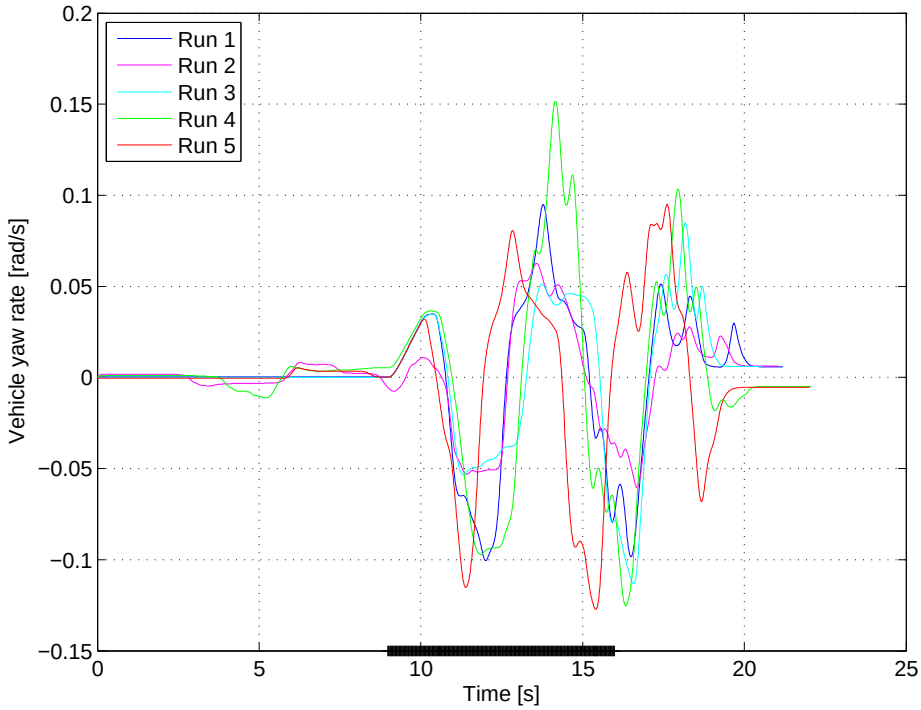

Figure 6.19: Combined yaw rate for 5 sidewind disturbance manoeuvres, using RTSM

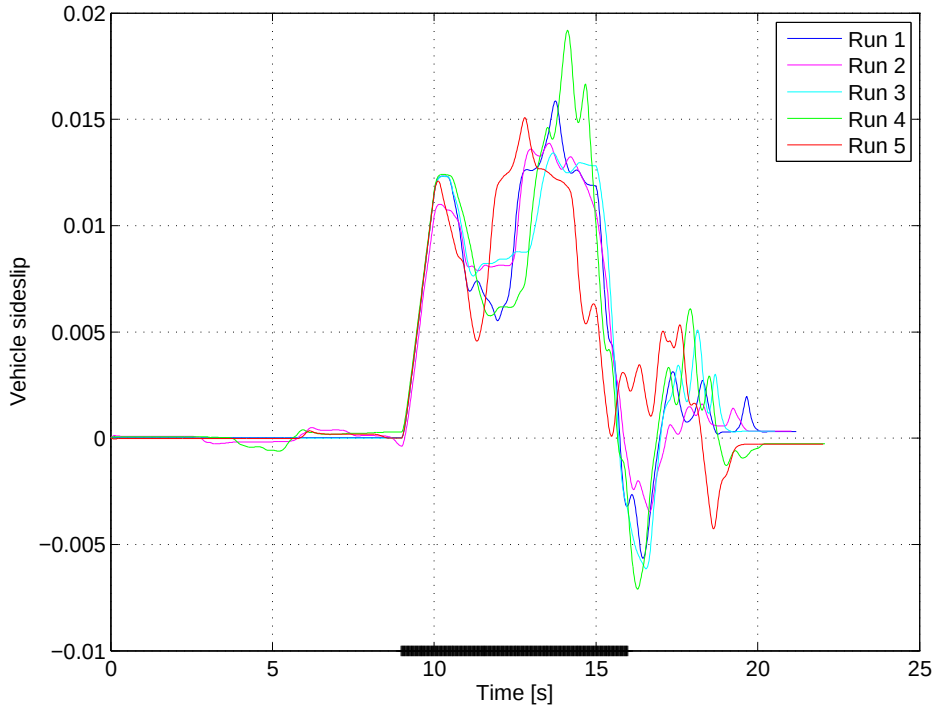

Figure 6.20: Combined sideslip for 5 sidewind disturbance manoeuvres, using RTSM

6.4.3 Driver steering input and yaw rate control

In this section the yaw rate channel of the feedback controller (channel 2) is activated and human input from the test rig is again used as an input. Therefore, the sidewind disturbance remains the same and acts on the vehicle in an identical manner (as per figure 6.14), and the driver continues to steer the vehicle as required to keep it on course.

The reference signal for yaw rate is a constant zero, as before. This should allow comparisons to be made with the vehicle when driver steering is the only input (see figures 6.16 to 6.20). Furthermore, this should help to ascertain if the yaw rate controller has a positive effect on the behaviour of the vehicle when use in conjunction with a human steering input. Figure 6.21 presents the simulation results for driver steering input with feedback control of yaw rate.

With the combined yaw rate control and driver interaction, only a small deviation of less than one metre to the left can be observed. It is very noticeable that the trajectory is less oscillatory when compared to the driver input trajectory plots in figure 6.16. The road wheel angle in figure 6.21(e) is applied from the human via the test rig, and equates to a peak value of 1.7° to the right for a steering wheel input.

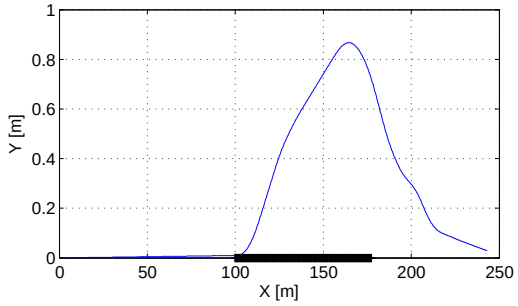

(a) Vehicle trajectory

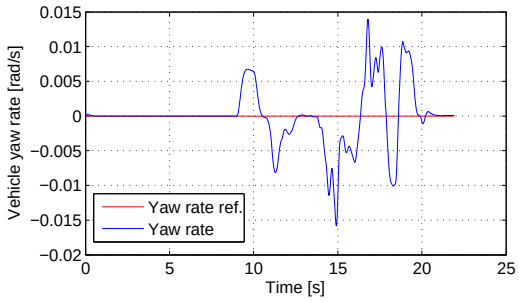

(b) Vehicle yaw rate

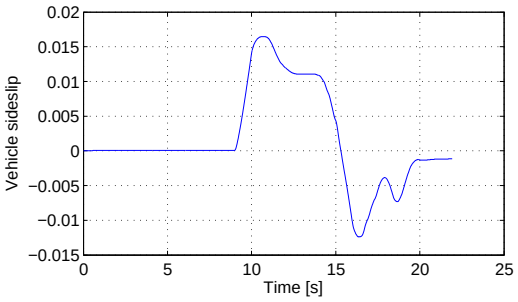

(c) Vehicle sideslip

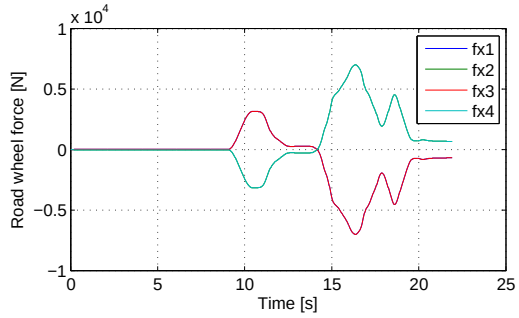

(d) Demanded longitudinal road wheel forces

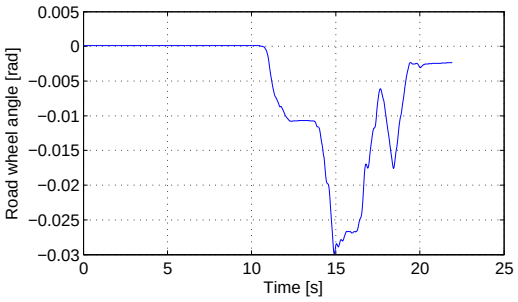

(e) Road wheel angle

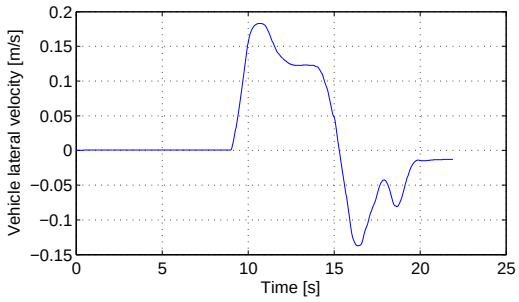

(f) Vehicle lateral velocity

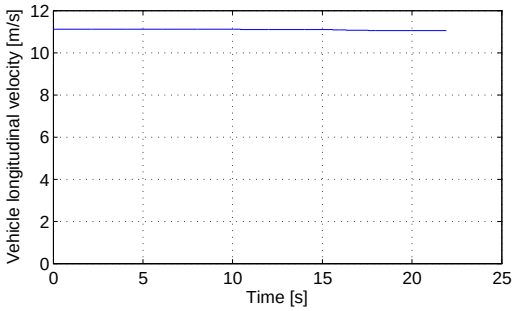

(g) Vehicle longitudinal velocity

Figure 6.21: Driver input and yaw rate control for the sidewind disturbance manoeuvre, using RTSM

In order to try and maintain the yaw rate at zero, longitudinal wheel forces are applied in conjunction with the steering angle, and the feedback controller demands the forces in figure 6.21(d), which are very close to the limit of what can be applied by the actuators. The yaw moment is generated from the differential style braking, and the direction of this moment changes after approximately 14 seconds. This large change in direction is due mainly to the feedback controller trying to counteract the large change in steering input from the driver.

Throughout the manoeuvre, the vehicle is steered heavily to the right to counteract the disturbing sidewind, and when this disturbance stops acting, the vehicle continues to travel to the right generating a positive yaw angle and yaw rate. It is therefore required of the feedback controller to address this issue and generate a counter-yaw rate. The yaw rate (figure 6.21(b)) changes very rapidly, and there are now three different inputs affecting the magnitude of it: the sidewind disturbance, the driver input and the yaw rate controller.

The vehicle sideslip in figure 6.21(c) is generated from the lateral velocity and the longitudinal velocity (figures 6.21(f) and 6.21(g) respectively). The change in longitudinal velocity is so small that it can be considered zero, so the shape of the sideslip response will be determined purely by the shape of the lateral velocity.

Comparing the yaw rate response (figure 6.21(b)) to the response of only the driver input in figure 6.19, shows that the yaw rate is now drastically reduced — on average by a factor of ten (from 0.1 rad/s to 0.01 rad/s). Similarly, the steer angle from the rig is reduced, but only by approximately 25%. It can also be seen that an increase in lateral velocity has led to an increase in sideslip, when compares to figure 6.20.

6.4.4 Driver steering input and sideslip control

Vehicle sideslip is now controlled instead of yaw rate, otherwise the setup remains the same as section 6.4.3.

The aim is to limit the vehicle sideslip to 0.0035 while the disturbance is acting on the vehicle. As before, this is performed by adjusting the longitudinal forces at the wheels. The value for the threshold was chosen since it is lower than the natural vehicle response of sideslip to the sidewind disturbance (figure 6.15). However, the sideslip response is 50% larger at times than the other natural responses for the rig test work. So it was deemed necessary to to choose this larger value to avoid altering the vehicle velocity too greatly that

the simulation may crash. It is however, very close to the 0.003 used elsewhere in this work.

The trajectory of the vehicle for this setup is shown in figure 6.22(a), and this controlled manoeuvre can instantly be seen to wander more than the yaw rate controlled simulation. However, it is not unlike the trajectories generated with the driver input in figure 6.16. During this manoeuvre, the desired longitudinal wheel forces are calculated by the sideslip controller, which results in an increase in the vehicle velocity of approximately 40% as per figure 6.22(g). As for the vehicle sideslip in figure 6.22(c), a reduction occurs between approx 12 and 15 seconds. There are a few other points when the vehicle sideslip starts to decrease sharply, which corresponds with a sharp turn of the road wheel (see figure 6.22(e)). This will naturally change β as v_y decreases towards zero and v_x increases.

As for the yaw rate of the vehicle, this has increased greatly in magnitude from the yaw rate controlled with driver steering input plot of figure 6.21(b), but is approximately the same as for the driver input only plots in figure 6.19. The demanded longitudinal wheel forces do not differ from one side of the vehicle to the other, indicating that they do not contribute to generating a yaw moment as expected. These forces are not excessively large, and within the limits of the actuators as discussed earlier. Finally, the driver's road wheel angle is again similar in magnitude to the 5 runs carried out earlier with only the driver's steering to counteract the sidewind disturbance. However, one important difference is visible in figure 6.22(e): it almost remains a negative angle for the duration of the manoeuvre, and it is a very smooth signal which does not change rapidly. This would indicate that the controller is working in tandem with the driver's steering angle, making it less sporadic and less like the driver steering only results.

With the sideslip controller active and an understanding of how the control effort changes the longitudinal velocity of the vehicle to alter the sideslip, the following would have been expected to occur during the manoeuvre. As the lateral velocity increases, the longitudinal velocity would also change to try and maintain the ratio of v_y to v_x to be less than the threshold. However, the varying driver input via the test rig, together with the delay in increasing the longitudinal velocity (i.e not instantaneous) makes it very difficult for the sideslip controller to be effective. As a result, the sideslip controller status in figure 6.22(h) shows that the controller is active for the full duration that the sidewind disturbance acts.

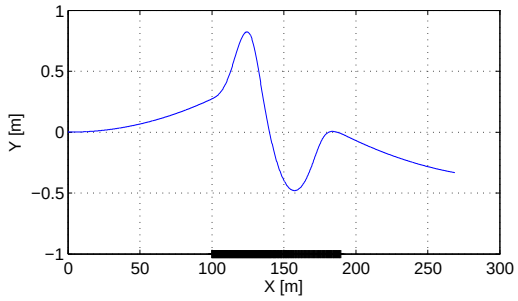

(a) Vehicle trajectory

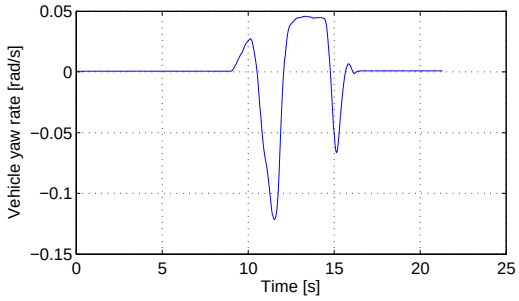

(b) Vehicle yaw rate

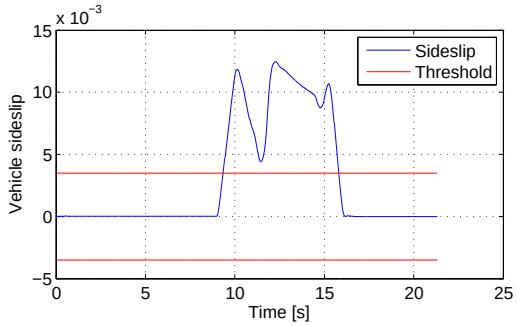

(c) Vehicle sideslip

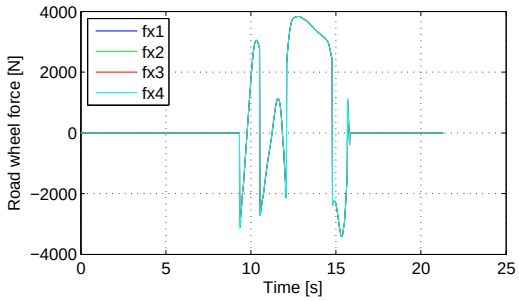

(d) Demanded longitudinal road wheel forces

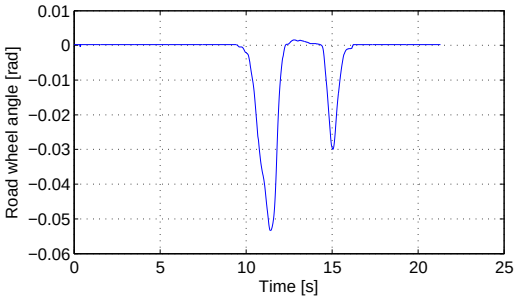

(e) Road wheel angle

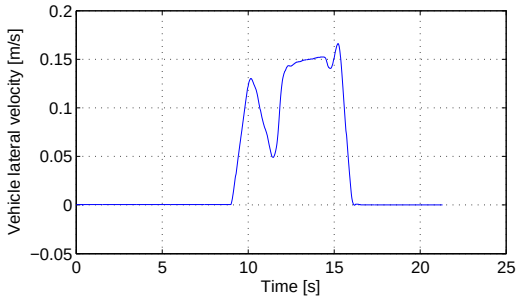

(f) Vehicle lateral velocity

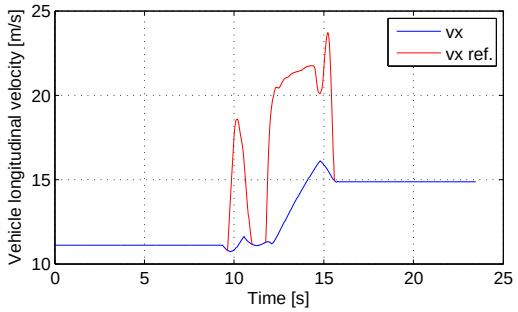

(g) Vehicle longitudinal velocity

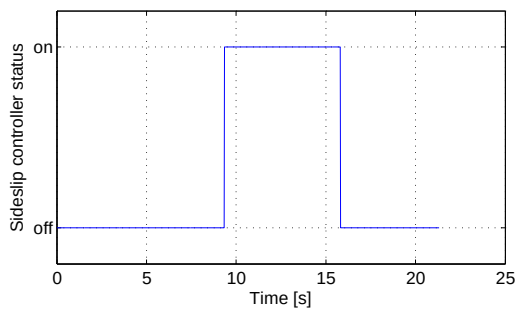

(h) Sideslip controller status

Figure 6.22: Driver input and sideslip control for the sidewind disturbance manoeuvre, using RTSM

6.4.5 Driver steering input and feedback control

This section attempts to reject the sidewind disturbance using both driver input via the test rig and simultaneous control of yaw rate and sideslip. Therefore, both channels of the feedback controller will be active, and the driver will again have visual feedback from the monitor to try and counteract the sidewind. Again there is no feedforward based steering applied, since this would be generated from the yaw rate reference signal — which is zero.

The trajectory of the vehicle is shown in figure 6.23(a) is a vast improvement on the driver input only case and any of the individual control simulations so far. However, the shape of the trajectory is comparable with figure 6.22. An improved yaw rate response can also be observed when both channels of the feedback controller are activated (see figure 6.23(b)). The magnitude of the controlled signal is smaller and there is less deviation from the maximum value to the minimum value of the signal, when compared to the driver only input plots. It is however, larger than was achieved in figure 6.21 for yaw rate control with driver input. The feedback controller demands the longitudinal wheel forces in figure 6.23(d) to achieve the simultaneous control objective. The difference in magnitude between the left and right hand side of the vehicle attempts to minimise the yaw rate error which has been generated by a combination of the sidewind disturbance and the driver's steering input. Peak values of 10,000N are experienced with both controllers working simultaneously, which is very large and exceeds the physical limits of the actuators. However, excluding the two peak values, results in forces which *are* within the actuator limits. When the steady state values are reached towards the end of the manoeuvre, a small force difference can be seen which corrects the yaw rate and controls it to the desired value of zero. Furthermore, from approximately 12 seconds to 17 seconds, the demanded wheel forces from the controllers contribute largely to minimising the yaw rate.

The other controlled signal, vehicle sideslip, can be seen to have improved in some areas. For example, on occasions the magnitude is smaller than the driver input in figure 6.20 and between 12 and 15 seconds it is reduced below the threshold value, allowing the controller to be turned off. However, less than two seconds later the lateral velocity increases two fold in magnitude (see figure 6.23(f)) which results in an excessively large vehicle sideslip.

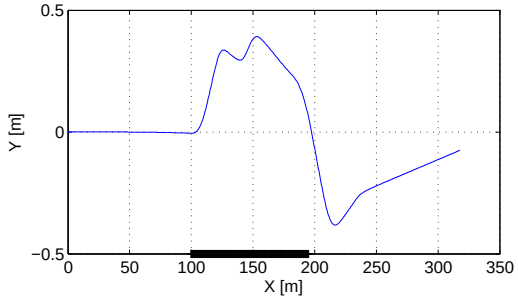

(a) Vehicle trajectory

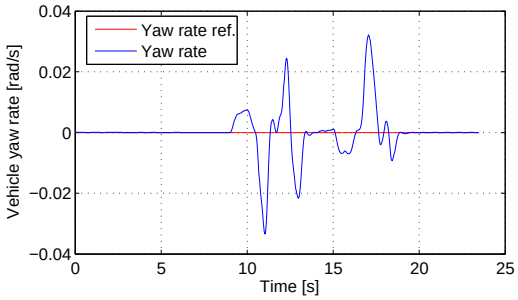

(b) Vehicle yaw rate

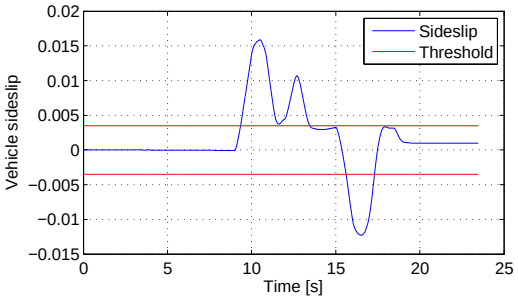

(c) Vehicle sideslip

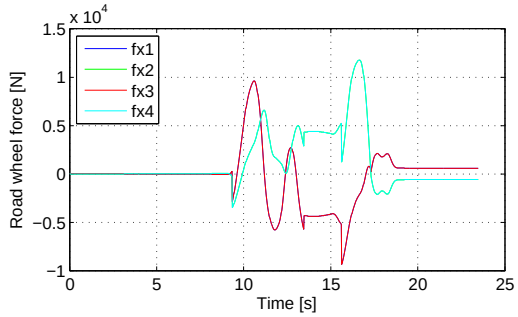

(d) Demanded longitudinal road wheel forces

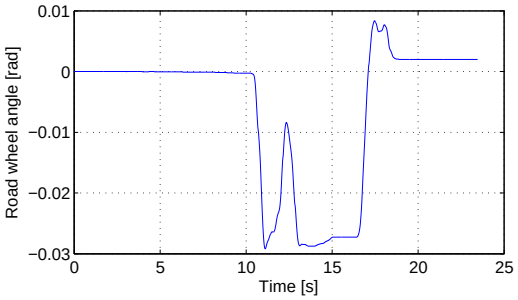

(e) Road wheel angle

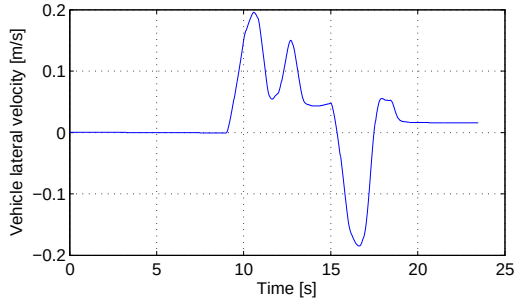

(f) Vehicle lateral velocity

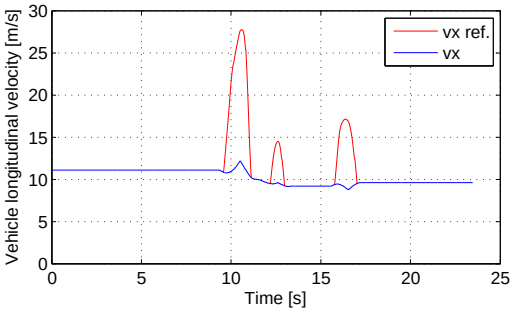

(g) Vehicle longitudinal velocity

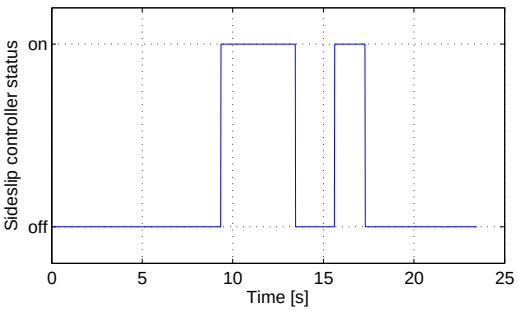

(h) Sideslip controller status

Figure 6.23: Driver input and feedback control for the sidewind disturbance manoeuvre, using RTSM

The vehicle velocity then must change at a similar rate and by a similar amount in order to decrease the sideslip. The velocity cannot change instantaneously and there will be an error between the desired velocity and the actual velocity. This is emphasised in figure 6.23(g) which shows the actual velocity plotted with the reference velocity $v_{x,ref}$. Like many of the other velocity plots when controlling vehicle sideslip, the reference velocity increases quickly since it is calculated instantaneously at each time step of the simulation, but the actual velocity cannot change as quickly.

The sideslip controller is only active once the threshold is exceeded. Throughout the manoeuvre, the actual longitudinal velocity does not change vastly in relation to the initial velocity. It was seen in previous simulation results that the final velocity can be very different (both smaller and larger) from the initial velocity. This would indicate that the driver input and simultaneous feedback control combination works well. For this manoeuvre and control combination, the driver's input in figure 6.23(e), is smooth and not sporadic like the initial five runs with only driver steering to counteract the disturbance as per figure 6.17. It is also interesting to see the effect that the controllers have on the vehicle in terms of yaw rate and road wheel angle. Between 9 and 15 seconds, the yaw rate signal does not have the same shape as the road wheel angle. Without the controllers active, they would normally both be similar.

Instead, the demanded longitudinal road wheel forces which are designed to regulate the yaw rate, can be seen to have a positive effect.

6.4.6 Feedback control - no driver input

In this section the sidewind disturbance is only counteracted by both channels of the feedback controller working simultaneously. Driver steering input from the test rig is not available here, and neither is the feedforward based steering signal - since the yaw rate reference is still set to zero. The sideslip threshold is still set to 0.0035.

The trajectory of the vehicle for this automatically controlled manoeuvre is shown in figure 6.24(a), and shows the vehicle drifting to the left by 0.75 metres and remains there. This drifting can be expected now that position is not being controlled by the driver using the interface test rig. However, longitudinally the vehicle does not travel as far as the other simulations, since the velocity has been greatly reduced by the sideslip controller.

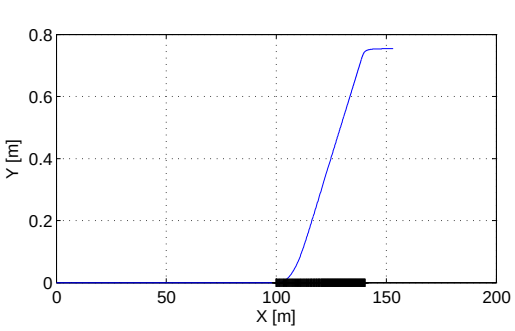

(a) Vehicle trajectory

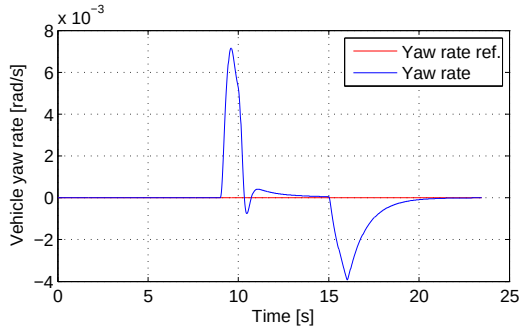

(b) Vehicle yaw rate

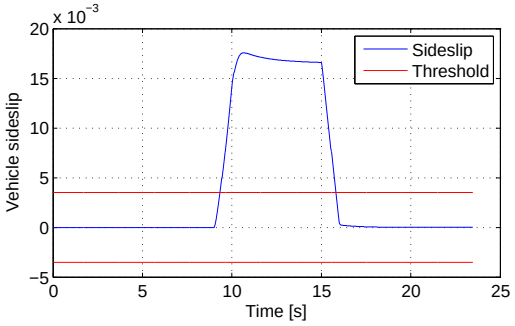

(c) Vehicle sideslip

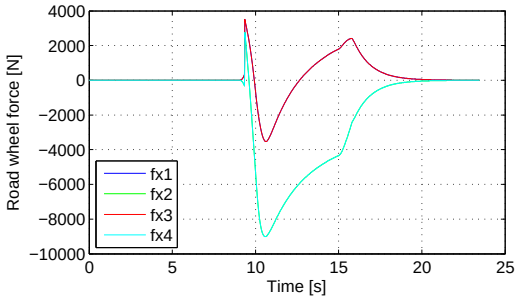

(d) Demanded longitudinal road wheel forces

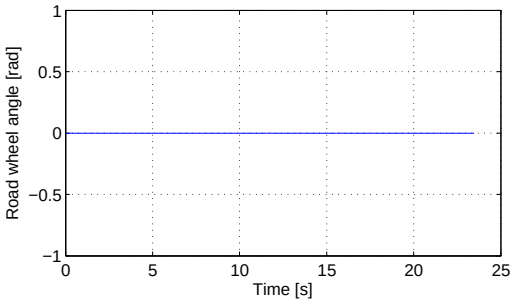

(e) Road wheel angle

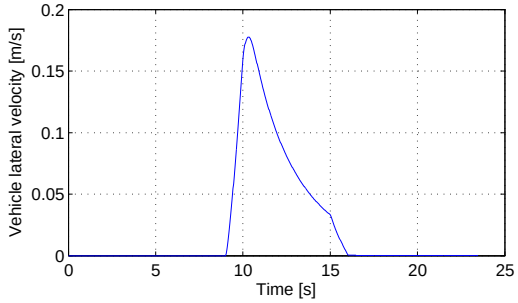

(f) Vehicle lateral velocity

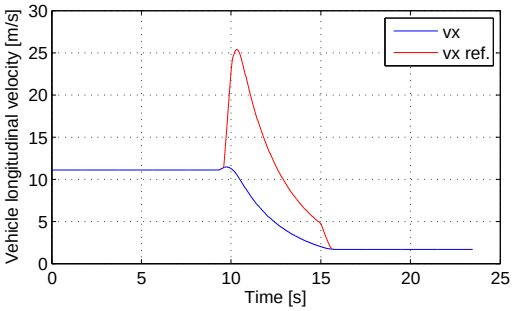

(g) Vehicle longitudinal velocity

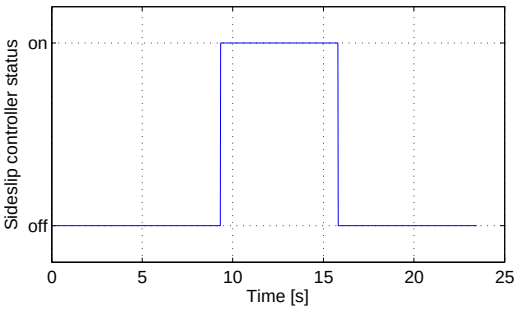

(h) Sideslip controller status

Figure 6.24: Feedback control for the sidewind disturbance manoeuvre, using RTSM

The much smaller velocity has an effect on all of the plots, with the exception of the road wheel angle plot in figure 6.24(e), which is constantly zero — as expected.

The vehicle yaw rate is well controlled to zero after the initial overshoot in both directions. The slow tracking back to zero after 15 seconds is due to the large decrease in the vehicle velocity. Upon comparison with the passive vehicle plots for the sidewind in figure 6.15, the peak yaw rate in the controlled manoeuvre is reduced by 80%, and is controlled to zero very effectively while the uncontrolled plot responds with a step response of 0.035 rad/s. This is the lowest peak value for yaw rate in any of the simulations performed.

However, the vehicle sideslip in figure 6.24(c) does not appear to be as responsive as the yaw rate. Looking at the signal in more detail together with the signals which are used to calculate it (v_y and v_x in figures 6.24(f) and 6.24(g) respectively), one is able to understand exactly what is happening during the manoeuvre. The sideslip controller demands a reduction in the vehicle velocity, which also results in a reduction in the lateral velocity. Furthermore, also controlling $\dot{\psi}$ to zero reduces the lateral velocity further. Overall, the ratio of v_y and v_x does not change much throughout the duration of the acting disturbance. The longitudinal wheel forces which are demanded by the two channels of the feedback controller are larger than previous individual simulations.

By the end of the manoeuvre, the vehicle is travelling at approximately 2 m/s, and has decelerated at a rate of 1.8 m/s^2 equating to approximately 0.18 g (where g is the gravitational acceleration constant equal to 9.81 m/s^2). These values of deceleration combined with the large reduction in v_x, could perhaps make the linear model invalid, based on the assumptions made in chapter 2. Unfortunately, only a small reduction in sideslip was achieved in return for the relatively large control effort.

6.4.7 Discussion

To assess the performance of both channels of the feedback controller, different setups were used involving the human interface system. Firstly, five different runs using only the test rig input and driver visual feedback to counteract the sidewind were carried out, and overall the results were fairly similar. A short break in between each run together with no time allocated to learn or revise the manoeuvres beforehand, helped to ensure that the experiments were both fair and realistic. Driver input was then considered in conjunction with one controlled

variable — first yaw rate control and then vehicle sideslip control. Finally, driver input was considered with simultaneous control using both channels of the feedback controller. For reference purposes, the vehicle response to the sidewind without any correction or control was recorded, as was the response to simultaneous control without any driver input.

These experiments have provided knowledge and insight into the behaviour of the vehicle, and the differing results have been recorded for the range of experiments. The driver only steering experiments recorded similar steer angles for each run to give satisfactory results in terms of vehicle position on the road. However, vehicle position is not a controlled variable in this work. It is controlled to some extent by the driver using the test rig steering wheel as the actuator.

More importantly, it has supplied a benchmark for the vehicle yaw rate and sideslip responses for a driver operating a vehicle in this scenario. If the controllers are to be of benefit, then these values must be improved upon.

The first of the controlled simulations was the driver input with feedback yaw rate control, for which good results were seen. In comparison to the five driver steering only inputs, the trajectory was only marginally improved. However, the yaw rate was reduced by a factor of ten with the controller active, although the demanded longitudinal wheel forces were at the limits of what is physically possible for the actuators to deliver.

When combining sideslip control and driver steering input, similar positive results were obtained. An improvement was seen in the trajectory, together with an increase in the velocity of the vehicle (approximately 36% increase from the start of the manoeuvre). This increase in velocity resulted in a slight decrease in sideslip angle. When comparing the peak yaw rate signals of this control setup with the driver only steering setup, the yaw rate can be seen to improve when only the sideslip control is activated. Again the demanded longitudinal wheel forces are large, but they are within the limits of the actuators. The main problem with this manoeuvre is that the sideslip controller remains active for the whole duration that the disturbance acts on the vehicle.

The next step was to include driver steering input from the test rig with simultaneous feedback control of yaw rate and sideslip. Overall, the results from this setup were mixed. Compared to the driver only steering results, the yaw rate was reduced for almost the whole manoeuvre, although on average it was twice the value observed for the yaw rate control and

driver input simulations. On the other hand, overall sideslip angle was reduced, but varied somewhat when the disturbance was acting. After the initial gust of force pushing the car to the left, there is a change in velocity. For the middle section, the velocity is of the correct magnitude in relation to the lateral velocity. However, when the road wheel angle is applied via the rig, the magnitude of v_y increases suddenly and the ratio of v_y to v_x is incorrect for the desired sideslip threshold value. By the end of this manoeuvre, the vehicle velocity had changed very little from its initial value. However, the sideslip controller was active for approximately 70% of the duration that the disturbance was acting. What is of most concern for this control setup, is the excessively large demanded wheel forces that are required to control sideslip and yaw rate. Unfortunately these exceed what is physically possible for the actuators to deliver.

The final simulation to be carried out was the automatic controller working simultaneously without any driver steering input from the test rig. Again, the yaw rate controller functioned very well, controlling to the desired value effectively and greatly reducing the effect of the disturbance on the vehicle yaw rate (in terms of peak magnitude). However, the sideslip controller did not have such a positive impact. The problem appears to be that the sideslip controller demands a reduction in v_x, but the change in v_x, together with the yaw rate controller trying to keep $\dot{\psi}$ to zero, results in a change in v_y. Unfortunately changing v_y instantaneously is easier than changing v_x instantaneously. Without the steering input from the driver, the vehicle velocity decreases by approximately 80%, and again the demanded wheel forces exceed the physical limits of the actuators. Finally, similar to the driver steering and sideslip control setup, the sideslip controller is active for 100% of the duration that the disturbance acts.

It can be concluded that the setup which works best for the controllers is to have both channels of the feedback controller active with driver steering input, where the driver's steering input interacts very well with the feedback controller. Interestingly, from the sidewind experiments it was observed that when only one variable was controlled and combined with the driver's steering input via the rig, the controlled variable decreased in magnitude as desired while the other variable did not deteriorate in performance. Instead it remained comparable with the driver only input simulation results, or improved slightly.

What has been noticed throughout all of the controlled scenarios is the less oscillatory

nature of the road wheel angle (which is, of course, proportional to the driver's steering input through the steering ratio) in comparison to the driver only input plots. this indicates that the feedback controller helps to alleviate the effort required from the driver using the test rig.

However, the yaw rate controller will work against any large steer inputs to minimise the effect on the vehicle. This was seen in figure 6.23, where a large steer angle has no effect on the vehicle yaw rate. The large demanded wheel forces from the yaw rate controller act to try and prevent the yaw rate increasing above zero in magnitude. Controlling yaw rate to zero for this manoeuvre is acceptable until the vehicle heads off its initial course of straight ahead. Once this happens, feedback steering (or position in general) is required if the vehicle is to continue travelling straight ahead. The vehicle position is of course controlled in real-time when the human interface input is used, with the driver closing the loop.

Table 6.1 has been created to enable a straightforward comparison of some performance indicators which have all been mentioned in the text above. The six rows represent the different controller architectures which are used while trying to counteract the sidewind disturbance. The four columns show some performance indicators, and are labelled as follows.

'**% chg in** v_x' is the percentage change in the the longitudinal velocity throughout the manoeuvre. A positive value indicates an increase in v_x, while a negative value indicates a decrease. '**% of** K_β **activity**' is the percentage of the disturbance duration that the sideslip controller is active. 'fx **within limits**' idicates whether the demanded wheel forces are within the actuator limits (Y=yes, N=no, BL=border line). '$\dot{\psi}$ **peak**' is the peak yaw rate (positive and negative values from the reference signal of zero).

Control	% chg in v_x	% of K_β activity	fx within limits	$\dot{\psi}$ peak (rad/s)
Uncontrolled	—	—	—	0.035
Driver only	—	—	—	0.15, -0.13
Driver and $\dot{\psi}$	—	—	BL	0.015, -0.015
Driver and β	+36	100	Y	0.05, -0.12
Driver and $\dot{\psi}$ and β	-12	71	N	0.03, -0.03
$\dot{\psi}$ and β	-82	100	N	0.008, -0.004

Table 6.1: Performance indicators for sidewind disturbance manoeuvre

Finally, the trajectory is an important factor when attempting to counteract a sidewind disturbance. Figure 6.25 shows the vehicle trajectories for all of the sidewind disturbance manoeuvres.

From this figure, comparisons can be easily made, and the simultaneous control combined with driver input via the test rig results in the least deviation (see figure 6.25(d)). With the results shown in table 6.1 and the trajectories in figure 6.25, it would appear that feedback control of both channels combined with driver input from the human interface test rig is the most successful setup.

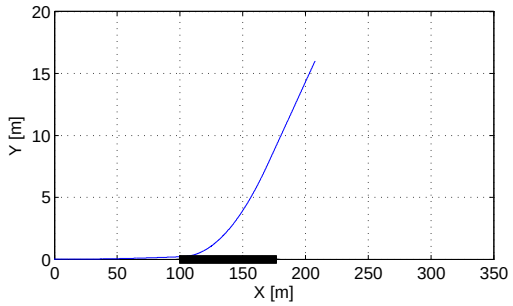

(a) Passive response

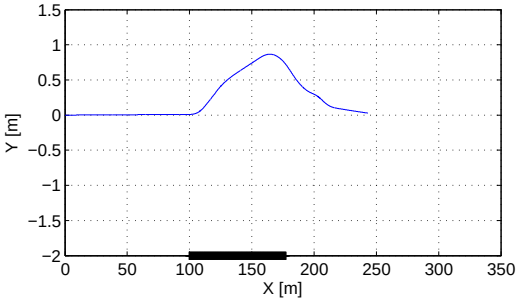

(b) Driver input and yaw rate control

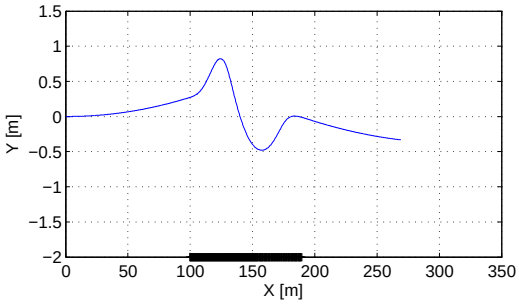

(c) Driver input and sideslip control

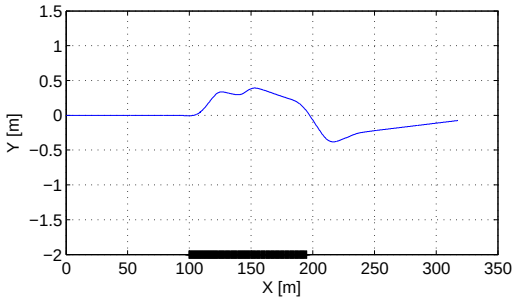

(d) Driver input and feedback control of both channels

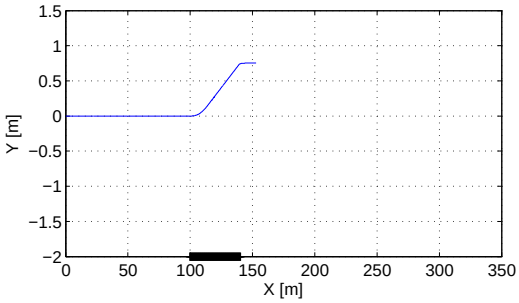

(e) Feedback control for both channels

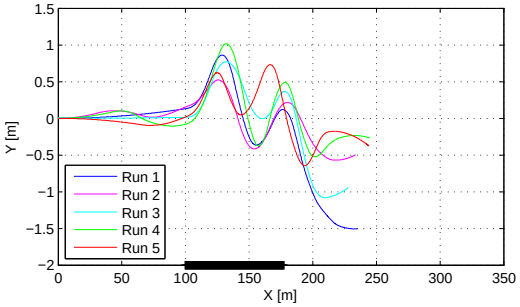

(f) Driver 1 steering input only

Figure 6.25: Vehicle trajectories for the sidewind disturbance manoeuvre

6.5 Conclusions

It has been shown through experiments with a human interface test rig and a 'human-in-the-loop' that the two channel feedback controller, with integrated front steering when applicable, is successful in completing the task of simultaneously controlling yaw rate and vehicle sideslip. Measures were taken to ensure that the behaviour of the controller and the driver of the test rig were comparable throughout the manoeuvres.

Lane change manoeuvres and disturbance input tests have been simulated with promising results. Both theory and simulation results have shown that simultaneous control can be achieved and can work well with driver input via a test rig.

However, it was evident from the simulation results that a large change in velocity is often required when regulating the vehicle sideslip. While the effect of braking the vehicle could be beneficial in emergency situations, it may be seen as detrimental in non-emergency situations.

Because of this large change in velocity that is often required, only small angle changes for sideslip are recommended, since a sharp decrease or increase in velocity can be detrimental to the purpose of the control, for two reasons. Firstly, the change in vehicle velocity may have an effect on controlling the yaw rate, and secondly, large demanded wheel forces may saturate the actuators. However, this change in velocity also occurs in other methods of simultaneous control of yaw rate and sideslip angle. Most noticeably, Vilaplana et al. [46], experienced a drop in velocity of 33% when using 4WS when controlling to the same values, allbeit with a larger initial vehicle velocity.

One possible improvement would be to control β to understeer, oversteer or neutral steer, all of which can be calculated from the difference between the front and rear slip angles whilst cornering. However, the problem of using the longitudinal velocity to control sideslip angle would still exist.

4WS and braking control to achieve simultaneous control of yaw rate and another lateral dynamic has been previously studied [49, 50]. Using the 4WS as the main control actuator would enable the braking system to be less active, since the lateral velocity would be directly influenced by both the front and rear wheel turn angle. This is a safer method of control compared to braking or accelerating the vehicle, to a value which may sometimes be double

or half the initial velocity.

When feedforward based steering was combined with the test rig input, the two steering angles (from the test rig and the feedforward based signal) were summed together. This gave some poor results which may be avoidable if a mathematical relationship between the two angles is generated. For example, the feedforward based steering angle could be weighted as a function of yaw rate error.

However, in some cases the human input from the rig interacted well with the feedback controller, especially the sidewind disturbance manoeuvre and the step disturbance input. It is important at this point to note that this could be the primary application for this sort of controller. As such, it is very desirable to integrate the control structures with the human interface test rig and assess how they function in conjunction with one another. Also, the test rig has enabled the driver's response to the manoeuvres to be obtained, and allow comparisons to be made with the different control structures.

Chapter 7

Conclusions and further work

This chapter draws conclusions for the work presented in this thesis, and in particular, the main aspects of the study. Some recommendations of how this work could be advanced and implemented in a production car will also be discussed.

7.1 Conclusions

It has been shown that linear controller design techniques can be used to control vehicle lateral dynamics using primarily the longitudinal wheel forces, whilst operating in the linear region of the tyre characteristic curve. This is has been demonstrated using a linearised three state vehicle model to design the control laws, and a complex 'black box' proprietary vehicle model, whose dynamics closely reflect a production saloon vehicle, to implement and test the controller.

The aims outlined in section 1.3 will be briefly discussed, followed by how the objectives were used to ensure the aims were met.

The first aim was to use the longitudinal wheel forces to simultaneously control vehicle yaw rate and sideslip. This was achieved by deriving a vehicle model which was suitable for controller design purposes. Control laws were derived using frequency based design and analysis techniques, and the controller was tested in a detailed nonlinear model.

The second aim was to integrate the feedback controller with some front wheel steering. This aim was purposely set to ascertain if enhanced performance could be achieved with the integrated control. This aim was met by calculating a symbolic based relationship between

front steering angle and vehicle yaw rate. Furthermore, the steering angle is dependent on vehicle velocity, which is important since v_x changes as the demanded longitudinal wheel forces change (due to the feedback control). The steering was implemented using a feedforward based approach to apply the angle direct to the model as an input.

The third aim stated that the control laws should be implemented into a human interface test rig and evaluated. To enable this to be achieved, three separate components were required to work together. The first is a steering test rig which accepts a steering angle from an operator (or driver) and processes it as an input. The second component is to have a vehicle model which is capable of interfacing with the test rig and running in real time. The final essential component is to provide visual feedback to the operator of the vehicle behaviour (the driver). This latter element feedsback the position of the vehicle to the driver, allowing test manoeuvres to be attempted in a realistic and meaningful manner. This aim was met and results were obtained, as described in chapter 6.

7.1.1 Vehicle modelling

The first objective of this work was to develop a vehicle model which is suitable for controller design purposes.

A three state linearised vehicle model representing longitudinal velocity, lateral velocity and vehicle yaw rate was derived and presented in chapter 2. A nonlinear vehicle model was also presented and was used to interact with the interface test rig. Finally, a proprietary nonlinear vehicle model was introduced and was the main source for evaluating the feedback and feedforward based controllers. All three of these models were compared to one another using standard step inputs for longitudinal wheel forces and road wheel angle.

While comparing the three vehicle models, it became apparent that the simulation model (VSM) that has been verified against a production saloon vehicle was significantly more oscillatory in behaviour than the other two presented models. However, the dynamic behaviour of yaw rate, vehicle sideslip and the vehicle velocity was very similar between the three vehicle models, which deemed them to be adequate for design and simulation purposes.

The outputs from the linearised vehicle model are the three states, v_x, v_y and $\dot{\psi}$. Sideslip is not a state of the model and hence is not an output. It can however, be calculated from two of the outputs v_x and v_y. Using the longitudinal velocity and lateral velocity to calculate

sideslip, it becomes clear that sideslip can be regulated by altering the ratio of lateral velocity to longitudinal velocity of the vehicle.

Feedforward based steering uses the same yaw rate reference value as the feedback controller. From this reference, inverse vehicle model equations were used to calculate a road wheel angle which will result in the desired yaw rate when applied to the model. Therefore, it is this steering angle that is applied to the vehicle model.

7.1.2 Controller design

The second objective of this work was to use the linear model to design and analyse a two-channel feedback controller using frequency based techniques, and was addressed in chapter 3.

This feedback controller was used to simultaneously control vehicle yaw rate and sideslip using the longitudinal wheel forces. Analysis of the open loop structure enabled controllers to be designed, ensuring that they met the design criteria for gain and phase margin and crossover frequency. System robustness and stability criteria were also specified beforehand to ensure the performance of the system is desirable.

A sum and difference approach is used in the control law, where the sum of the longitudinal wheel forces can be used to regulate vehicle sideslip, and the longitudinal wheel force difference left to right can be used to control vehicle yaw rate. A relationship is found between desired sideslip and vehicle velocity. Using this relationship together with the current lateral velocity allows all four longitudinal wheel forces to be used to regulate the longitudinal velocity. Therefore, the vehicle sideslip is controlled indirectly via regulating the vehicle velocity.

The third objective was to integrate front wheel steering with the feedback control structure, and evaluating the results to see if any benefits were achieved.

The steering angle was generated in chapter 2, and was applied to the model in a feedforward-based manner. It was referred to as 'feedforward based steering' since the equations that were used to generate it had a dependency on the vehicle velocity.

When controlling vehicle sideslip, a threshold is defined so that instead of controlling to a unique single value, sideslip is instead controlled to a threshold (or deadband) region around zero, $0 \pm \beta_{th}$. It is performed in this way to avoid numerical errors when attempting to control to values close to zero.

Within the feedback controller architecture, the reference signal for yaw rate was generated

offline while the reference value for the longitudinal velocity was calculated online using the current lateral velocity and the sideslip threshold value.

7.1.3 Controller evaluation

The next objective was to generate specific manoeuvres to adequately test the controllers.

This objective was addressed in chapter 5 by deriving three different manoeuvres. The first was a constant yaw rate test which enabled steady state values to be reached. The second manoeuvre was a gentle lane change that was based on the ISO standard for a double lane change. This manoeuvre is designed to test the controllers by demanding reference signals which vary in both magnitude and direction. Finally, the third manoeuvre was in the form of a disturbance acting on the vehicle, and was carried out in conjunction with the human interface test rig. The yaw rate reference signals required for the lane change manoeuvre were generated offline in this work. The requirement was to control yaw rate and sideslip, not to complete a lane change manoeuvre — for which feedback of the vehicle position would be required.

Overall, simultaneous control of vehicle yaw rate and sideslip has been shown to be possible using two different control architectures (feedback control and feedforward based steering combined with feedback control). Results were obtained through computer model simulation and hardware in the loop evaluation via the human interface test rig.

For each of these manoeuvres, the feedback controller was simulated and evaluated first, followed by feedforward based steering integrated with the feedback controller. The results were discussed and presented for both of these control setups.

7.1.4 Human interface test rig

The final aim of this work was to integrate the controller with a human interface test rig, and enable visual feedback of the vehicle trajectory in real-time. This is designed to enable the response of a human in the loop to be analysed and compared with that of the controllers.

This aim was addressed in chapters 4 and 6. Both of the control architectures were combined with a steering input from a human interface test rig, where a driver can attempt to complete the same test manoeuvres as the automatic controllers. To make this possible, real-time visual feedback to the driver via a PC monitor was implemented.

The third manoeuvre mentioned above was in the form of a disturbance input acting on the vehicle. The human interface test rig was used in chapter 6, and this third manoeuvre was implemented in two ways. The first disturbance was in the form of an additional steering input from the test rig, and the second disturbance was in the form of a sidewind acting on the vehicle.

Whilst completing the manoeuvres, the interface test rig allowed the reactions of the human driver to be compared to that of the controllers. Furthermore, it allowed human and controller interaction to be evaluated. Most previous studies use only vehicle simulations. In this work the simulations are extended to include a vehicle test rig to enable further assessment.

One main limitation of this work is the large demanded longitudinal wheel forces that are often required to complete the control objective. These large forces are often not practical to implement, and this naturally leads to an investigation of how this work could be developed further.

7.2 Further work

Firstly, improvements could be made to the linear three state vehicle model to make it better resemble a production vehicle. It was seen in the vehicle simulation results in chapter 5 that the longitudinal wheel forces demanded by the feedback controller were at times excessive and impractical. Due to the lack of both actuator dynamics and realistic traction limits, there are no limitations as to how much force can be delivered to the wheels. A different approach to design the controllers and a different controller structure, where these limitations are taken into account may result in more realistic controller outputs. For example, when using the very detailed nonlinear model (VSM), the controller never demanded wheel forces greater than what was deliverable from the vehicle. The LCDM which was derived in chapter 2, was designed using small input assumptions. Obviously the model becomes invalid if any of these assumptions are exceeded, which may have been the case with some of the combined feedback control and driver input simulations in chapter 6.

Another possible improvement could address the calculation of vehicle sideslip. Instead

of calculating vehicle sideslip from the ratio of lateral to longitudinal velocity, it could be calculated using the difference between the tyre slip angle at the front and rear wheels. This was briefly discussed in chapter 2, and can be used to determine if the vehicle is in oversteer, understeer or neutralsteer, and the vehicle could then be controlled relative to these conditions rather than a given threshold, if desired.

A further improvement would be to include automatic feedback control of steering (either 2WS or 4WS) with the feedback wheel force controller. It is reflected in the current literature that feedback steering control can also achieve simultaneous control, but has different properties to feedback braking control. For example, the vehicle speed will tend to decrease less during the manoeuvres and for the sidewind manoeuvre, the feedback steering would steer against the sidewind instead of using the feedback controller to alter the vehicle speed — which is the natural reaction.

7.2.1 Implementation

It has been observed in the results presented that the demanded wheel forces cause both accelerations and decelerations in vehicle velocity. It is possible to implement the demanded decelerations using currently available systems and actuators. These systems include Electronic Stability Program (ESP), Anti-lock Braking System (ABS) and potentially an actuator system like Electro-Hydraulic Braking (EHB) as is currently used on the Mercedes E class and SL models.

The main issue when implementing this work, is how to deliver the individual longitudinal wheel forces which represent acceleration. The most obvious answer is to use an engine management control system which demands power be sent to a particular wheel. This would most likely be implemented as the engine distributing the power to the driven wheels, and then combining this with individual wheel braking to effectively deliver torque to an individual wheel. However, the behaviour of such systems is generally slow.

One possible solution is to use an electronically controlled differential (e-diff). The problem with this system though, is that power can only be distributed to the slowest moving wheel, which in the case of the constant yaw rate manoeuvre, would be the inside wheel — the wrong wheel. Recently, a torque vectoring differential (TVD) or overdriven differential

as referred to in section 1.2 was launched in a production vehicle [1]. Furthermore, Audi plan a similar system in 2010. Such a system allows driveshaft torques to be controlled in direction and magnitude, and therefore wheel speeds can be independently regulated. Therefore, torque can be delivered to any wheel, at any point in time. Furthermore, some field tests show that the dynamics of such a system are favourable for this application. For example, an additional torque of 1600 Nm can be distributed across the axle to one wheel in less than two seconds, which highlights that progress is being made to enable such dynamic control systems to be implemented. Using a TVD in conjunction with the feedback controller could make it possible to deliver such forces to any wheel when requested. However, this would require improved control characteristics to enable it to function in a desired manner.

[1] BMW launched the X6 with a TVD as standard

Bibliography

[1] H. B. Pacejka and E. Bakker, "The magic formula tyre model," in *Proc. 1st International Colloquium on Tyre Models for Vehicle Dynamics Analysis, Vehicle System Dynamics*, vol. 21, pp. 1–19, 1993.

[2] "http://www.ntsb.gov/events/symp-rec/proceedings/authors/lehmmann.htm."

[3] "http://www.driveandsurvive.co.uk/cont5.htm."

[4] J. Gerstenmeir, "Electronic control unit for passenger car anti-skid (ABS)," in *Proc. Institute of Mechanical Engineers*, 1981.

[5] P. Wellstead and N. Pettit, "Analysis and redesign of an antilock brake system controller," *Proc. IEE Control Theory and Applications*, vol. 144, pp. 413–426, September 1997.

[6] J. W. Zellner, "An analytical approach to antilock brake system design," *SAE Technical Paper 840249*, 1984.

[7] B. R. Lee and K. H. Sin, "Slip-ratio control of ABS using sliding mode control," in *Proc. The 4th Korea-Russia International Symposium On Science and Technology*, vol. 3, pp. 72–77, IEEE, Piscataway, NJ, USA, 2000.

[8] Y. Chin, W. Lin, D. M. Sidlosky, and D. S. Ruley, "Sliding-mode ABS wheel-slip control," in *Proc. of the American Control Conf.*, vol. 1, (Chicago, IL, USA), pp. 1–5, June 1992.

[9] R. Bosch, *Automotive Handbook*. SAE, 5th ed., 2000.

[10] A. Müller, W. Achenbach, E. Schindler, T. Wohland, and F. W. Mohn, "Das Neue Fahrsicherheitssystem Electronic Stability Program von Mercedes Benz," *Automobiltechnische Zeitschrift*, vol. 11, pp. 656–670, 1994.

[11] D. Kim, K. Kim, W. Lee, and I. Hwang, "Development of mando ESP (Electronic Stability Program)," *SAE Technical Paper 2003-01-0101*, 2003.

[12] A. Morgando, "Linear approach to ESP control logic design," *SAE Technical Paper*, no. 2006-01-1017, pp. 153–162, 2006.

[13] A. T. V. Zanten, "Bosch ESP systems: 5 years of experience," *SAE Technical Paper 2000-01-1633*, 2000.

[14] A. Sigl and H. Demel, "ASR -traction control, state of the art and some prospects.," in *Proc. SAE international congress and exposition*, (Detroit, Michigan, USA), pp. 71–78, 1990.

[15] B.-C. Jang, Y.-H. Yun, and S.-C. Lee, "Simulation of vehicle steering control through differential braking," *International Journal of Precision Engineering and Manufacturing*, vol. 5, pp. 26–34, July 2004.

[16] N. Bajcinca, R. Cortesao, M. Hauschild, J. Bals, and G. Hirzinger, "Haptic control for steer-by-wire systems," in *Proc. International Conference on Intelligent Robots and Systems*, vol. 2, (Las Vegas, Nevada, USA), pp. 2004–2009, October 2003.

[17] L. Guvenc, B. A. Guvenc, T. Yigit, and E. S. Ozturk, "HiL system for steering controller tests," in *Proc. IEEE Conference on Control Applications*, vol. 1, pp. 13–18, June 23-25 2003.

[18] P. Setlur, J. Wagner, D. Dawson, and L. Powers, "A hardware-in-the-loop and virtual reality test environment for steer-by-wire system evaluations," in *Proc. American Control Conference*, vol. 3, (Denver, CO, United States), pp. 2584–2589, June 2003.

[19] Velardocchia and Sorniotti, "Hardware-in-the-loop (HIL) testing of ESP (Electronic Stability Program) commercial hydraulic units and implementation of new control strategies," *SAE Technical Paper 2004-01-2770*, 2004.

[20] T. Pilutti, G. Ulsoy, and D. Hrovat, "Vehicle steering intervention through differential braking," in *Proc. American Control Conference*, vol. 3, (Seattle, WA, USA), pp. 1667–1671, June 1995.

[21] P. Raksincharoensak, M. Shino, and M. Nagai, "Investigation of intelligent driving assistance system using direct yaw moment control," *Review of Automotive Engineering*, vol. 25, pp. 185–191, April 2004.

[22] H. Mouri and H. Furusho, "Research on automated lane tracking using linear quadrtic control: Control procedure for a curved path," *JSAE Review*, vol. 20, no. 3, pp. 325–329, 1999.

[23] G. Bevan, H. Gollee, and J. O'Reilly, "Automatic lateral emergency collision avoidance for a passenger car," *International Journal of Control*, vol. 80, no. 11, pp. 1751–1762, 2007.

[24] S. V. Drakunov, B. Ashrafi, and A. Rosiglioni, "Yaw control algorithm via sliding mode control," in *Proc. American Control Conference*, (Chicago, Illinois), pp. 580–583, June 2000.

[25] M. Lakehal-Ayat, S. Diop, Franc, and F. Lamnabhi-Lagarrigue, "Yaw rate control for a cornering 4wd vehicle," in *Proc. 14th International Symposium of Mathematical Theory of Networks and Systems (MTNS 2000)*, (Perpignan, France), June 2000.

[26] K. Yi, T. Chung, J. Kim, and S. Yi, "An investigation into differential braking strategies for vehicle stability control," *Proc. Institution of Mechanical Engineers, Part D: Journal of Automobile Engineering*, vol. 217, no. 12, pp. 1081–1094, 2003.

[27] V. Utkin, *Sliding Modes and Their Application in Variable Structure Systems*. Mir Publishers, Moscow, 1978.

[28] J. J. E. Slotine and W. Li, *Applied Nonlinear Control*. Prentice Hall, 1991.

[29] C. Zhao, W. Xiang, and P. Richardson, "Vehicle lateral control and yaw stability control through differential braking," in *Proc. IEEE International Symposium on Industrial Electronics*, (Montreal, Que., Canada), pp. 384–389, July 2006.

[30] Y. Fukada, "Slip-angle estimation for vehicle stability control.," *Vehicle System Dynamics*, vol. 32, no. 4, pp. 375–388, 1999.

[31] M. Boada, B. Boada, A. Munoz, and V. Diaz, "Integrated control of front-wheel steering and front braking forces on the basis of fuzzy logic," *Proc. Institution of Mechanical Engineers, Part D: Journal of Automobile Engineering*, vol. 220, pp. 253–267, 2006.

[32] J. Ahmadi, A. Ghaffari, and R.Kazemi, "Fuzzy logic based vehicle stability enhancement through combined differential braking and active front steering," in *Proc. ASME International Design Engineering Technical Conferences and Computers and Information in Engineering Conference*, vol. 6 C, (Long Beach, CA, United States), pp. 2417–2423, September 2005.

[33] F. Tahami, R. Kazemi, and S. Farhanghi, "A novel driver assist stability system for all-wheel-drive electric vehicles," *IEEE Transactions on Vehicle Technology*, vol. 52, pp. 683–692, May 2003.

[34] E. Esmailzadeh, A. Goodarzi, and G. Vossoughi, "Optimal yaw moment control law for improved vehicle handling," *Mechatronics (UK)*, vol. 13, pp. 659–675, September 2003.

[35] M. Nagai, M. Shino, and F. Gao, "Study on integrated control of active front steer angle and direct yaw moment," *JSAE Review*, vol. 23, pp. 309–315, July 2002.

[36] G. Burgio and P. Zegelaar, "Integrated vehicle control using steering and brakes," *International Journal of Control*, vol. 79, pp. 534–541, May 2006.

[37] M. Salman, Z. Zhang, and N. Boustany, "Coordinated control of four wheel braking and rear steering," in *Proc. American Control Conference*, vol. 1, (Chicago, IL, USA), pp. 6–10, June 1992.

[38] E. J. Davison and A. Godenberg, "Robust control of a general servomechanism problem: The servocompensator," *Automatica*, vol. 11, pp. 461–471, 1975.

[39] E. J. Davison and I. J. Ferguson, "The design of controllers for multivariable robust servomechanism problem using parameter optimization methods," *IEEE Transactions on Automatic Control*, vol. AC-26, no. 1, pp. 93–110, 1981.

[40] M. Salman, "Coordinated control of steering and braking," in *American Society of Mechanical Engineers, Applied Mechanics Division, AMD*, vol. 108, (Dallas, TX, USA), pp. 69–76, November 1990.

[41] J. He, D. A. Crolla, M. C. Levesley, and W. J. Manning, "Coordination of active steering, driveline, and braking for integrated vehicle dynamics control," *Proc. Insitute of Mechanical Engineers, Part D: Journal of Automotive Control*, vol. 220, pp. 1401–1421, May 2006.

[42] B. A. Guvenc, T. Acarman, and L. Guvenc, "Coordination of steering and individual wheel braking actuated vehicle yaw stability control," in *Proc. IEEE Intelligent Vehicles Symposium*, (Columbis, OH, USA), pp. 288–293, June 2003.

[43] B. A. Guvenc and L. Guvenc, "Robust steer-by-wire control based on the model regulator," in *Joint IEEE Conference on Control Applications and IEEE Conference on Computer Aided Control Systems Design*, (Glasgow, U.K.), pp. 435–440, 2002.

[44] B. A. Guvenc and L. Guvenc, "The limited integrator model regulator and it's use in vehicle steering control," *Turkish Journal of Engineering and Environmental Sciences*, vol. 1, pp. 473–482, 2002.

[45] A. Hac and M. Bodie, "Improvements in vehicle handling through integrated control of chassis systems," *International Journal of Vehicle Autonomous Systems*, vol. 1, no. 1, pp. 83–110, 2002.

[46] M. A. Vilaplana, O. Mason, D. J. Leith, W. E. Leithead, and J. Kalkkuhl, "Non-linear control of four-wheel steering cars with actuator constraints," in *Proc. IFAC conference*, (Barcelona), 2002.

[47] J. Ackermann, "Robust decoupling, ideal steering dynamics and yaw stabilization of 4WS cars," *Automatica*, vol. 30, no. 11, pp. 1761–1768, 1994.

[48] W. E. Leithhead and J. O'Reilly, "m-input, m-output feedback control by individual channel design," *International Journal of Control*, vol. 56, no. 6, pp. 1347–1397, 1992.

[49] Y. Jia, "Robust control with decoupling performance for steering and traction of 4WS vehicles under varying velocity-varying motion," *IEEE Transactions on Control systems Technology*, vol. 8, pp. 554–569, May 2000.

[50] S.-H. Yu and J. J. Moskwa, "Global approach to vehicle control: Coordination of four wheel steering and wheel torques," *Journal of Dynamic Systems, Measurement and Control, Transactions of the ASME*, vol. 116, pp. 659–667, December 1994.

[51] N. Matsumoto and M. Tomizuka, "Vehicle lateral velocity and yaw rate control with two independent control inputs," *Journal of Dynamic Systems, Measurement and Control, Transactions of the ASME*, vol. 114, pp. 606–613, 1992.

[52] H.-F. Lin and A. A. Seireg, "Vehicle dynamics and stabilization using a nonlinear tyre model with four-wheel steering and braking," *International Journal of Computer Applications in Technology*, vol. 11, no. 1-2, pp. 53–64, 1998.

[53] S. Horiuchi, K. Okada, and S. Nohtomi, "Effects of integrated control of active four wheel steering and individual wheel torque on vehicle handling and stability - a comparison of alternative control strategies," *Vehicle Systems Dynamics Supplement*, vol. 33, pp. 680–691, 1999.

[54] K. Fujita, K. Ohashi, K. Fukatani, S. Kamei, Y. Kagawa, and H. Mori, "Development of active rear steer system applying H infinity-μ synthesis," *SAE Technical Paper 981115*, 1998.

[55] R. Rajamani, *Vehicle Dynamics and Control*. Springer US, 2006.

[56] T. Akita, K. Satoh, and M. C. Gaunt, "Development of 4WS control algorithm for a SUV," *SAE Technical Paper 2002-01-1216*, 2002.

[57] M. Velardocchia, A. Morgando, and A. Sorniotti, "Four-wheel-steering control strategy and its integration with vehicle dynamics control and active roll control," *SAE Technical Paper 2004-01-1061*, 2004.

[58] C. R. Carlson and C. J. Gerdes, "Optimal rollover prevention with steer-by-wire and differential braking," in *Proc. ASME Dynamic Systems and Control*, vol. 72, (Washington, DC., United States), pp. 345–354, American Society of Mechanical Engineers, November 2003.

[59] A. S. Hauksdottir and R. E. Fenton, "Vehicle longitudinal controller.," in *Proc. 38th IEEE Vehicular Technology Conference*, pp. 218–222, June 15-17 1988.

[60] H. Dugoff, P. S. Fancher, and L. Segel, "An analysis of tire traction properties and their influence on vehicle dynamic performance," *SAE Paper No. 700377*, 1970.

[61] R. Sharp and M. Bettella, "On the construction of a general numerical tyre shear force model from limited data," *Journal of Automobile Engineering*, vol. 217, no. 3, pp. 165–172, 2003.

[62] A. Y. Maalej, D. A. Guenther, and J. R. Ellis, "Experimental development of tyre forces and moment models," *International Journal of Vehicle Design*, vol. 10, no. 1, pp. 35–50, 1989.

[63] O. Mokhiamar and M. Abe, "Active wheel steering and yaw moment control combination to maximize stability as well as vehicle responsiveness during quick lane change for active vehicle handling," *Proc. Institute of Mechanical Engineers, Part D: Journal of Automobile Control*, vol. 216, no. 2, pp. 115–124, 2002.

[64] W. Klier, A. Reim, and D. Stapel, "Robust estimation of vehicle sideslip angle - an approach w/o vehicle and tire models," *SAE Technical Paper 2008-01-0582*, 2008.

[65] U. Kiencke and A. Daiß, "Observation of lateral vehicle dynamics," in *Proc. 1996 IFAC World Congress*, (San Fransisco), pp. 7–10, July 1996.

[66] R. Daily and D. Bevly, "The use of GPS for vehicle stability control systems," *IEEE Transactions on Industrial Electronics*, vol. 51, pp. 270–277, April 2004.

[67] D. M. Bevly, J. C. Gerdes, and C. Wilson, "The use of GPS based velocity measurements for measurement of sideslip and wheel slip," *International Journal of Vehicle Mechanics and Mobility*, vol. 38, pp. 127–147, August 2002.

[68] "http://www.racelogic.co.uk."

[69] "Determination and control of vehicle sideslip using GPS: United states patent 6681180."

[70] A. Nishio, K. Tozu, H. Yamaguchi, K. Asano, and Y. Amano, "Development of vehicle stability control system based on vehicle sideslip angle estimation," *SAE Technical Paper 2001-01-0137*, 2001.

[71] S. Müller, M. Uchanski, and K. Hedrick, "Estimation of the maximum tire-road friction coefficient," *Journal of Dynamic Systems, Measurement and Control*, vol. 125, pp. 607–617, 2003.

[72] K. Kobayashi, K. Cheok, and K. Watanabe, "Estimation of absolute vehicle speed using fuzzy logic rule-based Kalman filter," in *Proc. American Control Conference*, vol. 5, pp. 3086–3090, 21-23 June 1995.

[73] F. Jiang and Z. Gao, "An adaptive nonlinear filter approach to the vehicle velocity estimation for ABS," in *Proc. IEEE International Conference on Control Applications*, (Anchorage, Alaska, USA), pp. 490–495, September 2000.

[74] K. Aström and B. Wittenmark, *Adaptive Control*. Addison-Wesley, 1995.

[75] L. Imsland, T. A. Johansen, T. I. Fossen, J. C. Kalkkuhl, and A. Suissa, "Vehicle velocity estimation using modular nonlinear observers," *Automatica*, vol. 42, pp. 2091–2103, 2006.

[76] H. F. Grip, L. Imsland, T. A. Johansen, T. I. Fossen, J. C. Kalkkuhl, and A. Suissa, "Nonlinear vehicle side-slip estimation with friction adaption," *Automatica*, vol. 44, pp. 611–622, 2008.

[77] M. C. Best, T. J. Gordon, and P. J. Dixon, "An extended adaptive Kalman filter for real-time state estimation of vehicle handling dynamics," *Vehicle System Dynamics*, vol. 34, no. 1, pp. 57–75, 2000.

[78] G. Hodgson and M. C. Best, "A parameter identifying a kalman filter observer for vehicle handling dynamics.," *Proc. Insitute of Mechanical Engineers, Part D: Journal of Automotive Control*, vol. 220, pp. 1063–1072, 2006.

[79] F. Yu, J.-W. Zhang, and D. A. Crolla, "A study of a Kalman filter active suspension system using correlation of front and rear wheel road inputs," in *Proc. Insitute of Mechanical Engineers, Part D: Journal of Automotive Control*, vol. 214, pp. 493–502, 2000.

[80] F. Yu and D. Crolla, "Wheelbase optimal control for active vehicle suspensions," *Chinese Journal of Mechanical Engineering*, vol. 11, no. 2, pp. 122–129, 1998.

[81] P. J. Venhovens and K. Naab, "Vehicle dynamics estimation using Kalman filters," *Vehicle System Dynamics*, vol. 32, pp. 171–184, August 1999.

[82] K. Naab and G. Reichart, "Driver assistance systems for lateral and longitudinal vehicle guidance - heading control and active cruise control," in *Proc. AVEC 94*, pp. 449–454, 1994.

[83] G. Reichart, R. Haller, and K. Naab, "Towards future driver assistance systems," *Automotive Technology International*, pp. 25–29, 1995.

[84] A. Hac and M. D. Simpson, "Estimation of vehicle side slip angle and yaw rate," *SAE Technical Paper 2000-01-0696*, 2000.

[85] H. Cherouat and S. Diop, "An observer and an integrated braking/traction and steering control for a cornering vehicle," in *Proc. American Control Conference*, vol. 3, (Portland, OR, United States), pp. 2212–2217, June 2005.

[86] H. Leffler, R. Auffhammer, R. Heyken, and H. Röth, "New driving stability control system with reduced technical effort for compact and medium class passenger cars," *SAE Technical Paper 980234*, 1998.

[87] K. Huh, S. Lim, J. Jung, D. Hong, S. Han, K. Han, H. Y. Jo, and J. M. yun, "Vehicle mass estimator for adaptive roll stability control," *SAE Technical Paper 2007-01-0820*, 2007.

[88] R. Rajamani and J. K. Hedrick, "Adaptive observers for active automotive suspensions: Theory and experiment," in *IEEE Transactions on Control Systems Technology*, vol. 3, pp. 86–93, 1995.

[89] D. Odenthal, T. Bunte, and J. Ackermann, "Nonlinear steering and braking control for vehicle rollover aoidance," in *Proc. European Control Conference*, (Gemany), 1999.

[90] S. Solmaz, M. Akar, and R. Shorten, "Adaptive rollover prevention for automotive vehicles with differential braking," in *Proc. International Federation of Automatic Control (IFAC) World Congress*, (Seoul, Korea), 2008.

[91] H. Leffler, "Consideration of lateral and longitudinal vehicle stability by function enhanced brake and stability control system," *SAE Technical Paper 940832*, 1994.

[92] M. J. Hancock, R. Williams, T. J. Gordon, and M. C. Best, "A comparison of braking and differential control of road vehicle yaw-sideslip dynamics," *Journal of Automobile Engineering*, vol. 219, pp. 309–327, 2004.

[93] N. Cooper, D. Crolla, M. Levesley, and W. Manning, "Integration of active suspension and active driveline to ensure stability while improving vehicle dynamics," *SAE Technical Paper 2005-01-0414*, 2005.

[94] H. Huchtkötter and H. Klein, "The effect of various limited slip differentials in front wheel drive vehicles on handling and traction," in *Proc. SAE International Congress and Exposition*, (Detroit, Michigan), pp. 133–134, 26-29 February 1996.

[95] Y. Ikushima and K. Sawase, "A study on the effects of the active yaw moment control," *SAE Technical Paper 950303*, pp. 425–433, 1995.

[96] K. Sawase and Y. Sano, "Application of active yaw control to vehicle dynamics by utilizing driving/braking force," *JSAE Rev*, vol. 20, pp. 289–295, 1999.

[97] B. Post, X. Kang, and C. Cymbal, "Method for improved yaw stabilization control by integration of a direct yaw control AWD system with a vehicle stability assist controller," *SAE Technical Paper 2008-01-1456*, 2008.

[98] H. T. Smakman, *Functional integration of slip control with active suspension for improved lateral vehicle dynamics*. PhD thesis, Delft University of Technology, 2000.

[99] S. Mammar, J. Sainte-Marie, and S. Glaser, "On the use of steer-by-wire systems in lateral driving assistance applications," in *Proc. IEEE International Workshop- Robot and Human Communication*, (Bordeaux-Paris), pp. 487–492, September 2001.

[100] T. D. Gillespie, *Fundamentals of Vehicle Dynamics*. Society of Automotive Engineers, 1992.

[101] G. P. Bevan, S. J. O'Neill, H. Gollee, and J. O'Reilly, "Performance comparison of collision avoidance controller designs," in *Proc. IEEE Intelligent Vehicles Symposium*, (Istanbul, Turkey), pp. 468–473, June 2007.

[102] U. Kiencke and L. Nielsen, *Automotive Control Systems*. Springer, 2000.

[103] W. Milliken and D. Milliken, *Race Car Vehicle Dynamics*. Society of Automotive Engineers, 1995.

[104] R. C. Dorf and R. H. Bishop, *Modern Control Systems*. Addison Wesley, 7 ed., 1995.

[105] G. F. Franklin, J. D. Powell, and A. Emami-Naeini, *Feedback Control of Dynamic Systems*. Prentice Hall, 4 ed., 2002.

[106] J. Hur, "Characteristic analysis of interior permanent-magnet synchronous motor in electrohydraulic power steering systems," *Industrial Electronics*, vol. 55, pp. 2316–2323, June 2008.

[107] D. D. Eisele and H. Peng, "Vehicle dynamics control with rollover prevention for articulated trucks," in *Proc. AVEC 2000, 5th Int'l Symposium on Advanced Vehicle Control*, (Ann Arbor, Michigan), pp. 123–130, August 2000.

[108] "International organization for standardization (1999), iso 3888: Passenger cars - test track for a severe lane-change manoeuvre part 1: Double lane-change."